The role of the mechanosensitive cation channel Piezo1 in the regulation of cardiac fibroblast function

Nicola Marusia Blythe

Submitted in accordance with the requirements for the degree of Doctor of Philosophy

The University of Leeds

Faculty of Medicine and Health

Leeds Institute of Cardiovascular and Metabolic Medicine

September, 2019

Funded by the British Heart Foundation

The candidate confirms that the work submitted is her own and that appropriate credit has been given where reference has been made to the work of others.

Acknowledgements

I must firstly say an enormous thank you to my supervisor, Dr Neil Turner, for his unrelenting support, guidance and encouragement over the past 4 years. Thank you for your reassurance, teaching me to be positive whilst discussing my science and being accepting of my holidays! I don't think I could have asked for a better teacher.

There is no doubt that I would not be in a position to complete my PhD without Professor David Beech, my supervisor during my undergraduate dissertation project and Masters in Research and co-supervisor during my PhD. Thank you for all of your guidance and scientific knowledge over the past 6 years and for giving me the opportunity and encouragement to undertake this PhD. I would also like to thank my other co-supervisors, Dr Mark Drinkhill for his supervision and for his work on the *in vivo* aspect of this project, and Dr Jing Li for her help during the early stages of my PhD and for the generation of the murine models.

I would like to thank all members of the Turner and Beech labs for their support during my studies. I have asked for guidance many times over the past 4 years and am grateful to my colleagues for always being on hand to offer their help and support. I must say a huge thank you to Dr Melanie Bettale who, as she was during my Masters, has been a fountain of knowledge and has always been there to listen to my scientific problems. Congratulations on your new addition to the family – I am so happy for you! I would also like to thank Dr Simon Futers who, over the past 2 years, has been an immense help to me regarding the mouse work required for my project; I don't think you could understand how much I appreciated this! I would also like to thank Melanie Reay for being on hand to offer advice, for making the mouse work a lot more bearable and for only laughing occasionally at my inadequacies. Thank you to Professor Katsuhiko Muraki for his efforts in patching cardiac fibroblasts which I know was a mammoth task and added a great deal to my project. I would also like to thank Dr Baptiste Rode for his part in generating the Piezo1 Het mice, to Beth for harvesting the M-R mice (and for always changing media on my cells whilst I was on holiday!) and to Dr Laeticia Lichtenstein for her assistance with the Piezo1-HA mice. I would also like

to thank Dr Karen Porter for the numerous vials of human cardiac fibroblasts which she has provided me with which I believe enhanced my thesis, and to Karen Hemmings for all things cardiac fibroblast-related! I wish to thank Dr Azhar Maqbool for conducting my transfer and progress reviews and for lending me reagents to complete my project. Thank you also to the Chemistry department at The University of Leeds, in particular Dr Kevin Cuthbertson for his work generating the Yoda1 analogues. I would also like to acknowledge Savithri Rangarajan for her assistance in analysing data from the PamGene kinase arrays.

I would also like to thank Dr Frans van Nieuwenhoven, who allowed me to spend a month in his lab at The University of Maastricht, which was a fantastic experience. I must also say thank you to Chantal Munts, who was a tremendous support whilst I was there. Thank you to Vasili Stylianidis for all of his work on Piezo1 in cardiac fibroblasts during his time in Leeds and for being a great host during my time in Maastricht. I also wish to thank Dr Joe Swift at The University of Manchester for allowing me to use the FlexCell machine and to Dr Hamish Gilbert for being an enormous help during experimentation.

There is no doubt that I would not have enjoyed this experience half as much without the people I have met along the way. I have been lucky enough to make fantastic friends during various stages of my PhD and I hope to stay in touch with all of them (Katie, Hannah, Beth, Kat, Lucia, Nele, Pete, Nick, Adam, Hollie, Katie S, Lara, Marj and Fiona). Thank you also to Ash and Alice who have been incredible housemates during my PhD and I am overjoyed to see them both complete their doctorates so successfully. Special thanks to the Drinky in Helsinki group for ensuring that I have some amazing memories from these past 4 years, putting up with me and for always being on hand to make me giggle. I know we will be friends for life. I must give particular thanks to Katie Musialowski who started this journey in the lab alongside me and since then has been a constant source of support. I am not sure how I will cope not seeing her face nearly every day as I have for the past 7 years since we lived together in Australia on our year abroad – thank you for everything.

Last but not definitely not least, I would like to extend my thanks to 3 very special people. Thank you to Harry who, since the week of my interview for this PhD position, has aimed to put a smile on my face. I know you are more fibreglass than fibroblast but I appreciate how you have tried to understand my PhD and the millions of miles that you have driven to spend time together over the past 5 years. Thank you to A&T for all of their support throughout my education, up to and including this PhD. Thank you for supporting me, always being a phone call away and for trying to make my life easier however possible. I am 100% sure that I would not have been able to complete this without you both.

A huge thank you to The British Heart Foundation for funding my PhD studentship and to the alumni at The University of Leeds for their donation towards my research expenses; without them, this work would not have been possible.

Abstract

Background

Cardiac fibroblasts are fundamental regulators of multiple aspects of cardiac function under both physiological and pathophysiological conditions. These cells contribute to cardiac inflammation, angiogenesis, fibrosis and cardiomyocyte hypertrophy and are therefore a potential therapeutic target for ameliorating adverse cardiac remodelling. Cardiac fibroblasts become activated upon mechanical stimulation; mechanically-activated ion channels have been implicated as sensors of mechanical stress in these cells. The mechanosensitive non-selective cation channel, Piezo1, has widespread physiological importance and although *Piezo1* mRNA expression has been detected in the murine heart, its role in the myocardium is poorly understood. The hypothesis is that Piezo1 is important for detecting mechanical stress in cardiac fibroblasts in order to affect cell function and phenotype.

Methods and Results

RT-PCR analysis indicated that *Piezo1* mRNA is expressed in cardiac fibroblasts at similar levels to endothelial cells and Fura-2 intracellular Ca^{2+} measurements using the Piezo1 agonist, Yoda1, validated Piezo1 as a functional ion channel in these cells. Yoda1-induced Ca^{2+} entry can be inhibited by non-specific Piezo1 blockers (gadolinium, ruthenium red) and affected proportionally by alterations in Piezo1 activity or mRNA expression. In addition to using chemical stimulation, Piezo1 could be activated using mechanical force generated by cell-attached patch clamp electrophysiology. Investigation into the effect of Yoda1 on selected cardiac remodelling genes indicated that Piezo1 activation induces the expression of tenascin C (TNC), a mechanosensitive glycoprotein, and interleukin-6 (IL-6), a pro-hypertrophic and pro-fibrotic cytokine, which are both known to be upregulated following cardiac injury. Piezo1 was demonstrated to have a role in regulating basal IL-6 levels; this appeared to be dependent on substrate stiffness and/or composition. Multiplex kinase activity profiling, combined with kinase inhibitor studies and phospho-specific western blotting, established that Ca^{2+} entry instigated by Piezo1 activation by Yoda1 stimulates concentration-dependent phosphorylation of both p38α MAPK and ERK. It was

revealed that it was p38α MAPK which mediated Yoda1-induced IL-6 expression and secretion. Src-family kinases were subsequently discovered to be the link between Piezo1 activation and p38 MAPK phosphorylation; three members of the kinase family were found to be expressed in cardiac fibroblasts. Preliminary data gathered using a myofibroblast-specific Piezo1 KO murine model implied that Piezo1 may promote cardiac remodelling following pressure overload and that its deletion may be advantageous in cardiac dysfunction.

Conclusion

In summary, this study reveals that cardiac fibroblasts express functional Piezo1 channels and that utilisation of Yoda1 to stimulate the opening of these channels is coupled to increased secretion of IL-6. This occurs via activation of Src-family kinases and p38 MAP kinase. Improved understanding of Piezo1 channels in cardiac fibroblasts may be necessary for achieving a greater appreciation of how cardiac fibroblasts sense mechanical stimuli in pathological conditions such as fibrosis and hypertrophy.

Table of contents

List of Tables

List of Figures

Abbreviations

ACE	Angiotensin-converting enzyme
ADME	Absorption, distribution, metabolism and excretion
AF	Atrial fibrillation
ANF	Atrial natriuretic factor
Ang II	Angiotensin II
APS	Ammonium persulfate
ARB	Angiotensin receptor blockers
ATP	Adenosine triphosphate
AT_1	Angiotensin II receptor type 1
BSA	Bovine serum albumin
Ca^{2+}	Calcium
CD31	Cluster of differentiation 31
CDK	Cyclin-dependent kinase
CF	Cardiac fibroblasts
CM	Cardiomyocytes
CO	Cardiac output
Ct	Cycle threshold
Ctrl	Control
CVD	Cardiovascular disease
DAPI	4',6-diamidino-2-phenylindole
DDR2	Discoidin domain-containing receptor 2
DHS	Dehydrated hereditary stomatocytosis
DMEM	Dulbecco’s modified Eagle’s medium
DMSO	Dimethyl sulfoxide
ECM	Extracellular matrix
EDH	Endothelium-dependent hyperpolarisation

EDP	End diastolic pressure
EDTA	Ethylenediaminetetraacetic acid
EF	Ejection fraction
EGM	Endothelial cell basal medium
ELISA	Enzyme linked immuno-sorbent assay
eNOS	Endothelial nitric oxide synthase
ER	Endoplasmic reticulum
ERK	Extracellular signal-regulated kinases
ESP	End systolic pressure
FAK	Focal adhesion kinase
FBS	Foetal bovine serum
FITC	Fluorescein isothiocyanate
FSP1	Fibroblast specific protein 1
Gapdh	Glyceraldehyde-3-phosphate dehydrogenase
Gd^{3+}	Gadolinium
GPCR	G-protein coupled receptor
GsMTx4	Grammostola spatulata mechanotoxin 4
HA	Hemagglutinin epitope
HEK-293	Human embryonic kidney 293
HEPES	4-(2-hydroxyethyl)-1-piperazineethanesulfonic acid
Het	Heterozygote
Hom	Homozygote
HRP	Horse radish-peroxidase
HUAEC	Human umbilical artery endothelial cells
HUVEC	Human umbilical vein endothelial cells
HW/BW	Heart weight to body weight ratio
HW/TL	Heart weight to tibia length ratio

IL	Interleukin
IP_3	Inositol-1,4,5-trisphosphate
IP_3R	Inositol-1,4,5-trisphosphate receptor
JNK	c-Jun N-terminal kinases
KO	Knockout
K2P	Two-pore domain potassium
LAD	Left anterior descending
LV	Left ventricular
mAb	Monoclonal antibody
MACS	Magnetic-activated cell sorting
MAPK	Mitogen activated protein kinase
MI	Myocardial infarction
MMP	Matrix metalloproteinase
NCLX	Mitochondrial Na^+/Ca^{2+} exchanger
NCX	Na^+-Ca^{2+} exchanger
NFAT	Nuclear factor of activated T cells
NMDG-Cl	N-methyl-D-glucamine chloride
PBS	Phosphate-buffered saline
PCR	Polymerase Chain Reaction
PDGFRA	Platelet derived growth factor receptor alpha
PEC	Pulmonary endothelial cells
PECAM-1	Platelet and endothelial cell adhesion molecule 1
PFA	Paraformaldehyde
Piezo1-HA	Hemagglutinin-tagged version of Piezo1
PIP_2	Phosphatidylinositol 4,5-bisphosphate
PI3K	Phosphatidylinositol-4,5-bisphosphate 3-kinase
PLC	Phospholipase C

PMCA	Plasma membrane Ca^{2+} ATPase
PTK	Protein tyrosine kinase
PV	Pressure-volume
PVDF	Polyvinylidene difluoride
RBC	Red blood cell
ROCK	Rho-associated kinase
r.t.	Room temperature
RT	Reverse transcription
RT-qPCR	Real time-quantitative polymerase chain reaction
RuR	Ruthenium red
RyR	Ryanodine receptor
SBS	Standard bath solution
SDS	Sodium dodecyl sulphate
SEM	Standard error of the mean
SERCA	Sarcoplasmic reticulum Ca^{2+} ATPase
SFK	Src-family kinase
siRNA	Short interfering RNA
SOCE	Store-operated Ca^{2+} entry
SSP	Staurosporine
STIM1	Stromal interaction molecule 1
STK	Serine-threonine kinase
SV	Stroke volume
SVEC	Saphenous vein endothelial cells
TAB1	TGF-β-activated protein 1 (TAK1)-binding protein 1
TAC	Transverse aortic constriction
TAE	Tris-acetate-EDTA
TAZ	Transcriptional coactivator with PDZ-binding motif

TBS	Tris-buffered saline
TBS-T	Tris-buffered saline-tween
Temed	N,N,N′,N′-Tetramethylethylenediamine
TGF-βR	Transforming growth factor-beta1 receptor
TGF-β1	Transforming growth factor-beta1
Thy1	Thymocyte differentiation antigen 1
TIMP	Tissue inhibitors of metalloproteinase
TNC	Tenascin C
TNF	Tumour necrosis factor
TWEK	TWIK-related potassium channel
TRP	Transient receptor potential
VEGF	Vascular endothelial growth factor
WT	Wild-type
YAP	Yes-associated protein
4OH-TM	4-hydroxytamoxifen
α-MHC	Alpha-myosin heavy chain
α-SMA	Alpha-smooth muscle actin
β-MHC	Beta-myosin heavy chain

Publications and Communications

Publications

First author:

Blythe N.M., Muraki K., Ludlow M.J., Stylianidis V., Gilbert H.T.J., Evans E.L., Cuthbertson K., Foster R., Swift J., Li J., Drinkhill M.J., van Nieuwenhoven F.A., Porter K.E., Beech D.J. and Turner N.A. (2019). Mechanically-activated Piezo1 channels of cardiac fibroblasts stimulate p38 mitogen-activated protein kinase and interleukin-6 secretion. ***Journal of Biological Chemistry***. 294(46), pp. 17395-17408.

Blythe N.M., Stylianidis V., Ludlow M.J., Gilbert H.T.J, Evans E.L., Cuthbertson K., Foster R., Swift J., Li J., Drinkhill M.J., van Nieuwenhoven F.A., Porter K.E., Beech D.J. and Turner N.A. (2019). Stimulation of cardiac fibroblast Piezo1 channels opposes myofibroblast differentiation and induces IL-6 secretion via Ca^{2+}-mediated p38 MAP kinase activation. Preprint available on ***bioRxiv***.

Turner N.A. & **Blythe N.M.** (2019). Cardiac fibroblast p38 MAPK: a critical regulator of myocardial remodelling. ***Journal of Cardiovascular Development and Disease***. 6(3), pp. 27.

Co-author:

Evans, E.L., Cuthbertson, K., Endesh, N., Rode, B., **Blythe, N.M.**, Hyman, A.J., Gaunt, H.J., Ludlow, M.J., Foster, R. and Beech, D.J. (2018). Yoda1 analogue (Dooku1) which antagonizes Yoda1-evoked activation of Piezo1 and aortic relaxation. ***British Journal of Pharmacology.*** 175(10), pp. 1744-1759.

Rubaiy, H.N., Ludlow, M.J., Henrot, M., Gaunt, H.J., Miteva, K., Cheung, S.Y., Tanahashi, Y., Hamzah, N., Musialowski, K.E., **Blythe, N.M.**, Appleby, H.L., Bailey, M.A., McKeown, L., Taylor, R., Foster, R., Waldmann, H., Nussbaumer, P., Christmann, M., Bon, R.S., Muraki, K., Beech, D.J. (2017). Picomolar, selective and subtype specific small-molecule inhibition of TRPC1/4/5 channels. ***Journal of Biological Chemistry*****.** 292(20), pp. 8158-8173.

Ludlow, M.J., Gaunt, H.J., Rubaiy, H.N., Musialowski, K.E., **Blythe, N.M.**, Vasudev, N.S., Muraki, K., Beech, D.J. (2017). (-)-Englerin A-evoked cytotoxicity is mediated by Na^+ Influx and counteracted by Na^+/K^+-ATPase. ***Journal of Biological Chemistry.*** 292(2), pp. 723-731.

Blythe N.M., Li J., Drinkhill M.J., Beech D.J. and Turner N.A. (2016). Piezo1 – a role in cardiac differentiation? Abstract – ***Heart***,102:A11.

Naylor, J., Minard, A., Gaunt, H.J., Amer, M.S., Wilson, L.A., Migliore, M., Cheung, S.Y., Rubaiy, H.N., **Blythe, N.M.**, Musialowski, K.E., Ludlow, M.J., Evans, W.D., Green, B.L., Yang, H., You, Y., Li, J., Fishwick, C.W.G., Muraki, K., Beech, D.J., Bon, R.S. (2016). Natural and synthetic flavonoid modulation of TRPC5 channels. ***British Journal of Pharmacology.*** 173(3), pp. 562-74.

Communications

Poster presentations:

Piezo1 activity and signalling in cardiac fibroblasts. **Nicola M Blythe**, Melanie J. Ludlow, Vasili Stylianidis, Hamish T. J. Gilbert, Elizabeth L. Evans, Kevin Cuthbertson, Richard Foster, Joe Swift, Jing Li, Mark J. Drinkhill, Frans A. van Nieuwenhoven, Karen E. Porter, David J. Beech and Neil A. Turner. The 14th International Symposium on Biomechanics in Vascular Biology and Cardiovascular Disease, Imperial College London (2019).

Piezo1 activity and signalling in cardiac fibroblasts. **Nicola M Blythe**, Jing Li, Azhar Maqbool, Mark J. Drinkhill, David J. Beech and Neil A. Turner. FBS-FMH symposium, University of Leeds (2018).

Piezo1 is a functional ion channel in cardiac fibroblasts. **Nicola M Blythe**, Jing Li, Mark J. Drinkhill, David J. Beech and Neil A. Turner. International Union of Physiological Sciences (IUPS) World Congress of Physiology, Rio de Janeiro (2017).

Piezo1 – a role in cardiac differentiation? **Nicola M Blythe**, Jing Li, Mark J. Drinkhill, David J. Beech & Neil A. Turner. The British Society for Cardiovascular Research (BSCR) Meeting, University of Leeds (2016).

Chapter 1 Introduction

1.1 Cardiovascular disease

According to the World Health Organisation, cardiovascular disease (CVD) is the leading cause of death worldwide, claiming the lives of 17.9 million people each year. The British Heart Foundation affirm that CVD is the cause of a quarter of deaths in the UK, with a total annual healthcare cost of a staggering £9 billion. Hypertension, hypercholesterolemia, cigarette smoking, inactivity, aging, genetics and diabetes all increase the likelihood of developing these diseases. CVD are a class of diseases which affect the heart, blood vessels and the vasculature of the brain. Some examples are: atherosclerosis, ischaemic heart disease, cerebrovascular disease, ischaemic stroke, haemorrhagic stroke, hypertensive heart disease, cardiomyopathy and myocarditis, atrial fibrillation, aortic aneurysm, peripheral vascular disease and endocarditis (Roth *et al.* 2017). This thesis will discuss some of the more common diseases associated with the myocardium.

1.1.1 Myocardial infarction

Coronary artery disease is the narrowing or blockage of the coronary arteries, usually caused by atherosclerosis, a thickening of the intimal and medial layers of arteries due to deposition of atheromatous plaques (Lahoz and Mostaza 2007). This restricts blood flow, which can result in inadequate supply of blood to the myocardium ("ischaemia") and a myocardial infarction (MI). Following MI, there is a multifaceted approach to repair the myocardium (Prabhu and Frangogiannis 2016). Ischaemia initiates the necrosis of cardiomyocytes and this rapidly triggers an intense inflammation response, involving the upregulation of proinflammatory cytokines and chemokines by cardiac and inflammatory cells, together with neutrophil and macrophage infiltration to clear necrotic cells and matrix debris (Bujak and Frangogiannis 2007; Turner 2016). Within a few days, inflammation is suppressed as inflammatory cells undergo apoptotic death and there is formation of granulation tissue comprising of newly synthesised extracellular matrix (ECM) and blood vessels and activated cardiac fibroblasts (Jourdan-

LeSaux, Zhang and Lindsey 2010). The final stage encompasses the healing of the myocardium, characterised by the upregulation of profibrotic and anti-inflammatory factors and scar formation (Chen and Frangogiannis 2013). As the infarct matures, “stress-shielding” of activated cardiac fibroblasts by the ECM prompts quiescence and normally triggers their apoptotic death (Chen and Frangogiannis 2013). However, it has been demonstrated that these cells can remain active in the infarct region up to 17 years post-MI (Willems *et al.* 1994).

1.1.2 Hypertension

Extensive growth of the left ventricle, termed left ventricular (LV) hypertrophy, is induced by factors such as prolonged and abnormal hemodynamic stress; this is known as pathological hypertrophy, but this term can also refer to the physiological adaptation to increased work load e.g. in athletes or during pregnancy (Shimizu and Minamino 2016). It is well established that persistently elevated blood pressure (“hypertension”) has been associated with LV hypertrophy and that LV hypertrophy is a risk factor for future cardiac events (Verdecchia *et al.* 1990; Vakili, Okin and Devereux 2001). Hypertrophy can be categorised into two subgroups: concentric hypertrophy, transpiring due to hypertension and subsequent sustained pressure overload, where wall thickness increases without chamber enlargement, or eccentric hypertrophy, occurring following chronic volume overload in which the volume of the chamber is augmented, with no increase in wall thickness (Rossi and Carillo 1991). The hypertrophic growth of cardiomyocytes is the leading response by which the heart lessens the stress on the LV wall imposed by pressure overload (González *et al.* 2018). The hypertrophic growth of myocytes is an attempt to maintain cardiac output but the subsequent remodelling consequently lowers ventricle compliance and can cause cardiac dysfunction. In addition to during pressure overload, myocardial hypertrophy is also part of the remodelling process following MI (Kahan and Bergfeldt 2005).

1.1.3 Heart failure

Adverse cardiac remodelling following MI or pressure overload can lead to heart failure (Schirone *et al.* 2017). Improved medical care following cardiac events

such as MI has resulted in increased patient survival and, therefore, the frequency of secondary complications such as heart failure has intensified. It is approximated that 1-2 % of adults in Western populations have heart failure (Mosterd and Hoes 2007), with the most common symptoms being breathlessness, fatigue and swollen lower limbs. The economic burden on the National Health Service is second only to stroke in the UK (Stewart *et al.* 2002) and the severity of the disease is most commonly assessed using the New York Heart Association Class guidelines. The classes range from I (mild), characterised as patients without limitation of physical activity to IV (severe), described as patients with the inability to carry out any physical activity without discomfort; symptoms may even be present at rest in this population.

Heart failure is a broad term described by the American Heart Association as “a complex clinical syndrome that results from any structural or functional impairment of ventricular filling or ejection of blood” (Yancy *et al.* 2013) and can occur due to dysfunction during systole and/or diastole. Systolic dysfunction is characterised by compromised contraction and ejection of blood, resulting in reduced ejection fraction, principally due to increased collagen deposition (Murtha *et al.* 2017). It has been suggested that this increased deposition may result in impairment of systolic function through disturbed coordination of myocardial excitation-contraction coupling (Janicki and Brower 2002). In contrast, in diastolic dysfunction, ejection fraction is preserved; however, there is impaired filling of the LV ventricle (Murtha *et al.* 2017). This is largely due to compromised ventricular relaxation or increased myocardial stiffness triggered by excessive ECM deposition which reduces the compliance of the ventricles (Federmann and Hess 1994).

1.2 Cardiac fibrosis

Nearly all aetiologies of heart disease, including MI and heart failure, involve pathological remodelling characterised by the excessive deposition of ECM proteins (“fibrosis”) (Travers *et al.* 2016). Fibrosis presents as interstitial (reactive) or replacement (reparative) fibrosis. Interstitial fibrosis is described as chronic expansion of the interstitium in order to maintain organ function (e.g. during pressure overload) without the initial loss of cardiomyocytes (Murtha *et al.* 2017).

This is accompanied by adaptive cardiomyocyte hypertrophy, in an attempt to preserve cardiac output while normalising wall stress (Biernacka and Frangogiannis 2011). Subsequently there may be necrosis and apoptosis of cardiomyocytes, possibly due to the augmented ECM surrounding hypertrophied cardiomyocytes giving rise to an inadequate supply of nutrients (Biernacka and Frangogiannis 2011). In contrast, replacement fibrosis involves necrotic cells being replaced with a collagen-rich scar, as occurs following MI (Murtha *et al.* 2017). Myocardial deposition of collagen has also been revealed in patients with diabetes (Heerebeek *et al.* 2008; Patil *et al.* 2011). Patil *et al.* (2011) demonstrated that the incidence of diastolic dysfunction is high in patients with type 2 diabetes mellitus, in the absence of coronary artery disease; the level of dysfunction correlated with the duration of diabetes and diabetic microangiopathies. Excessive diastolic left ventricular stiffness has been reported to be an important contributor to heart failure in these patients; this is presumed to be due to the deposition of collagen and advanced glycation end products (Heerebeek *et al.* 2008). Using a genetically-induced mouse model of type 2 diabetes mellitus generated by a point mutation in the leptin receptor, it was demonstrated that cardiac fibroblasts derived from diabetic hearts had elevated expression of several pro-fibrotic markers, including type I collagen and transforming growth factor-β (TGF-β), compared with those from non-diabetic hearts (Hutchinson *et al.* 2013). This pattern of protein expression was associated with myocardial stiffness and LV diastolic dysfunction (Hutchinson *et al.* 2013). This correlates with the finding that cardiac fibroblasts from type 2 diabetic patients possess a pro-fibrotic phenotype (Sedgwick *et al.* 2014).

Progressive cardiac fibrosis in heart failure is principally facilitated by the tissue-resident cardiac fibroblast, which becomes activated and differentiates into a myofibroblast (Khalil *et al.* 2017), these cells will be discussed in more detail below. Initially, fibrosis is an adaptive, protective mechanism required to avoid a loss of integrity in the mechanical strength of the ventricle following injury, which could lead to rupture due to LV wall thinning (Ma *et al.* 2014). For example, post-MI, an appropriate degree of fibrosis in the infarct zone is essential to replace necrotic cardiomyocytes (Talman and Ruskoaho 2016). However, over time, irreversible, adverse ventricular remodelling can contribute to the contractile demise of the organ (Porrello and Olson 2014). Fibrosis results in stiffening of the

heart, impairment of electrical conductivity and reduced contraction capacity and oxygen diffusion, thus exacerbating deleterious remodelling (Piek, de Boer and Silljé 2016).

1.3 Cardiac Remodelling

1.3.1 Extracellular matrix deposition

In physiology, the ECM provides structural support, acts as reservoir for cytokines and growth factors and enables communication of extracellular cues between cells (Valiente-Alandi, Schafer and Blaxall 2016). Following cardiac injury, the ECM undergoes remodelling and it is cardiac fibroblasts which are chiefly responsible for this regulation of the ECM. Cardiac fibroblasts secrete ECM proteins including proteins serving a structural role such as collagens, adhesive glycoproteins such as fibronectin and proteases named matrix metalloproteinases (MMPs) which degrade the ECM, along with their native inhibitors, tissue inhibitors of metalloproteinases (TIMPs) (Valiente-Alandi, Schafer and Blaxall 2016). Production of these proteins leads to cardiac remodelling (Dobaczewski, Gonzalez-Quesada and Frangogiannis 2010). Cardiac fibroblasts are known to secrete MMP-1,-2,-3,-9,-13,-14 and TIMP-1,-2,-3 and -4 in response to cardiac injury (Vanhoutte *et al.* 2006; Turner and Porter 2012); macrophages present in granulation tissue also contribute to the generation of MMPs (Iyer, Jung and Lindsey 2016). MMPs and TIMPs are important for ECM homeostasis in physiology but have also been demonstrated to participate in the development and progression of heart failure (Barton *et al.* 2003). Evidence suggests that MMP-1,-2,-3,-9 and TIMP-1 activity is associated with adverse pathophysiology and clinical outcomes in MI patients (Phatharajaree, Phrommintikul and Chattipakorn 2007); the correlation with MMP-9 expression is so strong that it has been suggested this molecule could be used as a predictor for cardiovascular mortality in patients with coronary artery disease (Blankenberg *et al.* 2003).

Cardiac fibroblasts also secrete matricellular proteins, which have regulatory, rather than structural, roles in the ECM; examples are periostin and tenascin-C (TNC). Periostin is scarcely expressed in the developed myocardium but can be more readily detected following myocardial injury or pressure overload

stimulation (Shimazaki *et al.* 2008; Stansfield *et al.* 2009). Mice deficient in periostin showed attenuated fibrosis following pressure overload and displayed improved ventricular performance after MI; however, animals were more susceptible to cardiac rupture (Oka *et al.* 2007; Shimazaki *et al.* 2008). As might be anticipated, inducible overexpression of myocardial periostin protected mice from rupture following MI and induced spontaneous hypertrophy with aging (Oka *et al.* 2007). TNC is highly expressed in development and repressed in the adult myocardium but, similarly to periostin, its levels soar following MI or pressure overload (Imanaka-Yoshida *et al.* 2001; Xia *et al.* 2009). It has been suggested that TNC loosens the adhesion of cardiomyocytes to connective tissue; this may aid in releasing surviving cardiomyocytes to reorganise their arrangement following cardiac injury (Imanaka-Yoshida *et al.* 2001).

Cardiac fibroblasts are the principal producers of TGF-β, a pleiotropic cytokine/growth factor. TGF-β stimulation of cardiac fibroblasts causes increased synthesis of collagen, fibronectin, proteoglycans, expression of contractile genes and triggers their subsequent differentiation into myofibroblasts (Eghbali *et al.* 1991; Villarreal *et al.* 1996). TGF-β signals via heterotetrameric complexes of type I and type II receptors in the plasma membrane (Heldin and Moustakas 2016). Of the three TGF-β isoforms (1-3), TGF-β1 is the predominant isoform and is found almost ubiquitously (Dobaczewski, Chen and Frangogiannis 2011). TGF-β receptor activation generates downstream intracellular signals through the Smad proteins (Shi and Massagué 2003) and alternative non-canonical pathways (Derynck and Zhang 2003). The overexpression of TGF-β in the mouse heart is associated with cardiac fibrosis and hypertrophy (Dobaczewski, Chen and Frangogiannis 2011). Incisional rat wounds treated with anti-TGF-β antibodies displayed an evident reduction in ECM deposition and scarring (Shah, Foreman and Ferguson 1995). Moreover, TGFβ1-deficient mice had an overt reduction in collagen deposition, accompanied by a pronounced inflammatory response which was ultimately lethal (Kulkarni *et al.* 1993). This is presumably due to the anti-inflammatory effects of TGF-β (Werner *et al.* 2000) which have been suggested to be important in promoting the resolution of post-MI inflammation.

1.3.2 Cardiomyocyte hypertrophy

In addition to being primarily responsible for the deposition of excessive ECM, cardiac fibroblasts are now recognised as being important direct regulators of cardiac hypertrophy via paracrine mechanisms (Gray *et al.* 1998; Fujiu and Nagai 2014; Kamo, Akazawa and Komuro 2015). Pathological hypertrophy gives rise to ventricular remodelling associated with systolic and diastolic dysfunction, inflammation and interstitial fibrosis, which can result in adverse outcomes, such as congestive heart failure, arrhythmia, and sudden death (Kamo, Akazawa and Komuro 2015). Cardiac hypertrophy triggers multiple molecular modifications, including genetic reprogramming (re-induction of various foetal genes and diminished adult genes) (Izumo, Nadal-Ginard and Mahdavi 1988). In fact, the re-expression of foetal genes, including β-myosin heavy chain (β-MHC) and atrial natriuretic factor (ANF) is an indicator of pathological hypertrophy (Pandya and Smithies 2011).

Fibroblasts synthesise a range of paracrine signalling molecules including growth factors, cytokines and microRNAs that can act to stimulate hypertrophy of cardiomyocytes (Fujiu and Nagai 2014; Kamo, Akazawa and Komuro 2015). Conditioned medium from cardiac fibroblasts isolated from pressure-overloaded rat hearts caused hypertrophy of cardiomyocytes; this could be inhibited by a TGF-β1 receptor antagonist, indicating that TGF-β is important in mediating cardiomyocyte hypertrophy (Cartledge *et al.* 2015). Interleukin-6 (IL-6), a pleiotropic cytokine which participates in cell growth, apoptosis, differentiation and survival, is produced by and can stimulate both cardiac fibroblasts and cardiomyocytes (Banerjee *et al.* 2009). The activity of IL-6 is modulated by binding to the IL-6Rα/gp130 signal transduction complex (Coles *et al.* 2007). Importantly, high levels of IL-6 are detected in patients with heart failure (Nian *et al.* 2004). It has since been reported that IL-6 is cardioprotective during acute injury to the myocardium but becomes pathogenic when elevated persistently (Fontes, Rose and Čiháková 2015). Initially, IL-6 protects myocytes from apoptosis (Smart *et al.* 2006); however, continuous activation of gp130 has been revealed to instigate pathological cardiac hypertrophy (Hirota *et al.* 1995; Kunisada *et al.* 1998). Cardiac hypertrophy is accompanied by increased IL-6 after 1 week of isoproterenol infusion (Cha *et al.* 2010) and genetic deletion of IL-6 has been shown to attenuate thoracic aortic constriction (TAC)- and

norepinephrine-induced LV hypertrophy in mice (Zhao *et al.* 2016a; Meier *et al.* 2009). IL-6 also directly induces cardiomyocyte hypertrophy in cultures of primary human cardiomyocytes and cardiac fibroblasts (Ancey *et al.* 2003). Bageghni *et al.* (2018) observed that IL-6 secretion from cardiac fibroblasts following isoproterenol infusion was dependent on the activity of p38α mitogen-activated protein kinase (MAPK). Fibroblasts can also modulate cardiomyocyte hypertrophy through signalling molecules such as fibroblast growth factor 2 (Bogoyevitch *et al.* 1994; Pellieux *et al.* 2001), insulin-like growth factor 1 (McMullen *et al.* 2004) and miR-21*, which is delivered to cardiomyocytes through fibroblast-derived exosomes (Duygu and Da Costa Martins 2015). The processes involved in cardiac remodelling which can lead to the development of heart failure are summarised in Figure 1.1.

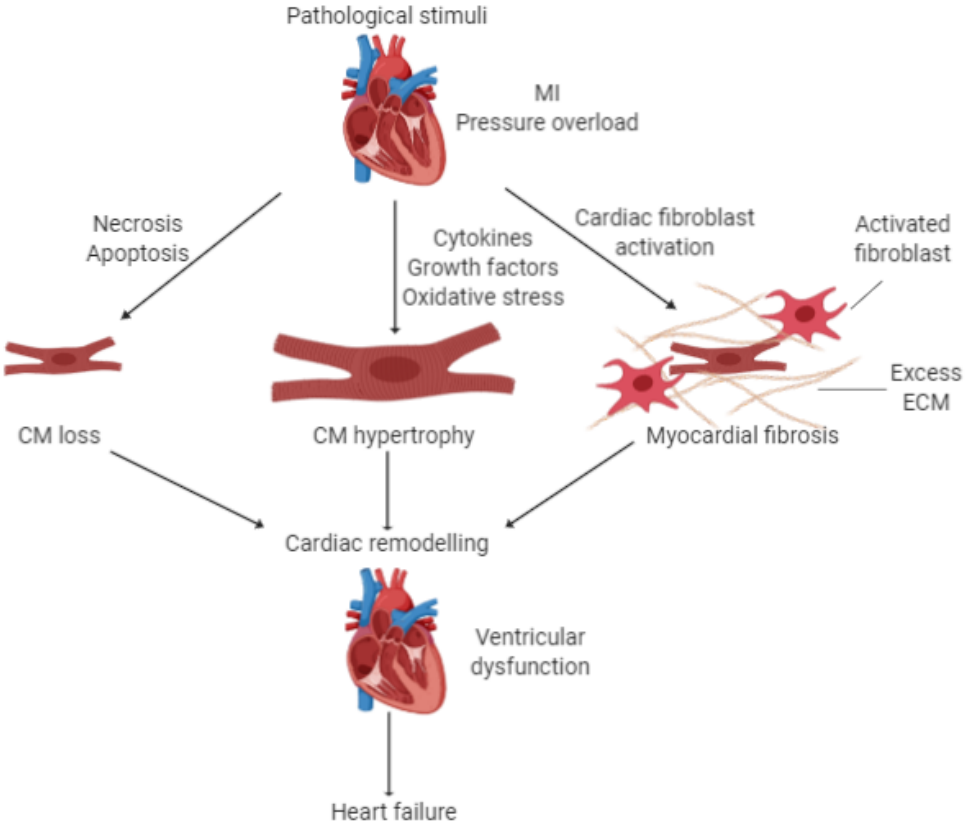

Figure 1.1 Mechanisms of pathological cardiac remodelling leading to heart failure. In response to pathophysiological stimuli such as ischemia or excessive mechanical load, various processes occur which contribute to cardiac remodelling. These include: cardiomyocyte loss, cardiomyocyte hypertrophy and the accumulation of excess ECM leading to fibrosis. These structural changes induce ventricular dysfunction, which can culminate in heart failure.

1.4 Cardiac fibroblasts

1.4.1 Characterisation of cardiac fibroblasts

During embryonic development, cardiac fibroblasts evolve from multiple sources; the epicardium was believed to be the chief source of cardiac fibroblasts found in the ventricular myocardium, with epicardial cells undergoing epithelial-to-mesenchymal transition (Dettman *et al.* 1998). This has been a source of debate as lineage tracing with the epicardial marker, *Tbx18*, revealed only one third of cardiac fibroblasts were *Tbx18*-expressing (Cai *et al.* 2008). However, more recent evidence demonstrated that 80 % of cardiac fibroblasts in the adult heart were derived from the epicardium (Moore-Morris *et al.* 2014). It has been reported that endothelial-to-mesenchymal transition and the recruitment of bone marrow-derived cells also contribute to the source of cardiac fibroblasts during cardiac fibrosis (Zeisberg *et al.* 2007; Fan *et al.* 2012).

It is recognised that cardiomyocytes constitute approximately 25-35% of total cardiac cells (Nag 1980) but the composition of the non-myocyte cardiac cell population has been disputed. It was originally suggested that fibroblasts accounted for the majority of the non-myocyte portion (Banerjee *et al.* 2007). However, with the availability of genetic tracers and enhanced flow cytometry techniques, it was verified by Pinto *et al.* (2016) that cardiac fibroblasts in fact represent a more minor population (<20 %) in the myocardium than endothelial cells, which are the most abundant cell type (>60 %).

Cardiac fibroblasts lack a basement membrane, display a cytoplasm with multiple processes and, *in vitro*, appear flat and spindle-shaped (Camelliti, Borg and Kohl 2005). The interconnected network of cardiac fibroblasts forms the fibrous, supportive skeleton of the myocardium, where they are spatially intermingled with cardiomyocytes (Fountoulaki, Dagres and Iliodromitis 2015). Cardiac fibroblasts are a highly heterogeneous cell population, depending on their origin or physiological state (Zeisberg and Kalluri 2010). For an extensive period, these cells were poorly characterised as the majority of markers were either non-specific or lacked sensitivity and this hindered investigation into this cell type (Camelliti, Borg and Kohl 2005). Early markers of cardiac fibroblasts, such as thymocyte differentiation antigen 1 (Thy1) and fibroblast specific protein 1 (FSP1), also identify endothelial cells, immune cells and pericytes (Kong *et al.*

2013; Hudon-David *et al.* 2007) and vimentin also labels other mesoderm-derived cells in the heart (Bursac 2014). More recently, lineage-tracing experiments relying on platelet-derived growth factor receptor-α (PDGFRα) and the collagen1a1-*GFP* reporter line being coexpressed successfully identified the majority of cardiac fibroblasts in the heart (Moore-Morris *et al.* 2014).

It was previously assumed that cardiac fibroblasts exclusively regulated ECM remodelling but it is now acknowledged that these cells have vital roles in several aspects of cardiac function in both physiological and pathophysiological circumstances (Porter and Turner 2009; Dostal, Glaser and Baudino 2015). Their functions include proliferation, migration, differentiation into a myofibroblast phenotype, ECM generation and degradation and secretion of cytokines and growth factors (Souders, Bowers and Baudino 2009; Fan *et al.* 2012). These roles grant cardiac fibroblasts the ability to contribute to cardiac disease and they have been considered as potential therapeutic targets. However, inadequate understanding of the regulatory mechanisms governing this cell type has so far been a hindrance.

1.4.2 Differentiation of cardiac fibroblasts

Cardiac fibroblasts are highly plastic cells with the ability to adjust their phenotype and function to meet the challenges of the mechanical load relentlessly inflicted upon the heart. In response to injury, stretch or cytokines such as TGF-β, fibroblasts become activated and differentiate (Souders, Bowers and Baudino 2009; Kendall and Feghali-Bostwick 2014; Herum *et al.* 2017a). The differentiated cells, which are absent in healthy myocardium and only appear after cardiac injury (Willems *et al.* 1994), are termed ‘myofibroblasts’. Myofibroblasts were first described in skin wounds, where they were suggested to be responsible for wound contraction (Gabbiani, Ryan and Majno 1971) by imparting mechanical tension on the surrounding ECM. They were named myofibroblasts due to features similar to smooth muscle cells such as cytoplasmic stress fibres containing alpha smooth muscle actin (α-SMA) (Ehrlich, Allison and Leggett 2006).

Following cardiac injury, profuse proliferation of myofibroblasts occurs to satisfy the temporarily high demand during cardiac remodelling. Historically, it was

presumed myofibroblasts were sourced from resident cardiac fibroblasts. This was challenged and it was established that cellular sources including endothelial cells, epithelial cells, mesenchymal stem cells, pericytes, smooth muscle cells and bone marrow-derived fibrocytes also participate in increasing myofibroblast numbers (van den Borne *et al.* 2009; Turner and Porter 2013). More recent studies using lineage-tracing have confirmed earlier thoughts that in fact the majority of myofibroblasts arise from tissue-resident cardiac fibroblasts (Kanisicak *et al.* 2016). The more contractile myofibroblasts increase collagen turnover, migrate towards chemokines released at the site of injury and secrete a number of cytokines, thus maintaining the inflammatory response to injury (Gabbiani 2003; Baum and Duffy 2011; Dostal, Glaser and Baudino 2015). The majority of myofibroblasts are thought to undergo apoptosis when ECM tension is restored, after the healing process (Kis, Liu and Hagood 2011).

Knowledge of the importance of myofibroblast differentiation following cardiac injury is well established but, more recently, it has been suggested that cardiac fibroblasts exhibit distinct phenotypes at different time points post-cardiac injury (Ma *et al.* 2017). Ma *et al.* (2017) suggested that, at day 1 post-MI, fibroblasts are pro-inflammatory, secreting pro-inflammatory mediators and MMPs. At day 7, fibroblasts are pro-reparative, secreting anti-inflammatory mediators and producing ECM and, at day 28, fibroblasts resume to a homeostatic-like phenotype. Recent in-depth molecular analyses and lineage-tracing experiments have supported the idea of a continuum of differentiation states in cardiac fibroblasts following MI (Fu *et al.* 2018; Mouton *et al.* 2019). The final differentiation state is referred to by Fu *et al.* (2018) as a “matrifibrocyte”, a specialised cell highly adapted to collagenous environments, which reinforces the mature scar. A schematic illustrating the process of myofibroblast differentiation is shown in Figure 1.2.

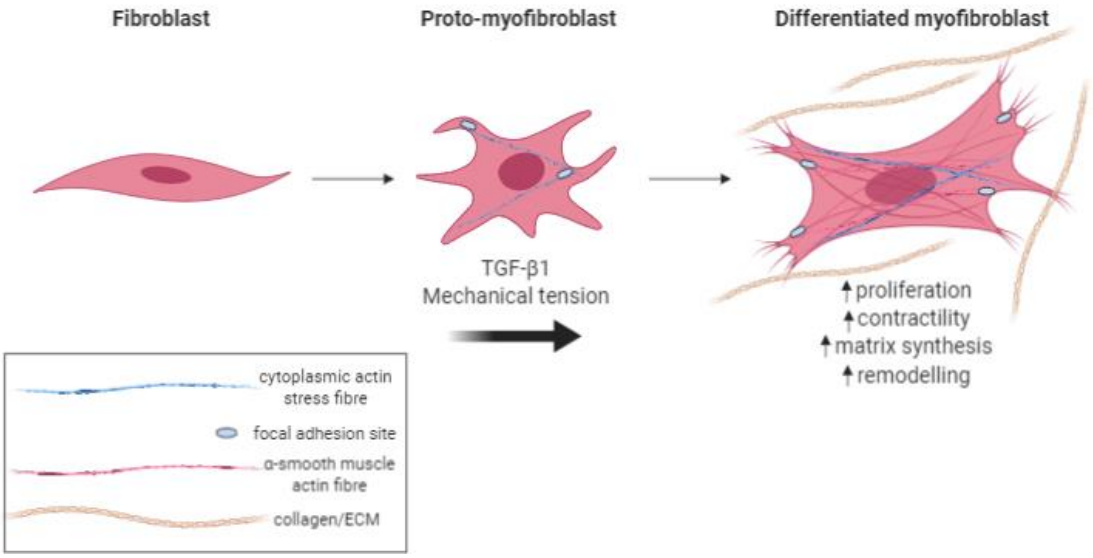

Figure 1.2 Model of cardiac fibroblast differentiation. *In vivo*, fibroblasts display neither stress fibres nor do they form adhesion complexes with the ECM. Under mechanical stress or when transforming growth factor (TGF)-β1 is present, fibroblasts differentiate into proto-myofibroblasts, which form cytoplasmic actin-containing stress fibres that terminate in focal adhesion complexes. Further exposure to TGF-β1 and mechanical stress promotes the modulation of proto-myofibroblasts into differentiated myofibroblasts, characterised by expression of α-smooth muscle actin in more extensively developed stress fibres. Functionally, differentiated myofibroblasts display an increase in proliferation, matrix synthesis and generate greater contractile force, which all enable cardiac remodelling. Figure is adapted from Tomasek *et al.* (2002).

1.4.3 Mechanical signalling in cardiac fibroblasts

It is obligatory that there is a balance in the heart between tissue being sufficiently resilient to endure the constant mechanical load but also compliant enough to allow contraction. Following cardiac injury, enhanced ECM synthesis leads to compliant ECM and cardiomyocytes being replaced by stiffer collagenous scar tissue, resulting in ECM stiffening (van Putten, Shafieyan and Hinz 2016). Young's Modulus (in Pa) can be used to determine the stiffness of tissue; this is the force per area (stress) needed to strain an elastic material (Solon *et al.* 2007). Healthy heart tissue has a Young's modulus of 10-15 kPa whereas fibrotic tissue

is on average 2-10-times stiffer (20-100 kPa) (van Putten, Shafieyan and Hinz 2016).

The impact of mechanical strain on cardiac fibroblast phenotype can be observed in fibroblasts cultured on compliant substrates such as soft collagen gels, which show little development of stress fibres, compared to fibroblasts grown on stiffer substrates which form stress fibres and are therefore characterised as myofibroblasts (Darby *et al.* 2014). Driesen *et al.* (2014) observed that a reduction in mechanical strain can promote the dedifferentiation of myofibroblasts. Mechanical stimulation of fibroblasts gives rise to a pronounced upregulation of ECM components and cytokine and growth factor expression, creating a pro-fibrotic environment (Chapman, Weber and Eghbali 1990; Hsieh *et al.* 2000; Yokoyama *et al.* 1999; Ruwhof *et al.* 2000). Moreover, the release of endothelin-1 and TGF-β from stretched cardiac fibroblasts act as paracrine mediators in cardiomyocyte hypertrophy (van Wamel *et al.* 2001). These studies indicate that mechanical load is important in the regulation of cardiac fibroblast gene expression.

1.5 Mechanotransduction in cardiac fibroblasts

Cells are able to sense mechanical cues from their surrounding environment (mechanosensing) and respond by transducing this information into biochemical signals (mechanotransduction) (Martino *et al.* 2018). Mechanotransduction is initiated at the interface between the plasma membrane and the ECM (Rustad, W Wong and Gurtner 2013). Mechanisms by which cardiac fibroblasts sense and respond to mechanical inputs remain enigmatic. In this section, a brief overview will be offered on the most prominent molecular mechanisms implicated in cardiac fibroblast mechanotransduction.

1.5.1 Integrins

Integrins are heterodimeric proteins consisting of one α and one β subunit which span the plasma membrane and participate in bi-direction signalling (Liu, Calderwood and Ginsberg 2000). There are at least 18 α and 8 β subunits known in humans; through different combinations of these subunits, 24 integrin

heterodimers can be generated (Takada, Ye and Simon 2007). Early studies established that integrins were fundamental for cell adhesion to the ECM but it has since been determined that they have a diverse range of functions including cell survival and migration, in addition to remodelling of the cellular cytoskeleton and focal adhesion (Manso, Kang and Ross 2009). Integrin-mediated signalling involves the binding of ECM proteins, such as fibronectin, vitronectin and laminin (Schlaepfer and Hunter 1998). Integrins are viewed as mechanosensitive as they provide a link between the contractile cytoskeleton and the ECM and permit fibroblasts to probe the mechanical state of the environment (van Putten, Shafieyan and Hinz 2016). Cardiac fibroblasts express at least 8 of the α subunits and 3 β subunits (Manso, Kang and Ross 2009); several of these are upregulated during cardiac fibrosis (Schroer and Merryman 2015).

1.5.1.1 TGF-β receptor type 1

The importance of TGF-β1 in fibrosis and cardiac hypertrophy has previously been discussed. TGF-β is secreted in an inactive protein complex consisting of TGF-β and latency-associated propeptide, which links to latent TGF-β binding protein 1 (Robertson *et al.* 2015). Upon integrin-binding caused by cell traction forces, such as during myofibroblast contraction, TGF-β is released from its complex in the ECM and subsequently activated to allow receptor binding (Wipff *et al.* 2007). Blocking of αvβ3 and αvβ5 integrins led to diminished TGF-β1 activation and α-SMA expression upon cardiac fibroblast contraction; the appearance of myofibroblasts was re-established upon addition of active TGF-β1 (Sarrazy *et al.* 2014). The activation of latent TGF-β1 is directly influenced by ECM compliance (Hinz 2015); on substrates of increased stiffness, cell contraction-mediated release of TGF-β1 from the ECM is augmented (Wipff *et al.* 2007). The mechanical properties of the ECM thereby modulate TGF-β1 activity and thus, TGF-β1-evoked induction of myofibroblasts.

1.5.1.2 Focal adhesions

Focal complexes are the first contacts that develop when a fibroblast interacts with the ECM during cell adhesion and migration; once a mechanically stable contact can be established between an activated integrin and ECM ligand, focal

complexes mature into larger focal adhesions, located at the termini of cytoskeletal actin stress fibres (Chiquet *et al.* 2009). This initiates the attachment of the cytoplasmic domain of the integrin to the cytoskeleton, which involves the recruitment of paxillin, phosphoproteins and vinculin, and is reliant on the presence of cytoskeletal tension (Katsumi *et al.* 2004). The transformation of focal complexes into focal adhesions is dependent upon the activation of Rho, a small GTPase, and its downstream target, Rho-associated kinase (ROCK) (Matthews *et al.* 2006). ROCK aids focal adhesion formation and increases cell contractility (Matthews *et al.* 2006). The Rho/ROCK pathway leads to actin cytoskeletal reorganisation, which facilitates myofibroblast differentiation and collagen synthesis (Ni *et al.* 2013). Fittingly, ROCK inhibitors have been suggested as promising anti-fibrotic agents in models of cardiac fibrosis *in vivo* (Li *et al.* 2012).

1.5.1.3 Talin

The adaptor protein talin can form a connection between integrins and the cytoskeleton upon mechanical stimulation (Critchley 2009). Talin-deficient mice displayed lessened pressure overload-induced cardiac fibrosis and improved cardiac function; this was linked to reduced MAPK signalling (Manso *et al.* 2013). Talin has also been reported to sense substrate stiffness; a rigid matrix caused talin to stimulate focal adhesion formation and nuclear translocation of Yes-associated protein (YAP) (Elosegui-Artola *et al.* 2017). The transcription factors, YAP and transcriptional coactivator with PDZ-binding motif (TAZ), have been discovered to be vital in mechanosensing. Mechanical inputs trigger nuclear translocation of the YAP/TAZ complex where it regulates gene expression (Dupont *et al.* 2011). Jin *et al.* (2018) demonstrated that inhibition of the YAP signalling pathway contributed to improved cardiac function in mice with dilated cardiomyopathy, in part due to a reduction in myofibroblast differentiation.

1.5.2 Syndecan-4

The syndecans are a family of four transmembrane proteins which each consist of an extracellular polysaccharide glycosaminoglycan chain that binds molecules in the ECM (Couchman 2010). Syndecan-4 has been reported to play a role in mechanotransduction (Bellin *et al.* 2009). Mice deficient in syndecan-4 expressed

reduced collagen I and III and markers of myofibroblast differentiation following aortic banding-evoked pressure overload (Herum *et al.* 2013). There is a lack of knowledge on how syndecan-4 transduces mechanical stress into intracellular signals but Herum *et al.* (2013) found that, upon cyclic stretch, the calcineurin/nuclear factor of activated T-cell (NFAT) pathway was activated in a syndecan-4-dependent manner in murine cardiac fibroblasts.

1.5.3 Angiotensin II receptor type 1

The Angiotensin II receptor type 1 (AT_1) receptor is a well-established G-protein coupled receptor (GPCR) proven to have substantial importance in the development of cardiac hypertrophy (Yasuda *et al.* 2008). Angiotensin II (Ang II) is known to act through the AT_1 receptor to induce collagen production and secretion from cardiac fibroblasts (Lijnen, Petrov and Fagard 2001). In addition, Yasuda *et al.* (2008) determined that mechanical stress could induce cardiac hypertrophy *in vivo* through the AT_1 receptor in mice deficient in angiotensinogen. It has been stated that the AT_1 receptor can be activated by mechanical stretch in cardiac fibroblasts in the absence of G-protein activation, through the scaffolding protein β-arrestin-2; this couples to activation of the c-Jun N-terminal kinase (JNK) signalling cascade (Dostal, Glaser and Baudino 2015). This has been suggested to be due to mechanical stretch triggering an AT_1 receptor-mediated conformational change in β-arrestin (Rakesh *et al.* 2010). Cardiac hypertrophy can also be induced by the activation of other GPCRs, such as the receptors for endothelin 1 and adrenoceptors; however, it has been reported that mechanical stretch does not induce activation in cells overexpressing these receptors so this effect appears to be specific to only some GPCRs (Yasuda *et al.* 2008).

1.5.4 Tenascin C

As previously discussed, TNC is an ECM glycoprotein, rather than being present in the plasma membrane, but has also been reported to be directly modulated by mechanical stress. Following MI, TNC is localised at the border zone between the intact and infarcted lesion; this is where the majority of tissue remodelling takes place and is a region that must withstand strong mechanical stress

(Imanaka-Yoshida *et al.* 2001). Correlating with this, inducing aortic stiffness and hypertension in mice with a deficiency in TNC evoked acute aortic dissection (Kimura *et al.* 2014). TNC expression was amplified in chick embryo fibroblasts subjected to cyclic strain within 3-6 h (Chiquet, Sarasa-Renedo and Tunç-Civelek 2004); this was independent of protein synthesis (i.e. a transcription factor) or any paracrine factor but found to be dependent on Rho/ROCK signalling factors (Chiquet, Sarasa-Renedo and Tunç-Civelek 2004). TNC has been shown to interfere with the action of fibronectin (Chiquet-Ehrismann *et al.* 1988). It has been speculated that, under high mechanical load, this is required to loosen matrix adhesion contacts and prevent overstretching (Chiquet *et al.* 2009).

1.5.5 Protein kinases

Integrins associate with or activate numerous non-receptor protein tyrosine kinases (PTKs) in response to tension; it is believed this triggers much of their downstream signalling (Schlaepfer and Hunter 1998; Seong *et al.* 2013). These include focal adhesion kinase (FAK), Src-family kinases (SFKs) and MAPKs. It has been demonstrated that FAK promotes cyclic stretch-induced, integrin-mediated proliferation and differentiation of cardiac fibroblasts (Dalla Costa *et al.* 2009) and FAK knockdown reduced fibrosis in response to chronic pressure overload in mice (Clemente *et al.* 2007). Integrins have been shown to play a vital role in mechanical stress-induced p38 MAPK activation and cardiac hypertrophy, through a FAK-Src-Ras pathway in the myocardium (Aikawa *et al.* 2002).

1.5.5.1 Src-family kinases

The SFKs are a group of membrane-associated intracellular proteins (Blk, Fgr, Fyn, Hck, Lck, Lyn, Src, and Yes) which act as important signalling mediators, playing key roles in cell morphology, motility, proliferation, and survival (Roskoski 2004). All SFKs have a C-terminal domain preceded by Src 2 and 3 homology domains (SH2 and SH3, respectively), a membrane-anchoring SH4 N-terminal region and a unique domain (a short sequence which varies between the family members) (Amata, Maffei and Pons 2014).

SFKs are regulated by phosphorylation which, at certain sites, induces activation, and at other sites initiates inhibition, due to the generation of a closed inactive conformation (Roskoski 2005). For example, phosphorylation of Y527 in c-Src, the prototype of the family, leads to an interaction between the phospho-residue and the SH2 domain, causing inactivity; dephosphorylation of phospho-Y527 by phosphatases permits opening of the structure and subsequent phosphorylation and activation (Anguita and Villalobo 2017). Activated SFKs can then modulate other proteins; Src and Fyn have been demonstrated to enable the activation of Rho GTPases in response to tension (Guilluy *et al.* 2011; Herum *et al.* 2017b).

1.5.5.2 p38 mitogen-activated protein kinases

The MAPKs are a family of kinases which participate in essential cell functions, such as gene regulation, proliferation, differentiation and mobility (Krishna and Narang 2008). p38 MAPKs are one of the four classical MAPK signalling cascades, the others being the extracellular signal-regulated kinases (ERK1/2), c-Jun N-terminal kinases (JNK1-3) and ERK5 (Figure 1.3) Stimulation of these cascades leads to sequential phosphorylation events; a MAP kinase kinase kinase (MAPKKK) phosphorylates a MAP kinase kinase (MAPKK) on specific serine/threonine residues and this subsequently triggers dual phosphorylation of the MAPK on specific threonine and tyrosine residues, as shown in Figure 1.3. Activated MAPKs influence cell function by phosphorylating downstream substrates or activating downstream kinases.

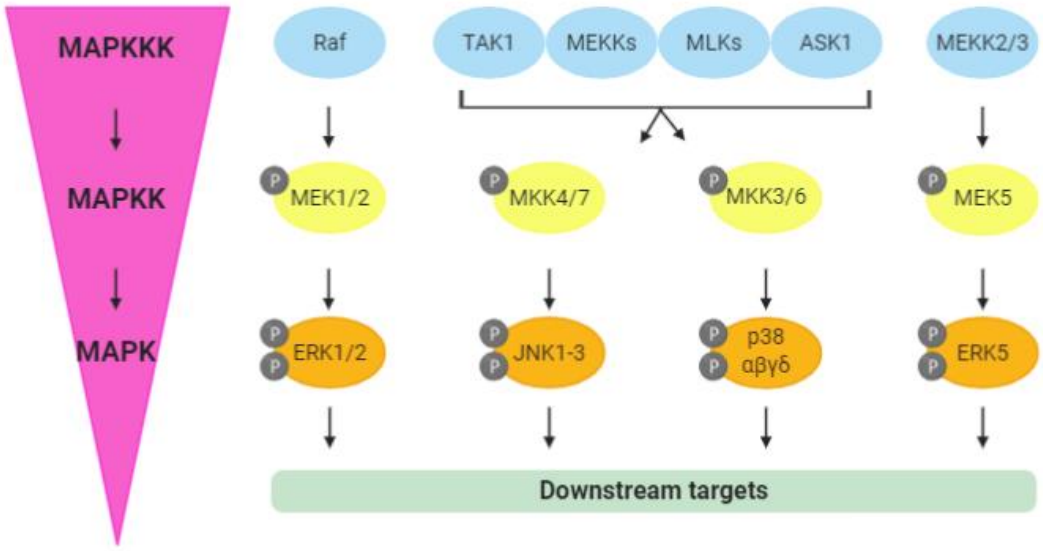

Figure 1.3 Canonical MAPK signalling. Schematic simplified representation of the classical MAP kinase (MAPK) pathways. These comprise a cascade of three kinases which phosphorylate (denoted by P) and activate each other consecutively. Mitogens, cytokines, and cellular stresses stimulate the MAPK pathways. MAPKs subsequently phosphorylate downstream substrates in the nucleus (e.g., transcription factors), cytosol, cytoskeleton, mitochondria and plasma membrane to affect cellular function. MAPK: Mitogen-activated protein kinase; MAPKK: Mitogen-activated protein kinase kinase; MAPKKK: Mitogen-activated protein kinase kinase kinase. Image taken from Turner and Blythe (2019).

The JNKs and p38 MAPKs are together termed stress-activated protein kinases (SAPKs) due to factors such as stresses and inflammation (e.g. ultraviolet light, oxidant stress, osmotic shock, infection and cytokines) triggering their activation (Kyriakis and Avruch 2001). These kinases are capable of regulating cell death, differentiation and inflammatory responses (Kyriakis and Avruch 2001). There are several upstream kinases capable of initiating the p38 phosphorylation cascade, including the MAPKKKs, TAK1, MEKK1-4, MLK3 and ASK1, and the MAPKKs, MKK3/6 (Figure 1.3). The p38 MAPK family is comprised of four isoforms, p38α/β/γ and δ; p38α and β are approximately 70% identical and p38γ and δ also show structural similarity. The α isoform is the most well-established of the four

and, unlike the other family members which demonstrate variances in expression between tissues and cell types, is ubiquitously expressed (Turner and Blythe 2019). It is known that the phosphorylation of transcription factors triggered by p38 MAPK activation can induce the reprogramming of cardiac gene expression (Heineke and Molkentin 2006). p38 can regulate both gene and protein expression via several mechanisms, including modulation of chromatin structure, transcription, mRNA stability and translation (de Nadal and Posas 2010; Turner and Blythe 2019). The MAPK-activated protein kinase, MK2, is reported to be important for regulation of mRNA stability (Turner and Blythe 2019).

MAPK signalling, as previously discussed, has been implicated in stimulating cardiac hypertrophy and fibrosis (Molkentin *et al.* 2017; Bageghni *et al.* 2018). This tallies with reports that the MAPK signalling cascade is initiated by stretch (Sugden and Clerk 1998). Cyclic mechanical load for 10-20 min has been revealed to activate the p38 MAPK signalling pathway, in addition to the JNK and ERK pathways, in foetal rat cardiac fibroblasts; p38 and ERK1/2 activation were found to be important for the regulation of collagen I expression following cyclic stress (Papakrivopoulou *et al.* 2004). The p38 pathway has been reported to be central for the induction of IL-6 secretion, a key molecule through which cardiac fibroblasts can modulate cardiomyocyte hypertrophy (Meléndez *et al.* 2010). p38 activation has been demonstrated to occur in response to various factors upregulated in cardiac remodelling, such as α and β-adrenergic receptor agonists, interleukin-1 (IL-1), interleukin-33 (IL-33), tumour necrosis factor (TNF)-α, Ang II and adenosine (Perez, Papay and Shi 2009; Bageghni *et al.* 2018; Turner 2011; Zhu and Carver 2012).

1.5.6 Ion channels

In addition to integrins, syndecans and the AT1 receptor, another method of cell surface mechanotransduction is via the passage of current through mechanosensitive ion channels (Figure 1.4) . Mechanical forces applied to the cell membrane have been revealed to induce calcium ion (Ca^{2+}) influx across the plasma membrane in cardiac fibroblasts (Kiseleva *et al.* 1996); this influx of Ca^{2+} ions into the cell leads to downstream signalling and changes in cardiac fibroblast function in normal physiology and disease states (Castella *et al.* 2010; Reed, Kohl

and Peyronnet 2014). In the next section, cellular Ca^{2+} handing mechanisms will be discussed, with a particular emphasis on mechanically-activated ion channels.

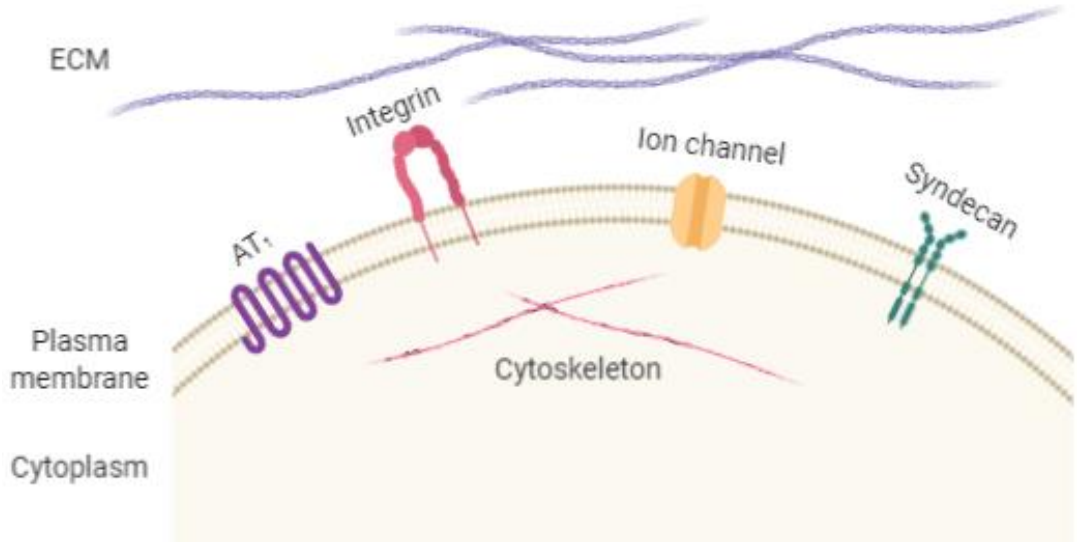

Figure 1.4 Cardiac fibroblast mechanotransduction at the plasma membrane. Simplified schematic of proteins participating in mechanotransduction at the plasma membrane of the cardiac fibroblast. These include: angiotensin II receptor type 1 (AT_1), integrins, ion channels and syndecans.

1.6 Ca^{2+} handling mechanisms

The cytosolic free calcium ion (Ca^{2+}_i) operates as a highly versatile second messenger in virtually all types of eukaryotic cells. Ca^{2+}_i regulates an extensive array of cellular processes including excitation-contraction coupling, gene transcription, cell growth, differentiation and apoptosis (Berridge, Lipp and Bootman 2000). In cardiac fibroblasts, intracellular Ca^{2+} is known to control various functions including ECM synthesis and cell proliferation (Zhang *et al.* 2014) and is a feature of many intracellular signalling pathways (Chen et al., 2010). However, Ca^{2+} signals in cardiac fibroblasts are not as well characterised as those in cardiac myocytes (Bers and Guo 2005).

Prolonged cytoplasmic Ca^{2+} overload can lead to cell death, and irregular Ca^{2+} signalling is defined as a key element of numerous diseases (Clapham 1995). It

has become apparent that abnormalities in calcium transport and signalling are associated with both cardiac hypertrophy and heart failure (Bers, Eisner and Valdivia 2003; Cartwright *et al.* 2011; Ritter and Neyses 2003). Therefore, mechanisms by which cells control cytosolic Ca^{2+} levels are carefully regulated. The standard intracellular Ca^{2+} concentration is 100 nM; this is 20,000-fold lower than the concentration found extracellularly (Clapham 1995). It is ion channels located within cell membranes which are depended upon to regulate Ca^{2+} ions in a controlled manner (Kondratskyi *et al.* 2015). An overview of the mechanisms involved in Ca^{2+} handling is illustrated in Figure 1.5.

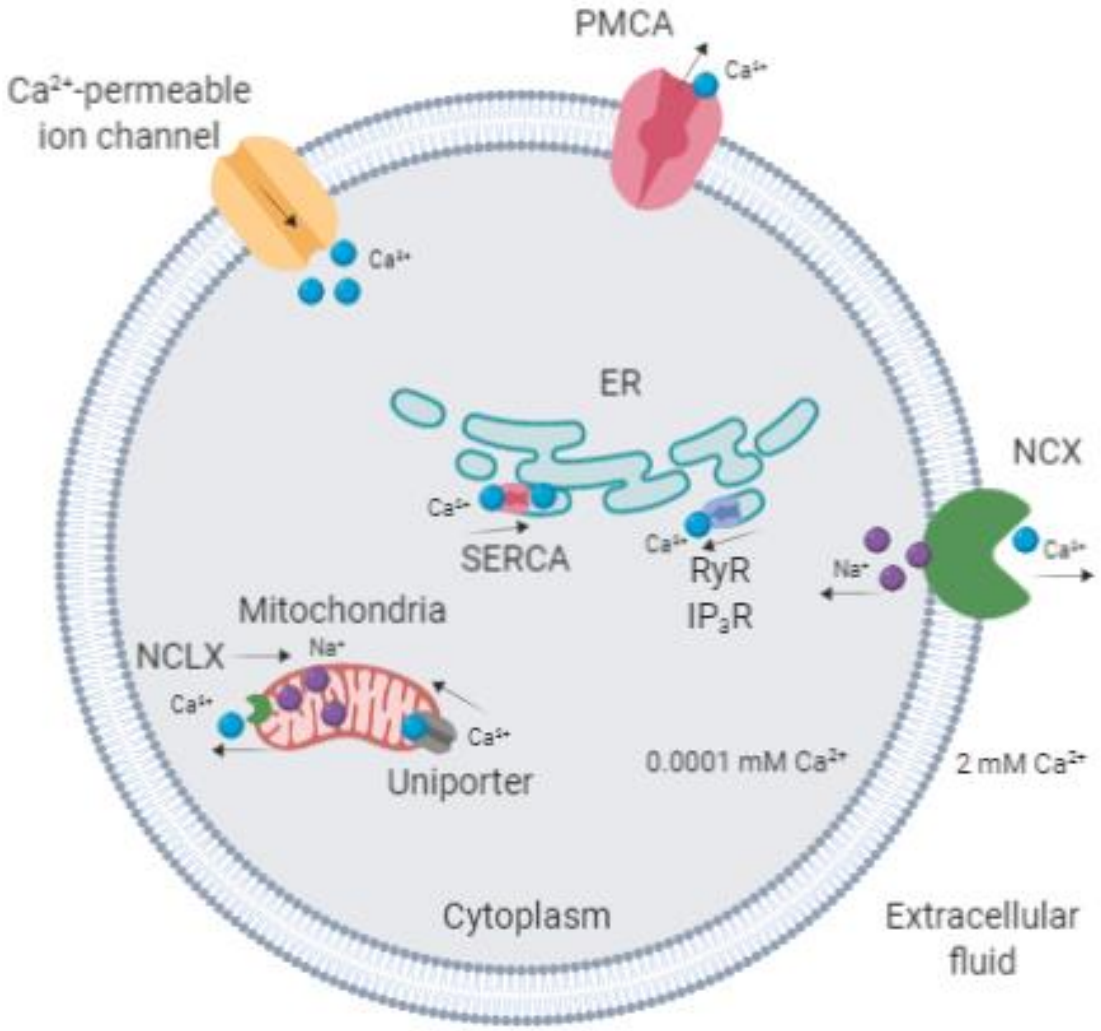

Figure 1.5 Overview of cellular Ca^{2+} handling. The intracellular Ca^{2+} concentration is carefully maintained by various membrane pumps and exchangers; these ensure a 20,000 fold gradient is kept constant. Ca^{2+} can enter the cell through Ca^{2+}-permeable ion channels in response to particular stimuli and is able to leave the cell through exchangers (Na^+/Ca^{2+} exchanger; NCX) and pumps (Plasma membrane Ca^{2+} ATPase; PMCA). Inside the cell, the majority of Ca^{2+} is stored in the endoplasmic reticulum (ER) where it is released through inositol-1,4,5-trisphosphate receptors (IP_3R) and ryanodine receptors (RyR) and recycled via the sarcoplasmic reticulum Ca^{2+} ATPase (SERCA) extrusion pump. Mitochondrial Ca^{2+} homeostasis is accomplished through Ca^{2+} uniporters and mitochondrial Na^+/Ca^{2+} exchangers (NCLX).

1.6.1 Ca^{2+} extrusion

Pumps and exchangers present in the plasma membrane and endoplasmic reticulum membrane are responsible for the extrusion of Ca^{2+} from the cytosol to achieve Ca^{2+} homeostasis. The Na^{+}/Ca^{2+} Exchanger (NCX) is located in the plasma membrane, exists in three isoforms (NCX1-3) and predominantly exports one Ca^{2+} ion for the uptake of three Na^{+} ions (Hilge 2012). This exchanger uses the electrochemical gradient of Na^{+} and has a high capacity for Ca^{2+} which enables the transport of many Ca^{2+} ions at a fast rate (Clapham 2007). The plasma membrane Ca^{2+}-ATPase (PMCA) pumps are high-affinity Ca^{2+} extruders, binding a single intracellular Ca^{2+} ion which is deposited to the extracellular space following conformational changes; this occurs in conjunction with the import of protons (Stafford *et al.* 2017). There are four known PMCA isoforms (PMCA1-4) (Strehler and Zacharias 2001). Notably, total PMCA4 knockout (KO) specifically from cardiac fibroblasts protected mice against pressure overload-induced cardiac hypertrophy by regulating Ca^{2+} signalling (Mohamed *et al.* 2016). The related ATPase of the sarco(endo)plasmic reticulum (SERCA), which has 3 isoforms, instead pumps Ca^{2+} from the cytosol into the endoplasmic reticulum (ER). It has a higher capacity for Ca^{2+} clearance than PMCA, removing two Ca^{2+} ions per ATP molecule hydrolysed (Stafford *et al.* 2017). RT-PCR analysis revealed NCX3, PMCA1,3,4 and SERCA1-3 were detected in human cardiac fibroblasts (Chen *et al.* 2010). Mitochondria also accumulate significant amounts of Ca^{2+} from the cytosol (Kirichok, Krapivinsky and Clapham 2004). The balance is mainly achieved by Ca^{2+} influx through the mitochondrial Ca^{2+} uniporter and efflux by the mitochondrial version of the Na^{+}/Ca^{2+} exchanger (NCLX) (Boyman *et al.* 2013).

1.6.2 Ca^{2+} release from stores

Intracellular Ca^{2+}-release channels on the sarcoplasmic reticulum of striated muscle (ryanodine receptors, RyRs) and on the endoplasmic reticulum of virtually all cell types (inositol 1,4,5-trisphosphate receptors, IP_3Rs) play crucial roles in Ca^{2+}-mediated signalling (Marks 1997). Three isoforms of RyR have been characterised (1-3) with RyR2 being expressed predominantly in cardiac muscle. RyR2 is activated during excitation-contraction coupling by Ca^{2+} influx via the

dihydropyridine receptor, a phenomenon referred to as Ca^{2+}-induced Ca^{2+} release (Marks 1997). IP_3R function is regulated by a classic second messenger cellular signalling pathway mediated by inositol 1,4,5-trisphosphate (IP_3), generated primarily by phospholipase C (PLC) metabolism of phosphoinositol-4,5-bisphosphate (PIP_2), in response to the stimulation of GPCRs by extracellular agonists (Santulli *et al.* 2017). This results in Ca^{2+} release from the ER. Chen *et al.* (2010) detected IP_3R1-3 mRNA expression, but not that of RyR, in human cardiac fibroblasts.

1.6.3 Ca^{2+} entry

Ion channels are transmembrane proteins which permit the passage of ions in response to a stimulus. There are two important properties which distinguish ion channels from simple aqueous pores. Firstly, they show ion selectivity, permitting only certain ions to pass; some ion channels are selective to specific ions whereas others discriminate ions only by charge. The second distinction is that ion channels are not continuously open, they are gated. The most common stimuli known to cause the opening of ion channels are: a change in voltage across the membrane (voltage-gated channels), the binding of a ligand (ligand-gated channels) and mechanical stress (mechanically-activated channels). Ion channels are extremely efficient; up to 100 million ions can pass through one open channel each second, a rate 10^5 times higher than the fastest rate of transport mediated by any known carrier protein (Alberts 2002). However, channels are not coupled to an energy source so are only able to mediate passive movement of ions down their electrochemical gradients across the lipid bilayer.

Voltage-gated Ca^{2+} channels are activated upon membrane potential changes and are able to transduce this into intracellular Ca^{2+} transients which orchestrate many physiological events in excitable cells (Catterall 2011). These events include rapid contraction in skeletal muscle cells, secretion of hormones in endocrine cells and initiation of synaptic transmission in neurons (Catterall 2011). The channels have been classified into three subfamilies named Cav1 (L-type), Cav2 and Cav3 (T-type) (Ertel *et al.* 2000). Despite the detection of mRNA expression of L-type and T-type Ca^{2+} channels in neonatal rat cardiac fibroblasts, their significance in fibroblast function is not clear (Ross and Jahangir 2016).

Ligand-gated ion channels are directly activated by the binding of an agonist to their extracellular domain and are sometimes referred to as ionotropic receptors; P2X receptors are examples of ligand-gated Ca^{2+} channels and their particular agonist is ATP (Mahaut-Smith, Taylor and Evans 2016). Chen *et al.* (2012) found that ATP activation of P2X receptors leads to proliferation and migration of human cardiac fibroblasts.

Store-operated Ca^{2+} entry (SOCE) is another Ca^{2+} influx mechanism in non-excitable cells, including fibroblasts. Orai proteins have been identified as store-operated channels and stromal interaction molecule 1 (STIM1) proteins as ER Ca^{2+} sensors in SOCE. Depletion of Ca^{2+} from the ER causes STIM to cluster at ER-plasma membrane junctions where it is able to activate Orai channels to allow Ca^{2+} entry into the cytosol. ER Ca^{2+} stores are refilled via SERCA. RT-PCR analysis has revealed expression of STIM1 and Orai1-3 in human cardiac fibroblasts (Chen *et al.* 2010). Human ventricular fibroblasts from patients with heart failure secrete increased collagen in comparison with those from non-failing hearts; this was shown to be related to an increase in Ca^{2+} entry via SOCE and enhanced expression of Orai1 (Ross *et al.* 2017). Another study unravelled SOCE as a key modulator in Ang II-induced cardiac fibrosis (Zhang *et al.* 2016).

1.7 Mechanically-activated ion channels

Detecting and responding to mechanical stimuli is an obligatory part of any living system. The plasma membrane is a target of external mechanical stimuli and mechanically-activated ion channels play a vital role in the physiology of mechanotransduction (Martinac 2004). They detect and transduce external mechanical cues into electrical and/or chemical intracellular signals in a diverse range of cell types. Mechanically-activated ion channels are implicated in a myriad of physiological processes, for example touch and pain sensation, hearing, blood pressure control and cell volume regulation (Hamill and Martinac 2001).

1.7.1 Selective cation stretch-activated channels

Kim (1993) first described whole-cell potassium-selective stretch-activated channel currents in cardiac cells. These channels are outwardly rectifying and lead to potassium exit from the cytoplasm. Two-pore domain potassium (K2P) channels have been revealed to be expressed in human cardiac tissue (Schmidt *et al.* 2017) and involved in cardiac arrhythmogenesis (Gurney and Manoury 2008). One of these, TWIK-related potassium channel (TREK)-1 is activated by numerous stimuli including pH, temperature, fatty acids, anaesthetics, membrane deformation or stretch (Patel and Honoré 2001). TREK-1 contributes to the 'leak' potassium conductance in cardiomyocytes which aids normal repolarisation (Goonetilleke and Quayle 2012). While cardiomyocyte-specific deletion of TREK-1 in mice resulted in cardiac dysfunction in response to pressure overload, TREK-1 deletion in fibroblasts prevented deterioration in cardiac function (Abraham *et al.* 2018). The authors confirmed this was associated with diminished cardiac fibrosis and reduced activation of JNK in cardiomyocytes and fibroblasts.

Although conventionally considered to be ligand-gated, Van Wagoner and Lamorgese (1994) obtained single-channel inside-out patch clamp recordings from neonatal rat atrial myocytes which demonstrated that patch pipette negative pressure increased K_{ATP} channel sensitivity. In normal metabolic conditions, K_{ATP} channels are inactivated. If ATP levels fall, K_{ATP} open probability increases. In the presence of stretch, this increase occurs at less reduced ATP levels (Peyronnet, Nerbonne and Kohl 2016). Stretch-preconditioning has been reported to reduce ischaemia-reperfusion injury but this is abolished when K_{ATP} channels are blocked (Kristiansen *et al.* 2005). Benamer *et al.* (2013) reported that MI in rats induced expression of functional K_{ATP} channels in scar and border zone cardiac fibroblasts.

The mechanosensitivity of voltage-gated sodium channels has been reported in heterologous expression studies (Beyder *et al.* 2010) and they are stated to be expressed in cultured ventricular fibroblasts (Li *et al.* 2009). Chatelier *et al.* (2012) showed that human atrial myofibroblasts display a fast inward voltage-gated sodium current, whereas no current was detectable in non-differentiated fibroblasts. Quantitative RT-PCR revealed 4-fold expression of the $Na_V1.5$ α-subunit in myofibroblasts when compared to fibroblasts, indicating that sodium current may be important in the fibrogenesis cascade.

1.7.2 Non-selective cation stretch-activated channels

Transient receptor potential (TRP) channels are a large superfamily consisting of 28 members which can be classified into 6 subfamilies according to sequence homology: TRPC (canonical), TRPV (vanilloid), TRPM (melastatin), TRPP (polycystin), TRPML (mucolipin) and TRPA (ankyrin). The proteins are Ca^{2+}-permeable non-selective cation channels that detect a wide variety of environmental stimuli. Stimuli range from vision to taste, smell, touch, hearing, proprioception and thermosensation (Liu and Montell 2015). Several of the channels have also been demonstrated to be involved in mechanosensation; TRPC6 and TRPV4 have been implicated in osmosensing (Wilson and Dryer 2014; Feetham *et al.* 2015). It has been reported that TRPC1/3/4/5/6/7 are all involved in cardiac hypertrophy but most of the studies demonstrate the involvement of TRPC channels in Ca^{2+} signalling in cardiomyocytes (Eder and Molkentin 2011; Nishida and Kurose 2008; Satoh *et al.* 2007). More recent studies have focussed on cardiac fibroblast TRP channels and imply that TRP channels may serve as a potential therapeutic target for cardiac fibrosis. Numerous TRP channels are highly expressed in cardiac fibroblasts from various sources; these are primarily TRPs from the TRPC (1-7), TRPV (2/4) and TRPM (6/7) subfamilies (Yue *et al.* 2013). Harada *et al.* (2012) demonstrated that TRPC3 expression was upregulated in atria from patients with atrial fibrillation (AF), goats with electrically maintained AF and dogs with tachypacing-induced heart failure. They found that TRPC3 channels in canine atrial fibroblasts were responsible for cardiac fibroblast proliferation and differentiation, through controlling Ca^{2+} influx that subsequently activates ERK signalling. TRPC6 has been proposed to promote TGF-β1- and Ang II-induced myofibroblast differentiation which aided wound healing in mice (Davis *et al.* 2012). In addition, Adapala *et al.* (2013) discovered that TRPV4 was important for TGFβ1-induced differentiation in rat cardiac fibroblasts *in vitro*; this effect was dependent on ECM stiffness. Although these TRP channels have been suggested to be mechanically-activated, there is ambiguity as to whether these channels sense force and act as primary transducers, or whether they have an indirect, supporting role as part of a downstream signalling pathway (Christensen and Corey 2007).

Peyronnet, Nerbonne and Kohl (2016) stated in a review on cardiac mechanically-activated ion channels that the two main molecular candidates for

non-selective cation stretch-activated channels were TRP channels and Piezo channels. Piezo proteins are a more recent discovery in this field (Coste *et al.* 2010) and their identification has significantly expanded understanding of mammalian, mechanically-activated currents and their functions. This family of proteins will be discussed in more depth below.

1.8 The Piezo family

Molecules responsible for many mechanically-activated cation channel activities remained elusive until 2010, when a novel family of ion channels was identified. Using RNA interference, Coste *et al.* (2010) discovered that Piezo1 (encoded for by the *Fam38a* gene) was responsible for a rapidly-activating current initiated in response to pressure stimulation in a mouse neuroblastoma cell line. The channel was named Piezo1 based on the Greek word for pressure, 'πίεση'. Piezo1 and Piezo2 (encoded by *Fam38b*) make up the Piezo family (Coste *et al.* 2010). Both proteins assemble to form functional channels which independently confer mechanically-activated non-selective cationic current (Coste *et al.* 2010). Piezo1 expression was observed to be highest in bladder, colon, kidney, lung and skin whereas strong expression of Piezo2 was revealed in bladder, lung and dorsal root ganglion sensory neurons (Coste *et al.* 2010). This correlates with more recent data published disclosing the role of Piezo2 in somatosensory mechanotransduction; the channel has been revealed to be important for light touch, pain and proprioception (Woo *et al.* 2014; Woo *et al.* 2015; Dubin *et al.* 2012).

1.8.1 Structure and activation of Piezo1

Mouse Piezo1 heterologously expressed in HEK-293 cells and purified was able to mediate mechanosensitive cationic currents when reconstituted into lipid bilayers (Coste *et al.* 2012; Syeda *et al.* 2016). This confirmed its ability to form an intrinsically mechanosensitive channel, without a requirement for other cofactors. Gnanasambandam *et al.* (2015) discovered that Piezo1 is permeable to monovalent ions (K^+, Na^+, Cs^+, Li^+) and most divalent ions (Ba^{2+}, Ca^{2+} and

Mg^{2+}, not to Mn^{2+}). Therefore, Piezo1 is a non-selective cation channel; however, Coste *et al.* (2010) suggested that Piezo1 displays a slight preference for Ca^{2+}.

The Piezo proteins were revealed not to possess sequence homology with any known class of ion channels (Zhao *et al.* 2016b). Piezo1 is a relatively large protein estimated to be 286 kDa in humans and 292 kDa in mouse (Soattin *et al.* 2016). Initial structural analysis suggested that Piezo1 formed a tetramer (Coste *et al.* 2012) but, in recent years, cryo-electron microscopy has enabled the full-length structure (2547 amino acids) of mouse Piezo1 to be resolved at a resolution of 4.8A˚ and this revealed the protein formed a trimeric propeller-like structure (Ge *et al.* 2015). Coste *et al.* (2012) first ascertained Piezo1 to be a multipass transmembrane protein and the protein is now suggested to possess an unprecedented 38 transmembrane domains, meaning a total of 114 transmembrane helices are present in the trimeric channel complex (Zhao *et al.* 2018).

Zhao *et al.* (2018) confirmed the findings of Ge *et al.* (2015) that mouse Piezo1 possesses a three-bladed, propeller-shaped architecture comprising of a central cap, three peripheral blades and three long intracellular beams (Figure 1.6). It is hypothesised that Piezo1 may use its peripheral blade regions to detect mechanical force (Ge *et al.* 2015). This was validated by the use of whole-cell electrophysiology on mutated and chimeric Piezo1 channels, which revealed the N-terminal blade structures are important for sensing force and mechanical activation, whereas the C-terminal cap region is important for efficient ion conduction and cation selectivity (Zhao *et al.* 2016b). Zhao *et al.* (2018) proposed that Piezo1 utilises its curved blades and long beams as a pivot to form a lever-like apparatus. The lever-like mechanism may enable Piezo1 channels to create a slight opening of the central pore, allowing cation-selective permeation.

In vitro, Piezo1 is able to respond to differing forms of mechanical stimulation including poking, suction, stretch, cell swelling and flow-induced shear stress (Coste *et al.* 2010; Li *et al.* 2014; Ranade *et al.* 2014; Miyamoto *et al.* 2014; Gudipaty *et al.* 2017). Membrane tension has also been shown to activate the channel (Cox *et al.* 2016; Lewis and Grandl 2015).

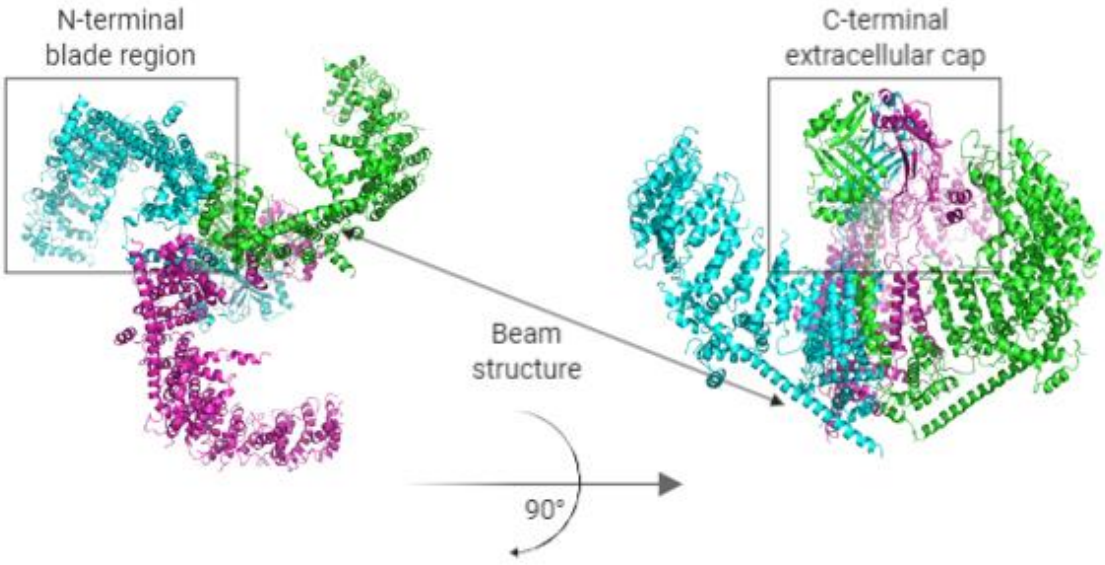

Figure 1.6 Cryogenic electron microscopy structure of the Piezo1 trimer. Intracellular view of the structure of the Piezo1 trimer, the three Piezo1 subunits are illustrated in different colours. On the right is the image rotated 90° to present the beam, blade and extracellular structures. Image adapted from Zhao *et al.* (2018).

1.8.2 Modulation of Piezo1 activity

1.8.2.1 Piezo1 activators

Syeda *et al.* (2015) developed a high-throughput screen in which over 3 million compounds were assessed for their ability to activate Piezo1 and Piezo2 in transfected HEK-293 cells using Ca^{2+} imaging. They identified and characterised a synthetic small molecule, Yoda1, which was able to activate human and mouse Piezo1 channels to cause Ca^{2+} influx, with no effect on Piezo2 channels.

Lipid bilayer experiments suggested that Yoda1 does not require other proteins or specific lipid domains to activate Piezo1, indicating that Yoda1 is acting directly on the channel or through alterations in membrane tension or curvature. Lacroix, Botello-Smith and Luo (2018) engineered chimeras of mouse Piezo1 and its Yoda1-insensitive paralog Piezo2 and identified a minimal region in Piezo1 located between the blade and pore (residues 1961-2063) required for Yoda1 sensitivity. The group suggest that the C-terminal part of this region has an important role in mediating the effects of Yoda1. Syeda *et al.* (2015) proposed

that Yoda1 stabilises the open state of Piezo1, rather than destabilising the closed state; this would explain why Yoda1 increases the sensitivity and slows inactivation kinetics of mechanically-induced responses. Prominent Yoda1-dependent calcium responses are also seen in the absence of externally applied forces. Yoda1 is the first known agonist of Piezo1 and has already been instrumental in facilitating studies aimed at clarifying the gating mechanism of Piezo1 and exploring its functional roles in various biological processes, without the need for mechanical stimulation. Yoda1 causes Ca^{2+} influx and subsequent dehydration of red blood cells (RBCs) in a similar manner to mechanical stretch (Cahalan *et al.* 2015). The compound can also mimic shear stress by activating endothelial nitric oxide synthase (eNOS) in human umbilical artery endothelial cells (HUAECs) and causing relaxation of murine mesenteric arteries (Wang *et al.* 2016). One disadvantage is that Yoda1 displays poor aqueous solubility above 20-30 μM (Syeda *et al.* 2015); therefore, improved agonists of the Piezo1 channel are necessary for any future translational research.

A subsequent high-throughput screen identified a set of two alternative chemical activators of Piezo1, named Jedi1 and Jedi2; both compounds specifically elicit concentration-dependent Ca^{2+} responses in cells transfected with mouse Piezo1, but not with mouse Piezo2 (Wang *et al.* 2018). Jedi was shown to activate Piezo1 through the extracellular side of the blade and activation required key mechanotransduction components, including two extracellular loops in the distal blade and two leucine residues in the proximal end of the beam (Wang *et al.* 2018).

1.8.2.2 Piezo1 inhibitors

Current antagonists of the Piezo1 channel, such as ruthenium red and gadolinium, are generic inhibitors of many cationic mechanically-activated currents (Coste *et al.* 2010). Ruthenium red has been revealed to act via the extracellular side of the channel, perhaps directly blocking the pore (Coste *et al.* 2012). A peptide toxin isolated from the venom of the Chilean rose tarantula spider, Grammostola spatulata mechanotoxin 4 (GsMTx4), has been shown to inhibit Piezo1 responses (Bae, Sachs and Gottlieb 2011) but also inhibits a range of endogenous cationic mechanosensitive channels (Suchyna *et al.* 2000).

GsMTx4 inhibits the channel only when applied from the extracellular side (Bae, Sachs and Gottlieb 2011) and is believed to function indirectly through interactions with plasma membrane lipids (Suchyna *et al.* 2004).

Our group at the University of Leeds generated analogues of Yoda1 using synthetic chemistry and tested them against the Piezo1 channel, with the aim of developing improved Piezo1 modulators and increasing knowledge on the structure-activity relationship for Yoda1 activation of Piezo1 (Evans *et al.* 2018). This led to the identification of Dooku1, an inhibitor of Yoda1-induced Piezo1 channel activity that blocks Yoda1-induced relaxation of aorta (Evans *et al.* 2018). Dooku1 only has activity against Yoda1-induced, rather than constitutive, Piezo1 channel activity, suggesting the compound may compete with Yoda1 or act allosterically at another site to reduce the binding or efficacy of Yoda1 (Evans *et al.* 2018). The discovery of a small molecule specific inhibitor of constitutive Piezo1 activity would be invaluable for future studies.

1.8.3 Expression and functional roles of Piezo1

Since the discovery of the Piezo1 channel as a molecular carrier of a mechanically-activated current in 2010, there has been a surge of activity to study this ion channel. Over the past 10 years, ground-breaking research has identified that Piezo1 is important for sensing pressure in numerous tissues throughout the body.

1.8.3.1 Cardiovascular functions

The physiological force of shear stress is vital for vascular development and function; Piezo1 has been verified as a direct sensor of shear stress (Li *et al.* 2014; Ranade *et al.* 2014). Li *et al.* (2014) found that global Piezo1 KO results in embryonic lethality in mice at day E9.5-11.5; growth retardation and less prominent vasculature in the yolk sac was observed in these animals, compared to wild-type (WT) animals. Endothelial-specific Piezo1 KO caused similar vascular defects during development, whereas heterozygote Piezo1 KO mice had no major phenotype. *In vitro*, the diminution of Piezo1 supressed tube formation and attenuated the migration of human umbilical vein endothelial cells (HUVECs) towards vascular endothelial growth factor (VEGF), a key stimulant of angiogenesis. Piezo1$^{-/-}$ embryonic endothelial cells had reduced shear stress-

evoked Ca^{2+} entry and showed directionless alignment, whereas endothelial cells isolated from $Piezo^{+/+}$ littermates exhibited cell alignment in the direction of blood flow. This study highlights the role of Piezo1 in vascular function.

Rode *et al.* (2017) addressed the role of Piezo1 in the adult vasculature, this required conditional disruption in mature mice. The group found that the channel was important for elevation of blood pressure during whole body physical activity by redistributing blood flow. Mice with conditional endothelial KO of Piezo1 had no obvious phenotype until performing exercise, when they displayed an attenuated increase in blood pressure in the mesenteric artery, compared to WT mice. Investigation into the mechanism revealed that Piezo1 opposed the relaxation mechanism, endothelium-dependent hyperpolarisation (EDH). Piezo1 channels depolarise endothelial cells, this then depolarises adjacent vascular smooth muscle cells, triggering contraction and thus vasoconstriction. During exercise, mesenteric arteries constrict to allow the redistribution of blood flow to skeletal muscles. Mice lacking endothelial Piezo1 had compromised physical performance, thought to be due to their inability to advantageously redistribute blood flow from the gut to skeletal muscles upon physical exercise. Wang et al. (2016) found that mice with induced endothelium-specific deletion of Piezo1 lost the ability to form nitric oxide and therefore induce vasodilation in response to flow and consequently mice developed hypertension.

Retailleau *et al.* (2015) established that smooth muscle Piezo1 plays a key role in the structural remodelling of resistance arteries upon Ang II-induced hypertension or when mechanoprotection was removed due to the deletion of filamin A, the actin crosslinking element which exerts a tonic repression on the opening of stretch-activated channels (Kainulainen *et al.* 2002). Deletion of smooth muscle filamin A stimulated Piezo1 opening; its increased activity induced structural remodelling of small-diameter arteries, even in the absence of hypertension. When Piezo1 was also deleted, hypertension-induced remodelling of caudal arteries was eradicated, suggesting that Piezo1 plays a role in the remodelling of vascular smooth muscle cells during hypertension.

1.8.3.2 Non-cardiovascular functions

McHugh *et al.* (2010) were the first to discover a functional role of the still uncharacterised *FAM38A* gene; they showed that siRNA knockdown of *FAM38A* in epithelial cells inactivates endogenous β1 integrin, reducing cell adhesion. Two years later, the same group demonstrated that knockdown of Piezo1 increased cell migration in lung epithelial cells and, as Piezo1 expression was depleted in small cell lung cancer lines, proposed that the loss of Piezo1 expression may cause increased cell migration and metastasis in lung tumours (McHugh *et al.* 2012). Data from Yang *et al.* (2014) differed; they demonstrated that the knockdown of Piezo1 attenuated cell mobility of gastric cancer cells. Contrasting roles for Piezo1 may imply that Piezo1 mediates differential signalling pathways in specialised cells.

Piezo1 has been associated with RBC volume homeostasis (Cahalan *et al.* 2015). When Yoda1 was used to activate Piezo1, Ca^{2+} influx was triggered which led to activation of a Ca^{2+}-activated K^+ channel; this activation caused osmotic loss of water and subsequent dehydration of RBCs. As expected, RBCs from blood cell-specific Piezo1 conditional KO mice were overhydrated and exhibited increased fragility (Cahalan *et al.* 2015).

Murine urothelial cells exhibited a Piezo1-dependent increase in cytosolic Ca^{2+} concentrations in response to mechanical stretch, which led to ATP release (Miyamoto *et al.* 2014). GsMTx4 inhibited the stretch-induced Ca^{2+} influx and subsequent ATP release in urothelial cells, suggesting a role for Piezo1 in sensing extension of the bladder urothelium. Piezo1 has been revealed to influence urinary concentration following dehydration or fasting, correlating with its prominent expression in the inner medulla (Martins *et al.* 2016). Urinary dilution and the decrease in urea concentration following rehydration are both significantly delayed in the absence of Piezo1 in collecting duct epithelial cells of adult mice, indicating that Piezo1 plays a functional role in the regulation of urinary osmolarity.

Romac *et al.* (2018) applied high pressure to pancreatic acinar cells using buffered saline solution, causing pancreatitis. GsMTx4 and acinar cell-specific genetic deletion of Piezo1 protected mice against pressure-induced pancreatitis, indicating a potential role for Piezo1 in pancreatitis development following abdominal trauma or pancreatic duct obstruction. Consistent with Piezo1

promoting pancreatitis, Yoda1 application into the pancreatic duct also induced pancreatitis (Romac *et al.* 2018).

1.8.4 Piezo1 in human disease

1.8.4.1 Dehydrated hereditary stomatocytosis

Mutations in the Piezo1 channel have been associated with an autosomal dominant hereditary haemolytic anaemia named dehydrated hereditary stomatocytosis (DHS), which is also referred to as hereditary xerocytosis (Albuisson *et al.* 2013; Andolfo *et al.* 2013; Zarychanski *et al.* 2012); the M2225R mutation was one of the first mutations discovered to be responsible for this disease (Zarychanski *et al.* 2012). The group confirmed that 3 members of the same family were homozygous for this particular mutation. The mutation caused an imbalance in intracellular cation concentrations which led to defective RBC membrane properties. Patients suffer from severe haemolytic anaemia with reticulocytosis, shortened RBC survival, stomatocytosis, hyperbilirubinemia and markedly altered erythrocyte sodium and potassium levels. This was the first report of human disease associated with a mutation in a mammalian mechanosensory transduction ion channel. Those investigating the properties of the mutated channel found that the DHS-associated mutation was a gain-of-function mutation which caused Piezo1 to exhibit delayed inactivation kinetics i.e. the channel remained open for longer, leading to increased Ca^{2+} influx (Albuisson *et al.* 2013; Bae *et al.* 2013).

Ma *et al.* (2018) engineered a mouse model of DHS and revealed that Plasmodium infection failed to cause cerebral malaria in these mice due to the action of Piezo1 in RBCs and T cells. The group subsequently found that a novel human gain-of-function PIEZO1 allele, E756del, was present in a third of the African population. The RBCs of patients were dehydrated and exhibited attenuated Plasmodium infection *in vitro*, suggesting this particular gain-of-function mutation is associated with malaria resistance.

1.8.4.2 Lymphatic dysplasia

Lymphatic endothelial cells are known to regulate the frequency and strength of lymphatic contraction in response to shear stress; intracellular Ca^{2+} is an important factor regulating lymphatic contraction (Jafarnejad *et al.* 2015). Failure of the lymphatic system to effectively drain interstitial fluid back to the blood results in lymphoedema. Loss-of-function mutations in Piezo1 have been associated with generalised lymphatic dysplasia, an autosomal recessive disease (Fotiou *et al.* 2015; Lukacs *et al.* 2015). Generalised lymphatic dysplasia is a rare form of primary lymphoedema affecting the whole body. High-throughput sequencing of a family with congenital lymphatic dysplasia identified heterozygosity for a splicing variant and a missense variant in Piezo1 (Lukacs *et al.* 2015). RBCs from affected individuals revealed severely diminished Piezo1 responses in response to Yoda1 and mechanical stimuli. The authors suggested that decreased function of the mutated Piezo1 may be due to reduced channel abundance in the plasma membrane.

1.8.4.3 Bicuspid aortic valve

Piezo1 has also been revealed to participate in cardiac development. It was found to be required for outflow tract and aortic valve development in zebrafish (Faucherre *et al.* 2019). Mechanical forces generated during the cardiac cycle were found to activate Piezo1 which initiates nitric oxide release in the outflow tract. Bicuspid aortic valve is a common congenital heart defect with increased prevalence of aortic dilatation and dissection (Giusti *et al.* 2017). Faucherre *et al.* (2019) followed up their results and investigated a cohort of bicuspid aortic valve patients; they found that novel variants of Piezo1 were detected in 3 probands; these were subsequently revealed to lead to inhibition of normal Piezo1 mechanosensory activity.

1.8.5 Piezo1 in the heart

Messenger RNA expression profiles of Piezo1 in various adult mouse tissues revealed its expression in the murine heart, whereas Piezo2 mRNA was barely detectable (Coste *et al.* 2010). Piezo1 has been demonstrated to be upregulated

following MI; expression was regulated by the Ang II-AT_1 receptor-ERK1/2 signalling pathway in neonatal rat ventricular myocytes (Liang *et al.* 2017), whereas Piezo1 was shown to be downregulated in a human cardiomyocyte cell line subjected to mechanical stretch (Wong *et al.* 2018). However, there are currently no reports on the role of Piezo1 in cardiac fibroblasts. Piezo1 is important for converting mechanical signals into changes in cell function, such as migration and differentiation (McHugh *et al.* 2012; Pathak *et al.* 2014). Mechanical stress is a mediator of the differentiation of cardiac fibroblasts into myofibroblasts and of cardiac hypertrophy (Wang *et al.* 2003; Ruwhof and van der Laarse 2000), which can both cause cardiac remodelling. It is possible that the mechanosensitive ion channel Piezo1 plays a role in transducing mechanical stress into cellular changes in cardiac fibroblasts. Unravelling specific roles of Piezo1 in cardiac fibroblasts may further our understanding of adverse cardiac remodelling and provide the foundation for the development of novel therapeutics to help patients suffering from heart failure.

1.9 Summary

Cardiac fibroblasts execute a wide array of physiological functions and are additionally implicated in numerous pathological circumstances, such as cardiac hypertrophy and fibrosis. A governing factor affecting fibroblast function during disease is mechanical stress. The molecular mechanisms by which cardiac fibroblasts sense mechanical stress remain largely elusive but mechanically-activated ion channels have been suggested to be important. The ability of Yoda1 to activate the mechanosensitive cation channel, Piezo1, without the need for mechanical stimulation has enabled a more practical and targeted approach to investigate Piezo1 channel functions. Recent reports of the importance of Piezo1 in the cardiovascular system and the fact that Piezo1 mutations have been implicated in human disease raises further interest regarding this channel in other cell types. Increased understanding of Piezo1 channel function may be beneficial in the quest to unravel the intricate mechanisms underlying cardiac fibroblast signalling in order to develop effective therapies for the treatment of diseases involving cardiac remodelling. Interventions targeting this pathologic remodelling would inevitably lead to significant advancements in the treatment of heart failure.

1.10 Aims and objectives

Overall aim

The overall aim of the project was to characterise Piezo1 expression, activity, function and downstream signalling pathways in cardiac fibroblasts *in vitro* and to determine the functional relevance of fibroblast Piezo1 in the normal and mechanically stressed heart *in vivo*.

Hypothesis

Piezo1 is important for detecting mechanical stress in cardiac fibroblasts, and activation of Piezo1 affects cardiac fibroblast function.

Objectives

1. To detect the expression of Piezo1 in murine and human cardiac fibroblasts.

2. To determine the effect of Yoda1 on intracellular Ca^{2+} entry levels in cardiac fibroblasts expressing endogenous Piezo1.

3. To use pharmacological tools and genetic methods to modulate Piezo1 expression in cardiac fibroblasts to examine whether Yoda1-induced Ca^{2+} entry is dependent on Piezo1.

4. To investigate the effects of Piezo1 activation on gene expression in cardiac fibroblasts using chemical and mechanical stimulation.

5. To characterise the downstream signalling pathways modulated by Piezo1 activation in cardiac fibroblasts.

6. To generate and validate a conditional fibroblast-specific Piezo1 KO mouse model.

7. To determine the functional relevance of Piezo1 in cardiac fibroblasts under pathological conditions.

Chapter 2 Materials and Methods

2.1 Chemicals and Reagents

Reagent	Solubility	Storage	Working conc	Vendor
Yoda1 analogues (2e, 2i, 2j, 2k (Dooku1), 159)	DMSO	-20°C, 10 mM	0.01-10 µM	Synthesised by the University of Leeds
11R-VIVIT		-20°C, 1 mM	10 µM	Merck
Adenosine triphosphate (ATP)	H_2O	-20°C, 20 mM	5-20 µM	Sigma-Aldrich
Fura-2 AM	DMSO	-20°C, 1 mM	2 µM	Invitrogen
Gadolinium	H_2O	r.t., 100 mM	10 µM	Sigma-Aldrich
Recombinant Human Interleukin 1α (IL1-α)	2% BSA in PBS	-20°C, 1 µg/mL	10 ng/mL	Invitrogen
KN-93	DMSO	-20°C, 10 mM	10 µM	Sigma-Aldrich
LY294002 hydrochloride				
Pluronic acid F-127		r.t., 10%	0.01%	
PD98059		-20°C , 18.7 mM	30 µM	Merck
PP1		-20°C, 10 mM	10 µM	Cayman Chemical
Probenecid	NaOH	r.t., made fresh	2.5 mM	Sigma-Aldrich
Ruthenium Red	H_2O	r.t., 30 mM	30 µM	
SB203580	DMSO	-20°C, 10 mM	10 µM	Merck
SP600125				Cambridge Bioscience
Staurosporine (SSP)		-20°C, 1 mM	1 µM	Sigma-Aldrich
Transforming growth factor (TGF)-β1	4 mM HCl & 1 mg/ml BSA in PBS	-20°C, 20 µg/mL	10 ng/mL	R&D Systems
Vascular endothelial growth factor (VEGF)	H_2O	-20°C, 30 µg/mL	30 ng/mL	Sigma-Aldrich
Yoda1	DMSO	-20°C, 10 mM	0.01-10 µM	Tocris

Table 2.1 Table of reagents. List of chemicals and reagents used throughout this thesis alongside their solvent/storage conditions and vendor.

Yoda1 analogues

Analogues of Yoda1 used in this study were synthesised by Kevin Cuthbertson in the School of Chemistry at The University of Leeds. All synthesised chemicals were purified by column chromatography or trituration and determined as >97% pure by 1H NMR (proton nuclear magnetic resonance) and 13C NMR (carbon-13 nuclear magnetic resonance). These were prepared as stock solutions of 10mM in dimethyl sulfoxide (DMSO) and used at a final concentration of 0.01-10 µM. 2e was utilised as a negative control throughout the study, 2k/Dooku1 as a Yoda1 antagonist and compound 159 as a potential Piezo1 agonist. The structure of Yoda1 and its analogues are displayed in Figure 3.15 and Figure 3.25. The screening of Yoda1 analogues was carried out alongside Elizabeth Evans.

Ionic solutions

Standard Bath Solution (SBS), mM: NaCl 134, KCl 5, $MgCl_2$ 1.2, $CaCl_2$ 1.5, HEPES 10, D-Glucose 8; pH was titrated to 7.4 with NaOH. Ca^{2+}-free SBS was prepared by omitting $CaCl_2$ and addition of 0.4 mM EGTA.

Phosphate Buffered Saline (PBS), mM: KCl 2.68, KH_2PO_4 1.47, NaCl 136.89 and Na_2HPO_4-$7H_2O$ 8.06.

2.2 Cell culture

2.2.1 Mouse cell isolation and culture

2.2.1.1 Mouse cardiac fibroblast culture

Adult C57BL/6J mice were euthanised according to guidelines of The UK Animals (Scientific Procedures) Act 1986. Hearts were extracted and digested in 1.5 mg/mL collagenase solution (Worthington) at 37°C for 90 min, with occasional agitation. The supernatant was collected, washed and resuspended in Dulbecco's Modified Eagle's medium (DMEM) with high glucose, pyruvate, no glutamine (#21969035, Invitrogen) supplemented with 10% foetal bovine serum (FBS) (Biosera), 1% L-glutamine (Gibco) and 1% penicillin/streptomycin (Sigma-Aldrich) and plated in a 25 cm^3 tissue culture flask for 30 min, which allowed for preferential attachment of fibroblasts. Non-adherent cells were removed and

medium was changed. The next day, cells were washed and medium replaced; cells were grown until confluence was reached and subsequently passaged. Cells were studied at passages 1-2 to minimise phenotypic changes induced by prolonged culturing. Cells were kept in serum-free DMEM for 16 h prior to treatment in order to collect RNA, lysates and conditioned media.

2.2.1.2 Mouse pulmonary endothelial cell culture

$CD146^+$ pulmonary endothelial cells (PECs) from WT mice were isolated with immunomagnetic microbeads (Miltenyi) and cultured in MV2 medium (Promocell), supplemented with 10% FBS and 1% penicillin/streptomycin. Cells were studied at passage 1. These cells were obtained by Dr Katy Paradine; RNA was extracted and qRT-PCR used to quantify *Piezo1* mRNA expression.

2.2.1.3 Mouse cardiomyocyte isolation

Adult mouse cardiomyocytes (CM) were isolated from ventricles of 8 week old WT mice. Hearts were cannulated through the aorta and perfused with perfusion buffer (124.5 mM NaCl, 10 mM HEPES, 11.1 mM glucose, 1.2 mM NaH_2PO_4, 1.2 mM $MgSO_4$, 4mM KCl, 25 mM Taurine; pH 7.34) containing 10 mM butanedione monoxime for 5 min followed by perfusion buffer containing 1 mg/mL type 2 collagenase, 0.05 mg/mL protease and 12.5 μM $CaCl_2$ for 7-15 min until suitable digestion was observed. Ventricles were gently cut in perfusion solution containing 10% FBS and 12.5 μM $CaCl_2$ and filtered. This step was repeated in perfusion solution containing 5% FBS and 12.5 μM $CaCl_2$ and, finally, perfusion solution containing only 12.5 μM $CaCl_2$. The filtrate was pelleted by gravity for 5 min before resuspension in perfusion buffer containing 0.5 mM $CaCl_2$. This step was repeated with increasing concentrations of $CaCl_2$ (1.5 mM, 3.5 mM, 8 mM and 18 mM). Finally, the cell pellet was resuspended in 1 ml Trizol. These cells were obtained from David Eisner's group at The University of Manchester by Elizabeth Evans; RNA was extracted and qRT-PCR used to quantify *Piezo1* mRNA expression.

2.2.1.4 Cardiac cell fractionation

Non-myocyte cardiac cell fractions were prepared as described previously (Bageghni et al, 2018). Briefly, collagenase-digested mouse heart tissue was filtered through a 30 µm MACS smart strainer (Miltenyi) to remove cardiomyocytes. Non-myocytes were then separated into two fractions using a cardiac fibroblast magnetic antibody cell separation kit, according to the manufacturer's instructions (MACS; Miltenyi). 'Non-fibroblasts' (endothelial cells and leukocytes which were *Pecam1*-positive) were collected in fraction 1 and 'fibroblasts' (*Col1a1*/*Col1a2*/*Ddr2*/*Pdgfra*-positive) were collected in fraction 2, as previously characterised (Bageghni *et al.* 2018). RNA was extracted and qRT-PCR used to quantify specific cellular markers and *Piezo1* mRNA expression in the different fractions.

2.2.2 Human cell culture

2.2.2.1 Human cardiac fibroblasts

Biopsies of human atrial appendage were obtained from patients undergoing elective coronary artery bypass grafting at the Leeds General Infirmary. Biopsies from patients were obtained following local ethical committee approval (reference 01/040) and informed patient consent. Cardiac fibroblasts were harvested, cultured and characterised as described previously (Turner *et al.* 2003). Cells were taken from liquid nitrogen storage and maintained in DMEM, supplemented with 10% FBS, 1% L-glutamine and 1% penicillin/streptomycin. Experiments were performed on human cardiac fibroblasts from passages 2-5. Serum-free DMEM was used for 1 h prior to treatments and subsequent collection of RNA, lysates and conditioned media.

2.2.2.2 Human saphenous vein endothelial cells (SVECs)

Samples of undistended saphenous vein were collected from patients undergoing coronary artery bypass grafting at the Leeds General Infirmary. Local ethical committee approval (reference CA01/040) and informed patient consent were obtained. SVECs were isolated as has been described previously (Bauer *et al.* 2010) and aliquots frozen in liquid nitrogen for long term storage. Cells were taken

from liquid nitrogen storage and maintained in Endothelial Cell Basal Medium (EGM™-2, Lonza), supplemented with 2% FBS and the following growth factors supplied as a bullet kit (EGM™-2 SingleQuots™ Kit, Lonza): 10 ng/mL VEGF, 5 ng/mL human basic fibroblast growth factor, 1 µg/ml hydrocortisone, 50 ng/ml gentamicin, 50 ng/ml amphotericin B, 10 µg/ml heparin and 10 µg/ml ascorbic acid. Experiments were performed on human SVECs from passages 3-7.

2.2.2.3 Human umbilical vein endothelial cells

HUVECs from pooled donors were purchased from Lonza and cultured in EGM™-2 medium, supplemented as described above for SVECs. Cells were utilised at passage 2-3.

2.2.3 HEK-293 cell culture

All HEK-293 cells were maintained in DMEM supplemented with 10% FBS and 1% penicillin/streptomycin. Non-transfected HEK T-Rex™-293 cells were used as control cells.

2.2.3.1 HEK-T-REx-hPiezo1 cells

Cells which overexpress human Piezo1 upon induction with tetracycline were created by Dr Baptiste Rode as described in Rode *et al.* (2017) using HEK T-REx™-293 cells (Invitrogen). To induce expression, cells were incubated with 1 µg/mL tetracycline (Sigma) for 24 h prior to experiments. qRT-PCR and western blotting were used to validate the cell line.

2.2.3.2 HEK-T-REx-mPiezo1 cells

Cells which overexpress mouse Piezo1 were created by Dr Melanie Ludlow. pcDNA3_mouse Piezo1_IRES_GFP, a kind gift from Ardem Patapoutian (Coste *et al.* 2010), was used as a template to clone the mouse Piezo1 coding sequence into pcDNA4/TO. Overlapping mouse Piezo1 (Fwd: GTAACAACTCCGCCCCATTG, Rev: GCTTCTACTCCCTCTCACGTGTC) and pcDNA4/TO (Fwd: GACACGTGAGAGGGAGTAGAAGCCGCTGATCAGCCTC-GACTG, Rev: CAATGGGGCGGAGTTGTTAC) PCR products were assembled

using Gibson Assembly (New England Biolabs) (Gibson *et al.* 2009). This construct does not contain tetracycline operator sequences. HEK T-REx™-293 cells were transfected with pcDNA4/TO-mPiezo1 using Lipofectamine 2000 (Invitrogen) and treated with 200 µg/mL zeocin (InvivoGen) to select for stably transfected cells. Individual clones were isolated and analysed for expression using intracellular Ca^{2+} measurements and Yoda1.

All cells were maintained in a humidified incubator with 5% CO_2, 95% air at 37°C. Once cells reached 90% confluence, cells were washed with PBS and passaged into cell culture flasks or seeded into tissue culture plates using Trypsin-EDTA (Gibco), or Detachin (Genlantis) for HUVECs, at 37°C for 5 min.

2.3 Intracellular Ca^{2+} measurements

Changes in intracellular Ca^{2+} (Ca^{2+}_i) concentration upon agonist-evoked channel activation were measured using Fura-2 (Invitrogen) and the FlexStationII^{384} fluorescence plate reader (Molecular Devices).

2.3.1 Fura-2 acetoxymethyl ester (Fura-2 AM)

Fura-2 AM is a high affinity, ratiometric intracellular Ca^{2+} indicator dye which permits the measurement of intracellular Ca^{2+} concentration (Ca^{2+}_i). Ratiometric dyes allow for the accurate measurement of intracellular Ca^{2+} concentrations whilst minimising the effects of unequal dye loading, unequal cell number and leakage, therefore leading to more reproducible results (Grynkiewicz, Poenie and Tsien 1985). The acetoxymethyl ester (AM) form is membrane permeable and once inside the cell, the AM group is cleaved by non-specific esterases to produce the charged and active form (Fura-2) which is able to bind Ca^{2+} with high affinity. Fura-2 is excited at 340 nm and 380 nm and has an emission wavelength of 510 nm; the excitation spectra is shown in Figure 2.1. Once bound to Ca^{2+}, there is a spectral shift in Fura-2 absorption which is proportional to the intracellular concentration of Ca^{2+}, increasing emission from excitation at 340 nm and decreasing emission from excitation at 380 nm. A change in intracellular Ca^{2+} concentration (ΔCa^{2+}_i) causes a change in the ratio (ΔF340/380). An increase in this ratio indicates an increase in intracellular Ca^{2+}.

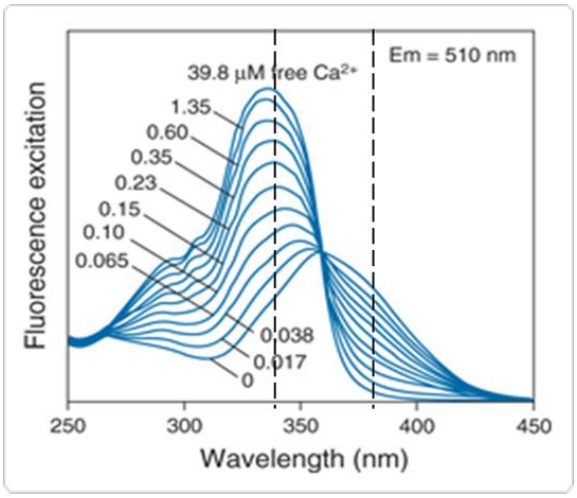

Figure 2.1 Fluorescence excitation spectra of Fura-2. The fluorescence excitation spectra of Fura-2 in various free calcium concentrations. An increase in intracellular Ca^{2+} causes the Fura-2 fluorescence emission intensity at 510 nm to increase at excitation wavelength 340 nm and decrease at 380 nm. The two excitation wavelengths are indicated on the image. Image adapted from Life Technologies.

2.3.2 High throughput Ca^{2+} measurements using the FlexStation III^{384}

Intracellular Ca^{2+} measurements were made using the FlexStationIII^{384}, a bench-top high-throughput fluorescence plate reader that can be utilised for kinetic fluorescence experiments using either a 96 or 384 well-based assay. The automated device has 3 drawers which are able to hold the tips, the assay plate and the compound plate. A built-in 8-head dispenser is programmed to add compounds from the compound plate into the assay plate containing cells. SOFTmax PRO 4.7.1 software (Molecular Devices) is able to select the desired excitation wavelengths (340 nm and 380 nm), the emission wavelength (510 nm), the time course of the experiment and amount of compound addition. Experiments were performed at r.t. (21 ± 2°C).

2.3.3 Experimental Protocol

HEK T-REx™-293 were seeded onto Bio-One™ CELLCOAT™ Poly-D-Lysine coated 96-well plates (Grenier); the poly-D-lysine improved adherence of HEK

cells throughout the assay. A seeding density of 50,000 cells per well was used for HEK cells. Cardiac fibroblasts and HUVECs were seeded onto clear non-coated 96 well plates (Corning) at a seeding density of 20,000 and 25,000 cells per well, respectively. All cells were grown to confluence overnight at 37°C in a 5% CO_2 incubator.

On the day of experimentation, cells were incubated for 1 h at 37°C in 1.5 mM Ca^{2+} SBS containing 2 µM Fura-2 AM and 0.01% pluronic acid. Pluronic acid is a mild detergent that has been found to facilitate the solubilisation of water-insoluble dyes. During all Fura-2 assays involving cardiac fibroblasts, probenecid (Sigma-Aldrich) was present throughout all stages of the experiment; this is an inhibitor of non-specific plasma membrane anion transport and is used to reduce leakage of Fura-2 AM. It was freshly prepared in 1 M NaOH and diluted to a final concentration of 2.5 mM. After 1 h, cells were washed with 1.5 mM Ca^{2+} SBS and incubated for 30 min at r.t. prior to recordings to allow for de-esterification of Fura-2 AM. During this time, if applicable, inhibitors were added. These steps were performed with all solutions and cells protected from light.

After the wash or pre-incubation stage, the assay plate, compound plate and FlexStation tips were loaded into the FlexStation. The FlexStation transferred solution from the compound plate into the assay plate wells, at a 1:2 dilution. For experiments involving the addition of a compound to the assay plate where there was no prior incubation with the compound, the compound was prepared at 2x the desired final concentration so that the further 1:2 dilution ensured the compound was the desired concentration. For pre-incubation, the drug was added to the compound plate at 1x to maintain its concentration. Baseline fluorescence ratios were recorded at 60 seconds; these were subtracted from values taken at the peak Ca^{2+} entry. Recordings were taken every 5 seconds for a total of 150 or 300 seconds. 'Zero baseline' traces are displayed in figures when baseline Ca^{2+} levels remain consistent. The DMSO concentration was kept constant throughout the experiment (< 0.1%).

2.3.4 Hypotonic assay

Following loading with Fura-2 AM, cells were kept in SBS for 30 min at r.t. If an inhibitor was utilised, it was present during this 30 min. The compound plate

contained solutions of varying hypotonicity. Na^+ was replaced in the SBS with N-methyl-D-glucamine chloride (NMDG-Cl) (Sigma) to allow us to control the osmolarity of the solution. 135 mM NMDG-Cl was used as an isotonic control and NMDG-Cl was used at decreasing concentrations (135-55 mM), with solutions becoming increasingly hypotonic. More hypotonic solutions induce increasing movement of water into the cells by osmosis, causing cell swelling and increased membrane tension, this was done in an attempt to activate the Piezo1 channel. This assay was developed by Dr Melanie Ludlow.

2.4 Transfection with small interfering RNA (siRNA)

2.4.1 Murine cardiac fibroblasts

The knockdown of Piezo1 was conducted using small interfering RNA (siRNA). These double stranded sequences of mRNA are complementary to the gene of interest (Piezo1). The siRNA transfection results in inhibition of mRNA which therefore reduces the expression of the target protein. Murine cardiac fibroblasts were grown to 80% confluence. A final concentration of 10 nM Piezo1-specific Silencer Select Pre-Designed siRNA (#4390771, siRNA ID: s107968, Ambion, Life Technologies) or Silencer Select Negative Control No. 1 siRNA (#4390843, Ambion, Life Technologies) was added to 250 µL OptiMEM (Gibco) with 7.5 µL Lipofectamine RNAiMAX Reagent (Life Technologies) in OptiMEM (Gibco), as per the manufacturer's instructions. This was incubated at r.t. for 20 min and then added to one well of a 6-well plate holding 2.25 mL 0.4 % FBS-containing DMEM (without antibiotics). Medium was replaced with full-growth DMEM 24 h later and cells were used for experimentation after 48-72 h. The negative control was a non-targeting siRNA control with no significant homology to sequences in the human genome and was transfected into adjacent wells. During optimisation of murine Piezo1-specific siRNAs, cells were also transfected with 10 or 20 nM Piezo1-specific Smartpool siRNA (#L-061455-00-0005, Dharmacon) or negative control siRNA (#D-001810-10-05, Dharamcon), using 1.35% Lipofectamine 2000 in OptiMEM. However, siRNAs from Ambion were used throughout experimentation. Sequences of control and Piezo1-specific siRNAs can be found in Table 2.2.

2.4.2 Human cardiac fibroblasts

Human cardiac fibroblasts were grown to 90% confluence. 20 nM Piezo1-specific Silencer Select Pre-designed siRNA (#4392422, siRNA ID: s18891, Ambion) or ON-TARGETplus Non-targeting Pool siRNA (#001810, Dharmacon) was added to 200 µL Opti-MEM (Gibco) with 3 µL Lipofectamine 2000. This was incubated at r.t. for 20 min and then added to one well of a 6-well plate holding 800 µL 0.4% FBS-containing DMEM media (without antibiotics). Fresh full-growth DMEM media was added after 4.5 h and cells were used for experimentation 48-72 h after transfection. 20 nM Piezo2-specific Smartpool siRNA (Dharmacon cat. #L-013925-02-005) was also employed, alongside the control siRNA stated above, using the same protocol. Sequences of control and Piezo1/Piezo2-specific siRNAs can be found in Table 2.2.

Gene	Species	Control sequence (5' to 3')	Specific sequence (5' to 3')
Piezo1	Mouse (Dharmacon)	UGGUUUACAUGUCGACUAA UGGUUUACAUGUUGUGUGA UGGUUUACAUGUUUUCUGA UGGUUUACAUGUUUUCCUA	GAAAGAGAUGUCACCGCUA GCAUCAACUUCCAUCGCCA AAAGACAGAUGAAGCGCAU GGCAGGAUGCAGUGAAGCGA
Piezo1	Mouse (Ambion)	Proprietary information	CGUCAAAUACUGGAUCUAU
Piezo1	Human	UGGUUUACAUGUCGACUAA UGGUUUACAUGUUGUGUGA UGGUUUACAUGUUUUCUGA UGGUUUACAUGUUUUCCUA	GCCUCGUGGUCUACAAGAU
Piezo2			UCGAAAGAAUAUCGCUAAA UCGGAAAUAGCAACAGAUA GGAACUAAUUGCCCGUGAA CUAUGGUAUUAUGGGAUUA

Table 2.2 Sequences of control and siRNAs specific for Piezo1 and Piezo2. Small interfering RNAs with 4 sequences are Dharmacon ON-TARGET plus SMARTpool siRNAs with a pool of 4 siRNAs as a single reagent.

2.5 RNA isolation, cDNA preparation and real time quantitative polymerase chain reaction (RT-qPCR)

2.5.1 RNA isolation from cultured cells

To collect RNA from a fully confluent 6 well plate, media was removed, cells were washed with 1 mL PBS, applied with 250 µL trypsin and incubated for 5 min. It was confirmed that cells were detached and then 3 mL ice-cold PBS was applied to cells and transferred into a 15 mL falcon tube. This step was repeated and the falcon tube was centrifuged at 600 g for 6 min. The supernatant was discarded and the falcon tube was left upside down to air-dry. Pellets were stored at -80°C until RNA isolation.

All subsequent steps were performed in a designated RNA preparation area using dedicated pipettes, sterile filter tips and autoclaved plastics. RNA was isolated using the Aurum™ Total RNA Mini Kit (Bio-Rad), according to the manufacturer's instructions. Briefly, this involved utilising a stringent reagent composed of guanidine isothiocyanate and β-mercaptoethanol for efficient sample lysis, followed by purification on silica membrane in a spin-column format. A DNase digestion stage was used to remove any contaminating genomic DNA. At the final stage, RNA was eluted in 80 µL (6 well plate) or 60 µL (12 well plate) elution solution. RNA was quantified using the Nanodrop (ThermoScientific); RNA concentrations obtained were in the range of 20-100 ng/µl. The ratio of absorbance at 260 nm and 280 nm was used to assess RNA purity and a ratio of ~2.0 was generally accepted as pure; lower values indicate the presence of proteins that absorb strongly at or near 280 nm. The ratio at 260/230 was used as a secondary measure of nucleic acid purity; expected values were 2.0-2.2. Lower ratios indicated the presence of organic contaminants, such as phenol, which absorb at 230 nm. RNA was stored at -80°C until RT-PCR was carried out.

2.5.2 RNA isolation from whole heart tissue

RNA was isolated from whole heart using a phase-separation technique. The apex of the heart was lysed using 1 mL ice-cold TriZol (Sigma) in a 2 mL tube, with a 5mm stainless steel bead present (Qiagen). This was then homogenised using the TissueLyser II (Qiagen) at 26 Hz for 30 seconds; this stage was

performed 4 times to ensure thorough tissue lysing. The solution was transferred to a sterile 1.5 mL Eppendorf tube and 200 µL phenol-chloroform (Sigma-Aldrich) was added. The solution was shaken vigorously for 15 seconds and subsequently left for 2 min at r.t. before undergoing centrifugation (12,000g, 15 min, 4°C) to separate the phases – RNA in the superior aqueous layer, DNA at the interface and protein in the inferior organic phase. The RNA-containing phase was transferred to a new Eppendorf and RNA was precipitated with an equal volume of ice-cold isopropanol, inverted and incubated at r.t. for 10 min. The sample was then centrifuged (12,000g, 15 min, 4°C) to pellet the RNA, followed by a wash step with 75% ethanol. The sample was vortexed to wash the pellet, left for 5 min and then spun (12,000g, 5 min, 4°C). The pellet was resuspended in 75% ethanol once more and spun down a final time (12,000g, 5 min, 4°C). Ethanol was carefully removed and the pellet was air-dried for 5 min at r.t. RNA was dissolved in 30 µL nuclease-free water on ice and stored at -80°C.

2.5.3 qRT-PCR using TaqMan Gene Expression Assays

2.5.3.1 Reverse transcription

The reverse transcription stage is used to convert mRNA to cDNA prior to real-time PCR. 5 µL RNA was incubated at 70°C for 10 min and then left to cool on ice. cDNA was synthesised using the Reverse Transcription System (Promega) based on the manufacturer's instructions. Based on a total of 20 µL reaction mix, 2 µL RNA was added to a tube containing: 4 µL $MgCl_2$ (25 mM), 2 µL 10x reverse transcriptase buffer, 2 µL dNTP (10 mM), 1 µL random primers, 0.5 µL RNasin, 0.6 µL AMV reverse transcriptase and made up with 7.9 µL nuclease-free water. The solutions were mixed and centrifuged and cDNA was synthesised at 25°C for 10 min, 42°C for 15 min and then incubated at 95°C for 5 min to terminate the reaction in a T100™ Thermal Cycler (Bio-Rad). The cDNA was then used for real-time PCR application.

2.5.3.2 Quantitative reverse transcription polymerase chain reaction (qRT-PCR)

PCR relies on rounds of DNA synthesis (cycles) via the action of DNA polymerase and is used to exponentially amplify specific regions of DNA. A positive reaction in qRT-PCR is detected by a fluorescent signal. The Ct (cycle threshold) is the intersection between an amplification curve and a threshold line (this was set at 0.2) (Figure 2.2). This number of cycles is a relative measure of the concentration of target in the PCR reaction. Ct levels are inversely proportional to the amount of target in the sample, e.g. the lower the Ct value, the larger the amount of target nucleic acid in the sample.

A master mix was made ensuring a solution containing 10 µL Taqman Universal PCR Master Mix and 0.5 µL Taqman primer/probe sets (both Applied Biosytems), made up to 18 µL with nuclease-free water, could be added into each well of a 96-well semi-skirted with raised rim PCR plate (Starlab). After cDNA preparation, 2 µL of sample was added into each well containing Taqman Universal PCR Master Mix with primer/probe set. Subsequently, the plate was spun to ensure solution was collected at the bottom of the well.

qRT-PCR was performed in duplicate using an Applied Biosystems™ 7500 PCR System. DNA was amplified for 2 min at 50°C, 10 min at 95°C, followed by 50 amplification cycles (15 seconds at 95°C and 60 seconds at 60°C). Mouse and human primers utilised are shown in Table 2.3 and Table 2.4, respectively. The expression of the target in a sample is compared to that of a housekeeping gene, typically a constitutive gene which is uniformly expressed with low variance under both control and experimental conditions. Data are expressed as a percentage of housekeeping gene mRNA expression: mouse Gapdh (Mm99999915_g1) or human GAPDH (Hs99999905_m1), using the formula $2^{-\Delta Ct}$ x 100. When multiple housekeeping genes were utilised, the geometrical average of the reference gene Ct values were calculated (Vandesompele *et al.* 2002). Data were analysed using 7500 Software v2.3.

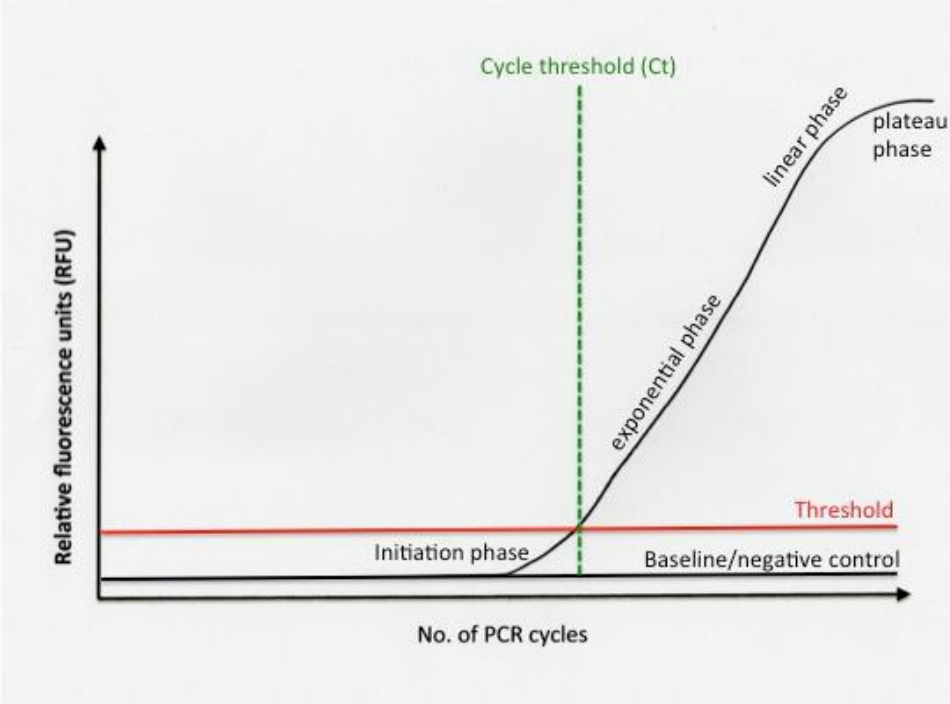

Figure 2.2 qRT-PCR amplification curve. An illustration of an amplification curve of a qRT-PCR reaction. The first few cycles represent the initiation phase, where the number of amplicons present is too low to produce a fluorescent signal. As the amount of fluorescence increases, the threshold line is exceeded; the number of cycles at this point is known as the cycle threshold (Ct). Image taken from Nordic BioSite.

Gene of interest	Protein	Primer code
Acta2	Alpha-smooth muscle actin	Mm00725412_s1
Actb	Beta-actin	Mm00607939_s1
Col1a1	Collagen 1	Mm01302043_g1
Col3a1	Collagen 3	Mm01254476_m1
Ddr2	Discoidin domain-containing receptor 2	Mm00445615_m1
Fam38a	Piezo1	Mm01241545_g1
Gapdh	Glyceraldehyde 3-phosphate dehydrogenase	Mm99999915_g1
Hprt	Hypoxanthine guanine phosphoribosyltransferase	Mm03024075_m1
Il1β	Interleukin-1β	Mm00434228_m1
Il6	Interleukin-6	Mm00446190_m1
Mmp3	Matrix metalloproteinase 3	Mm00440295_m1
Mmp9	Matrix metalloproteinase 9	Mm00442991_m1
Myh6	Alpha myosin heavy chain	Mm00440354_m1
Myh7	Beta myosin heavy chain	Mm01319006_g1
Nppa	Atrial natriuretic factor	Mm01255747_g1
Pdgfra	Platelet Derived Growth Factor Receptor Alpha	Mm00440701_m1
Pecam-1	Platelet And Endothelial Cell Adhesion Molecule 1	Mm01242584_m1
Postn	Periostin	Mm01284919_m1
Tgf-β1	Transforming growth factor beta1	Mm01178820_m1
Tnc	Tenascin-C	Mm00495662_m1

Table 2.3 Mouse primers used for qRT-PCR using Taqman primers. Table includes the catalogue numbers for mouse primers used to amplify genes of interest in qRT-PCR experiments; all are supplied by Applied Biosystems (Thermo Fisher Scientific).

Gene of interest	Protein	Primer code
FAM38A	Piezo1	Hs00207230_m1
GAPDH	Glyceraldehyde 3-phosphate dehydrogenase	Hs99999905_m1
IL6	Interleukin-6	Hs00174131_m1
TNC	Tenascin-C	Hs01115665_m1

Table 2.4 Human primers used for qRT-PCR using Taqman primers. Table includes the catalogue numbers for human primers used to amplify genes of interest in qRT-PCR experiments; all are supplied by Applied Biosystems.

2.5.4 qRT-PCR using SYBR™ Green

2.5.4.1 Reverse transcription

Reverse transcription of mRNA was performed using Superscript™ III Reverse Transcriptase (Invitrogen). Complementary DNA (cDNA) was synthesised by mixing 300 ng of RNA with 2 µL random primers (Promega), made up with nuclease-free water; this was heated for 7 min at 75ºC. Subsequently, the following were added to each sample: 4 µL 5x RT buffer, 0.5 µL M-MLV transcriptase, 1 µL dNTP, 0.5 µL RNase OUT™, 0.2 µL DTT (all Invitrogen) and nuclease-free water. Non-reverse transcribed (-RT) control solutions were prepared and tested in parallel. The solutions were mixed, centrifuged and incubated for 10 min at r.t., 1 h at 37°C followed by 5 min at 95°C. Complementary DNA was then used for qRT-PCR.

2.5.4.2 Quantitative reverse transcription polymerase chain reaction (qRT-PCR)

qRT-PCR was carried out using SYBR Green I (Bio-Rad) on a LightCycler (Roche). SYBR Green I binds to double stranded DNA and fluoresces when excited at 470 nm. The emission of light at 530 nm is significantly enhanced in the DNA bound, compared to the unbound, state. Each reaction contained the following: 5 µL of iTaq™ Universal SYBR® Green Supermix (containing antibody-mediated hot-start iTaq DNA polymerase, dNTPs, $MgCl_2$, SYBR® Green I dye,

enhancers and stabilizers), 0.75 µL of both forward and reverse primers (2 µM) and 2.5 µL nuclease-free water. This was made as a master mix and 9 µL was added into each well of a 96-well plate, before the addition of 1 µL cDNA. The plate was spun to ensure solution was collected at the bottom of the well. Primer sequences are displayed in Table 2.5. Reactions were run with a standard 2-step cycling program, 95 °C for 10 s and 60 °C for 40 s, for 40 cycles. The relative abundance of target genes amplified by RT-PCR were calculated relative to a housekeeping gene (*β-ACTIN/GAPDH*) using the $2^{-\Delta Ct}$ analysis method. Primer efficiencies were also tested; the efficiencies of primers for *Piezo1* and *Piezo2* are shown in Figure 3.4 as an example. Efficiencies were calculated by performing a serial dilution of RNA and calculating Ct values. Ct values were plotted and efficiencies calculated using the slope of the line. *Piezo1* and *Piezo2* primer efficiencies were 97 % and 83 %, respectively. As these were both over 80 %, they were judged to be accurate enough to be used for analysis. However, due to a 14 % difference in efficiency between the two primer sets, mean data of *Piezo1* and *Piezo2* mRNA expression relative to housekeeper were adjusted to take into account the respective efficiencies of the primer sets.

Gene of interest	Primer sequence (5' to 3')
Human *β-ACTIN*	Fwd: TCGAGCAAGAGATGGC Rv: CATCCAACGAAACTACCTTCA
Human *BLK*	Fwd: CTCTCAGGCTGGTCAGGAAA Rv: CAGAGCCTTCATCACGTTGG
Human *FGR*	Fwd: TGGCTTCCTTGATAGTGGCA Rv: CTGGGAATGCAGCCAGTTTT
Human GAPDH	Fwd: AGATCATCAGCAATGCCTCC Rv: CATGAGTCCTCCCACGATAC
Human FAM38A	Fwd: AGATCTCGCACTCCAT Rv: CTCCTTCTCACGAGTCC
Human FAM38B	Fwd: ATGGCCTCAGAAGTGGTGTG Rv: ATGTCCTTGCATCGTCGTTTT
Human *FYN*	Fwd: TCACCAAAGGAAGAGTGCCA Rv: CAAAAGTGGGGCGTTCTTCA
Mouse *Gapdh*	Fwd: AGGTCGGTGTGAACGGATTTG Rv: TGTAGACCATGTAGTTGAGGTCA
Human *HCK*	Fwd: CCACAGAGAGCCAGTACCAA Rv: TTCCAGTCCAACCTACCCAC
Human *LCK*	Fwd: CAACCTGGTTATCGCTCTGC Rv: TGGCCACAAAATTGAAGGGG
Human *LYN*	Fwd: CCACTATAGCTGGGAGGGTG Rv: GGCAAGAGAAGGCGGTATTG
Mouse *Fam38A*	Fwd: AGGACTTCCCCACCTATTGG Rv: CCAGGGATGAGGATACTGGAAAA
Mouse *Fam38B*	Fwd: ATGTGCGTTCCGGTACAATGG Rv: TGTGTCCTTGCATCGTTGCT
Human *SRC*	Fwd: AAACCCTGCCCTCCTTAGAC Rv: TCCTGAGGATGACAGAGGGA
Human *YES*	Fwd: GCTGGTTGATATGGCTGCTC Rv: CGACCATACAGTGCAGCTTC

Table 2.5 Primers used for qRT-PCR using SYBR™ Green. Table includes the sequences for forward and reverse primers (Sigma-Aldrich) used to amplify genes of interest in qRT-PCR experiments.

2.5.4.3 Agarose gel electrophoresis

PCR products were loaded onto a 1 % agarose gel containing SYBR™ Safe DNA Gel Stain (1:10,000) (Invitrogen), which binds DNA and allows visualisation of products upon exposure to ultraviolet light, and analysed by gel electrophoresis

to confirm product size. Agarose gels were prepared by boiling 1 g molecular biology grade agarose (Eurogentec) in 100 mL Tris-acetate-EDTA (TAE) buffer (Fisher Scientific). PCR reaction solutions were mixed with 6 x loading buffer containing the following: 2.5% Ficoll-400, 11 mM EDTA, 3.3 mM Tris-HCl (pH 8.0), 0.017% SDS and 0.015% bromophenol blue (New England Biolabs) and loaded on to the gel. The size of the product was compared to 100 bp DNA Ladder (New England Biolabs). Human brain RNA was purchased from Ambion (ref: AM7962) as a positive control. Electrophoresis was performed at a constant voltage of 85 V for 50 min. DNA was visualised by illumination using Syngene's G:BOX Chemi XT4 and GeneSys image acquisition software.

2.6 Western blotting

2.6.1 Solutions

Lysis buffer, used to lyse cells and make up samples to the required volume

10 mM Tris, pH 7.4, 150 mM NaCl, 0.5 mM EDTA, 0.5% NP-40. Minutes iComplete protease inhibitors (Roche 1:500) and PhosSTOP phosphatase inhibitors (Roche 1:500) were added prior to lysing.

Sample (loading) buffer (4x), used to dilute samples prior to loading on the gel

200 mM Tris pH 6.8, 8% SDS, 40% glycerol, 8% mercaptoethanol, 0.1% bromophenol blue.

Separating gel buffer, used to prepare separating gel

45.42 g Tris-base in 250 mL of distilled water, pH 8.8.

Stacking gel buffer, used to prepare stacking gel

6 g Tris-base in 100 mL of distilled water, pH 6.8.

Running (electrophoresis) buffer, used to run the samples

190 mM glycine, 25 mM Tris-base, 1% SDS.

Transfer buffer, used for the transfer stage

190 mM glycine, 25 mM Tris-base, 20% methanol.

Tris-buffered saline (TBS), used to wash membranes following transfer stage

150 mM NaCl, 20 mM Tris-base, pH 7.4.

Tris-buffered saline-Tween (TBS-T), used to make 5 % milk which antibodies were diluted in and also used to wash membranes following incubation with antibodies

150 mM NaCl, 20 mM Tris-base, 0.1% Tween-20, pH 7.4.

2.6.2 Cell treatment and lysis

Cells were grown to confluence in a 6 well plate; prior to treatment, cells were serum-starved overnight to dampen basal activation/phosphorylation of signalling proteins. Pretreatment of cells with inhibitors was carried out prior to treatment with an agonist where appropriate. Cells were treated with vehicle (DMSO) or compound in serum-free medium, at the appropriate time-points prior to lysing. Medium was removed and cells were immediately washed with 1 mL ice-cold PBS to halt all phosphorylation/dephosphorylation events. Cells were put on ice and PBS was removed and replaced with 65 µL ice-cold lysis buffer per well for 5 min. Cells were harvested using a cell scraper and samples were kept on ice for 30 min. Samples were spun for 10 min at 14,000 g at 4ºC and supernatant was taken into a new Eppendorf tube to remove unsolubilised cell debris.

2.6.3 Protein quantification

Protein quantification was performed on the supernatant using DC™ Protein Assay (BioRad). This is a dye-binding assay in which a differential colour change occurs which indicates protein concentration. Absorbance was measured using a plate reader at a wavelength of 750 nm. Comparison was made to a BSA standard curve (0-1333.3 µg/mL) and protein concentrations were derived from this. Samples were stored at -20 ºC until western blotting was performed.

2.6.4 Preparation of gels

	Separating gel	Stacking gel
Distilled H_2O	4.3 mL	2.81 mL
Ultra Pure ProtoGel® 30% acrylamide (National Diagnostics)	3 mL	0.83 mL
Separating/stacking gel buffer	2.5 mL	1.25 mL
10% sodium dodecyl sulphate (SDS) (VWR™)	100 µL	50 µL
10% ammonium persulphate (APS) (Sigma-Aldrich)	100 µL	50 µL
N,N,N′,N′-Tetramethylethylenediamine (Temed) (Sigma-Aldrich)	4 µL	5 µL

Table 2.6 Recipe for polyacrylamide gels. Quantities needed for producing two 10% SDS polyacrylamide gels.

2.6.5 Western blotting

10-30 µg of protein sample (depending on protein being analysed) was mixed with one-quarter volume of SDS-reducing sample buffer and heated at 90°C for 5 min to ensure complete denaturation of the proteins. Samples were loaded alongside 4 µL Precision Plus Protein™ Dual Colour ladder (Bio-Rad) or 10 µL HiMark™ Pre-Stained High Molecular Weight Protein Standard (Invitrogen), depending on the size of the protein of interest. Separation occurred on either 7.5 or 10% gels, depending on the size of the target protein. Electrophoresis was carried out for approximately 90 min at a constant current of 20 mA per gel in SDS-containing running buffer using PowerPac Basic™ (Bio-Rad). SDS is an anionic detergent which disrupts the secondary structures of proteins to create linear, negatively charged structures. An electrical charge across the gel leads to movement of negatively charged proteins towards the positively charged electrode. The distance each protein travels is inversely proportional to its size and molecular weight.

Polyvinylidene fluoride (PVDF) membrane (Immobilon-P, Merck) was soaked in methanol for 20 seconds before a rinse in water. The gel, filter paper and PVDF

membrane were soaked in transfer buffer for approximately 10 min. After resolution by electrophoresis, protein samples were transferred to the PVDF membrane using Bio-Rad wet transfer system at a constant current of 350 mA for 2 h in transfer buffer. After completion of the transfer, the membrane was rinsed once for 5 min in Tris-buffered saline (TBS) and incubated for 1 h in TBS containing Tween (TBS-T) containing 5% non-fat dried milk to block non-specific background binding. Membranes were then labelled overnight with primary antibodies diluted in TBS-T containing 5% milk and placed on a roller at 4°C. Table 2.7 contains a list of primary antibodies and dilutions used. The next morning, after 6 x 5 min washes in TBS-T on a rocker, the membrane was incubated with secondary horseradish-peroxidase (HRP) donkey anti-mouse, rabbit or rat secondary antibodies (1:5000/10000, Jackson ImmunoResearch) in TBS-T containing 5% milk for 1 h at r.t. on a roller, before another 6 x 5 min washes with TBS-T on a rocker. Membranes were probed with phosphorylation antibodies and then reprobed with total expression antibodies from different species. In the case of phospho-ERK, blots were placed in stripping buffer (Thermo-Scientific) for 15 min, washed and blocked in 5% milk after probing for p-ERK before probing for total ERK. This was necessary due to prior phospho-ERK antibody binding impairing total ERK antibody binding.

2.6.6 Protein visualisation

SuperSignal Femto detection reagents (Pierce Science) were used to detect immunolabelled protein bands. Membranes were imaged using Syngene's G:BOX Chemi XT4 and GeneSys image acquisition software. Data were analysed using Image J software (NIH) by calculating the mean intensity of each band and normalising it to that of α-tubulin or the total protein loading control.

Protein	Antibody	Dilution	Vendor
α-tubulin	0945-Tubulin (DM1A) Mouse mAb	1:2000	Cell Signalling Technology #3873
Piezo1	BEEC-4 (DLAKGGTVEYANEKHMLALA)	1:1000	Cambridge Biosciences
Piezo1-HA	Anti-HA High Affinity Rat mAb (clone 3F10)	1:3000	Roche #11867423001
phospho-p38α MAPK	(Thr180Tyr182) (3D7) Rabbit mAb	1:250	Cell Signalling Technology #9215
p38α	(L53F8) Mouse mAb	1:500	Cell Signalling Technology #9228
phospho-p44/42 MAPK (Erk1/2)	phospho-p44/42 MAPK (Erk1/2) (Thr202/Tyr204) (E10) Mouse mAb	1:5000	Cell Signalling Technology #9106
p44/42 MAPK (Erk1/2)	p44/42 MAPK (Erk1/2) (137F5) Rabbit mAb	1:4000	Cell Signalling Technology #4695
TNC	(EGF Like Domain) (4F10TT) Mouse mAb	1:200	Tecan #JP10337

Table 2.7 Primary antibodies used for Western Blotting. Summary of primary antibodies used along with their dilution factor, vendor and catalogue number, mAb: monoclonal antibody.

2.7 Mechanical stimuli experiments

2.7.1 Patch clamp electrophysiology

Human cardiac fibroblasts were seeded and grown to 80% confluence on glass coverslips (Thermo Scientific, thickness 0.15 mm) in 24 well plates. Cells were transfected with control or Piezo1-specific siRNA, where applicable. After 72 h of transfection, ionic currents were recorded through cell-attached patches using standard patch-clamp technique in voltage-clamp mode. Patch pipettes had resistance of 4–6 MΩ when filled with pipette solution. Ionic solution of composition (mM): CsCl 145, $MgCl_2$ 2, HEPES 10, ATP 5, GTP 0.1, EGTA 1 (titrated to pH 7.2 using CsOH) was used in the pipette. The bath solution was SBS. Recordings were at a constant holding potential of +80 mV (applied to the

patch pipette). 200 ms pressure steps were applied to the patch pipette with an interval of 10 s using High Speed Pressure Clamp HSPC-1 System (ALA Scientific Instruments, USA). All recordings were made with an Axopatch-200B amplifier (Axon Instruments, Inc., USA) equipped with Digidata 1550B and pClamp 10.6 software (Molecular Devices, USA) at room temperature. Currents were filtered at 2 kHz and digitally sampled at 20 kHz. Data were analysed using pClamp 10.6, MicroCal Origin 2018 (OriginLab Corporation, USA) software package. Patch clamp experiments were performed by Katsuhiko Muraki.

2.7.2 Application of shear stress

To generate shear stress, fibroblasts were plated in a 6-well plate, grown to confluence and placed on an orbital shaker (SSM1, Stuart) rotating at 153 rpm with an orbit of 16 mm for 24 h. Cells were cultured in 2 mL of media; meaning shear stress at the edge of the wells was ~10 dyn/cm^2 (Dardik *et al.* 2005). RNA was extracted from cells and used for RT-PCR.

2.7.3 Mechanical stretch

Human cardiac fibroblasts were seeded at 1x10^5 cells/well on collagen-coated silicon membranes (BioFlex® 6-well culture plates, Dunn Labortechnik, Germany). 72 h after transfection, cells were stretched in serum-free medium using an FX-4000 or FX-5000 Flexercell® Tension™ System (Flexcell International) to equibiaxially elongate the cell-seeded elastic membrane against a cylindrical loading post using a vacuum (Figure 2.3). These experiments were performed at either The University of Maastricht (Dr Frans van Nieuwenhoven's laboratory) or The University of Manchester (Dr Joe Swift's laboratory). This apparatus has been used previously to stretch cardiac fibroblasts (Fu et al., 2016). Elongation of 10% in surface area at 1 Hz was applied to the cells for 6 or 24 h. A 6-well stretching plate was housed inside the incubator (37°C, 5% CO_2) alongside unstimulated cells adhered to Bioflex® plates which served as controls. RNA was extracted and RT-PCR was used to quantify gene expression or lysates were collected for western blotting.

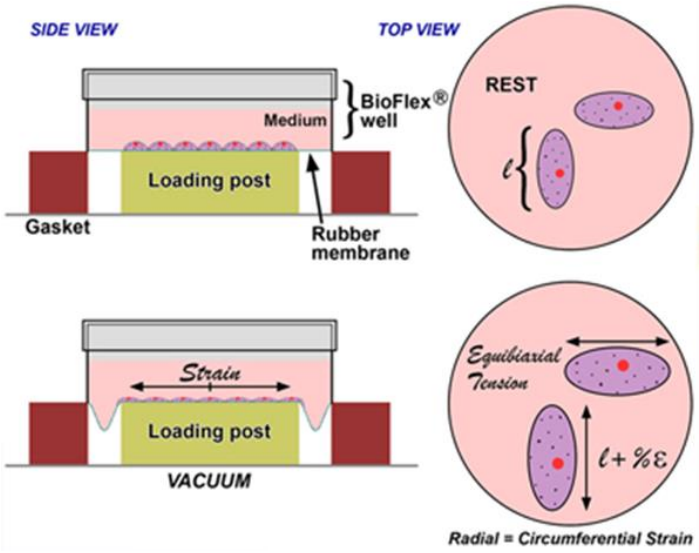

Figure 2.3 Mechanism utilised for stretching cardiac fibroblasts. Mechanism of the Flexercell® Tension™ System (Flexcell International) which equibiaxially elongates the elastic membrane against a cylindrical loading post using a vacuum in order to stretch cells. Image taken from Flexcell® International Corporation.

2.7.4 Substrate stiffness experiments

ExCellness® PrimeCoat 35 mm dishes and 24-well plates were used to assess the impact of substrate stiffness on gene expression. Dishes and plates were coated with fibronectin in serum-free media (10 µg/mL) and kept at 37^{0}C for at least 1 h prior to plating of cells. Murine cardiac fibroblasts were isolated and plated in one well of a 6-well plate. When confluent, these cells were seeded into a 24-well plate. The following day, cells were transfected with control and Piezo1-specific siRNA and left for 48 h. At this point, cells transfected with both control and Piezo1-specific siRNA were seeded into wells of three 24-well plates: one of 10 kPa stiffness, one of 30 kPa stiffness and a tissue culture plate and left to grow for 24 h. After 24 h, RNA was collected to perform RT-PCR to measure gene expression.

These levels of stiffness were chosen as a study using atomic force microscopy to evaluate the elastic modulus of healthy and ischemic tissue in a rat heart found that the elastic modulus of healthy heart tissue was in the range of 10-15 kPa, while the respective value of ischemic tissue was around 50 kPa (Berry *et al.* 2006). Normal cell culture plastic is up to 500,000 times stiffer.

2.8 Immunocytochemistry

Murine cardiac fibroblasts were seeded and grown to 80% confluence on glass coverslips (Thermo Scientific, thickness 0.15 mm) in 24 well plates. Cells were treated for 24 h with vehicle or 10 µM Yoda1 in the presence or absence of TGF-β1 (10 ng/ml), where applicable. Cells were washed in PBS, fixed in 4% paraformaldehyde (PFA) for 10 min at r.t. and washed with Tris-saline to quench PFA. Cells were permeabilised with 0.1% Triton™ X-100 (Sigma-Aldrich) in PBS for 10 min, before blocking with 1% BSA in PBS for 30 min to prevent non-specific antibody binding. Primary antibodies were diluted in 1% BSA in PBS solution and incubated with cells for 60 min at r.t. Cells were stained for vimentin (C-20, #sc-7557, Santa Cruz Biotechnology), α-SMA (clone 1A4, #A2547, Sigma-Aldrich) or CD-31 (#ab28364, Abcam). Primary antibodies were used at 1:100 (vimentin and α-SMA) or 1:50 (CD-31). After washing with PBS, cells were incubated with the relevant species-specific fluorescent dye-conjugated secondary antibodies (Jackson ImmunoResearch) in the dark for 30 min at r.t. Secondary antibodies were used at 1:300 in 1% BSA solution. Following this, coverslips were mounted onto glass slides using Prolong Gold Antifade Reagent (Invitrogen) containing DAPI (4',6-diamidino-2-phenylindole) to label the nuclei. Slides were kept at r.t. overnight to allow mounting media to set and imaged using a LSM 880 confocal microscope (Zeiss).

2.9 LIVE/DEAD cell viability assay

The LIVE/DEAD™ Viability/Cytotoxicity Kit (ThermoFisher Scientific) enables dual colour discrimination of a population of live cells from a dead cell population, based on plasma membrane integrity and esterase activity. Live cells are determined by the presence of intracellular esterase activity, determined by the enzymatic conversion of the non-fluorescent, cell-permeant calcein-AM to the fluorescent calcein. Calcein is retained within live cells, producing a uniform green fluorescence (excitation/emission ~495 nm/~515 nm). Ethidium homodimer enters cells with compromised cell membranes and displays an increase in fluorescence upon binding nucleic acids, producing a red fluorescence in dead cells (excitation/emission ~495 nm/~635 nm). Ethidium homodimer however cannot permeate cells with intact membranes.

Murine cardiac fibroblasts were plated in 12 well plates (Corning) at 80% confluency and incubated overnight (37°C, 5% CO_2). Vehicle (DMSO), Yoda1 (10 µM) or Staurosporine (SSP; 1 µM) were applied the following day and cells were incubated for an additional 24 h prior to commencing the assay. SSP isolated from Streptomyces sp. (Sigma-Aldrich), a non-specific protein kinase inhibitor, was utilised as a positive control to induce cell death (Bombeli *et al.* 1997). A working solution was prepared containing 2 µM calcein AM and 4 µM ethidium homodimer in 10 mL sterile PBS; 500 µL was applied to each well following removal of media and PBS wash. Cells were left for 30 min at r.t., protected from light. Cells were imaged using the IncuCyte® ZOOM Live Imaging System (Essen Bioscience, Michigan). The total number of fluorescent cells in each well was calculated using inbuilt algorithms, using an average from 9 images per well. The mean data are shown as the number of live cells relative to the total number of cells.

2.10 ELISA

Conditioned media were collected after treatment with stimuli, centrifuged to remove cellular debris and stored at -20 °C for analysis. Supernatants were thawed and enzyme linked immuno-sorbent assay (ELISA) performed to determine the levels of IL-6. Commercially available ELISA kits were utilised. The concentration of mouse IL-6 in medium was measured using Mouse IL-6 Quantikine ELISA Kit (M6000, R & D Systems), according to the manufacturer's instructions. The concentration of human IL-6 in medium was measured using Human IL-6 DuoSet ELISA (DY206-05, R & D Systems) which was used alongside DuoSet ELISA Ancillary Reagent Kit 2 (DY008, R & D Systems), according to the manufacturer's instructions.

Briefly, a 96-well plate was coated overnight at r.t. with IL-6 capture antibody in coating buffer. The following day, wells were blocked with BSA in PBS for 1 h at r.t. and then washed (these stages were only necessary for the Human IL-6 DuoSet ELISA). Conditioned media and IL-6 standards were added to the plate for 2 h at r.t; samples were diluted 1:5-1:30 depending on the experiment. This was followed by a wash stage and addition of IL-6 detection antibody for 2 h at r.t. After a wash step, Streptavidin-HRP was added for 20 min, followed by

substrate solution (equal volume of H_2O_2 and Tetramethylbenzidine) for 20 min, both stages were performed in the dark. The reaction was terminated using stop solution (2N H_2SO_4) and the plate was gently tapped to mix the colour before absorbances were read at 450 nm; readings at 570 nm were subtracted to correct for optical imperfections in the plate.

2.11 Collagen gel contraction assay

The collagen gel contraction assay was performed as described previously in 24-well plates (Van Nieuwenhoven et al., 2013). Wells were coated with 1% bovine serum albumin (Sigma) in PBS at 37 °C for 1 h. Collagen gels were prepared by mixing type I rat tail collagen solution (Merck) with 2 x concentrated DMEM (Merck), supplemented with 88 mM $NaHCO_3$, and then immediately mixing with 50,000 freshly trypsinised murine cardiac fibroblasts per gel. Gels were allowed to solidify at 37 °C for 1 h. Following solidification, gels were released from the sides of the well by addition of 0.5 mL DMEM with 0.4 % FBS containing either vehicle, Yoda1, compound 159 (both 10 µM) or 10 ng/ml TGF-β1. In RNA interference experiments, murine cardiac fibroblasts were transfected using control or Piezo1-specific siRNA 48 h prior to the commencement of the gel contraction assay. When PD98059 was tested, either vehicle or 30 µM PD98059 were applied in DMEM after 1 h of solidification, then Yoda1 or vehicle was added after another 1 h. Gels were photographed and weighed 24 h later to assess their relative contraction. Collagen gel area was calculated using ImageJ and displayed as gel area relative to the total area of the well.

2.12 Multiplex kinase activity profiling

PamGene Serine-Threonine Kinase (STK) and Tyrosine Kinase (PTK) multiplex activity assays were used to investigate STK and PTK activity, respectively. Confluent murine cardiac fibroblasts (n=6) in a 6-well plate were treated for 10 min with vehicle (DMSO) or Yoda1. Cells were washed with ice-cold PBS and lysed by addition of 100 µL M-PER mammalian extraction buffer (Thermo Fisher Scientific), containing 1:100 Halt phosphatase and Halt protease inhibitor cocktails (Pierce) for 15 min on ice. Cell extracts were cleared by centrifugation

for 10 min at 14,000 g at 4°C and protein concentrations were determined using the DC™ Protein Assay (BioRad). Aliquots were prepared and snap-frozen in liquid nitrogen.

6 and 1.2 µg of protein was loaded onto each PamChip (shown in Figure 2.4) for the Protein Tyrosine Kinase (PTK) array protocol and the Serine-Threonine Kinase (STK) array protocol, respectively. The phosphorylation of PamChip peptides were monitored using the PamStation 12 from PamGene (Hertogenbosch, Netherlands). Kinase(s) in the sample actively phosphorylate substrates on the PamChip, in the presence of ATP. Images are taken every 5 minutes to generate real time kinetics data (Figure 2.4). The PTK array was a single-step reaction. Cell extracts, ATP, and fluorescein isothiocyanate (FITC)-labelled pY20 antibody were incubated on the chip, and the phosphorylation of the individual tyrosine peptides was viewed by fluorescence detection in real time. The STK array was a two-step reaction. First, the cell extracts, ATP, and the primary antibody mixture were incubated with the chip for 110 min. Then, the secondary FITC-labelled antibody was added.

The STK Array consists of 140 serine/threonine containing peptides and 4 positive control phosphorylated peptides, resulting in 144 peptides per array. Each peptide represents a 15-amino-acid sequence, of which 13 residues are derived from a putative phosphorylation site in human proteins. The PTK Array consists of 196 peptides with known phosphorylation sites. Peptide sequences are derived from the literature or computational predictions and are correlated with one or multiple upstream kinases. Signal intensities were analysed in the BioNavigator software (PamGene) as Yoda1-treated versus DMSO treatment after 10 min. Permutation analysis gave a specificity score (mapping of peptides to kinases) and a significance score (difference between treatment groups) for each kinase. The median total of these two scores was used to rank kinase hits. Statistical analysis was performed by Savithri Rangarajan (PamGene).

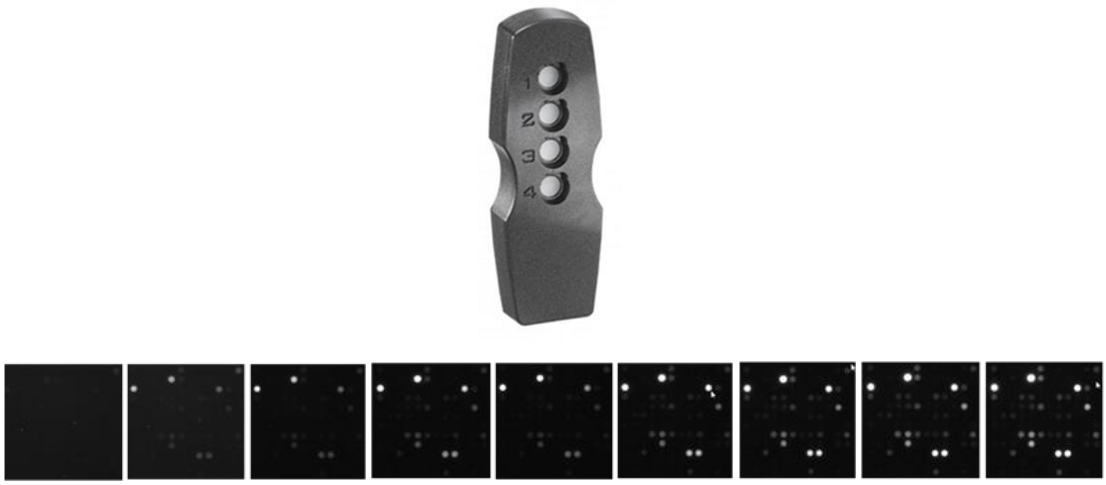

Figure 2.4 A PamChip and the phosphorylation signals generated. The PamChip contains 4 peptide arrays, composed of aluminum oxide. This material is approximately 60 µm thick and has a porous structure which maximises binding kinetics. The sample and labelled antibodies are dispensed onto a PamChip, which is then placed in the PamStation12. Below are some images of example phosphorylation signals; real time kinetics data are taken every 5 minutes. Images taken from PamGene.

2.13 Transgenic mice

2.13.1 Animal husbandry and ethics

All animal use was authorised by the University of Leeds Animal Ethics Committee and The Home Office, UK under project licenses 40/3523, P144DD0D6 and P65AC17DB. Animals were housed in Optimice individually ventilated cages (Animal Care Systems) with bedding of Pure'o Cell (Datesand) at 21°C, 50-70% humidity with light/dark cycle 12/12 h in a sterile animal unit. RM1 diet (SpecialDiet Services, Witham, UK) was available *ad libitum* and mice were allowed free access to triple filtered Hydropac water. Mice were housed with their littermates with a maximum of 5 mice per cage. Breeding pairs or trios (1 male with up to 2 females) were established when necessary; mating programmes required mice of at least 6 weeks of age and ideally less than 6 months of age. Offspring were weaned at 21 days of age. All animals were treated humanely and were checked on a daily basis to assess their general well-being.

2.13.2 Genotyping

Progeny resulting from breeding cages were genotyped ~14-21 days post-partum. Ear notches (2 mm) were taken from each mouse and this also enabled identification of individual animals. Tissue digestion was achieved with 0.5 mg/mL proteinase K (Ambion) in 0.5 mL lysis buffer (50 mM EDTA, 10 mM Tris-HCl (pH 8.0), 1% SDS) for 24 h at 37°C. After incubation, the tubes were mixed vigorously to break up any remaining tissue. 0.4 mL phenol/chloroform/isoamyl alcohol (Sigma-Aldrich) was added. Samples were kept for 15 min at r.t. and agitated frequently. Samples were then centrifuged at 13,200 rpm for 15 min to separate the phases. The upper (DNA-containing) phase was transferred to a fresh tube with an equal volume of isopropanol (Fisher-Scientific) and 0.1 volume of 3 M NaCl. Tubes were inverted gently before being left to stand for 30 min at r.t., while the DNA precipitated. After a 45 minute centrifugation step at 13,200 rpm, DNA pellets were washed with 0.5 mL 70% ethanol, air dried and re-suspended in 65 µL TE buffer (10 mM Tris, 1 mM EDTA buffer, pH 8.0) before being left to stand for 30 min before PCR was performed.

The presence of *Cre*, *lacZ*, *loxP* and a deletion of *Piezo1* were detected by PCR. Each reaction contained the following: 2.5 µL 10x ThermoPol Reaction Buffer, 0.5 µL Deoxynucleotide (dNTP) Solution Mix, 0.25 µL Taq DNA Polymerase (all New England Biolabs), 1 µL each of forward and reverse primers (25 µM), 0.5 µL DNA and nuclease-free water to give a final volume of 25 µL. Reactions were carried out using the T100™ Thermal Cycler. Reaction conditions were as follows: 1 minute 93°C; 29 cycles x 20 seconds 93°C, 3 min 68°C; followed by a hold step at 4°C. Sequences of primers and expected product sizes are shown in Table 2.8.

PCR products were subjected to gel electrophoresis on agarose gels and visualised as described in 2.5.4.3. Example genotyping results are shown below in Figure 2.5 and in Chapter 6, alongside the relevant murine models.

Gene of interest	Primer sequence (5' to 3')	Vendor	Product size (bp)
Cre	Fwd: GCATTACCGGTCGATGCAACGAGTGATGAG Rv: GAGTGAACGAACCTGGTCGAAATCAGTGCG	Invitrogen	408
lacZ	Fwd: AATGGTCTGCTGCTGCTGAAC Rv: GGCTTCATCCACCACATACAG	Sigma	225
loxP	Fwd: GGAGGGTTGCTTGTTGGATA Rv: ACTCATCTGGGTGAGGTTGC		189
Deletion of *Piezo1*	Fwd: ACCACCTGAGAAGTTGTCCC Rv: ACTCATCTGGGTGAGGTTGC		379

Table 2.8 Genotyping primers. Table includes sequences of forward and reverse primers used to amplify genes of interest for PCR genotyping experiments, along with their predicted product size.

2.13.3 Piezo1-modified transgenic mice

2.13.3.1 Piezo1-HA murine model

CRISPR-Cas9 technology was used to develop a transgenic C57BL/6 mouse globally expressing a mutated hemagglutinin (HA)-tagged version of Piezo1 (Piezo1-HA). This was done as current anti-Piezo1 antibodies are non-specific. The HA sequence was introduced between amino acids A2439 and D2440. 2 day embryos were electroplated using AltR crRNA:tracrRNA:Cas9 complex. Zygotes were implanted into 0,5-post coitum pseudopregant mice. Genotypes were determined using real-time PCR with specific probes designed for each gene (Transnetyx, Cordova, TN). Cardiac fibroblasts were isolated from WT, heterozygote (HA-Het) and homozygote (HA-Hom) mice and lysed. Cardiac fibroblasts from HA-Hom mice were isolated and transfected with control or Piezo1-specific siRNA and lysed. These samples were used for western blotting.

2.13.3.2 Global Piezo1$^{+/-}$ murine model

C57BL/6 mice carrying global disruption of the Piezo1 gene with a *lacZ* insertion flanked by FRT sites have been described previously (Li *et al.* 2014). This line

generates WT mice and mice globally heterozygous for Piezo1 (Piezo1$^{+/-}$); these mice are referred to as Het mice throughout. Analysis of Piezo1 disruption was performed by genotyping using primers for *lacZ* (primer sequences shown in Table 2.8). An example gel imaged to identify genotypes can be seen in Figure 2.5. Mice of varying ages and sexes were used for culturing cells for experiments.

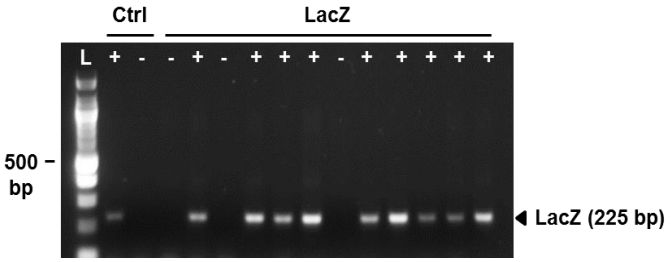

Figure 2.5 An example gel used to identify genotypes of mice from the Piezo1$^{+/-}$ line. PCR genotyping for presence of the *lacZ* site (225 bp) in DNA extracted from ear notches from 12 mice. Gels indicate positive and negative controls and L=100 bp ladder.

2.13.3.3 Piezo1 M2240R murine model

The Piezo1 M2240R gain of function mice (referred to as M-R mice), which have a mutation equivalent to the human mutation M2225R (Zarychanski *et al.* 2012), were generated using CRISPR/Cas9 by the Manchester Transgenic Facility, Dr Melanie Ludlow and Elizabeth Evans (University of Leeds). The gRNA was designed to direct Cas9-mediated cleavage of Piezo1 6 bp upstream of the target methionine codon and possesses no off-target sites with less than 3 mismatches elsewhere in the genome (binding sequence 5' GGGCGCUCAUGGUGAACAG 3'). A 120 nucleotide single-stranded homology directed repair (ssHDR) template was designed to incorporate the methionine to arginine missense mutation, in addition to silent mutations introducing a Mlu1 restriction enzyme recognition site to facilitate genotyping (5'ccacccgtcccctgagcctgaggggctccatgctgagcgtgcttccatcc-ccagccaTTAttTacGCGTagcgcccagcagccatccattgtgccattcacaccccaggcctacgagga g 3'; capital letters denote the mutated bases) (Sigma Aldrich).

The gRNA, delivered as an alt-R crRNA combined with tracrRNA (Integrated DNA Technologies, Illnois, USA), Cas9 protein (Thermo Fisher check) and ssHDR template were microinjected into C57BL/6 mouse zygotes, and implanted into

females (by Manchester Transgenic Animal Facility). Successful gene editing of pups was identified by Mlu1 digestion of PCR amplicons (Fwd: 5' TCTGGTTCCCTCTGCTCTTC 3', Rv: 5' TGCCTTCGTGCCGTACTG 3') and confirmed by DNA sequencing following subcloning into pCRTM-Blunt (Invitrogen). Further genotypes were determined by RT-PCR with specific probes designed for each gene (Transnetyx). Cardiac fibroblasts were isolated from 8-12 week-old male mice and used for experiments.

2.13.4 Piezo1 knockout murine models

2.13.4.1 *Cre-loxP* technology

Genetic manipulation to generate Piezo1 KO mice was performed using the *Cre-loxP* system. *Cre-loxP* reactions are affected by the orientation and location of two *loxP* sites. When *loxP* sequences are orientated in the same direction, *Cre* recombinase mediates removal of the DNA segment between the two sites. Usually, *Cre* and *loxP* strains are developed independently and then crossed.

Cre recombinase can be linked to a form of mutated oestrogen receptor (*CreER(T)*) to enable conditional deletion. 4-hydroxytamoxifen (4OH-TM), the active metabolite of tamoxifen, binds to the mutated oestrogen receptor, which allows *CreER(T)* to move to the nucleus and here, recombination occurs, causing targeted deletion of the gene between two *loxP* sites. Without 4OH-TM exposure, gene excision does not occur.

2.13.4.2 Tamoxifen administration

Tamoxifen free base (Sigma-Aldrich) was dissolved in corn oil at 20 mg/mL and shaken overnight at 200 rpm, 37°C to aid dissolution. 100 mg/kg tamoxifen was administered intraperitoneally (i.p.), daily, for 5 consecutive days using a 0.5 mL U-100 insulin syringe and 29G 13mm needle. This protocol induces *Cre* activity (and hence floxed gene deletion) that is restricted to the cell type which express the particular promoter utilised. Therefore, only Cre^{+} mice will have a deletion of Piezo1 in the chosen cells; Cre^{-} mice, injected with tamoxifen, were used as control animals.

2.13.4.3 Fibroblast-specific Piezo1 knockout murine model

Two murine models were generated in order to obtain an inducible (myo)fibroblast-specific Piezo1 KO mouse and both will be discussed. The first was an inducible fibroblast-specific Piezo1 KO mouse line established by crossing C57BL/6 mice expressing tamoxifen-inducible *Cre* recombinase under a fibroblast-specific promoter (obtained from Chris Denton, UCL) with C57BL/6 mice expressing a modified Piezo1 gene where exons 19-23 are flanked by *loxP* sites (Li *et al.* 2014). Fibroblast specificity of the Piezo1 deletion was determined by a 6 kb transcriptional enhancer sub-cloned from the far-upstream region of the mouse collagen I gene (*Col1a2*), linked to an endogenous minimal promoter (Zheng *et al.* 2002). This generated a *Col1a2-Cre-ER(T)-Piezo1*$^{flx/flx}$ mouse line. Strains homozygous for floxed *Piezo1* alleles but heterozygous for *Cre* were obtained. Therefore, subsequent breedings yielded exclusively *Cre*$^{+}$ *Piezo1*-floxed mice (experimental) and *Cre*$^{-}$ *Piezo1*-floxed mice (control). This is illustrated in Figure 2.6. *Col1a2*, is expressed in all fibroblasts, therefore the *Col1a2-Cre-ER(T)* line induces gene deletion in cardiac (and other) fibroblasts; it has previously been confirmed that there is no effect on other type I collagen-producing cells (Denton *et al.* 2001; Denton *et al.* 2005). *Col1a2-Cre-ER(T)-Piezo1*$^{flx/flx}$ KO mice (i.e. *Cre*$^{+}$ *Piezo1*$^{flx/flx}$) were compared alongside control littermates (i.e. *Cre*$^{-}$ *Piezo1*$^{flx/flx}$). Identification of correct genotype was performed by using genotyping primers for *loxP* and *Cre* (primer sequences are shown in Table 2.8). Male and female mice were injected at 3 weeks of age with tamoxifen for five consecutive days to induce *Cre* activity and facilitate *loxP*-directed deletion of exons 19-23 of *Piezo1* in fibroblasts; this is illustrated in Figure 2.7. Hearts were harvested 7 days after the last injection of tamoxifen and cardiac fibroblasts were cultured.

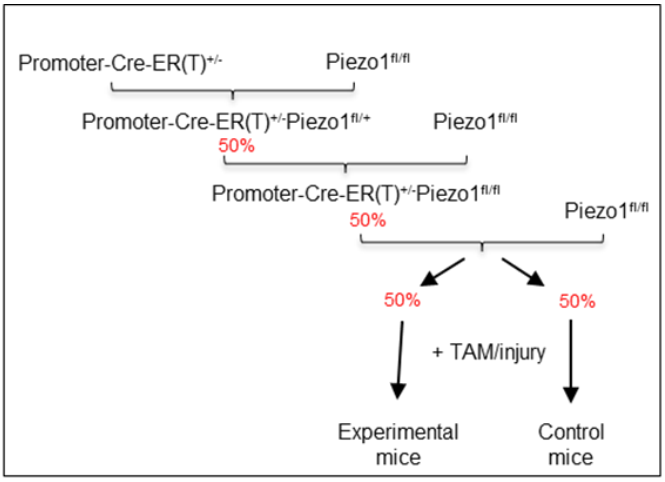

Figure 2.6 Breeding strategy for generation of Piezo1 knockout mice. Breeding strategy for generation of both the *Col1a2-Cre-Piezo1*$^{flx/flx}$ and *Postn-Cre-Piezo1*$^{flx/flx}$ murine models.

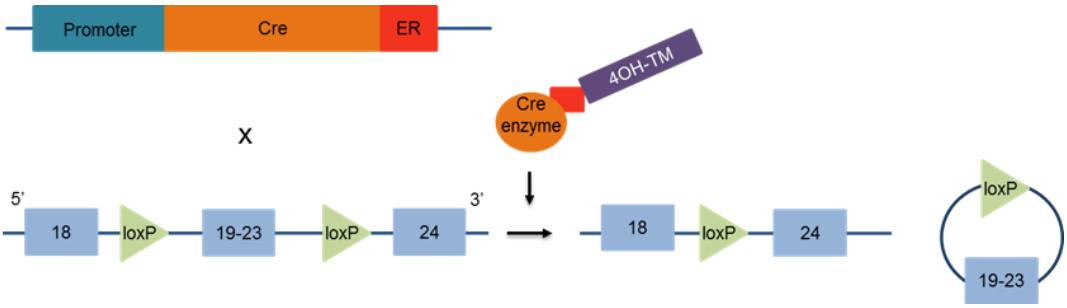

Figure 2.7 Gene deletion using the *Cre-loxP* system. The tamoxifen inducible *Cre* enzyme is linked to a mutant oestrogen receptor (ER), under the control of a fibroblast-specific transcriptional enhancer from the *Col1a2* gene or the myofibroblast specific promoter *Postn*, depending on the murine model. When *Cre* and a floxed *Piezo1* allele are present, exposure to 4OH-TM causes *Cre*ER(T) to excise exons 19-23 of *Piezo1* as a circular piece of DNA.

2.13.4.4 Myofibroblast-specific Piezo1 knockout murine model

The second model was a tamoxifen-inducible, myofibroblast-specific Piezo1 KO mouse line. This was established by crossing C57BL/6 mice expressing myofibroblast-specific, tamoxifen-inducible *Cre* recombinase under the *Postn* promoter (Molkentin *et al.* 2017), with C57BL/6 mice expressing a modified

Piezo1 gene with exons 19-23 flanked by *loxP* sites (Li *et al.* 2014) to generate a *Postn-Cre-Piezo1*$^{flx/flx}$ mouse line (shown in Figure 2.6). The method for deletion of exons 19-23 in shown in Figure 2.7. The *Postn-Cre* line is a Mer-Cre-Mer (MCM) model; the tamoxifen inducible Cre recombinase is flanked by two modified estrogen receptor ligand binding domains and is more potent than the ER(T) Cre used in the Col1a2-promotor mice (shown in Figure 2.6). This was purchased from The Jackson Laboratory (JAX stock #029645). Strains homozygous for floxed Piezo1 alleles but heterozygous for *Cre* were obtained (i.e. *Cre*$^{+}$*/Piezo1*$^{flx/flx}$). Therefore, subsequent breedings yielded exclusively *Cre*$^{+}$ Piezo1-floxed mice (experimental) and *Cre*$^{-}$ *Piezo1*-floxed mice (control). Periostin is expressed almost exclusively in myofibroblasts in areas of tissue injury (Kanisicak *et al.* 2016), therefore this line induces gene deletion in cardiac (and other) myofibroblasts without effect on other cells types. Experimental mice (i.e. *Cre*$^{+}$ *Piezo1*$^{flx/flx}$) were compared to control mice (i.e. *Cre*$^{-}$ *Piezo1*$^{flx/flx}$). Identification of correct genotypes was performed using genotyping primers for *loxP* and *Cre* (primer sequences are shown in Table 2.8).

2.13.5 Cardiac injury models

2.13.5.1 Experimental myocardial infarction model

A permanent left anterior descending (LAD) coronary artery ligation model of experimental MI was performed on 5% isoflurane-anaesthetised male mice (10-12 weeks of age) by Dr Mark Drinkhill. Following intubation, mice were ventilated at a tidal volume of 140 µL and a respiratory rate of 120/min with 1.5% isoflurane and 100% oxygen. The LAD was ligated at the edge of the left atrium using 8-0 prolene suture and occlusion confirmed by observing pallor of the anterior LV wall. Experimental mice were compared to sham-operated animals, which underwent a similar surgical procedure without tying the ligature. Data from sham animals are from a previous study (Bageghni *et al.* 2019), where Millar pressure-volume conductance catheter data were obtained by Dr Mark Drinkhill and RT-PCR data by Dr Sumia Bageghni.

2.13.5.2 Experimental thoracic aortic constriction model

Female mice aged 10-12 weeks were utilised for TAC surgery performed by Dr Mark Drinkhill. The TAC model results in pressure overload due to partial occlusion of the transverse aorta. This procedure often leads to cardiac hypertrophy, a common compensatory mechanism in the pressure overloaded heart and, in some animals, will result in heart failure over time. TAC was performed as described by deAlmeida, van Oort and Wehrens (2010). Briefly, mice were anaesthetised with 5% isoflurane. Following intubation, mice were ventilated at a tidal volume of 140 µL and a respiratory rate of 120/min with 1.5% isoflurane and 100% oxygen. Under a dissecting microscope, a sternal split of the cranial 1/3 of the sternum allowed an 8-0 silk ligature to be tied around the ascending aorta and a 26G blunted needle, which was subsequently removed. Experimental mice were compared to animals undergoing a sham procedure (surgery without banding of the aorta).

2.13.5.3 Analysis following cardiac injury

Mice were injected with tamoxifen for 5 consecutive days the week after surgery in order to induce *Cre* activity and facilitate *loxP*-directed deletion. Tamoxifen injections were carried out by Dr Simon Futers. Physiological measurements of cardiac function were obtained at the end of the experimental period (4 weeks after surgery) by Millar conductance pressure-volume (PV) catheter analysis as previously described by Frentzou et al. (2015). Briefly, mice were anesthetised with isoflurane, and body temperature was maintained with a heating pad before inserting a 1.4 F miniature PV catheter (ADInstruments) into the left ventricle via the right carotid artery and ascending aorta. Data were collected using the MPVS-300 PV system (ADInstruments) and PV loop analysis was performed with Chart 8 Pro software (ADInstruments). Dr Mark Drinkhill carried out the PV measurements and was blinded to the genotype of the animals. Stroke volume, ejection fraction, cardiac output, end systolic/diastolic pressure, end systolic/diastolic volume, heart rate, blood pressure and myocardial contractility were calculated. The heart was removed and washed; ventricles were cleaned of blood, blotted, and weighed. Heart weight/body weight ratio (mg/g) was recorded prior to further processing of cardiac tissue. Left tibias were also harvested and length was recorded; heart weight/tibia length was also recorded as another

indicator of cardiac weight index (mg/mm). RNA was prepared from the apex of the heart to evaluate cardiac gene expression, as was DNA to check for a deletion of Piezo1.

2.14 Data analysis

OriginPro 2015 (OriginLab, Northampton, MA, USA) was used for data analysis and presentation. Averaged data are presented as mean ± SEM, where “n” represents the number of independent experiments and “N” indicates the total number of replicates within the independent experiments (multiwall assays). For comparisons between two sets of data, a Student’s t-test was used. For multiple comparisons, a one-way ANOVA was used with Tukey’s post-hoc test. $P<0.05$ was considered statistically significant; *$P<0.05$, **$P<0.01$ and ***$P<0.001$. No significant difference is indicated by NS ($P>0.05$). For EC_{50} and IC_{50} determination, data were normalised to vehicle and curves were fitted using the Hill1 equation.

2.15 Figures

BioRender was utilised for the generation of all schematic figures in Chapter 1 and summary figures.

Chapter 3 Piezo1 is expressed and functional in cardiac fibroblasts across species

3.1 Introduction

Cardiac fibroblasts respond to a wide range of mechanical signals in physiology and pathophysiology. It is known that increased mechanical stimulation of fibroblasts results in enhanced ECM synthesis and expression of various cytokines and growth factors (Carver *et al.* 1991; Yokoyama *et al.* 1999). This implies that mechanical stress plays an important role in the regulation of cardiac fibroblast function but there are still many unknowns in this field. Mechanically-activated ion channels have been implicated as sensors of mechanical stress in cardiac fibroblasts (Reed, Kohl and Peyronnet 2014). Over the past 10 years, since Coste *et al.* (2010) discovered the Piezo1 family of proteins, there has been a vast amount of literature published discussing Piezo1 and its roles of sensing mechanical activation in a broad range of tissues. In a review by Herum *et al.* (2017b), it was suggested that the most solid data for a stretch-activated channel in cardiac fibroblasts would be Piezo1, as the electrophysiological properties of this channel are similar to that of endogenous cardiac non-selective cation stretch-activated channels. The objective of this study was to consider the role of Piezo1 in cardiac fibroblasts.

3.2 Aims

The main aims of this chapter were to investigate whether Piezo1 was present in murine and human cardiac fibroblasts, to ascertain if the Piezo1 agonist, Yoda1, could activate endogenous cardiac fibroblast Piezo1 channels to cause Ca^{2+} entry and to ascertain that this response was dependent on Piezo1. It was also explored whether mechanical stimuli could be used to activate the Piezo1 channel in cardiac fibroblasts.

3.3 Methods

Immunocytochemistry (Section 2.7), RT-PCR (Section 2.5) and Ca^{2+} measurements calculated using the FlexStation and the Ca^{2+} indicator, Fura-2 (Section 2.3) were first utilised to characterise murine cardiac fibroblasts. *Piezo1* mRNA expression was investigated using RT-PCR in cultured and freshly isolated murine cardiac fibroblasts and cultured human cardiac fibroblasts; this was compared with its expression levels in other cardiac cell types. Intracellular Ca^{2+} measurements were performed to examine whether the Piezo1 activator, Yoda1, could induce Ca^{2+} entry in cardiac fibroblasts. When this was confirmed, chemical antagonists (Section 2.1), two Piezo1-modified murine models (Section 2.13.3) and siRNA targeting Piezo1 (Section 2.4) were utilised to assess the involvement of Piezo1 in Yoda1-evoked Ca^{2+} entry. Alongside, novel Yoda1 analogues (Section 2.1) were tested for their ability to induce Ca^{2+} influx or inhibit Yoda1-evoked Ca^{2+} entry in cells overexpressing Piezo1, in order to increase knowledge of the structure-activity relationship for Yoda1 activation of Piezo1. Finally, various methods were then used to mechanically activate cardiac fibroblasts; it was investigated whether cardiac fibroblasts displayed Piezo1-like currents following hypotonicity (Section 2.3.4) or pressure patch-clamp recording experiments (Section 2.11.1).

3.4 Results

3.4.1 Characterisation of murine cardiac fibroblasts

To study Piezo1 in cultured cardiac fibroblasts, it was imperative to ensure that fibroblast cell cultures were not contaminated with endothelial cells, cells known to contain high levels of Piezo1 (Li *et al.* 2014). Immunocytochemistry of cultured murine cardiac fibroblasts was used to verify that cells exhibited the expected myofibroblast phenotype which is classically observed in cultured fibroblasts mechanically activated by the rigid plastic of cell culture (Hinz *et al.* 2007). It was confirmed that cells stained positively for vimentin and α-smooth muscle actin (α-SMA) and that no cells stained positively for the endothelial marker PECAM-1 (CD31) (Figure 3.1). HUVECs were stained for PECAM-1 alongside, as a positive control (Figure 3.1). Negative control staining without any primary antibody applied was performed to illustrate that secondary antibody was not binding non-specifically (Figure 3.1).

RT-PCR analysis of cultured murine cardiac fibroblasts revealed low levels of *Pecam1* mRNA and an absence of alpha-myosin heavy chain (*Myh6*) mRNA, a cardiac myocyte marker, but much higher mRNA expression of two common fibroblast markers, discoidin domain-containing receptor 2 (*Ddr2*) and platelet derived growth factor receptor alpha (*Pdgfra*) (Figure 3.2).

Throughout this study, the FlexStation and the Ca^{2+} indicator, Fura-2, were used to record intracellular Ca^{2+} events. VEGF binds to receptors on endothelial cells; cardiac fibroblasts do not express these receptors. VEGF was able to induce Ca^{2+} entry in HUVECs as expected, whereas murine cardiac fibroblast cultures were unresponsive to VEGF, further confirming that cardiac fibroblast cultures were free of endothelial cell contamination (Figure 3.3).

These data indicate that the cells present in our cultures are cardiac fibroblasts, the majority of which showed a myofibroblast phenotype, with no evidence for contamination by other cell types.

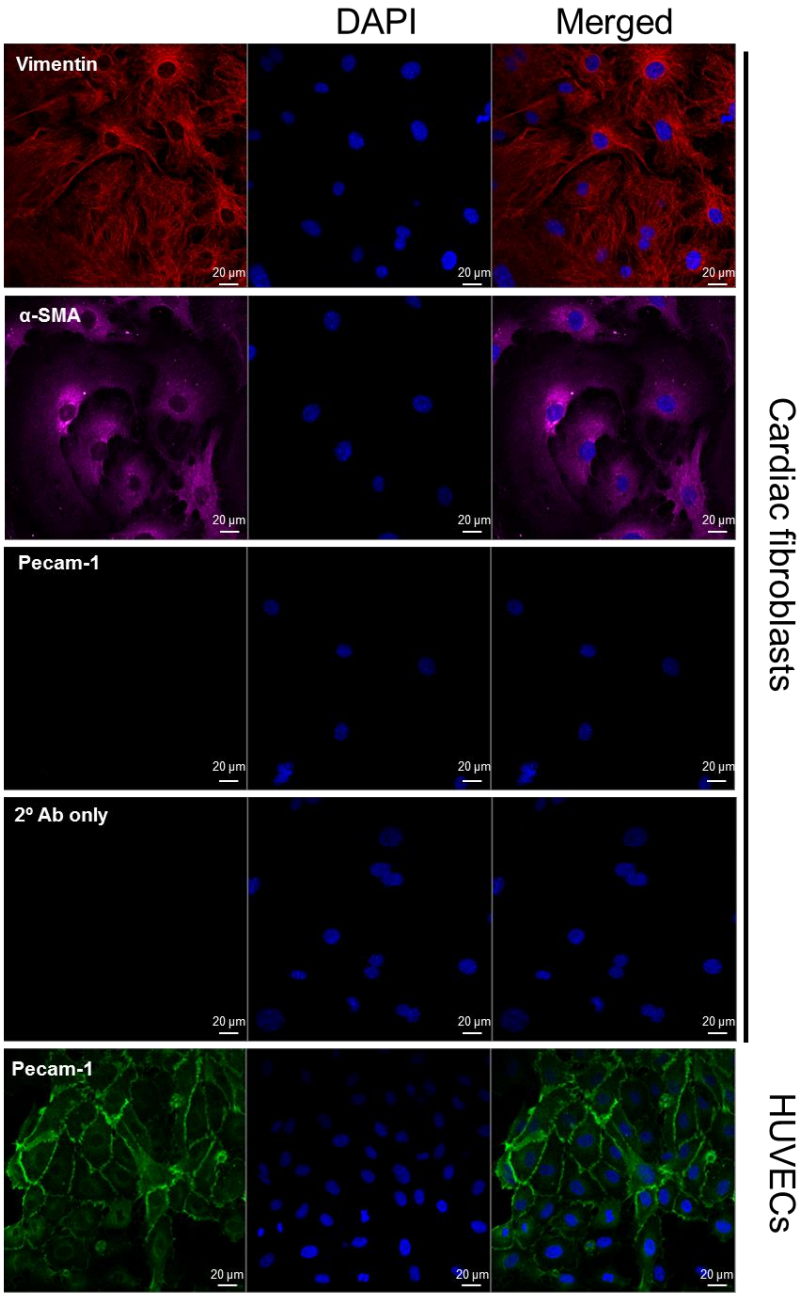

Figure 3.1 Characterisation of murine cardiac fibroblasts using immunocytochemistry. Representative images of cultured murine cardiac fibroblasts stained for vimentin (red), α-SMA (purple) and PECAM-1 (green). HUVECs are stained for PECAM-1 (green) as a positive control in the bottom panel. DAPI staining (blue) identifies nuclei. Secondary antibody only staining (without primary antibody) in cardiac fibroblasts acts as a negative control. Scale bar = 20 μm.

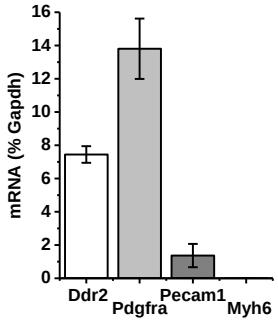

Figure 3.2 Cell-specific markers in cultured murine cardiac fibroblasts. RT-PCR analysis of various cardiac cell markers: *Ddr2*, *Pdgfra* (both fibroblast markers), *Pecam1* (endothelial cell marker) and *Myh6* (cardiomyocyte marker) in cultured murine cardiac fibroblasts (n=3). Expression levels expressed as a % of the housekeeping gene, *Gapdh*.

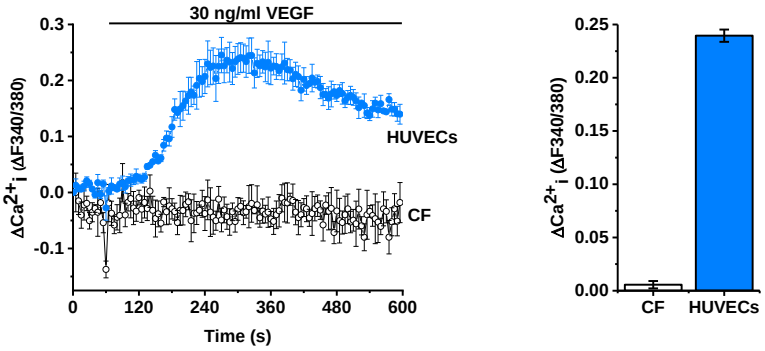

Figure 3.3 Response of cultured murine cardiac fibroblasts to VEGF. Representative intracellular Ca^{2+} traces, using the FlexStation and the Ca^{2+} indicator, Fura-2, when cultured murine cardiac fibroblasts and HUVECs were applied with 30 ng/mL VEGF at 60 seconds. The maximum Ca^{2+} entry induced is utilised for the mean data, which is shown in a bar chart (n/N=2/6).

3.4.2 Detection of Piezo1 expression in cardiac fibroblasts

Despite knowledge that *Piezo1* mRNA can be detected in mouse heart (Coste *et al.* 2010), it is currently unknown whether Piezo1 is expressed in cardiac fibroblasts. Experiments were undertaken to measure *Piezo1* mRNA expression in cultured human and mouse cardiac fibroblasts and mouse cardiac cell fractions, and Piezo1 protein expression was investigated in cultured mouse cardiac fibroblasts.

3.4.2.1 *Piezo1* mRNA is expressed in cultured cardiac fibroblasts

For the accurate comparison of gene expression by RT-PCR, it is imperative to know the efficiency of the primers used (Svec *et al.* 2015). The efficiencies of the primers used to analyse *Piezo1* and *Piezo2* mRNA expression were calculated (Figure 3.4A); here, the efficiencies were 97 % and 83 %, respectively. Primer efficiencies were taken into account when calculating the relative messenger RNA expression levels of *Piezo1* and *Piezo2*. Messenger RNA encoding Piezo1 was detected at a higher level than Piezo2 in cultured murine cardiac fibroblasts (Figure 3.4B,C).

Messenger RNA encoding Piezo1 was detected in both murine and human cultured cardiac fibroblasts (Figure 3.5). *Piezo1* mRNA expression levels in murine cardiac fibroblasts were similar to those observed in murine pulmonary endothelial cells (Figure 3.5). *PIEZO1* mRNA expression levels in human cardiac fibroblasts were observed to be 25% higher than in human saphenous vein endothelial cells and double that in HUVECs (Figure 3.5); cells known to express high levels of *Piezo1* mRNA (Li *et al.* 2014). These data confirm Piezo1 is expressed in cardiac fibroblasts at similar levels to those found in endothelial cells from various sources.

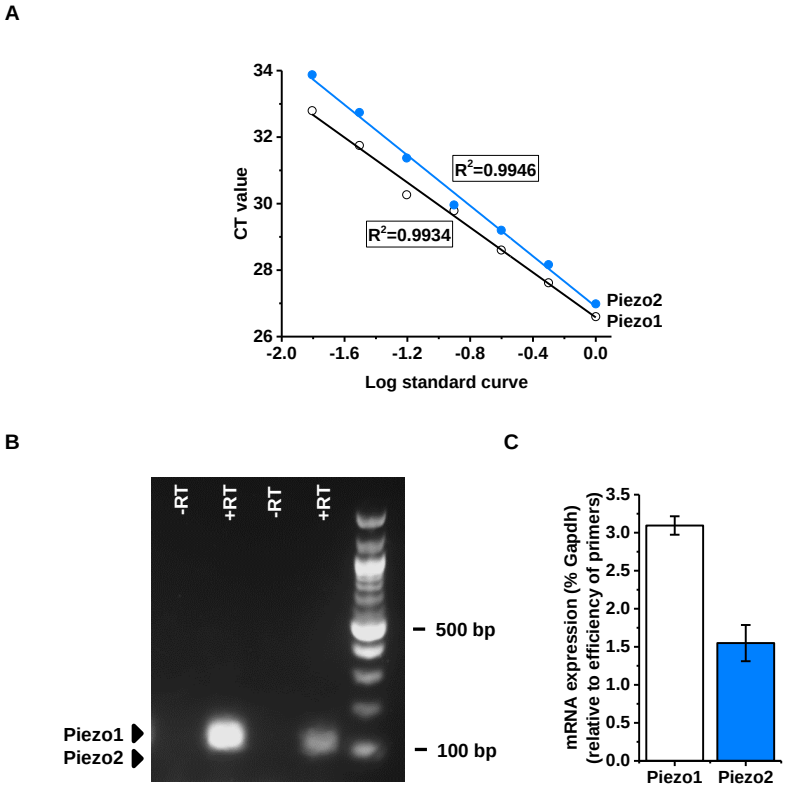

Figure 3.4 Expression levels of *Piezo1* and *Piezo2* mRNA in murine cardiac fibroblasts. (A) Graph illustrating the efficiency of the primers used during RT-PCR analysis of *Piezo1* and *Piezo2* mRNA expression, the R^2 value is indicated next to each line. Efficiencies: *Piezo1* primers: 97 %, *Piezo2* primers: 83 %. **(B)** End-point PCR products obtained using primers for *Piezo1* and *Piezo2* in murine cardiac fibroblasts. Lanes with (+RT) and without (-RT) reverse transcriptase reaction are indicated; this was performed to confirm there was no genomic DNA contamination. **(C)** Mean data of *Piezo1* and *Piezo2* mRNA expression as a % of housekeeping control (*Gapdh*), relative to the efficiency of each primer set (n=3).

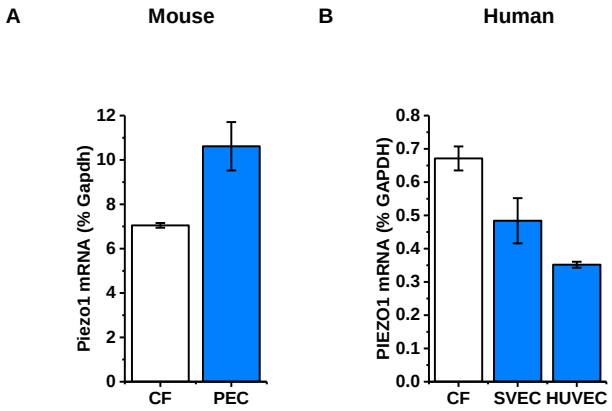

Figure 3.5 Expression of *Piezo1* mRNA in cultured murine and human cardiac fibroblasts in comparison to endothelial cells. RT-PCR analysis of *Piezo1* mRNA expression in **(A)** murine cardiac fibroblasts (CF; n=3) compared to pulmonary endothelial cells (PEC; n=5) and **(B)** human cardiac fibroblasts (CF; n=6) compared to human saphenous vein endothelial cells (SVEC, n=3) and human umbilical vein endothelial cells (HUVEC; n=3). Expression measured as % of housekeeping control (*Gapdh/GAPDH*).

3.4.2.2 *Piezo1* mRNA is expressed in the fibroblast fraction of the heart

A magnetic antibody cell separation (MACS) technique (Bageghni *et al.* 2018) was used to successfully separate cell types isolated from mouse heart, as shown by RT-PCR analysis of different fractions with cell-specific markers. It was verified that the fibroblast-enriched fraction had much higher expression of *Col1a2* mRNA than the endothelial cell-enriched fraction (50-fold higher) and separately isolated mouse cardiomyocytes (230-fold higher) (Figure 3.6). In addition, the endothelial cell-enriched fraction exhibited a much higher mRNA level of the endothelial marker *Pecam1* (CD31) than the fibroblast and myocyte fractions (Figure 3.6). Isolated cardiomyocytes expressed almost 10 times the mRNA expression of *Myh6* than the other fractions (Figure 3.6). This validated our separation technique.

Housekeeping genes should not vary in the samples under investigation or in response to treatment. It has been demonstrated that housekeeping gene expression can fluctuate considerably and it has been suggested that, in order to calculate expression levels accurately, values should be normalised to multiple housekeeping genes, rather than only one (Vandesompele *et al.* 2002). With this in mind, expression levels of *Piezo1* mRNA in cardiac cell types were normalised using geometric averaging of multiple internal control genes (*Gapdh*, *Actb* and *Hprt*). It was confirmed that *Piezo1* mRNA was expressed in the fibroblast-enriched (*Col1a2*-positive) fraction of freshly isolated cells from mouse heart at approximately two-thirds of the level of that in the endothelial cell-enriched (*Pecam1*-positive) fraction (Figure 3.7). The level of *Piezo1* expression in murine cardiac fibroblasts is displayed alongside data which demonstrates much lower expression of *Piezo1* mRNA in murine cardiac myocytes (Figure 3.7). These data further confirm that Piezo1 is expressed in murine cardiac fibroblasts and illustrate that cardiac fibroblasts and endothelial cells are the major cell types expressing Piezo1 in the heart, whilst cardiomyocytes have relatively low expression in comparison.

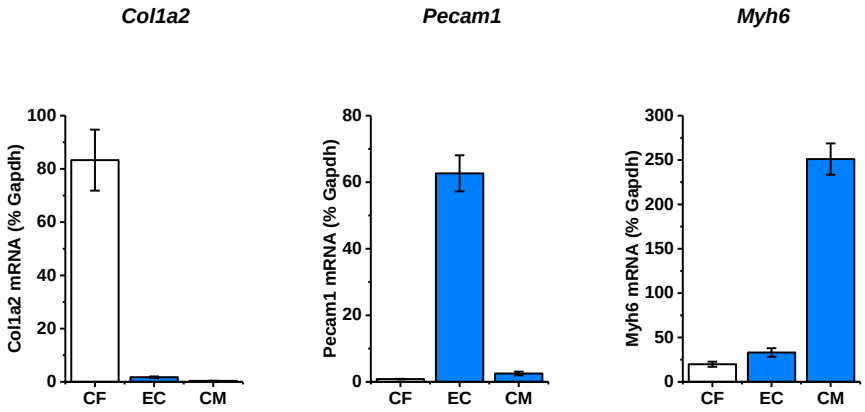

Figure 3.6 Validation of the separation of cardiac cell types using cell-specific markers. RT-PCR analysis of *Col1a2* (fibroblast marker), *Pecam1* (endothelial cell marker) and *Myh6* (cardiomyocyte marker) mRNA expression in the fibroblast-enriched fraction (CF) and endothelial cell-enriched fraction (EC) isolated from murine heart using magnetic antibody cell separation technique (n=4), compared to the expression in freshly isolated cardiomyocytes (CM) from different mice (n=3). Expression measured relative to housekeeping control (*Gapdh*).

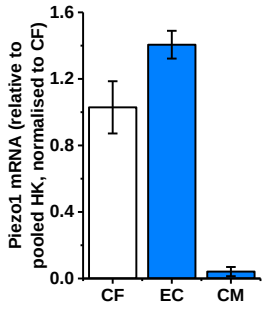

Figure 3.7 *Piezo1* mRNA expression in the fibroblast fraction of the whole heart. RT-PCR analysis of *Piezo1* mRNA expression in the fibroblast-enriched fraction (CF) and endothelial cell-enriched fraction (EC) isolated from murine heart using magnetic antibody cell separation technique (n=4) compared to in freshly isolated cardiomyocytes (CM) from different mice (n=2). Expression was measured relative to 3 different housekeeping genes (*Gapdh*, *Actb*, *Hprt*) and normalised to CF.

3.4.2.3 Piezo1 protein is detected in murine cardiac fibroblasts

Commercially available anti-Piezo1 antibodies are non-specific, and are unable to convincingly detect endogenous Piezo1. To overcome this, CRISPR-Cas9 technology was used to develop a transgenic mouse globally expressing a mutated hemagglutinin (HA)-tagged version of Piezo1 (Piezo1-HA) at endogenous levels. This HA tag enables the identification of Piezo1 using anti-HA antibodies by western blotting. Piezo1-HA was expressed in cardiac fibroblasts isolated from a Piezo1-HA homozygote mouse and, as expected, was expressed at lower levels in a Piezo1-HA heterozygous mouse; no band was detected in a WT mouse (Figure 3.8). This confirms that mRNA is translated and Piezo1 protein is expressed in murine cardiac fibroblasts.

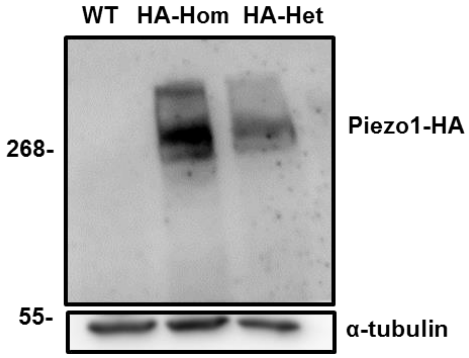

Figure 3.8 Detection of Piezo1 protein in murine cardiac fibroblasts. Piezo1 protein detected by western blotting in cardiac fibroblasts isolated from a CRISPR-generated murine model in which native Piezo1 was modified to contain a HA tag. Samples from a WT mouse, a mouse heterozygous for Piezo1-HA and a mouse homozygous for Piezo1-HA were immunoblotted with anti-HA antibody, followed by an α-tubulin antibody to confirm equal protein loading. A band was detected at the expected size: 295 kDa.

3.4.3 Expression of *Piezo1* mRNA in cardiac fibroblasts is unaltered by various stimuli

Knowledge of how the Piezo1 gene is regulated is limited. Therefore, investigation was undertaken to understand whether the expression of Piezo1 was affected by stimuli which are important in fibroblast function.

3.4.3.1 Confluency of cardiac fibroblasts has no effect on *Piezo1* mRNA expression

It has been reported that Piezo1 may act as a homeostatic sensor to control epithelial cell numbers. When epithelial cells become too crowded, they activate Piezo1 to trigger extrusion and apoptosis of cells (Eisenhoffer *et al.* 2012). Conversely, Gudipaty *et al.* (2017) found that cell division occurs in regions of low cell density, where epithelial cells are stretched, through activation of the Piezo1 channel. Therefore, Piezo1 appears to act as a homeostatic sensor to control epithelial cell numbers by participating in these two opposing processes. For this reason, it was examined whether confluency of cardiac fibroblasts had an effect on *Piezo1* mRNA expression. Murine cardiac fibroblasts were plated at varying densities and RNA was extracted 48 h later; there was no significant change in *Piezo1* mRNA expression between different conditions (Figure 3.9). This established that plating cells at different densities during experimentation was unlikely to have an effect on results as *Piezo1* mRNA expression would be unchanged.

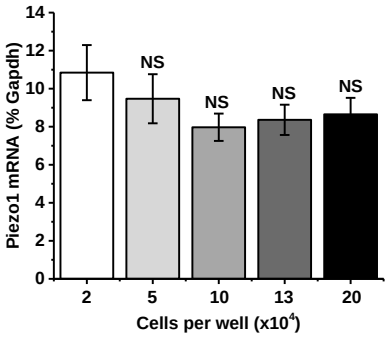

Figure 3.9 Effect of cell confluency on *Piezo1* mRNA expression in murine cardiac fibroblasts. RT-PCR analysis of *Piezo1* mRNA in murine cardiac fibroblasts plated at different levels of confluency, ranging from 2-20 x 10^4 cells per well of a 12 well plate, prior to RNA extraction 48 h later. Expression is measured as % of housekeeping control (*Gapdh*), P=NS, not significant following an ANOVA with Tukey's post-hoc test (n=3).

3.4.3.2 Cytokines do not affect *Piezo1* mRNA expression in murine cardiac fibroblasts

Two main stimuli have been reported to promote cardiac fibroblast differentiation: TGF-β1, a cytokine which is produced at the onset of pathology (Dobaczewski et al., 2010), and mechanical stress (Hinz *et al.* 2001). Cardiac fibroblasts stimulated with TGF-β1 *in vitro* have accelerated differentiation into myofibroblasts, measured by increased α-SMA expression and collagen synthesis (Samuel *et al.* 2004). Conversely, IL-1α has an inhibitory effect on the phenotypic switch of human cardiac fibroblasts to myofibroblasts induced by TGF-β1. For example, IL-1α has been shown to inhibit TGF-β1-induced increase in α-SMA protein expression and collagen gel contraction in human cardiac fibroblasts (van Nieuwenhoven *et al.* 2013). Therefore, with respect to myofibroblast differentiation, TGF-β1 and IL-1α have opposing effects in cardiac fibroblasts.

It was investigated whether modifying the differentiation state of cardiac fibroblasts using these factors had an effect on *Piezo1* mRNA expression. RT-PCR analysis of *Piezo1* mRNA expression revealed no change when murine cardiac fibroblasts were treated for 24 h with increasing concentrations of TGF-β1 or IL1-α, compared to cells treated with vehicle (Figure 3.10A,B). Hence, altering the differentiation state of cardiac fibroblasts did not affect expression of *Piezo1* mRNA. This is important as prolonged culture of cardiac fibroblasts leads to their differentiation (Santiago *et al.* 2010); these data give confidence that this will not affect the investigation into the role of Piezo1.

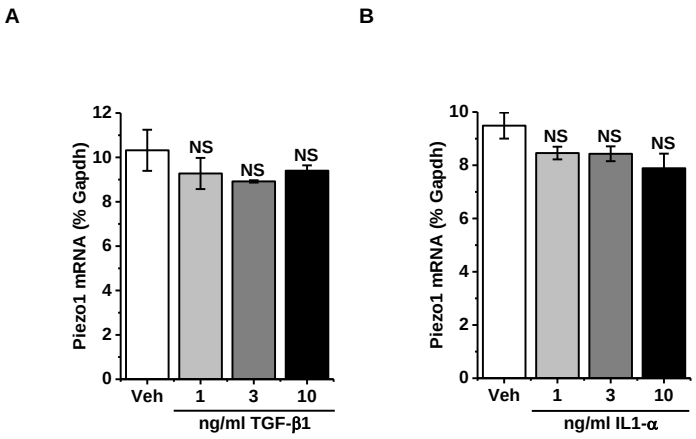

Figure 3.10 Effect of cytokines on *Piezo1* mRNA expression in murine cardiac fibroblasts. RT-PCR analysis of *Piezo1* mRNA in murine cardiac fibroblasts treated for 24 h with various concentrations of **(A)** TGF-β1 or **(B)** IL1-α, compared to cells treated with vehicle. Expression is measured as % of housekeeping control (*Gapdh*), P=NS, not significant following an ANOVA with Tukey's post-hoc test (n=3).

3.4.3.3 Mechanical stress has no effect on *Piezo1* mRNA expression

Piezo1 is a mechanosensitive ion channel, therefore it was investigated whether the application of mechanical stimuli to cardiac fibroblasts had an effect on *Piezo1* mRNA expression. Jin *et al.* (2015) have previously demonstrated that mechanical activation due to compressive stimuli significantly upregulated *Piezo1* mRNA expression after 30 min in human periodontal ligament cells and this was maintained over a 12 h time period. Three methods were employed to apply mechanical stress to cells; namely shear stress, altered substrate stiffness and cyclic stretch.

Shear stress applied to cells at ~10 dyn.cm^{-2} using an orbital shaker for 24 h had no effect on *Piezo1* mRNA expression in murine cardiac fibroblasts, in comparison with cells kept under static conditions (Figure 3.11A).

Mouse cardiac fibroblasts cultured on substrates of 'physiological' stiffness (a Young's elastic modulus of 8 kPa; (Berry *et al.* 2006)) maintain a quiescent phenotype, whereas those cultured on stiffer substrates mimicking fibrosis (20-100 kPa; (Berry *et al.* 2006)) express higher levels of α-SMA and exhibit increased cell area (Herum *et al.* 2017a), indicative of cell differentiation to the myofibroblast phenotype. Murine cardiac fibroblasts were grown on tailored culture substrates (10 kPa, 30 kPa and tissue culture plastic which is approximately 1x10^{6} kPa) for 24 h. Cells showed a trend for decreased expression of *Piezo1* mRNA with decreased stiffness of substrate (10 kPa) but this was not quite statistically significant, possible due to the low number of replicates (Figure 3.11B).

Cardiac fibroblasts are exposed to cyclic mechanical stretch with every heartbeat, at a frequency of ~1 Hz in humans. When cyclic stretch was applied to human cardiac fibroblasts for 6 h at 1 Hz, *PIEZO1* mRNA expression was unaltered, compared with cells kept under static conditions (Figure 3.11C). Together, these data convey that *Piezo1* mRNA expression in cardiac fibroblasts is unchanged when cells are activated using "outside-in" mechanical forces, i.e. forces arising from shear flow or stretch. However, *Piezo1* mRNA expression may be upregulated cells when cells actively generate mechanical forces, for example, while probing the stiffness of the ECM.

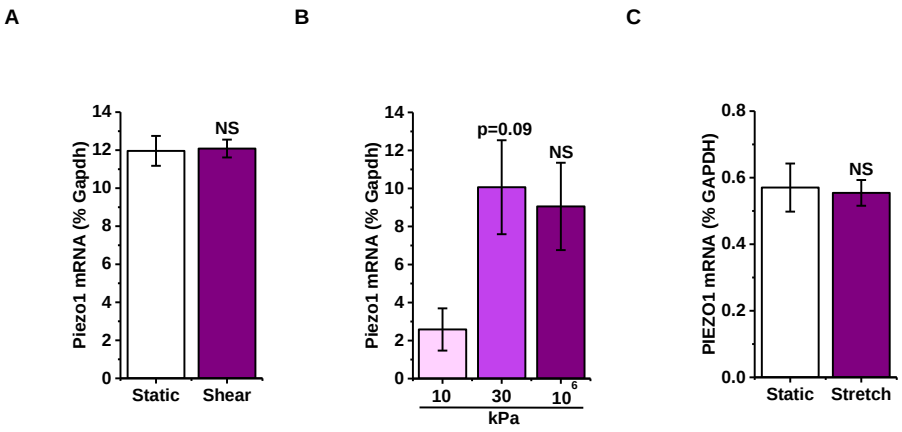

Figure 3.11 Effect of mechanical stimuli on *Piezo1* mRNA expression levels. **(A)** RT-PCR analysis of *Piezo1* mRNA levels in murine cardiac fibroblasts stimulated with shear stress via an orbital shaker for 24 h, compared to cells kept under static conditions, P=NS, not significant following a t-test (n=3). **(B)** RT-PCR analysis of *Piezo1* mRNA expression in murine cardiac fibroblasts grown on substrates of differing stiffness: 10 kPa, 30 kPa and tissue culture plastic which is approximately 10^6 kPa for 24 h, P=0.09, P=NS, not significant following an ANOVA with Tukey's post-hoc test (n=3). **(C)** RT-PCR analysis of *PIEZO1* mRNA levels in human cardiac fibroblasts stimulated with 6 h cyclic stretch (1 Hz, 10 % stretch), in comparison with cells kept under static conditions, P=NS, not significant following a t-test (n=3). All expression levels are expressed relative to the relevant housekeeper, *Gapdh*/*GAPDH*.

3.4.4 Novel small modulators of Piezo1

Pharmacological compounds which selectively modulate Piezo1 channels are attractive laboratory tools as they allow for study of the channel without the need for mechanical force. The first chemical activator of Piezo1, named Yoda1, was discovered by Syeda *et al.* (2015) and has since been widely used to investigate Piezo1 channel pharmacology. A library of ~3.25 million compounds was screened as activators of Piezo1 or Piezo2 using high-throughput Ca^{2+} imaging. Yoda1 was found to be an agonist of both human and mouse Piezo1 when overexpressed in otherwise Piezo1-null cells and was, importantly, unable to activate the Piezo2 channel (Syeda *et al.* 2015). The compound was able to activate purified Piezo1 channels reconstituted in an artificial bilayer, indicating that Yoda1 can activate Piezo1 channels in the absence of other cellular components (Syeda *et al.* 2015). Yoda1-induced Ca^{2+} entry was dependent on calcium influx, as the chelation of extracellular calcium using EGTA dramatically reduced responses, whilst depletion of intracellular calcium stores had no effect (Syeda *et al.* 2015). Yoda1 was utilised in the present study to investigate endogenously-expressed Piezo1 channels in cardiac fibroblasts.

3.4.4.1 Validation of the process used for screening Yoda1 analogues

Piezo1 pharmacology is limited; inhibitors of the channel are restricted and these tend to be general inhibitors of many mechanosensitive channels (Coste *et al.* 2010). Although Yoda1 is a useful research tool for facilitating the study of Piezo1 channels, its solubility is poor (Syeda *et al.* 2015). To develop improved Piezo1 modulators, increased knowledge of the structure-activity relationship for Yoda1 activation of Piezo1 is essential. The Department of Chemistry at the University of Leeds synthesised Yoda1 analogues and, as part of this project, these were tested against the Piezo1 channel in the search for an improved agonist or a specific antagonist of the Piezo1 channel.

To reliably study the effects of Yoda1 analogues on overexpressed Piezo1 channels, tetracycline-inducible human Piezo1 was stably incorporated into HEK 293 T-REx™ cells. These cells, referred to as HEK-T-REx-hPiezo1 throughout, expressed *PIEZO1* mRNA following tetracycline induction (Figure 3.12A). *PIEZO1* mRNA expression was not observed in control ‘WT’ HEK 293 T-REx™

cells without Piezo1 incorporation (referred to as HEK-T-REx) (Figure 3.12A). Similarly, western blotting with an anti-Piezo1 antibody confirmed Piezo1 protein expression following induction with tetracycline in HEK-T-REx-hPiezo1 cells but not in control HEK-T-Rex cells. (Figure 3.12B). Therefore, these cells could be used as a model with which to investigate Piezo1 activation by analogues of Yoda1.

Intracellular Ca^{2+} was measured prior to, and after, application of various concentrations of Yoda1. As expected, Yoda1 increased the levels of intracellular Ca^{2+} in HEK-T-REx-hPiezo1 cells (Figure 3.13A). Due to poor solubility of Yoda1, the recommended maximum concentration of Yoda1 is 10-20 μM (Syeda et al., 2015). HEK-T-REx-hPiezo1 cells applied with tetracycline displayed a concentration-dependent Ca^{2+} entry in response to Yoda1, with an EC_{50} of 1.85 μM (Figure 3.13A). No Ca^{2+} entry was observed in cells treated with vehicle (DMSO) (Figure 3.13A). Control HEK-T-REx cells exhibited a lack of Ca^{2+} entry when treated with Yoda1 (Figure 3.13B); cells were viable, as shown by the Ca^{2+} influx in response to ATP.

In order to confirm that Yoda1 could also activate mouse Piezo1 channels, a HEK 293 T-REx™ cell line heterologously expressing mouse Piezo1 was used; these cells will be referred to as HEK-T-REx-mPiezo1 throughout. As expected, Yoda1 also increased the levels of intracellular Ca^{2+} in these cells (Figure 3.14A). The Ca^{2+} entry occurred in a concentration-dependent manner with a Yoda1 EC_{50} of 0.33 μM; no Ca^{2+} influx occurred upon treatment with vehicle (Figure 3.14A). The induction of Ca^{2+} entry was absent in control HEK-T-REx cells (Figure 3.14B), despite a large increase in intracellular Ca^{2+} being observed when ATP was applied. These data confirmed that the experimental detection system for both human and mouse Piezo1 was functioning correctly.

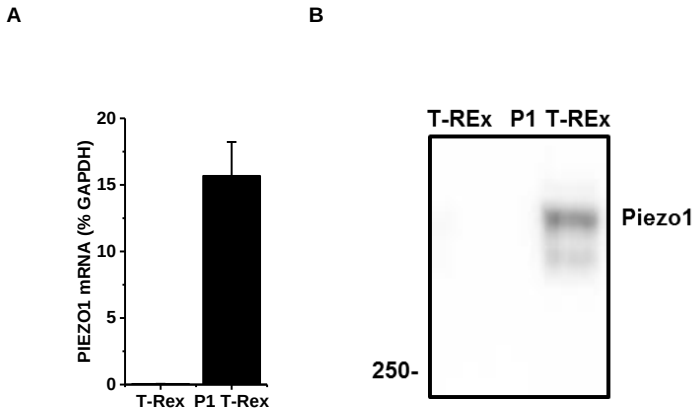

Figure 3.12 Validation of the HEK cell line used for screening Yoda1 analogues. (A) RT-PCR analysis of *PIEZO1* mRNA levels relative to housekeeper (*GAPDH*) in control HEK-T-REx (T-Rex) and Piezo1-expressing HEK-T-REx-hPiezo1 (P1 T-Rex) cells (n=3). **(B)** Western blot performed using the BEEC-4 anti-Piezo1 antibody in HEK-T-REx (T-REx) and HEK-T-REx-hPiezo1 (P1 T-REx) cells. A band was detected at the expected size: 286 kDa.

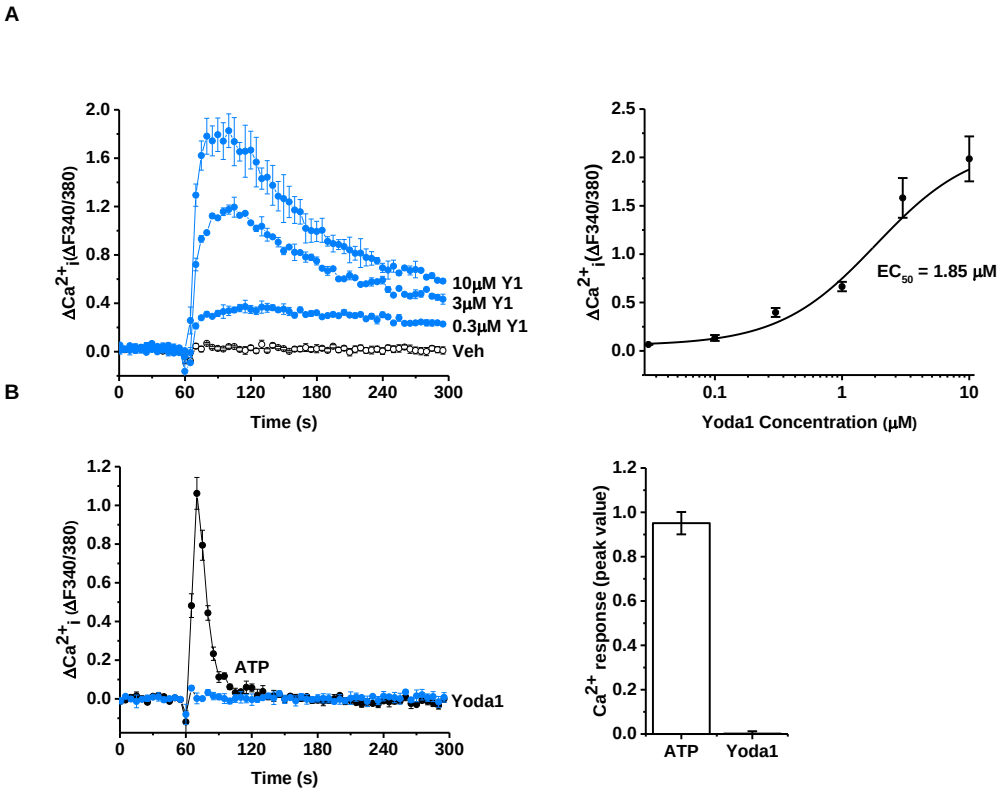

Figure 3.13 Effect of Yoda1 when human Piezo1 is overexpressed in an otherwise null cell line. (A) Ca^{2+} entry evoked by varying concentrations of Yoda1 application at 60 seconds, ranging from 0.03-10 μM in HEK-T-REx-hPiezo1 cells. Vehicle control is illustrated by the open circles. Mean data are displayed as a concentration-response curve and the fitted curve is plotted using a Hill Equation indicating the 50 % maximum effect (EC_{50}) of Yoda1 (n/N=3/9). **(B)** Representative trace and mean data of the Ca^{2+} entry evoked by 10 μM Yoda1 or 20 μM ATP in control T-REx cells without overexpression of human Piezo1 (n/N=3/9).

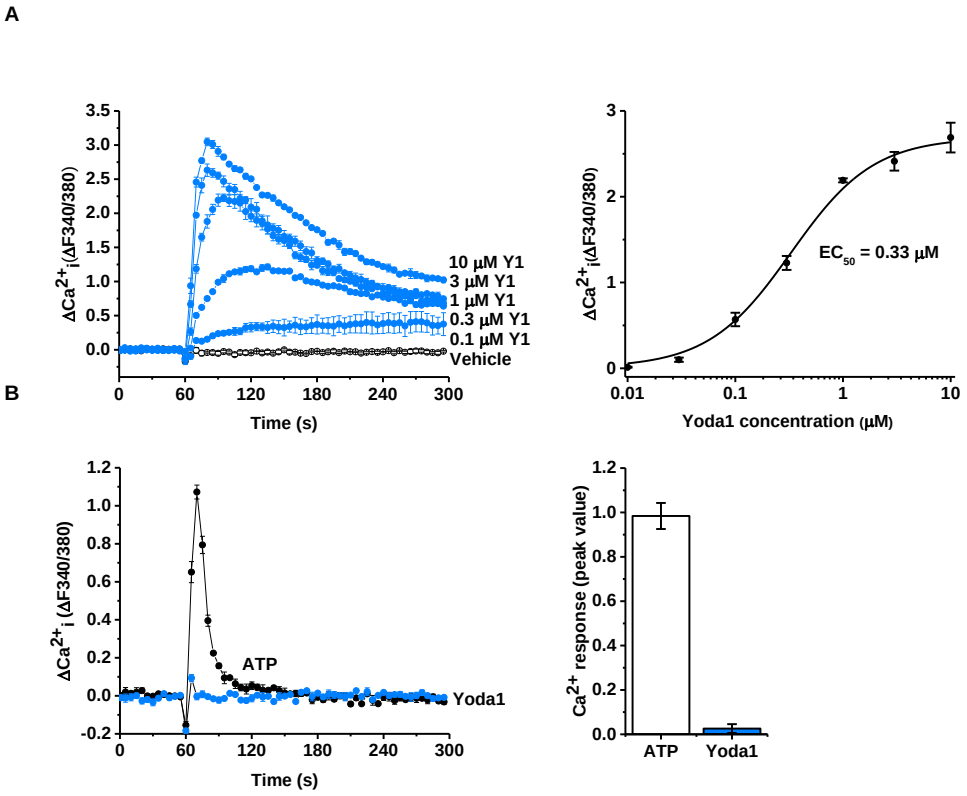

Figure 3.14 Effect of Yoda1 when mouse Piezo1 is overexpressed in an otherwise null cell line. (A) Ca^{2+} entry evoked by varying concentrations of Yoda1 application at 60 seconds, ranging from 0.01-10 µM in HEK-T-REx-mPiezo1 cells. Vehicle control is illustrated by the open circles. Mean data are displayed as a concentration-response curve and the fitted curve is plotted using a Hill Equation indicating the 50 % maximum effect (EC_{50}) of Yoda1 (n/N=3/9). **(B)** Representative trace and mean data of the Ca^{2+} entry evoked by 10 µM Yoda1 or 20 µM ATP in control HEK-T-REx cells without overexpression of mouse Piezo1 (n/N=3/9).

3.4.4.2 Small molecule screening

3.4.4.2.1 Novel Piezo1 agonists

A number of Yoda1 analogues were screened during this study; some are presented and discussed here. Their structures and modifications from Yoda1 are shown in Figure 3.15A. Analogues were screened at a concentration of 10 μM for their ability to cause Ca^{2+} entry in HEK-T-REx-hPiezo1 cells and this was compared with the Ca^{2+} influx observed with the same concentration of Yoda1. Representative intracellular Ca^{2+} traces are shown in Figure 3.17A-D, alongside the mean data (Figure 3.16E). Compounds 2e and 2k/Dooku1 had no effect on intracellular Ca^{2+} levels (Figure 3.16A,D). Compounds 2i and 2j appeared to be partial agonists of the Piezo1 channel but had lower activity than Yoda1 (Figure 3.16B,C).

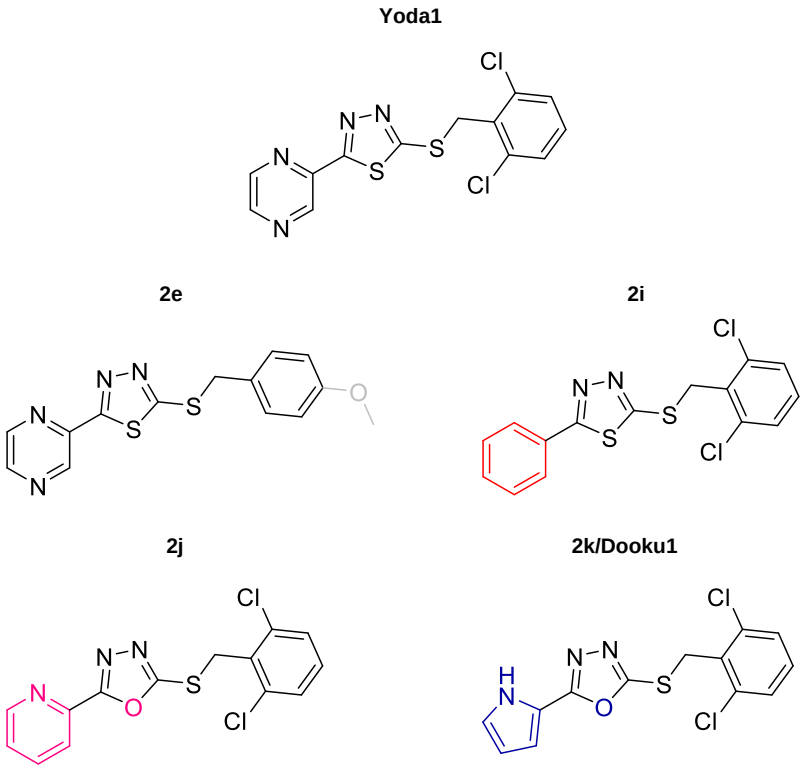

Figure 3.15 Chemical structures of Yoda1 and its analogues. Chemical structures of Yoda1 and some chosen analogues tested in the screen; modifications from the Yoda1 structure are highlighted with colour.

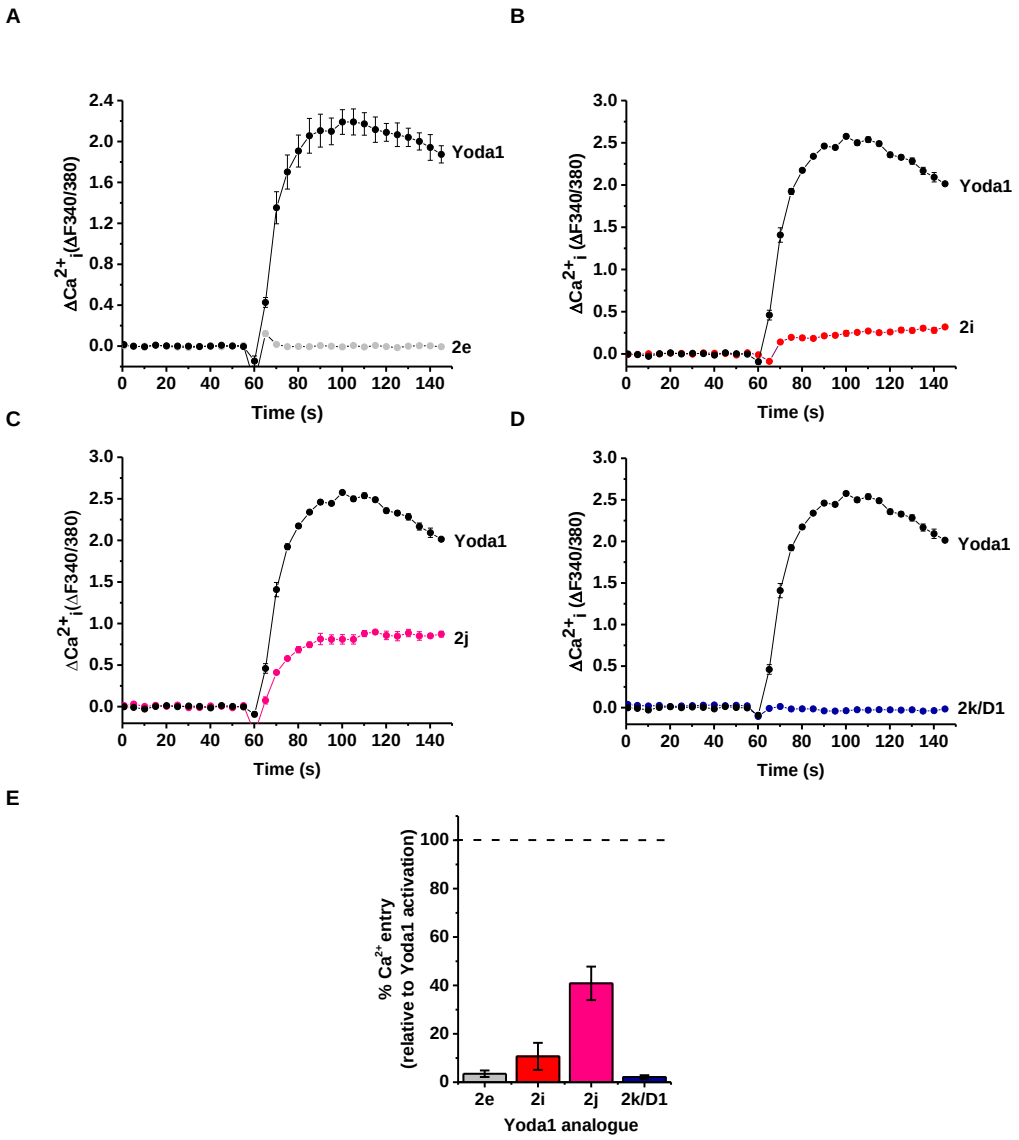

Figure 3.16 Screen of Yoda1 analogues for their ability to induce Ca^{2+} entry in a Piezo1-overexpressing cell line. Intracellular Ca^{2+} measurement representative traces for four analogues of Yoda1 which were tested as part of a larger screen. HEK-T-REx-hPiezo1 cells were exposed to 10 μM Yoda1 alongside **(A)** 2e, **(B)** 2i, **(C)** 2j and **(D)** 2k/Dooku1. **(E)** Mean data are displayed as a bar chart, data are calculated as a % of Yoda1 activation (n/N=5/15).

3.4.4.2.2 Novel Piezo1 antagonists

The same compounds were then tested as antagonists of the Piezo1 channel. 10 µM of each analogue was used to pretreat HEK-T-REx-hPiezo1 cells for 30 min, prior to addition of 2 µM Yoda1. This was then compared to the Ca^{2+} influx in cells pretreated with vehicle alone before application of Yoda1. Representative intracellular Ca^{2+} traces are shown in Figure 3.17A-D, alongside the mean data (Figure 3.17E). It was observed that compound 2e has no effect on Yoda1-evoked Ca^{2+} entry (Figure 3.17A). Due to compound 2e having no agonist or antagonist activity against the Piezo1 channel, it was utilised in future experiments as a negative control to ascertain that effects were Yoda1-specific. Initially, compounds 2i and 2j seemed to inhibit Ca^{2+} entry instigated by Yoda1 (Figure 3.17B,C). However, as was previously illustrated in Figure 3.16C,D, they also had agonist activity against the channel; this is shown once more by the elevated baseline Ca^{2+} signal compared with vehicle control (Figure 3.17B,C). Therefore, these compounds would not be appropriate to be utilised as antagonists of Yoda1. Compound 2k, now known and published as Dooku1 (Evans *et al.* 2018), inhibited Yoda1-evoked Ca^{2+} entry without any agonist activity, as demonstrated by the unchanged baseline Ca^{2+} signal (Figure 3.17D). These initial data highlighted compound 2k/Dooku1 as a potential Yoda1 antagonist. From this point onwards the compound will be referred to as Dooku1.

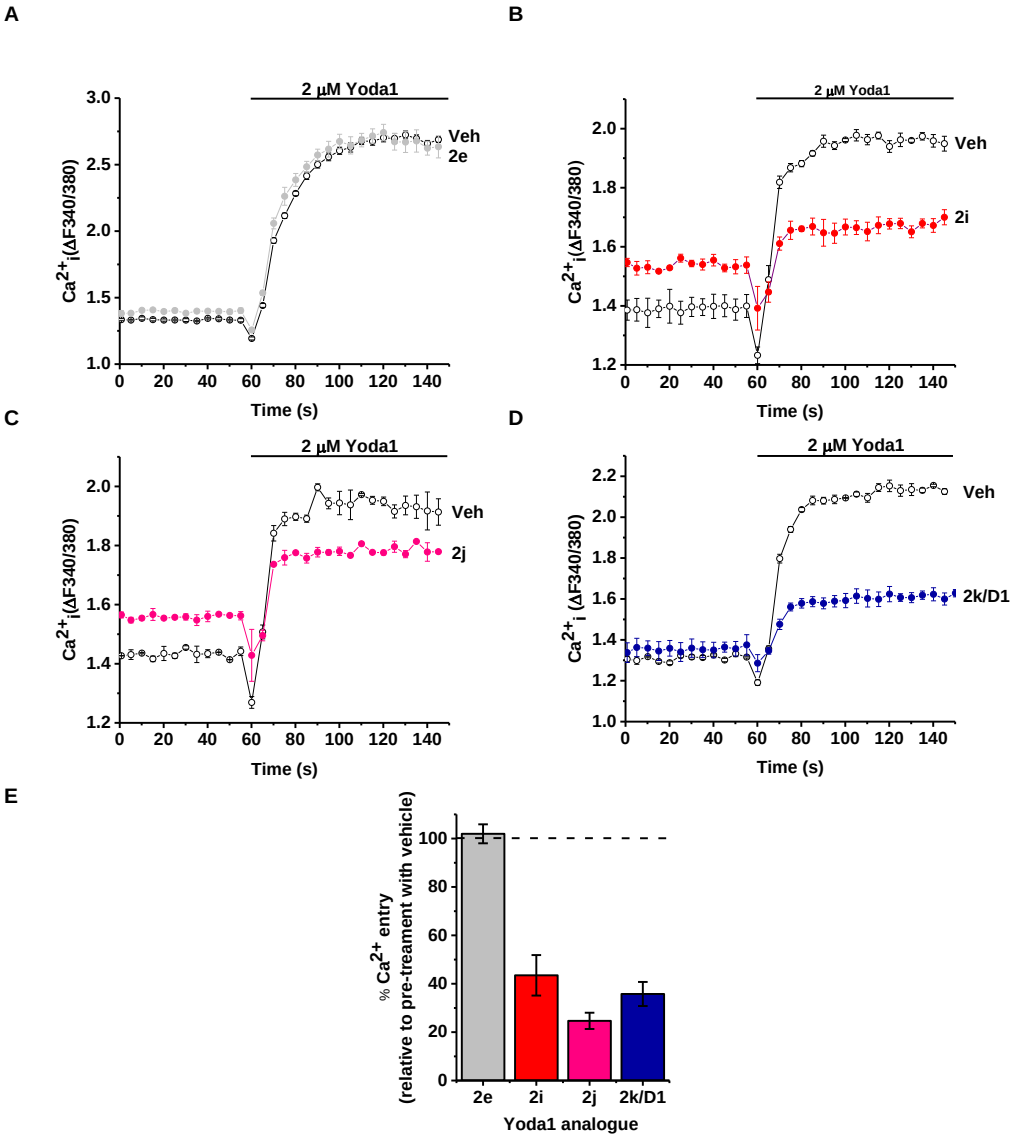

Figure 3.17 Screen of Yoda1 analogues for their ability to inhibit Yoda1-evoked Ca^{2+} entry in a Piezo1-overexpressing cell line. Intracellular Ca^{2+} measurement representative traces for four analogues of Yoda1 which were tested as part of a larger screen. HEK-T-REx-hPiezo1 cells were pretreated with **(A)** 2e, **(B)** 2i, **(C)** 2j or **(D)** 2k/Dooku1 alongside vehicle only (DMSO) for 30 min and then activated using 2 µM Yoda1 at 60 seconds. **(E)** Mean data are displayed as a bar chart, data are calculated relative to the Ca^{2+} response when cells were pretreated with vehicle only (n/N=5/15).

3.4.4.2.3 Identification of Dooku1 as a Yoda1 antagonist

Further experimentation revealed Dooku1 caused a concentration-dependent inhibition of Yoda1-induced Ca^{2+} entry, with an IC_{50} value of 1.30 μM in HEK-T-REx-hPiezo1 cells (Figure 3.18A). 2 μM Yoda1 was used to activate Piezo1 in this assay as this was the approximate EC_{50} value (Figure 3.13). Inhibition was incomplete at 10 μM but higher concentrations of Dooku1 were not investigated due to solubility limitations. The same experiment was performed in HEK-T-REx-mPiezo1 cells; Dooku1 was again able to produce a concentration-dependent inhibition of Yoda1-induced Ca^{2+} entry, with an IC_{50} value of 2.80 μM (Figure 3.18B). Here, 0.5 μM Yoda1 was utilised for activation as this was the respective EC_{50} value (Figure 3.14). Further work on Dooku1 illustrated that this compound was selective for Piezo1 channels and had no effect on ATP-mediated or store-operated Ca^{2+} entry (Evans *et al.* 2018). It was also shown that Dooku1 could inhibit Yoda1-evoked Ca^{2+} influx through endogenous Piezo1 channels in HUVECs (Evans *et al.* 2018).

These data have provided insight into the structure-activity relationship of Piezo1 channel activation by Yoda1, with the goal of generating novel small-molecule tools for investigating Piezo1 channel function. Dooku1 was identified, which effectively antagonises Yoda1-induced Piezo1 channel activity, distinguishing it from constitutive Piezo1 channel activity. As previously discussed, there are emerging roles of Piezo1 in physiology but it is not yet clear whether activating or inhibiting the channel may be advantageous. Gaining knowledge of Piezo1 channel interactions with small molecules promises to be an important aspect of the overall effort to understand Piezo1 biology.

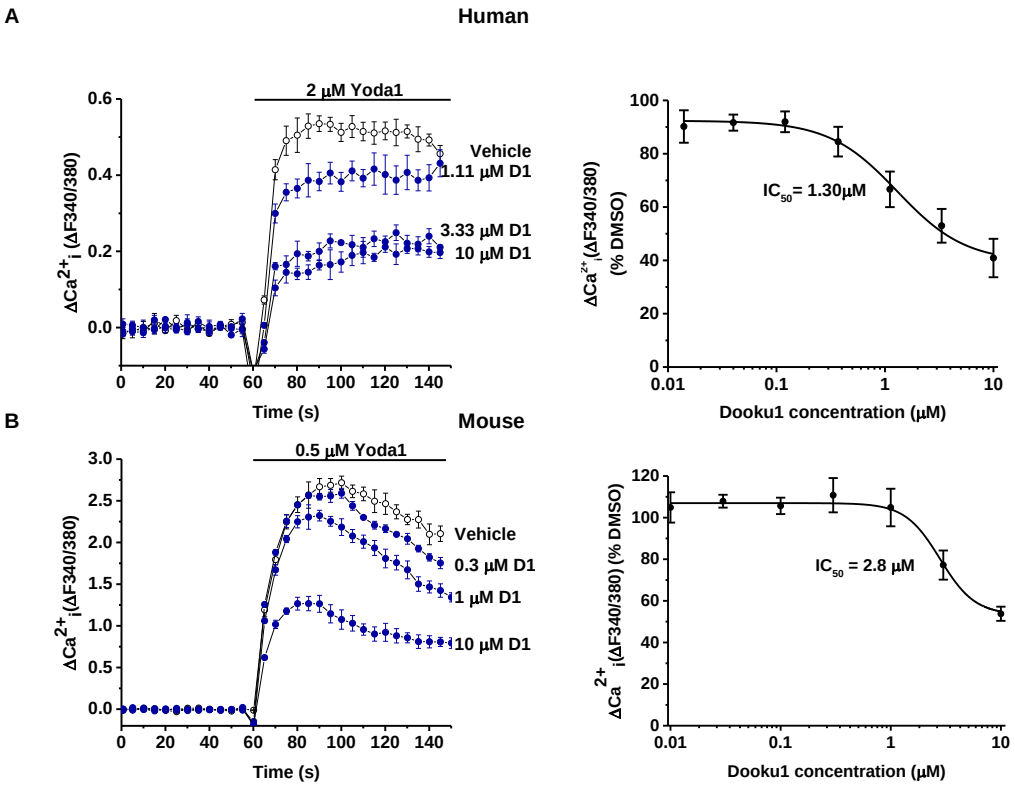

Figure 3.18 Effect of a Yoda1 antagonist, Dooku1, on Yoda1-evoked Ca^{2+} entry through human and mouse Piezo1. Ca^{2+} entry in **(A)** HEK-T-REx-hPiezo1 cells evoked by 2 μM Yoda1 application and **(B)** HEK-T-REx-mPiezo1 cells evoked by 0.5 μM Yoda1 at 60 seconds after cells have been pretreated for 30 min with various concentrations (0.01-10 μM) of Dooku1. Mean data are displayed as concentration-response curves and the fitted curves are plotted using a Hill Equation indicating the 50 % inhibitory effect (IC_{50}) of Dooku1 against Yoda1-evoked Ca^{2+} entry (n/N=3/9).

3.4.5 Piezo1 is a functional ion channel in cardiac fibroblasts

3.4.5.1 Optimising the intracellular Ca^{2+} measurement assay

Having demonstrated that cardiac fibroblasts express Piezo1 mRNA and protein (Section 3.4.2), we proceeded to investigate whether Piezo1 protein was able to form a functional ion channel in these cells. Firstly, it was examined whether Yoda1 could activate endogenous Piezo1 channels in cardiac fibroblasts. Using the standard Fura-2 Ca^{2+} indicator assay, it was revealed that Yoda1 elicited an increase in intracellular Ca^{2+} in murine and human cardiac fibroblasts (Figure 3.19A,B). However, this increase was relatively small and would make future results from experiments manipulating this response difficult to interpret. It was hypothesised that this may be due to extrusion of the Fura-2 indicator in fibroblasts, as has been observed previously in Chinese hamster ovary (CHO) cells (Edelman *et al.* 1994), rather than low Piezo1 activity *per se*. Hence, probenecid, a compound which prevents secretion and sequestration of the Fura-2 indicator (Di Virgilio, Steinberg and Silverstein 1989), was included in the bath solution to enable more robust Ca^{2+} responses to be observed. When probenecid was present in the SBS throughout the experiment, the Ca^{2+} entry signal was amplified by 3-4-fold in both murine and human cardiac fibroblasts; this made results easier to decipher (Figure 3.19A,B). Therefore, this compound was used in all future Ca^{2+} measurements involving cardiac fibroblasts.

In order to determine the optimal cardiac fibroblast number to use for the Fura-2 assay using the FlexStation, varying densities of murine cardiac fibroblasts (20,000-60,000) were plated in 96-well plates. 20,000 cells displayed the optimum Ca^{2+} response to 10 µM Yoda1 (Figure 3.20). Therefore, going forward, murine cardiac fibroblasts were seeded at 20,000 cells per well for FlexStation experiments.

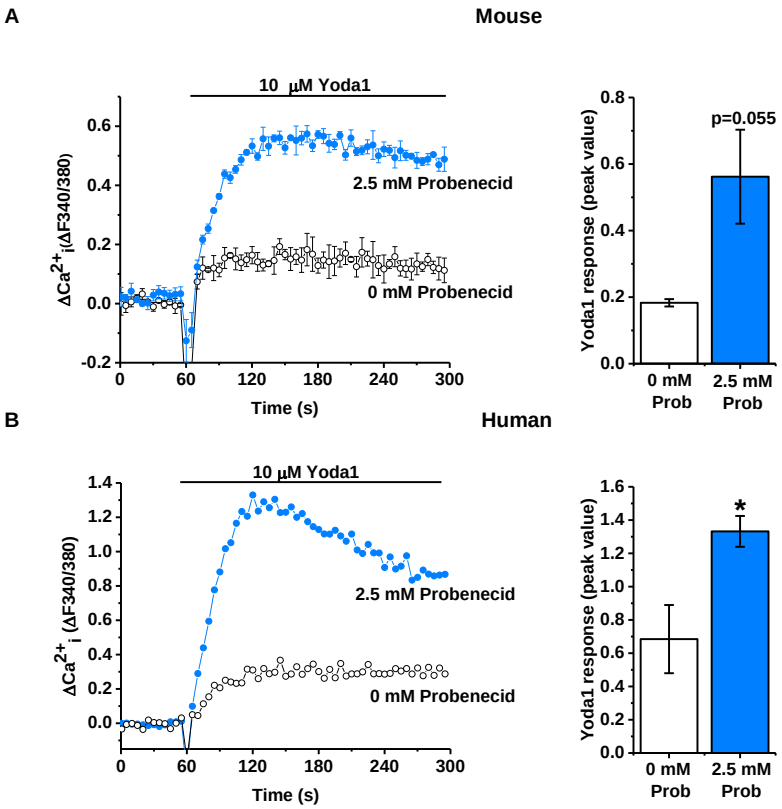

Figure 3.19 Effect of probenecid on the Yoda1-induced Ca^{2+} influx in murine and human cardiac fibroblasts. Representative Ca^{2+} traces illustrating the Ca^{2+} entry evoked by 10 μM Yoda1 in **(A)** murine and **(B)** human cardiac fibroblasts in the presence of 2.5 mM probenecid, compared to 0 mM probenecid in the SBS throughout experimentation. The mean data are displayed as bar charts, *P<0.05 following a t-test (n/N=3/9).

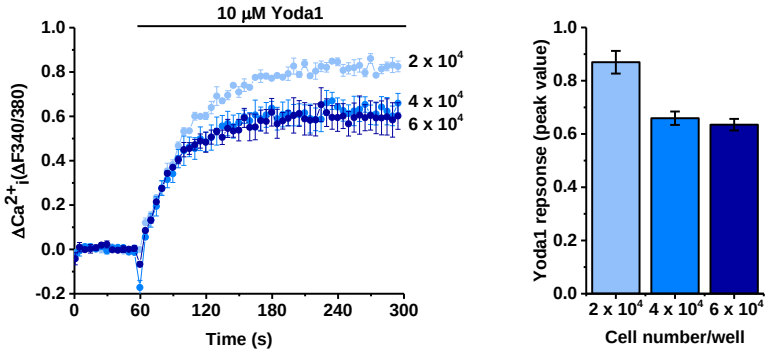

Figure 3.20 Optimisation of cardiac fibroblast cell number for the Fura-2 assay. Representative Ca^{2+} traces illustrating the Ca^{2+} entry evoked by 10 µM Yoda1 in murine cardiac fibroblasts plated at different densities ranging from 20,000 to 60,000 cells/well. The mean data are displayed alongside (n/N=3/9).

3.4.5.2 Yoda1 causes Ca^{2+} entry in murine cardiac fibroblasts

Application of Yoda1 increased intracellular Ca^{2+} levels in a concentration-dependent manner in cardiac fibroblasts with a detectable effect being observed at 0.3 μM and the maximal response at 10 μM; the 50 % maximum effect (EC_{50}) of Yoda1 was calculated to be 0.72 μM (Figure 3.21A). This was almost identical to the EC_{50} generated in human cardiac fibroblasts in similar experiments (0.71 μM) (Figure 3.21B). The poor solubility of Yoda1 limits meaningful interpretation of the EC_{50} value as concentrations above 10uM could not be prepared. These data were highly comparable with those from HEK-T-REx-mPiezo1 cells, in which the EC_{50} of Yoda1 was 0.33 μM (Figure 3.14) or HEK-T-REx-hPiezo1 cells, where the EC_{50} of Yoda1 was 1.85 μM (Figure 3.13). These data confirm that the Piezo1 agonist, Yoda1, causes Ca^{2+} entry in murine and human cardiac fibroblasts.

It was important to confirm that Yoda1 was activating plasma membrane Piezo1 channels and inducing Ca^{2+} entry, rather than causing Ca^{2+} release from intracellular stores. To investigate this, murine and human cardiac fibroblasts were maintained in either media containing EGTA to chelate free Ca^{2+} or in media with physiological levels of extracellular Ca^{2+} (1.5 mM) and activated using Yoda1. The Ca^{2+} signal was abolished completely in human cardiac fibroblasts and reduced by >90 % in murine cardiac fibroblasts when extracellular Ca^{2+} was absent (Figure 3.22A,B), confirming Yoda1 is activating plasma membrane Piezo1 channels. However, as the response was not fully abolished in the absence of extracellular Ca^{2+} in murine cardiac fibroblasts, there is the possibility that some functional Piezo1 channels may be present on intracellular membranes.

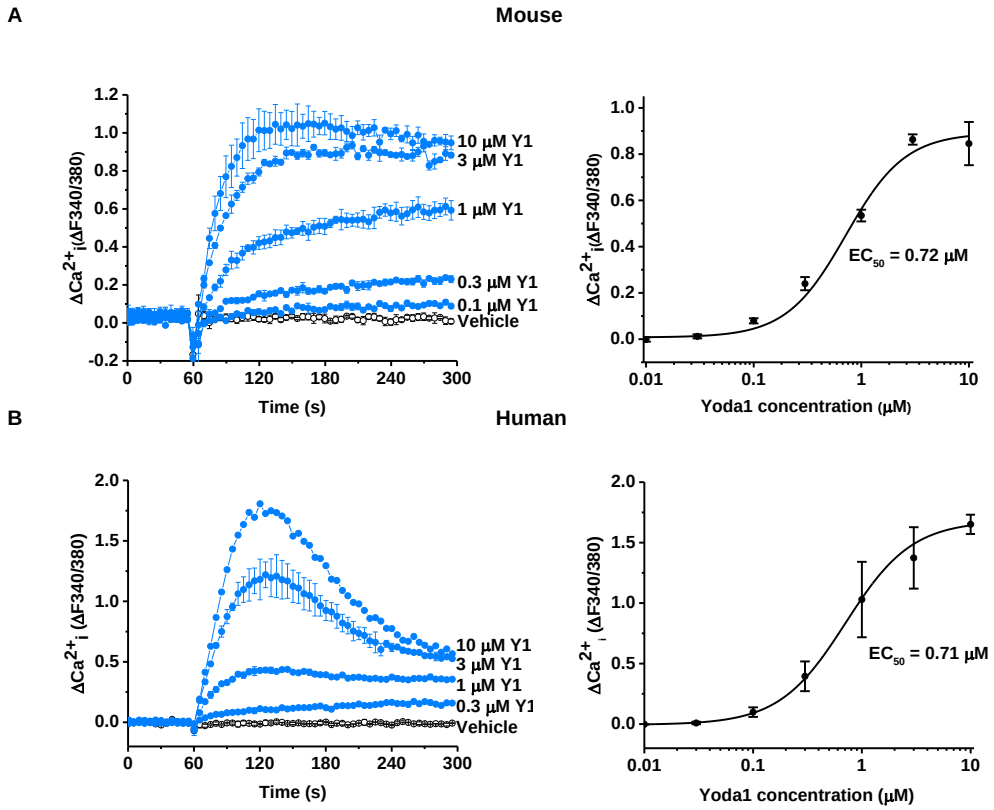

Figure 3.21 Effect of Yoda1 on the intracellular Ca^{2+} concentration in cardiac fibroblasts. Ca^{2+} entry evoked by varying concentrations of Yoda1 (0.01-10 µM) applied at 60 seconds to **(A)** murine and **(B)** human cardiac fibroblasts. Vehicle control is illustrated by the open circles. Mean data are displayed as concentration-response curves and fitted curves are plotted using a Hill Equation indicating the 50 % maximum effect (EC_{50}) of Yoda1 (n/N=3/9).

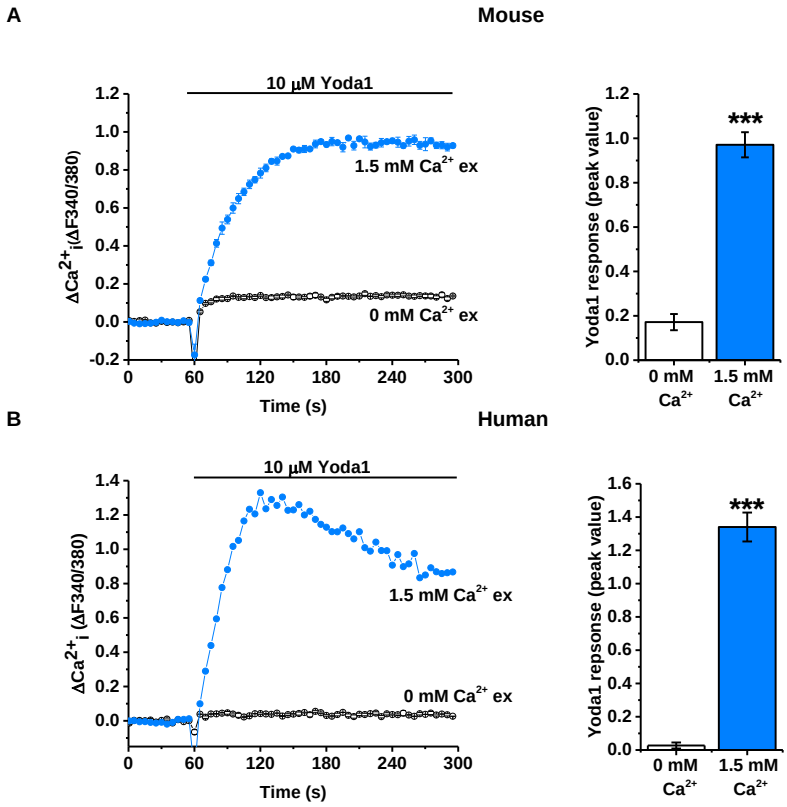

Figure 3.22 Effect of extracellular Ca^{2+} on Yoda1-evoked Ca^{2+} influx in cardiac fibroblasts. Representative Ca^{2+} traces indicating the Ca^{2+} entry evoked by 10 µM Yoda1 in **(A)** murine and **(B)** human cardiac fibroblasts in the presence or absence of extracellular Ca^{2+}. Mean data are shown in bar charts, ***P<0.001 following a t-test (n/N=3/9).

3.4.6 Piezo1 has the expected pharmacological properties in cardiac fibroblasts

After confirming that Yoda1 evokes Ca^{2+} entry in cardiac fibroblasts, it was essential to investigate if this was Piezo1-mediated. Therefore, chemical inhibition of Piezo1 was explored. Gadolinium and ruthenium red, both non-specific inhibitors of mechanosensitive ion channels including Piezo1 (Coste *et al.* 2010), were used to inhibit Yoda1-evoked Ca^{2+} entry. Yoda1 was used at a sub-maximal dose of 2 μM, which was estimated to be the approximate EC_{85} in both murine and human cardiac fibroblasts (Figure 3.21A,B). Murine cardiac fibroblasts pre-incubated with either of the two inhibitors exhibited significantly reduced Yoda1-evoked Ca^{2+} entry (>70 % reduction in both cases) (Figure 3.23A). The data were very similar in human cardiac fibroblasts, where again the inhibitors significantly reduced the Ca^{2+} influx in response to Yoda1 (Figure 3.23B). Using knowledge from previous studies exploiting these compounds, these findings are consistent with the theory that Piezo1 channels are mediating the Ca^{2+} response to Yoda1 in cardiac fibroblasts.

Yoda1-evoked Ca^{2+} entry was significantly reduced by >50 % by the novel antagonist of Yoda1, Dooku1, in both mouse (Figure 3.24A) and human (Figure 3.24B) cardiac fibroblasts. These data show that Dooku1 can effectively inhibit Yoda1-induced Ca^{2+} entry through the endogenous Piezo1 channel, in addition to in overexpression systems.

The Yoda1 analogue, compound 159, is an agonist of Piezo1 discovered during subsequent structure-activity relationship investigations of the Yoda1 compound series. Compound 159 has higher solubility compared to Yoda1, probably due to the addition of its carboxylic acid group; the structures can be compared in Figure 3.25. Analysis of intracellular Ca^{2+} levels revealed that compound 159 activated Piezo1 in a similar manner to Yoda1 in murine cardiac fibroblasts (Figure 3.25B). As the compound has better physicochemical properties, it may be suited to further development as a lead candidate in the future.

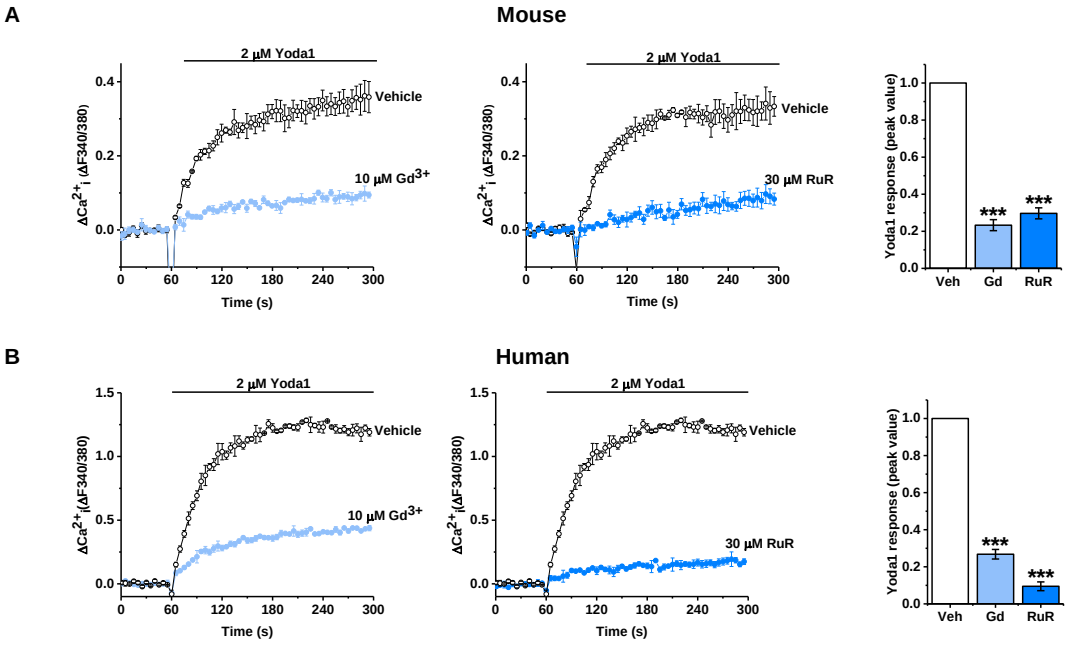

Figure 3.23. Effect of Piezo1 inhibitors on Yoda1-evoked Ca^{2+} entry in cardiac fibroblasts. Representative intracellular Ca^{2+} traces from **(A)** murine and **(B)** human cardiac fibroblasts exposed to 10 µM gadolinium (Gd^{3+}), 30 µM ruthenium red (RuR) or vehicle for 30 min before activation of Piezo1 by application of 2 µM Yoda1. Mean data are shown following normalisation to vehicle-treated cells, ***P<0.001 versus vehicle-treated cells following an ANOVA with Tukey's post-hoc test (n/N=3/9).

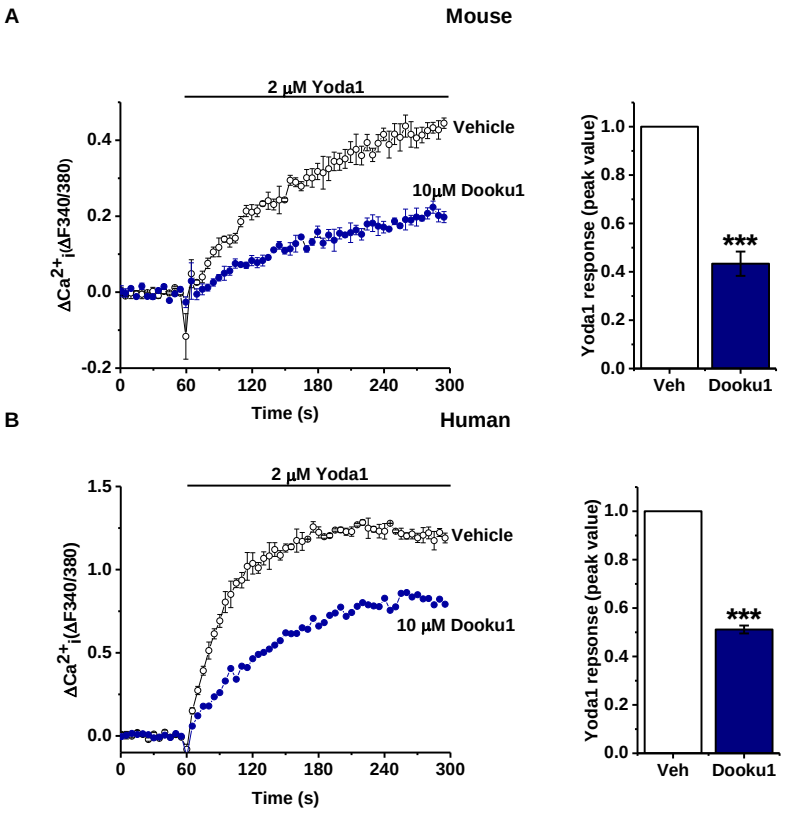

Figure 3.24. Effect of Dooku1 on Yoda1-evoked Ca^{2+} entry in cardiac fibroblasts. Representative intracellular Ca^{2+} traces and mean data from **(A)** murine and **(B)** human cardiac fibroblasts exposed to 10 µM Dooku1 or vehicle for 30 min before activation of Piezo1 by application of 2 µM Yoda1. Mean data were normalised to vehicle-treated cells, ***P<0.001 versus vehicle-treated cells following a t-test (n/N=3/9).

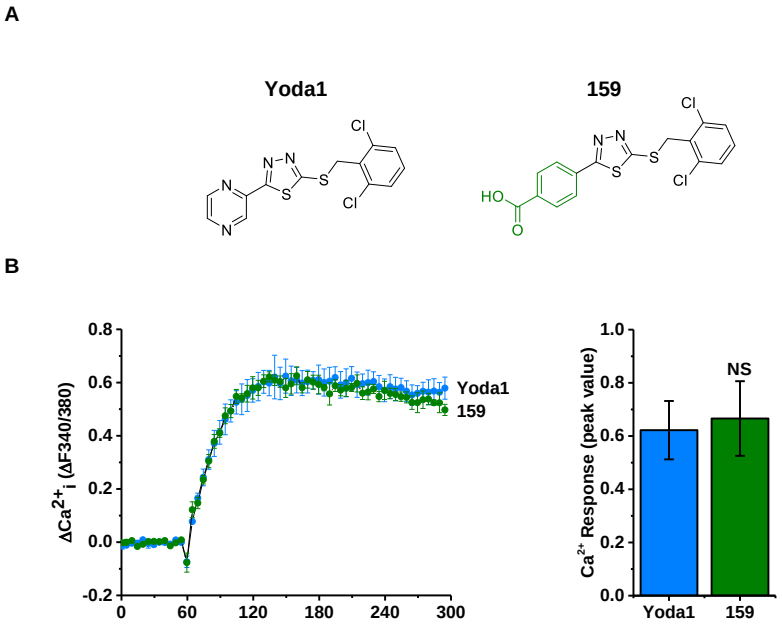

Figure 3.25. Effect of the novel compound, 159, on Yoda1-evoked Ca^{2+} entry in murine cardiac fibroblasts. (A) Chemical structures of Yoda1 and compound 159; chemical modifications of compound 159 from Yoda1 are shown in green. **(B)** Representative intracellular Ca^{2+} traces and mean data from murine cardiac fibroblasts exposed to 10 μM Yoda1 or compound 159, P=NS, not significant following a t-test (n/N=3/9).

3.4.7 Yoda1-evoked Ca^{2+} entry is mediated via Piezo1

3.4.7.1 Genetically modifying the Piezo1 gene causes changes in Yoda1-evoked Ca^{2+} entry

Despite inhibitors of the Piezo1 channel being useful molecular tools for acutely blocking the channel and investigating its pharmacology, these are non-selective pore blockers. Consequently, it was imperative to use a complementary molecular biology approach to confirm that Yoda1 responses were due to Piezo1 activation. Two *Piezo1*-modifed murine models were utilised; the first was a global heterozygous Piezo1 KO and the other was a line in which Piezo1 contained a gain-of-function mutation (M2240R).

A global homozygous Piezo1 full KO has previously been revealed to profoundly disturb the developing vasculature and be embryonically lethal within days of the heart beating (Li *et al.* 2014). Hence, the Ca^{2+} entry elicited by Yoda1 application was investigated in cardiac fibroblasts isolated from a global heterozygous (Het) $Piezo1^{+/-}$ KO mouse, which was viable. The Het $Piezo1^{+/-}$ KO mouse displayed reduced alignment of endothelial cells but had no major phenotype (Li *et al.* 2014). RT-PCR analysis confirmed the predicted 50 % reduction in *Piezo1* mRNA expression in cardiac fibroblasts derived from $Piezo1^{+/-}$ hearts, compared with those isolated from WT mice (Figure 3.26A). The Ca^{2+} entry upon Yoda1 application was also reduced by 50 % (Figure 3.26B), indicating that the scale of the Yoda1 response in these cells is proportional to the amount of Piezo1 expression. ATP was used as a positive control to validate that all cells had the equivalent Ca^{2+} content; the response to ATP was similar in cells from WT and $Piezo1^{+/-}$ mice (Figure 3.26C).

The first report of the M2225R mutation in Piezo1 in humans was by Zarychanski *et al.* (2012). Investigations into the properties of the mutated channel revealed that the mutation caused the Piezo1 channel to exhibit delayed inactivation kinetics, leading to a gain-of-function mutation which caused the channel to remain open for longer, leading to increased Ca^{2+} influx (Albuisson *et al.* 2013; Bae *et al.* 2013). A mouse line was generated, using CRISPR/Cas9 technology, in which mice had a M2240R mutation in Piezo1 globally; this is the mouse equivalent of the human M2225R mutation. These mice are referred to as M-R mice throughout this thesis. Cardiac fibroblasts from M-R mice displayed over a

doubling of the Ca^{2+} entry in response to Yoda1 activation, compared with cardiac fibroblasts from WT mice (Figure 3.27A). Cardiac fibroblasts from both sets of mice were confirmed to display identical ATP-evoked Ca^{2+} entry (Figure 3.27B). Together, these data using cells from genetically modified mice indicate that Yoda1-induced Ca^{2+} entry in cardiac fibroblasts is dependent on Piezo1 expression and activity.

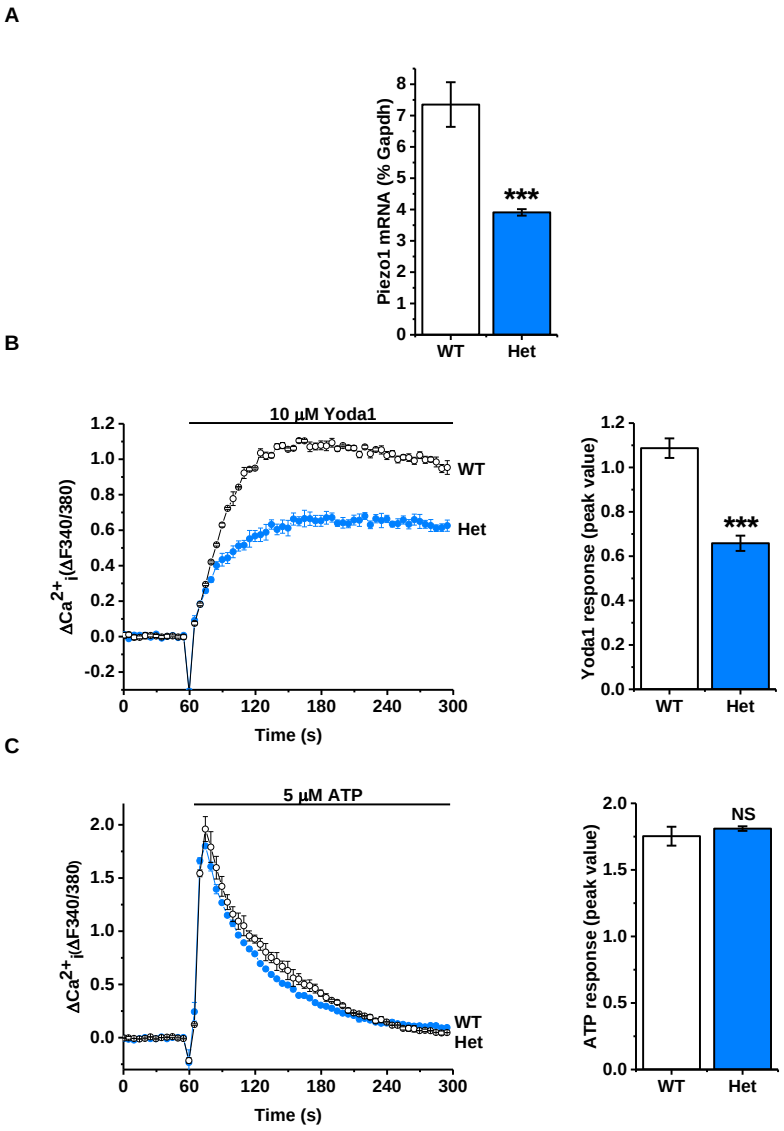

Figure 3.26 Effect of altering *Piezo1* mRNA expression on Yoda1-evoked Ca^{2+} entry in murine cardiac fibroblasts. (A) RT-PCR analysis of *Piezo1* mRNA expression in cultured murine cardiac fibroblasts isolated from wild-type (WT) and Piezo1$^{+/-}$ (Het) mice. Expression is measured as % of housekeeping control, *Gapdh*, ***P<0.001 following a t-test (n=8). **(B)** Representative Ca^{2+} traces and mean data illustrating Ca^{2+} entry elicited by 10 µM Yoda in cardiac fibroblasts from WT (n/N=8/24) and Piezo1$^{+/-}$ Het mice (n/N=5/15), ***P<0.001 following a t-test. **(C)** Representative Ca^{2+} traces and mean data illustrating the Ca^{2+} entry evoked by 5 µM ATP in cardiac fibroblasts from WT (n/N=4/12) and Piezo1$^{+/-}$ Het (n/N=3/9) mice, P=NS, not significant following a t-test.

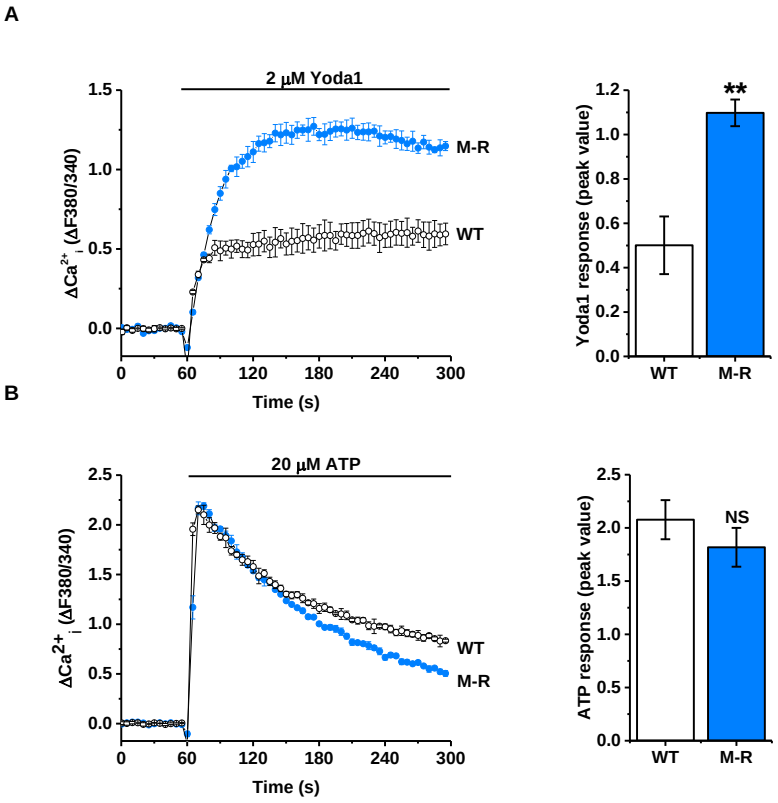

Figure 3.27 Effect of altering Piezo1 activity on Yoda1-evoked Ca^{2+} entry. **(A)** Representative Ca^{2+} traces and mean data illustrating Ca^{2+} entry elicited by 2 µM Yoda in cardiac fibroblasts from wild-type (WT; n/N=3/9) and gain-of-function M2240R Piezo1-mutated mice (M-R; n/N=5/15) mice, **P<0.01 following a t-test. **(B)** Representative Ca^{2+} traces and mean data illustrating the Ca^{2+} entry evoked by 20 µM ATP in cardiac fibroblasts from wild-type (WT; n/N=3/9) and gain-of-function Piezo1-mutated mice (M-R; n/N=5/15) mice, P=NS, not significant following a t-test.

3.4.7.2 Yoda1-induced Ca^{2+} entry is abolished by Piezo1-specific siRNA

A complementary method to the transgenic studies was sought to confirm the relationship between Piezo1 and Yoda1-evoked Ca^{2+} entry. This was the utilisation of siRNA targeting *Piezo1* to genetically disrupt its expression. Optimisation was required to source an appropriate siRNA which silenced mouse Piezo1 but had no off-target effects. Higher concentrations of siRNA are more likely to cause off-target effects; therefore, the aim was to acquire an siRNA which could silence Piezo1 at a low concentration. Murine cardiac fibroblasts were transfected with two Piezo1-specific siRNAs from different suppliers at different concentrations, alongside their respective control siRNAs and a transfection protocol in the absence of siRNA (mock transfection). The effectiveness of gene silencing was evaluated by RT-PCR 48 h after transfection. There was no difference in *Piezo1* mRNA expression between mock-transfected cardiac fibroblasts and cells transfected with control siRNA (Figure 3.28). 10 nM Piezo1-specific siRNA from Dharmacon achieved a 46 % reduction in *Piezo1* mRNA expression; the respective figure for Ambion Piezo1-specific siRNA was 53 % (Figure 3.28). There was minimal difference between *Piezo1* mRNA expression following transfection with 10 nM or 20 nM of siRNA (Figure 3.28). Therefore, 10 nM of Ambion Piezo1-specific siRNA was selected for use in subsequent experiments to silence *Piezo1* in murine cardiac fibroblasts to minimise any off-target effects.

With further optimisation of the protocol, Piezo1-specific siRNA decreased *Piezo1* mRNA expression by 80 % in murine cardiac fibroblasts (Figure 3.29A). The resulting Piezo1 knockdown markedly reduced the Yoda1-evoked Ca^{2+} entry by 84 % which was consistent with the level of *Piezo1* mRNA knockdown (Figure 3.29B); control siRNA was without effect. Similar data were obtained using human cardiac fibroblasts, in which Piezo1-specific siRNA knocked down *PIEZO1* mRNA levels by 77 %, compared to cells treated with a control siRNA (Figure 3.29C). Once again, this dramatically reduced Yoda1-evoked Ca^{2+} entry (by 62 %) (Figure 3.29D). Thus, it was confirmed that Ca^{2+} influx in response to Yoda1 was dependent on Piezo1 and proportional to its expression levels.

To confirm that Piezo1 siRNA could also reduce Piezo1 protein levels, and to also confirm that the band detected in cardiac fibroblasts isolated from mice with hemagglutinin (HA)-tagged Piezo1 (Piezo1-HA) in Figure 3.8 was Piezo1, cardiac

fibroblasts isolated from these mice were transfected with control siRNA and siRNA targeting Piezo1. Piezo1-HA protein was not detected in WT mice, as expected (Figure 3.30). In cardiac fibroblasts from Piezo1-HA mice transfected with control siRNA, a 295 kDa band corresponding to Piezo1 protein was detected; however in Piezo1-specific siRNA-transfected cells, Piezo1 protein expression was fully knocked down, confirming that this band is Piezo1 (Figure 3.30).

Through the combined use of pharmacological blockers of the Piezo1 channel, murine models with genetic disruption of *Piezo1*, and Piezo1-specific siRNA, it has been confirmed that the Ca^{2+} influx observed in cardiac fibroblasts activated by Yoda1 is due to Piezo1.

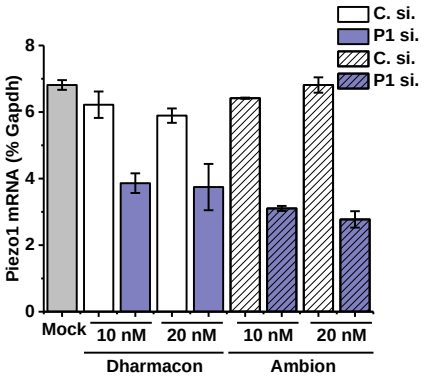

Figure 3.28 Optimisation of Piezo1-specific siRNA protocol. RT-PCR analysis of *Piezo1* mRNA expression 48 h after transfection of murine cardiac fibroblasts with Piezo1-specific (P1) siRNA from two different suppliers (purple bars), with their accompanying control (C) siRNA (white bars), alongside mock-transfected cells (grey bar). Expression is measured as % of housekeeping control, *Gapdh* (n=2).

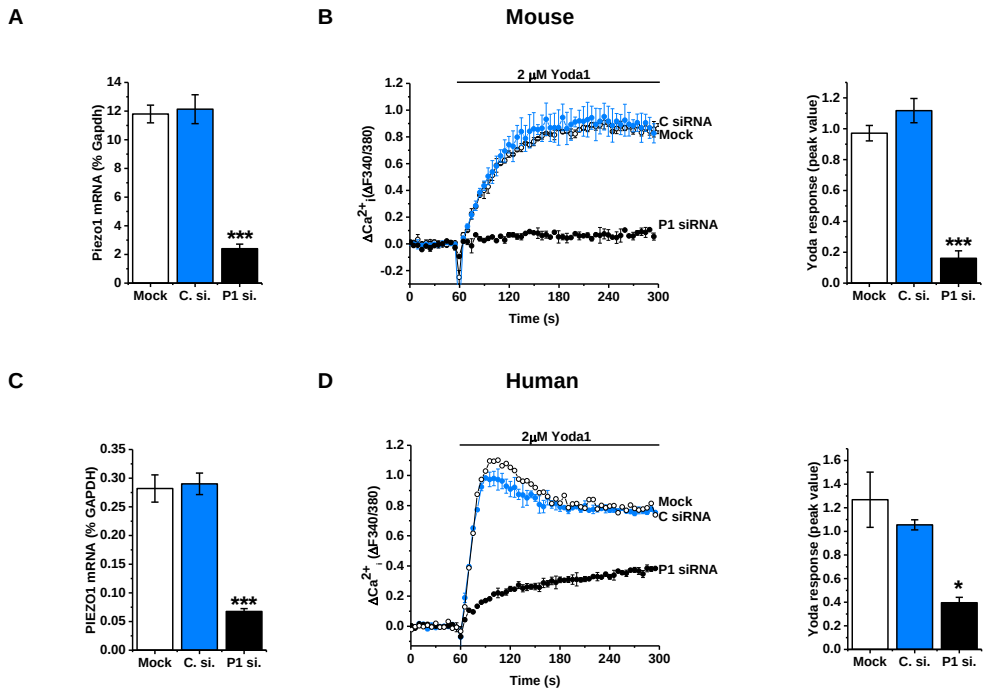

Figure 3.29 Effect of Piezo1 knockdown on Yoda1-evoked Ca^{2+} entry in murine and human cardiac fibroblasts. (A) RT-PCR analysis of *Piezo1* mRNA expression following transfection of murine cardiac fibroblasts with no siRNA (mock), control (C) siRNA or Piezo1-specific (P1) siRNA. Expression is measured as % of housekeeping control, *Gapdh*, ***P<0.001 versus mock-transfected cells following an ANOVA with Tukey's post-hoc test (n=3). **(B)** Representative Ca^{2+} traces and mean data showing the response of murine cardiac fibroblasts to 2 μM Yoda1 after transfection with Piezo1-specific (P1) siRNA, compared to mock-transfected cells and cells treated with control (C) siRNA, ***P<0.001 versus mock-transfected cells following an ANOVA with Tukey's post-hoc test (n/N=3/9). **(C)** As for (A) but in human cardiac fibroblasts, ***P<0.001 versus mock-transfected cells following an ANOVA with Tukey's post-hoc test (n=3). **(D)** As for (B) but in human cardiac fibroblasts, *P<0.05 versus mock-transfected cells following an ANOVA with Tukey's post-hoc test (n/N=3/9).

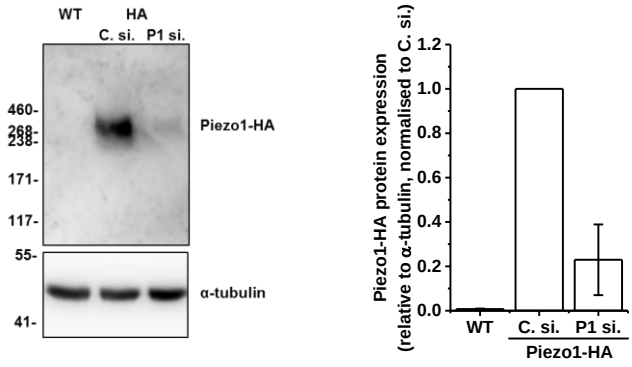

Figure 3.30 Effect of Piezo1-specific siRNA on protein levels in murine cardiac fibroblasts. Representative image and mean densitometric data of Piezo1 protein detected by western blotting in cardiac fibroblasts isolated from a CRISPR-generated murine model in which Piezo1 was modified to contain a HA tag. Samples from WT and Piezo1-HA mice were transfected with control (C) or Piezo1-specific (P1) siRNA and immunoblotted with anti-HA antibody, followed by an α-tubulin antibody to confirm equal protein loading (n=3). Data are normalised to control siRNA (C. si.). A band is detected at the expected size: 295 kDa.

3.4.8 Mechanical activation of Piezo1 in cardiac fibroblasts

3.4.8.1 Hypotonic stress evokes Ca^{2+} entry in murine cardiac fibroblasts in a Piezo1-independent manner

Increased deposition of ECM has been correlated with high glucose levels seen in diabetes; Tang *et al.* (2007) demonstrated that high glucose promoted production of collagen types I and III in rat cardiac fibroblasts through an ERK1/2 pathway. Osmotic swelling and increased stretch of cells transpire in the infarcted or pressure-overloaded myocardium and these factors can increase cardiomyocyte hypertrophy and mediate fibrotic responses through the activation of cardiac fibroblasts (Lu *et al.* 2012). Moreover, Piezo1 has been implicated in volume control in RBCs; RBCs from blood-cell-specific Piezo1 KO mice are overhydrated whereas activation of Piezo1 using Yoda1 causes calcium influx and subsequent dehydration of RBCs (Cahalan *et al.* 2015). A 96-well plate assay was developed to elicit hypotonic stress in cardiac fibroblasts, to determine whether this activated Piezo1. The FlexStation and Fura-2 assay were again utilised to investigate intracellular Ca^{2+} levels and a buffer was used in which Na^{+} was replaced with decreasing concentrations of NMDG-Cl to make solutions increasingly hypotonic. 135 mM NMDG-Cl was used as an isotonic control throughout all experiments. Firstly, it was assessed whether murine cardiac fibroblasts respond to hypotonic stimulation. Application of decreasing concentrations of NMDG-Cl, which causes cells to swell and pressure to increase, caused transient increases in intracellular Ca^{2+} levels in a concentration-dependent manner (Figure 3.31), indicating that these cells are responsive to hypotonic stress.

Subsequently, the involvement of Piezo1 channels in hypotonic stress-evoked Ca^{2+} entry was assessed. The non-selective cation channel ion pore blocker, gadolinium ($+Gd^{3+}$), or its vehicle, were used to pretreat murine cardiac fibroblasts to establish whether Ca^{2+} entry into cells was affected. Vehicle-treated cardiac fibroblasts showed concentration-dependent hypotonic responses (Figure 3.32A). However, these responses were reduced by 70 % when gadolinium was used prior to the addition of NMDG-Cl solutions (Figure 3.32A). The EC_{50} values without and with gadolinium pretreatment were comparable at 74.3 mM and 76.8 mM, respectively (Figure 3.32B,C), indicating that the remaining Ca^{2+} influx is likely due to the activation of mechanosensitive ion

channels which have not been inhibited. These data indicate that mechanosensitive non-selective cation channels, such as Piezo1, may be facilitating the increase in intracellular Ca^{2+} induced by cell swelling.

A more specific approach of gene silencing was employed to analyse whether Piezo1 channels specifically were responsible for the Ca^{2+} entry evoked by cell swelling. Piezo1-specific siRNA had no effect on intracellular Ca^{2+} levels in response to hypotonic stress in murine cardiac fibroblasts, compared to cells transfected with control siRNA (Figure 3.33A). This can be seen clearly in the mean data illustrating Ca^{2+} entry evoked by the most hypotonic solution (Figure 3.33B,C). Together with the Gd^{3+} experiments, these data suggest that the hypotonicity-evoked Ca^{2+} response in cardiac fibroblasts is mediated by a ion channel, but that it is not Piezo1.

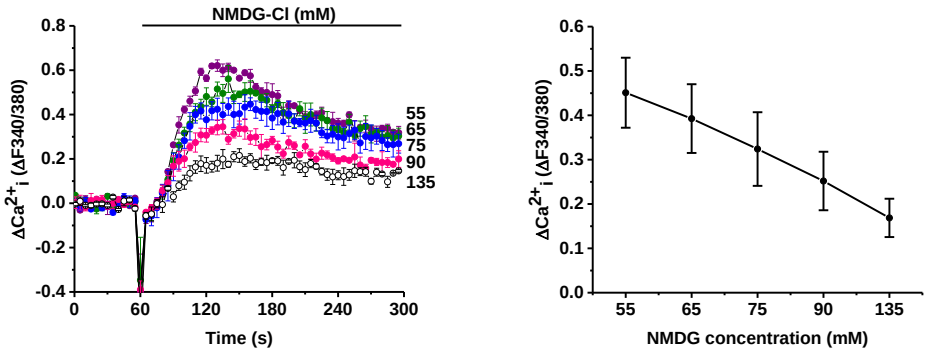

Figure 3.31 Effect of hypotonic stress on intracellular Ca^{2+} levels in murine cardiac fibroblasts. Representative intracellular Ca^{2+} measurement traces and mean data from murine cardiac fibroblasts during application of a range of concentrations of NMDG-Cl (55-90 mM) which evoke hypotonic stress, alongside an isotonic solution (135 mM) (n/N=3/9).

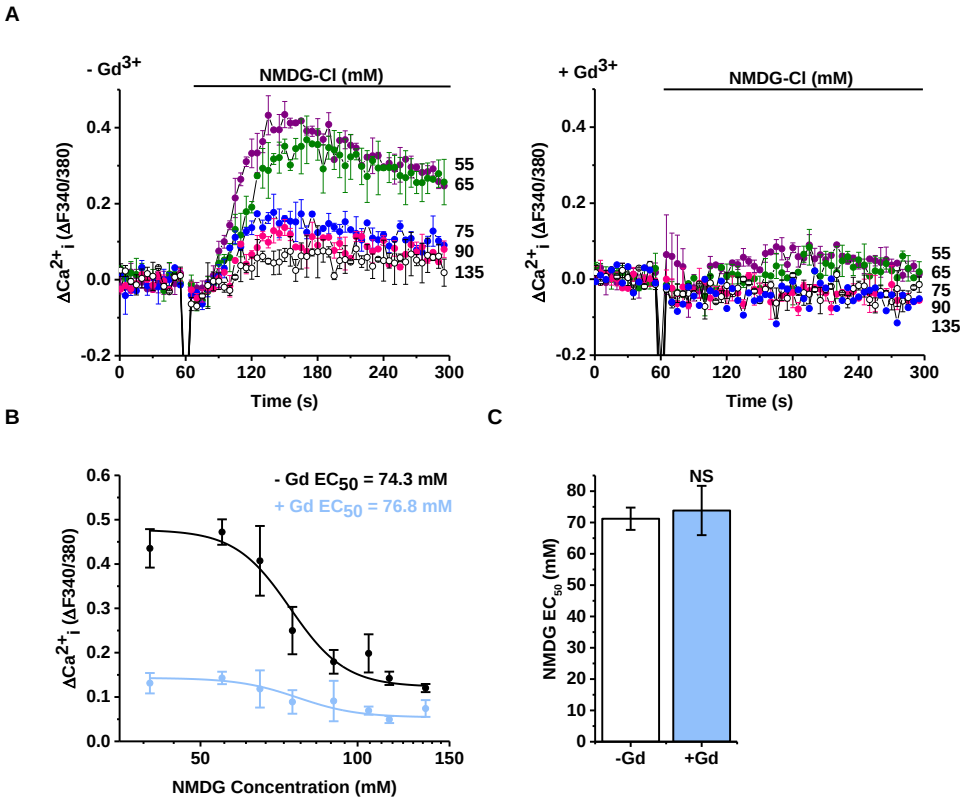

Figure 3.32 Effect of gadolinium pretreatment on Ca^{2+} entry evoked by hypotonicity. (A) Example intracellular Ca^{2+} measurement traces from murine cardiac fibroblasts during application of varying concentrations of NMDG-Cl (55-135 mM). Left: after 30 min pretreatment with the vehicle of gadolinium (-Gd^{3+}). Right: After 30 min pretreatment with 10 µM gadolinium (+Gd^{3+}). **(B)** Concentration-response data from the type of experiments in (A) (n/N=3/9). The fitted curve is a Hill equation indicating the 50 % maximum effect (EC_{50}) at 74.3 mM NMDG without gadolinium pretreatment and 76.8 mM NMDG with gadolinium pretreatment. **(C)** Mean data are shown in a bar chart comparing the EC_{50} values from three independent repeats, P=NS, not significant following a t-test.

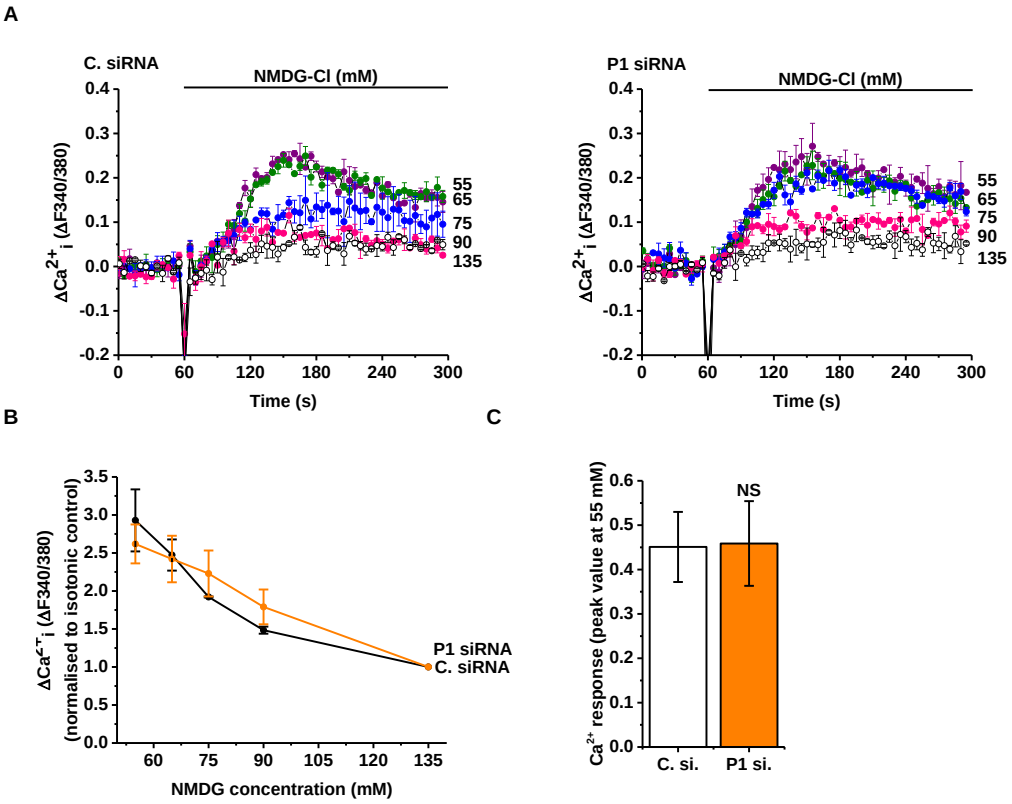

Figure 3.33 Effect of Piezo1 knockdown on the response of murine cardiac fibroblasts to hypotonicity. (A) Example intracellular Ca^{2+} measurement traces from murine cardiac fibroblasts during application of varying concentrations of NMDG-Cl (55-135 mM). Left: cells transfected with control (C) siRNA. Right: cells transfected with Piezo1-specific (P1) siRNA. **(B)** Concentration-response data for NMDG-Cl from the type of experiments in (A), data are normalised to isotonic control (135 mM NMDG-Cl) (n/N=3/9). **(C)** Mean data for the peak response at 55 mM for the experiment in (A), P=NS, not significant following a t-test (n=3).

3.4.8.2 Human cardiac fibroblasts express mechanically-activated ionic currents which depend on Piezo1

Cell-attached patch recordings were used as an alternative method to mechanically activate Piezo1 in cardiac fibroblasts. Mechanical force was applied to patches using a fast pressure-clamp system which generated pressure pulses and increased membrane tension. Increased pressure caused increased current in human cardiac fibroblasts (Figure 3.34A,B), consistent with the presence of Piezo1 channels (Coste *et al.* 2010; Bae *et al.* 2013). The currents were noisy which suggests the presence of multiple individual channels producing the overall current. The pressure required for 50% activation was estimated to be -61.3 mmHg (Figure 3.34A). To test if currents were Piezo1-dependent, human cardiac fibroblasts were transfected with control or Piezo1-specific siRNA. Piezo1 siRNA-transfected cells showed no meaningful current in response to pressure steps, unlike in cells transfected with control siRNA (Figure 3.34B,C). Data for all 45 recordings show that pressure-activated currents were more common in the control siRNA-transfected cells (Figure 3.34D) than in Piezo1 siRNA-transfected cells (Figure 3.34E). This was shown to be statistically significant and, therefore, these data suggest that human cardiac fibroblasts express mechanically activated Piezo1 channels.

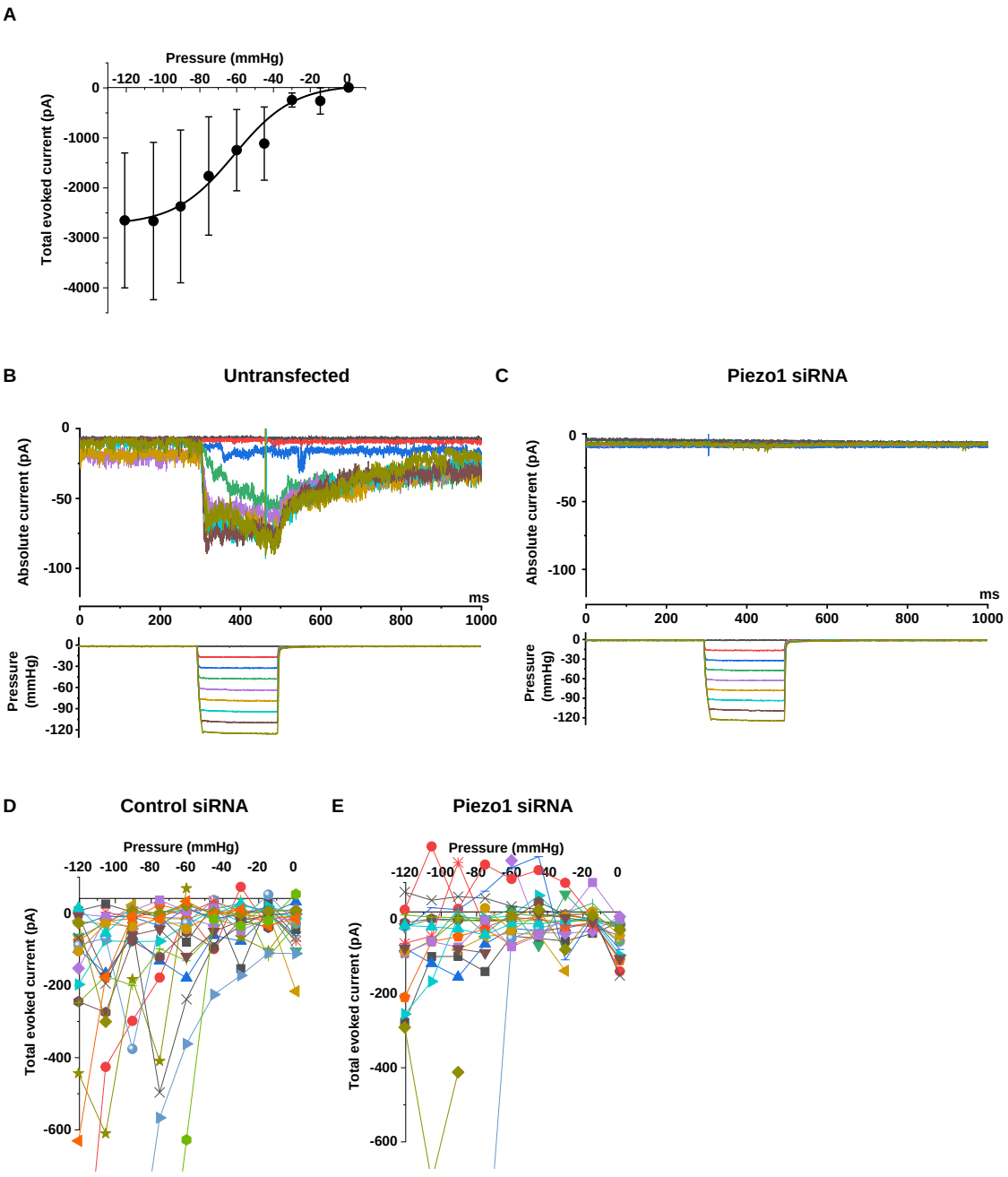
A
Pressure (mmHg)
-120 -100 -80 -60 -40 -20 0
Total evoked current (pA)
0
-1000
-2000
-3000
-4000
B
Untransfected
Absolute current (pA)
0
-50
-100
ms
0 200 400 600 800 1000
Pressure (mmHg)
0
-30
-60
-90
-120
C
Piezo1 siRNA
Absolute current (pA)
0
-50
-100
ms
0 200 400 600 800 1000
Pressure (mmHg)
0
-30
-60
-90
-120
D
Control siRNA
Pressure (mmHg)
-120 -100 -80 -60 -40 -20 0
Total evoked current (pA)
0
-200
-400
-600
E
Piezo1 siRNA
Pressure (mmHg)
-120 -100 -80 -60 -40 -20 0
Total evoked current (pA)
0
-200
-400
-600

Figure 3.34 Effect of Piezo1 knockdown on ionic currents evoked by mechanical pressure in human cardiac fibroblasts. (A) Recordings were made from cell-attached patches on human cardiac fibroblasts. A constant holding voltage of +80 mV was applied to the patch pipette and a rapid pressure clamp system applied 200-ms negative pressure (suction) steps to the patch pipette of increasing magnitude. Mean ± SEM data are shown for experiments in which the total current during 180-ms of each pressure pulse was summed (n=7-8 patches per data point). The fitted curve is the Boltzmann function, which gave a mid-point for 50% activation of -61.3 mmHg. **(B)** Example data from an untransfected cell analysed in (A). The colour of the pressure steps (lower panel) matches the colour of the current traces in the upper panel. **(C)** As for (B) but from a cell transfected with Piezo1 siRNA. **(D,E)** Individual data from cells transfected with control siRNA (D, n=24) or Piezo1 siRNA (E, n=21). Two-way ANOVA comparison with Tukey's post-hoc test of control v Piezo1 siRNA gave *P<0.05 over all pressure steps. Experiments were performed by Professor Katsuhiko Muraki.

3.5 Discussion

The heart experiences electrical, biochemical, and mechanical stimulations as it contracts; thus, cardiac cells express mechanosensitive apparatus which is capable of detecting mechanical stimulation (Peyronnet, Nerbonne and Kohl 2016). There is currently no information on Piezo1 in cardiac fibroblasts, despite knowledge that they express other mechanically-activated ion channels (Yue, Xie and Nattel 2011) and that the molecular mechanisms by which they sense mechanical signals remain elusive (Hinz and Gabbiani 2010). For these reasons, the aims of this study were to examine the chemical and mechanical activation of Piezo1 in cardiac fibroblasts.

Messenger RNA encoding Piezo1 was detected in the murine heart by Coste *et al.* (2010). There have since been publications investigating Piezo1 expression in cardiomyocytes (Liang *et al.* 2017; Wong *et al.* 2018) but none exploring the ion channel in cardiac fibroblasts. The only current publication on Piezo1 in fibroblasts from other sources is a recent paper by Chubinskiy-Nadezhdin *et al.* (2019). In that study, RT-PCR and immunofluorescent staining were used to confirm the presence of native Piezo1 in a mouse fibroblast cell line and functional expression of Piezo1 was illustrated using calcium measurements. The current study is the first to establish that cultured cardiac fibroblasts express *Piezo1* mRNA. It was established that *Piezo2* mRNA expression was expressed at lower levels than *Piezo1* mRNA. This result was expected as Coste *et al.* (2010) found there to be low expression of *Piezo2* in whole heart; this protein has been shown to be more important in somatosensation (Woo *et al.* 2014; Woo *et al.* 2015; Dubin *et al.* 2012).

Cultured murine and human cardiac fibroblasts expressed *Piezo1* mRNA at levels similar to those found in endothelial cells from various sources, cells known to express high levels of functional Piezo1 (Li *et al.* 2014). *Piezo1* mRNA expression was revealed to be approximately 25-times higher in cardiac fibroblasts than cardiomyocytes. This finding correlates with data from Liang *et al.* (2017) who found that Piezo1 was only expressed at low levels in mouse ventricular myocytes isolated from control animals but was significantly increased in myocytes isolated from mice that had undergone MI. Alongside demonstrating that *Piezo1* mRNA is expressed in cultured cardiac fibroblasts, expression in freshly isolated murine cells was also verified in the present study. This indicates

that *Piezo1* is expressed in native cardiac fibroblasts, and that its expression is not due to alterations in phenotype induced by culturing. Piezo1 protein was detected in cardiac fibroblasts with the use of a novel transgenic mouse globally expressing a mutated hemagglutinin (HA)-tagged version of Piezo1, developed using CRISPR-Cas9 technology. This allowed the identification of Piezo1 using anti-HA antibodies by western blotting; this was essential as current Piezo1 antibodies are non-specific. This transgenic mouse will be invaluable for future studies into Piezo1, for example, for immunocytochemistry or immunoprecipitation experiments to investigate Piezo1 localisation or interacting partners, respectively. The aforementioned paper by Liang *et al.* (2017) found that Piezo1 mRNA and protein expression were enhanced by Ang II in neonatal rat ventricular myocytes via an AT1 receptor-ERK1/2 pathway but, generally, information on how Piezo1 expression is regulated is scarce. Applying mechanical stimuli directly to cells or altering the confluency or differentiation state of cardiac fibroblasts had no effect on *Piezo1* mRNA expression. These findings were beneficial to the study as they confirmed that effects observed throughout were due to Piezo1 activity, rather than due to altered Piezo1 expression. However, there was a hint that, although *Piezo1* mRNA expression is unchanged when cells are activated using “outside-in” mechanical forces, i.e. forces arising from shear flow or stretch, expression may be downregulated when cells themselves generate less mechanical force (on softer substrates), i.e. traction forces caused by changes in the local environment. Cellular traction forces have been demonstrated to generate Piezo1-mediated Ca^{2+} flickers in the absence of externally-applied mechanical forces (Ellefsen *et al.* 2019).

One major disadvantage of using Yoda1 to activate Piezo1 is its lack of drug-like properties i.e. it has poor solubility, a short half-life and a high clearance rate (Kevin Cuthbertson PhD thesis, 2019). Investigation into the properties of analogues of Yoda1 has provided increased knowledge of the structure-activity relationship of Piezo1 channel activation by Yoda1. The goal is to generate novel small-molecule tools for investigating Piezo1 channel function, such as an agonist with improved absorption, distribution, metabolism and excretion (ADME) properties or a specific antagonist of the Piezo1 channel. Yoda1 appears to have a very tight structure-activity relationship as any slight structural changes have drastic effects on the activity of the compound. Syeda *et al.* (2015) have

previously demonstrated that the effect of Yoda1 appears to critically depend on the dichlorophenyl group, as similar compounds lacking the chlorines were not identified in their screen. Data published by Evans *et al.* (2018) confirmed the dichlorophenyl moiety of Yoda1 to be essential for activating the Piezo1 channel when overexpressed in HEK-293 cells. This is illustrated herein as compounds containing the dichlorophenyl group, 2i and 2j, were partial agonists of Piezo1 whereas compound 2e, which lacks the dichlorophenyl group, was inactive. Using this logic, it was unexpected that compound 2k/Dooku1 did not trigger Ca^{2+} influx, due to the compound possessing a dichlorophenyl group. Experiments performed to analyse the ability of the same Yoda1 analogues to inhibit Piezo1 revealed that compound 2k/Dooku1 was in fact able to block Yoda1-evoked Ca^{2+} influx. These data confirmed that the dichlorophenyl group is important for compounds interacting with the channel in any way, whether as agonists or antagonists. This screening process led to the development of Dooku1 as a small-molecule which antagonises Yoda1-evoked Piezo1 channel activation (Evans *et al.* 2018). Dooku1 inhibits Yoda1-evoked Piezo1 activation but is unable to block physiological Piezo1 channels (Evans *et al.* 2018). Therefore, it is probable that its binding site is the same as for Yoda1 and the compound prevents Yoda1 from binding to the Piezo1 channel. Despite being unable to block constitutively active Piezo1 channels, Dooku1 provides a useful tool compound to study Yoda1-evoked Piezo1 channel activation and signalling.

Further screening of Yoda1 analogues led to the discovery of compound 159. *In vitro* ADME analysis demonstrated that, compared to Yoda1, KC159 had greater solubility and did not precipitate in aqueous solution until it reached 76.6 µM (Kevin Cuthbertson PhD thesis, 2019). Additionally, KC159 had a half-life almost 40-times greater than Yoda1 and a clearance rate 35-times lower than Yoda1. This analogue of Yoda1 was proven to be able to evoke similar Ca^{2+} influx to its parent compound in murine cardiac fibroblasts. These characteristics render KC159 a more desirable drug with which to analyse Piezo1-mediated signalling and to take forward for *in vivo* investigation but more work is needed to further characterise this compound.

Despite demonstrating mRNA and protein expression of Piezo1, it was vital to corroborate that Piezo1 formed a functional channel in cardiac fibroblasts. This was performed using the Piezo1 chemical activator, Yoda1 (Syeda *et al.* 2015).

The advantage of utilising a chemical agonist over mechanical activation to stimulate Piezo1 channel opening is the specificity. While the latter could activate a plethora of cellular mechanosensors, Yoda1 is specific to Piezo1, with no agonist activity against other ion channels, including Piezo2 (Syeda *et al.* 2015). Using the Ca^{2+} indicator, Fura-2, it was established that Yoda1 had EC_{50} values of 0.72 μM and 0.71 μM in murine and human cardiac fibroblasts, respectively, implying that Piezo1 forms a functional, Ca^{2+}-permeable channel in cardiac fibroblasts. When artificially overexpressed in cell lines, the respective data on mouse (EC_{50} = 0.33 μM) and human (EC_{50} = 1.85 μM) Piezo1 overexpressed in HEK T-REx-293 cells were somewhat lower than those originally reported in HEK-293 cells transiently transfected with mouse (EC_{50} = 17.1 μM) or human (EC_{50} = 26.6 μM) Piezo1 (Syeda *et al.* 2015). The data were more comparable with a previous report from our laboratory where Evans *et al.* (2018) demonstrated an EC_{50} of 0.23 μM in HUVECs. As discussed, Yoda1 has poor solubility so could only be used at concentrations up to 10 μM; therefore these EC_{50} values are estimates and, along with the fact that the data was produced by different groups, could be the reason for any discrepancies. When cardiac fibroblasts were pretreated in the absence of extracellular Ca^{2+}, the Yoda1 response was blunted in murine cells and completely abolished in human cells, indicating that the majority of the response is through plasma membrane Piezo1 channels. The residual response in murine cardiac fibroblasts may be due to Yoda1 activating Piezo1 channels present in internal store membranes and triggering the release of Ca^{2+}; previous reports have demonstrated expression of Piezo1 in the endoplasmic reticulum (McHugh *et al.* 2010). This would need to be investigated further in cardiac fibroblasts, however, it is evident that the majority of the Ca^{2+} influx observed in response to Yoda1 is mediated by Ca^{2+} entry from extracellular sources.

The ability of common inhibitors of mechanosensitive ion channels, gadolinium and ruthenium red (Coste *et al.* 2010), and the novel Yoda1 antagonist, Dooku1 (Evans *et al.* 2018), to decrease Yoda1-evoked Ca^{2+} entry in murine and human cardiac fibroblasts correlated with the expected properties of the channel. We further verified that the Yoda1-evoked Ca^{2+} influx in cardiac fibroblasts was proportional to the expression and activity of Piezo1. Small interfering RNA-mediated knockdown of Piezo1 or the use of cells from a global $Piezo1^{+/-}$

heterozygous KO mouse model both reduced Yoda1-evoked Ca^{2+} entry and this was proportional to the expression of *Piezo1* mRNA expression. Li *et al.* (2014) generated and characterised the Piezo1 heterozygous KO mouse and found that, although the animals were phenotypically normal, there were differences in the organisation of endothelial cells lining the vessels (a more cobblestone-like appearance rather than the linear appearance in the direction of flow seen in *Piezo1*$^{+/+}$ littermate controls). In addition, Ca^{2+} entry due to Yoda1 was amplified in cardiac fibroblasts isolated from mice with a global gain of function M2220R mutation in Piezo1, which is the murine equivalent of the human M2225R mutation (Zarychanski *et al.* 2012). The mutation causes an imbalance in intracellular cation concentrations, leading to defective RBC membrane properties. This has since been revealed to be due to delayed inactivation kinetics of the Piezo1 channel, leading to a gain-of-function mutation which causes the channel to remain open for longer, allowing increased Ca^{2+} influx (Albuisson *et al.* 2013; Bae *et al.* 2013). This renders patients with severe haemolytic anaemia in a disease named dehydrated hereditary stomatocytosis. The CRISPR-generated mice utilised also display symptoms of anaemia (Evans et al. unpublished). Thus, it was confirmed that Yoda1 responses observed in cardiac fibroblasts were unequivocally due to the activation of Piezo1.

Despite hypotonicity-evoked Ca^{2+} signals being observed in murine cardiac fibroblasts which were able to be inhibited by gadolinium, knockdown of Piezo1 by specific siRNA had no effect on this Ca^{2+} influx. It may be that alternative non-selective cation channels are responsible for the changes in intracellular Ca^{2+} levels. It is known that many of the TRP channels are expressed in cardiac fibroblasts and have been associated with activation due to mechanical stretch (Yue *et al.* 2013). Several of these, for example, TRPV2 (Muraki *et al.* 2003) and TRPV4 (Vriens *et al.* 2004), have been shown to be activated by osmotic cell swelling and can also be inhibited by Gd^{3+} (Bouron, Kiselyov and Oberwinkler 2015).

Cell-attached patch clamp electrophysiology was used as an alternative method to mechanically activate Piezo1 in human cardiac fibroblasts. The amplitude of the current was greatly variable between patches; it is suggested that the variable amount of suction needed to form the initial seal was a contributor to this variability (larger suction leading to lesser mechanically-activated currents) but it

was shown that increased pressure pulses generated increased inward current. The estimated pressure for 50% activation (-61.3 mmHg) varies from previous work which suggested that overexpressed human Piezo1 channels require -43 mmHg for 50% activation (Bae *et al.* 2013); this difference may be due to the impact of the native environment (Romero *et al.* 2019). The kinetics of the currents were relatively slow and did not inactivate which disagrees with data on overexpressed Piezo1 channels (Coste *et al.* 2010). However, it has been proposed that endogenous Piezo1 channels have slower kinetics and do not inactivate or inactivate slowly (Li *et al.* 2014; Del Mármol *et al.* 2018). Piezo1-specific siRNA was utilised to test if the currents were Piezo1-dependent. Pressure-activated currents were more frequent in control siRNA-transfected cells, in comparison with the Piezo1-siRNA-transfected group. It is proposed that the only 2 large recordings in the Piezo1 siRNA-transfected group were from cells unsuccessfully transfected with Piezo1-specific siRNA, as transfection efficiency was estimated to be 90 %. These data therefore suggest that Piezo1 can be activated using mechanical stimuli in cardiac fibroblasts.

Together, data in this chapter have established that, in both mouse and human cardiac fibroblasts, Piezo1 mRNA is expressed and Piezo1 protein is translated and able to form a functional cation channel. Piezo1 mRNA expression remained unaffected when cardiac fibroblasts were stimulated using cytokines and mechanical stimuli such as shear stress and stretch but its expression appeared to be decreased when cells were plated on softer substrates. The Piezo1 channel had the expected pharmacological properties and the Yoda1-induced Ca^{2+} entry was dependent on Piezo1 expression, as evidenced by a variety of methods. Mechanical force applied via cell-attached patch clamp electrophysiology was able to evoke ionic currents in human cardiac fibroblasts; this occurred in a Piezo1-dependent manner.

Chapter 4 Yoda1-induced activation of Piezo1 alters the expression of remodelling genes in cardiac fibroblasts

4.1 Introduction

Cardiac fibroblasts are the fundamental cell type responsible for ECM homeostasis in health and its remodelling in heart disease. Cardiac fibroblasts produce both structural ECM proteins (e.g. collagens, fibronectin) and MMPs, which enzymatically digest ECM proteins. The activity of MMPs is regulated at the level of transcription, by activation of the precursor zymogens and by the inhibition by TIMPs (Nagase, Visse and Murphy 2006). Cardiac fibroblasts also synthesise and secrete a variety of bioactive molecules, including cytokines, active peptides and growth factors, which function in the myocardium in autocrine and/or paracrine fashions (Fan *et al.* 2012). In response to changes in haemodynamic burden of the heart, mechanical stress (generated by ECM stiffness) induces the differentiation of fibroblasts into myofibroblasts, cells with increased expression of α-SMA, periostin and pro-fibrotic cytokines (Deb and Ubil 2014; Turner and Porter 2013; Oka *et al.* 2007). If this burden persists, it can lead to the disproportionate accumulation of fibrillar collagen (fibrosis) and adverse cardiac remodelling.

4.2 Aims

In the previous chapter, it was established that Piezo1 is expressed by cardiac fibroblasts and acts as a mechanosensitive ion channel in this cell type. The primary aims of this chapter were to investigate whether activating the channel, using chemical activation, such as Yoda1, or mechanical stimulation, leads to changes in the expression of genes associated with fibroblast function and cardiac remodelling.

4.3 Methods

Cardiac fibroblasts were treated with the Piezo1 activator, Yoda1, and it was assessed whether the compound had any effect on cell viability using the LIVE/DEAD cell assay, as described in Section 2.8. Gene expression was analysed using RT-PCR (Section 2.5). It was then investigated whether Yoda1-induced changes in gene expression were dependent on Piezo1; this was performed utilising Piezo1-modified murine models (Section 2.13.3) and siRNA targeting Piezo1 (Section 2.4). It was also explored whether mechanical stimulation (shear stress, controlling substrate stiffness or cell stretching, which are described in Section 2.11) induced similar changes in gene expression and, again, whether these were dependent on the activity of the Piezo1 channel.

4.4 Results

4.4.1 Activation of Piezo1 and the effect on gene expression

4.4.1.1 Yoda1 has no impact on cardiac fibroblast viability after 24 h of treatment

To gain insight into the functional role of Piezo1 activation in cardiac fibroblasts, the effect of activating the Piezo1 channel using Yoda1 was investigated. A LIVE/DEAD cell viability assay was firstly performed to identify whether Yoda1 had any effect upon murine cardiac fibroblast viability over prolonged time periods. A maximal concentration of 10 µM Yoda1 was utilised, as this was the highest concentration used throughout the study. When applied with Yoda1, 90 % of cardiac fibroblasts were alive after 24 h treatment (illustrated by green staining), compared to 97 % after treatment with the vehicle control; this difference was not statistically significant (Figure 4.1). 1 µM staurosporine (SSP) was used as a positive control as a compound which causes cell death; SSP treatment resulted in 38 % cell death as visualised by the increased red staining (Figure 4.1). This suggests that an extended period of Yoda1 exposure does not adversely affect cardiac fibroblast viability. It is notable that Yoda1 induced a morphological change in the cells towards a more spindle-like, less rhomboid shape, in comparison with vehicle-treated cells; this will be discussed in more detail in section 4.4.2.

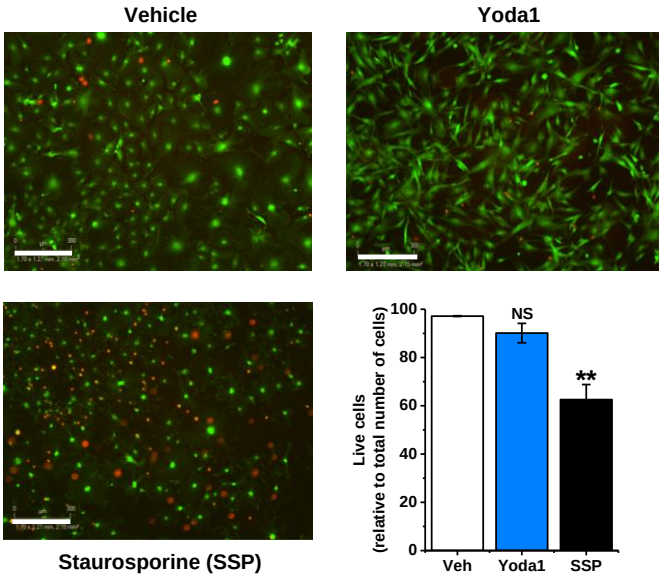

Figure 4.1 Effect of 24 h Yoda1 treatment on murine cardiac fibroblast viability. Representative images from the LIVE/DEAD cell viability assay performed on cultured murine cardiac fibroblasts treated with either vehicle, 10 μM Yoda1 or 1 μM staurosporine (SSP) for 24 h. Green indicates live cells; red indicates dead cells. Scale bar = 300 μm. Bar chart displays mean data of viable cells as a percentage of total cells, **P<0.01, P=NS, not significant versus vehicle-treated cells following an ANOVA with Tukey's post-hoc test (n=3).

4.4.1.2 Activating Piezo1 causes changes in the expression of key remodelling genes

The expression of remodelling genes following 24 h treatment with 0.5-10 μM Yoda1 was investigated by RT-PCR. Prolonged Yoda1 treatment did not modulate *Piezo1* gene expression itself (Figure 4.2A). However, three genes associated with myofibroblast differentiation were altered. Expression of *Acta2* mRNA, the gene that encodes α-SMA, decreased by over 50 % following 10 μM Yoda1 treatment (Figure 4.2B) and expression of the gene encoding the profibrotic cytokine TGF-β (*Tgfb1*) was significantly reduced in a concentration-dependent manner (Figure 4.2C). Expression of *Postn* mRNA, the gene encoding periostin, a described marker of the myofibroblast that is expressed in adult tissues only after injury (Snider *et al.* 2009), was also significantly decreased by Yoda1 treatment at concentrations greater than 2 μM for 24 h (Figure 4.2D). As with *Piezo1* mRNA expression, Yoda1 treatment did not affect expression of genes involved in ECM turnover, including collagens I and III (Col1a1, Col3a1) or Mmp3 or Mmp9 (Figure 4.2E-H).

In contrast, the expression levels of *Tnc*, a molecule closely associated with tissue injury and active inflammation, was significantly increased after treatment with Yoda1 (Figure 4.2I). A concentration-dependent increase in mRNA expression of the inflammatory/hypertrophic cytokine interleukin-6 (*Il6*) was also observed; with a significant 4-fold increase in response to 10 μM Yoda1 (Figure 4.2J). This was not a generic inflammatory response, as mRNA levels of the proinflammatory cytokine *Il1β* remained unchanged by Yoda1 treatment (Figure 4.2K). These data reveal that activation of Piezo1 using Yoda1 is coupled to altered expression of key genes associated with fibroblast function.

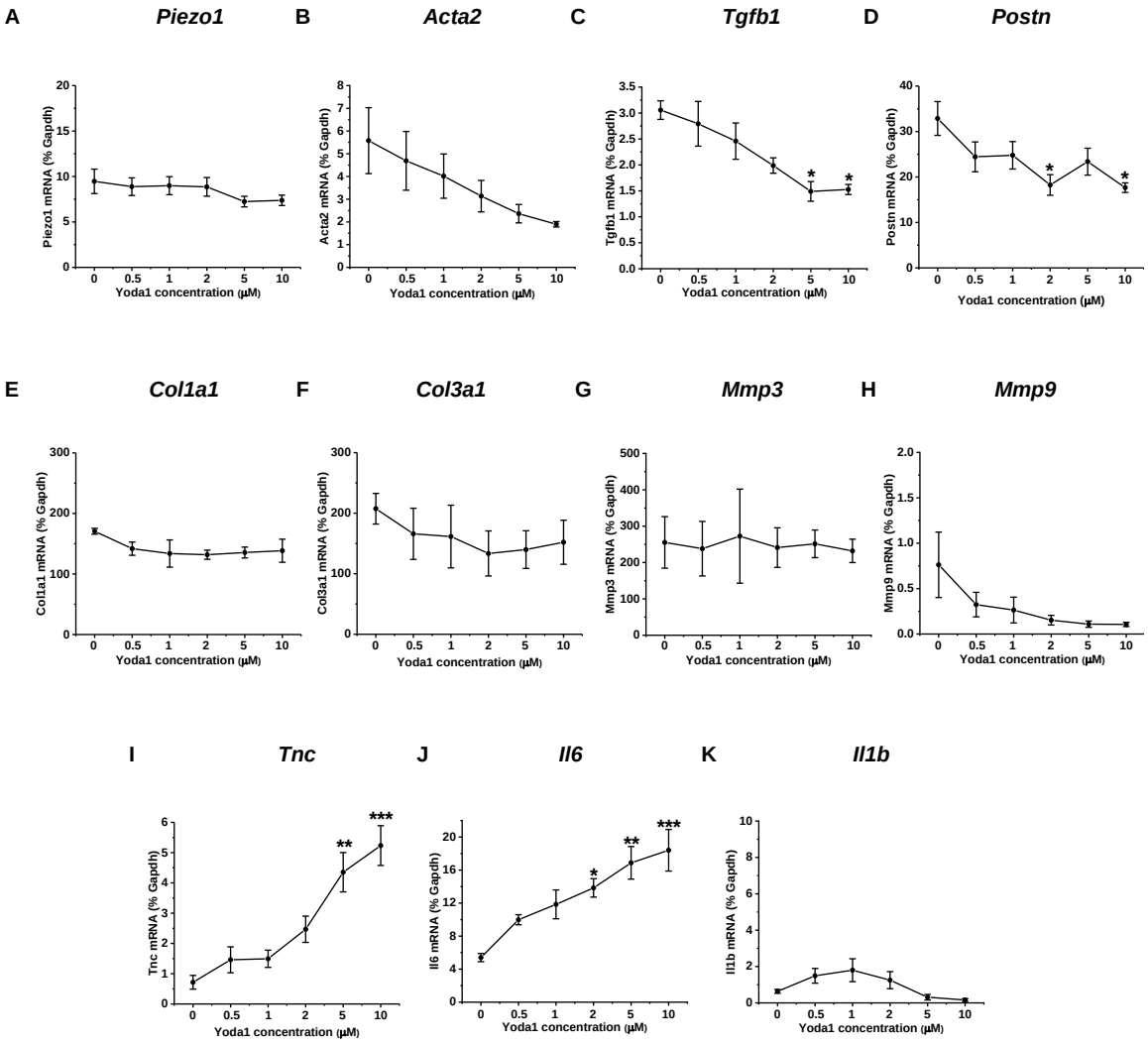

Figure 4.2 Effect of Yoda1 on the expression of genes associated with fibroblast function. (A-K) RT-PCR analysis of 11 genes in murine cardiac fibroblasts treated with concentrations of Yoda1 ranging from 0.5-10 μM, or DMSO vehicle, for 24 h. All mRNA expression levels were normalised to those of the housekeeping gene, *Gapdh*, *P<0.05, **P<0.01, ***P<0.001 versus vehicle-treated cells following an ANOVA with Tukey's post-hoc test (n=3).

4.4.2 The effect of Yoda 1 on genes associated with myofibroblast differentiation

TGF-β1 is a cytokine released from a variety of inflammatory cells which migrate in large numbers to damaged or fibrotic tissue (Darby *et al.* 2014); but activated cardiac fibroblasts are the primary producers (Chen *et al.* 2004). TGF-β1 stimulates cardiac fibroblast proliferation, differentiation, migration, apoptosis and initiates the deposition of ECM via the upregulation of collagens and TIMPs and downregulation of MMPs (Leask and Abraham 2004); these processes all exacerbate the pro-fibrotic environment. TGF-β1 is the factor which largely regulates fibroblast to myofibroblast differentiation in order to drive effective wound healing and, despite an increase in this cytokine being associated with most of the fibrotic diseases in humans (Border and Noble 1994), regulatory mechanisms remain unclear. The transition of fibroblasts into myofibroblasts is accompanied by the upregulation of α-SMA both *in vitro* and *in vivo* (Santiago *et al.* 2010) and α-SMA is a commonly used marker to identify activated myofibroblasts. Given the important role of myofibroblast differentiation in cardiac remodelling, the finding that the expression of three genes associated with myofibroblast differentiation (*Acta2*, *Postn*, *Tgfb1*) were downregulated following Yoda1 treatment was intriguing. Therefore, the effect of Piezo1 activation on markers of cardiac myofibroblasts was examined further.

4.4.2.1 Expression of markers of myofibroblast differentiation following Yoda1 treatment

The Yoda1-induced reduction in *Acta2* and *Tgfb1* mRNA expression data (Figure 4.2B,C) appeared to correlate with the morphological change towards a more spindle-like shape observed in cardiac fibroblasts following prolonged exposure to Yoda1 (Figure 4.1), which is indicative of a less differentiated state. The time courses of the Yoda1-induced decrease in *Acta2* and *Tgfb1* mRNA expression were investigated. *Acta2* mRNA expression was briefly increased after 2 h Yoda1 treatment, but was then reduced by a third after 24 h treatment, compared to control-treated cells (Figure 4.3A). *Tgfb1* mRNA expression also decreased by approximately a third after 24 h of Yoda1 treatment (Figure 4.3B). Despite both markers of myofibroblast differentiation showing a decrease at 24 h, the

difference in the area under the curves was not statistically significant between vehicle- and Yoda1-treated cells (Figure 4.3A,B), indicating unchanged mRNA expression over the entire 24 h period.

To more specifically explore whether the Yoda1-induced decrease in *Acta2* and *Tgfb1* mRNA expression at 24 h was due to the Piezo1 channel and not a non-specific effect of Yoda1, siRNA targeting Piezo1 was utilised. As expected, there was a significant reduction in *Acta2* mRNA expression (Figure 4.4A) and a trend for a decrease in *Tgfb1* mRNA expression (Figure 4.4B) following Yoda1 treatment in murine cardiac fibroblasts transfected with control siRNA. These outcomes were unaffected by the use of Piezo1-specific siRNA (Figure 4.4A,B), indicating that these effects of Yoda1 may be Piezo1-independent.

To investigate if α-SMA protein expression was affected by Yoda1-evoked Piezo1 activation, murine cardiac fibroblasts were stained for α-SMA following Yoda1 treatment, with either vehicle or TGF-β1 present. TGF-β1 treatment increased the expression and organisation of α-SMA fibres and led to larger cells (Figure 4.5A), consistent with a myofibroblast phenotype, as has been shown previously in human cardiac fibroblasts (van Nieuwenhoven *et al.* 2013). α-SMA immunocytochemistry of cultured murine cardiac fibroblasts revealed that, as in Figure 4.1, Yoda1 treatment had the opposite effect and altered the morphology of fibroblasts to a smaller, more spindle-like, less rhomboid shape, in comparison with vehicle-treated cells (Figure 4.5A). When cells were exposed to both TGF-β1 and Yoda1, cell morphology was more similar to control untreated cells (Figure 4.5A). Together, the mRNA and cell morphology data indicate that Piezo1 activation using Yoda1 is opposing myofibroblast differentiation. However, it was apparent that untreated cardiac fibroblasts already exhibited a myofibroblast phenotype, as shown by the appearance of α-SMA fibres, which are absent from undifferentiated cardiac fibroblasts, indicating that cells have already undergone differentiation to some extent in culture (Figure 4.5A).

A similar experiment was performed to quantify the effect of Yoda1 on α-SMA protein expression in murine cardiac fibroblasts by western blotting. α-SMA was expressed in vehicle-treated cells and did not increase further in response to TGF-β1 treatment (Figure 4.5B). This differed from data in human cardiac fibroblasts where α-SMA protein levels were upregulated by TGF-β1 treatment (van Nieuwenhoven *et al.* 2013). These data again indicate that the cardiac

fibroblasts were already differentiated in culture. It became apparent that Yoda1 did not reduce α-SMA protein levels (Figure 4.5B).

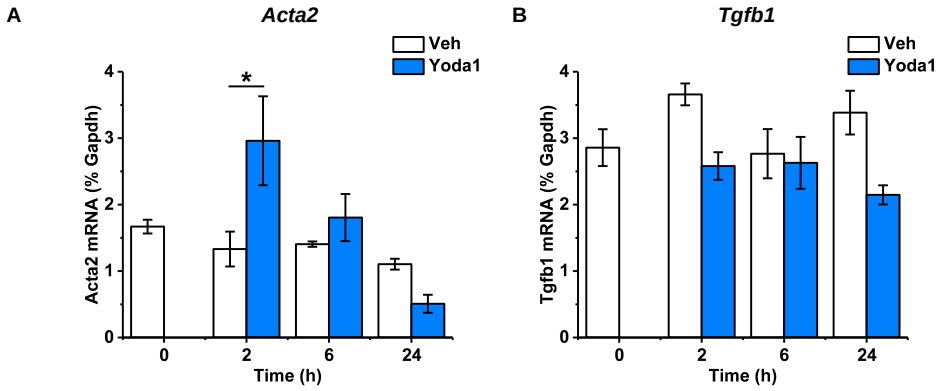

Figure 4.3 Time course of *Acta2* and *Tgfb1* mRNA expression following Yoda1 treatment. Murine cardiac fibroblasts were treated with vehicle or 10 µM Yoda1 for 0, 2, 6 or 24 h before measuring **(A)** *Acta2* and **(B)** *Tgfb1* mRNA expression, relative to *Gapdh*, *P<0.05 following an ANOVA with Tukey's post-hoc test (n=3).

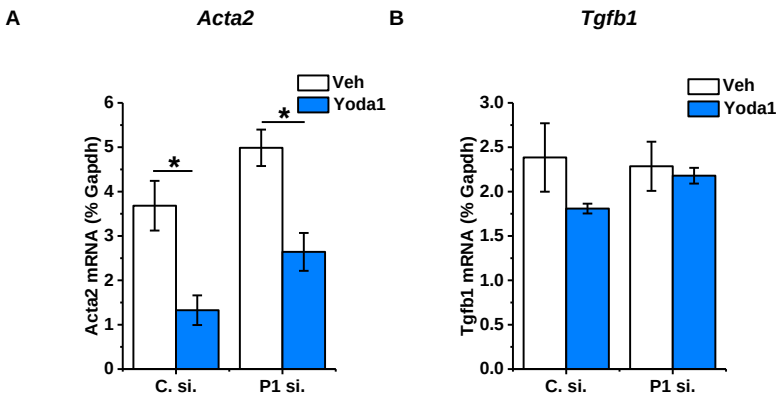

Figure 4.4 Effect of Piezo1-specific siRNA on *Acta2* and *Tgfb1* mRNA expression following Yoda1 treatment. Murine cardiac fibroblasts were transfected with control (C) or Piezo1-specific (P1) siRNA and subsequently treated with either vehicle or 10 μM Yoda1 for 24 h before measuring **(A)** *Acta2* and **(B)** *Tgfb1* mRNA expression by RT-PCR, relative to *Gapdh*, *P<0.05 following an ANOVA with Tukey's post-hoc test (n=3).

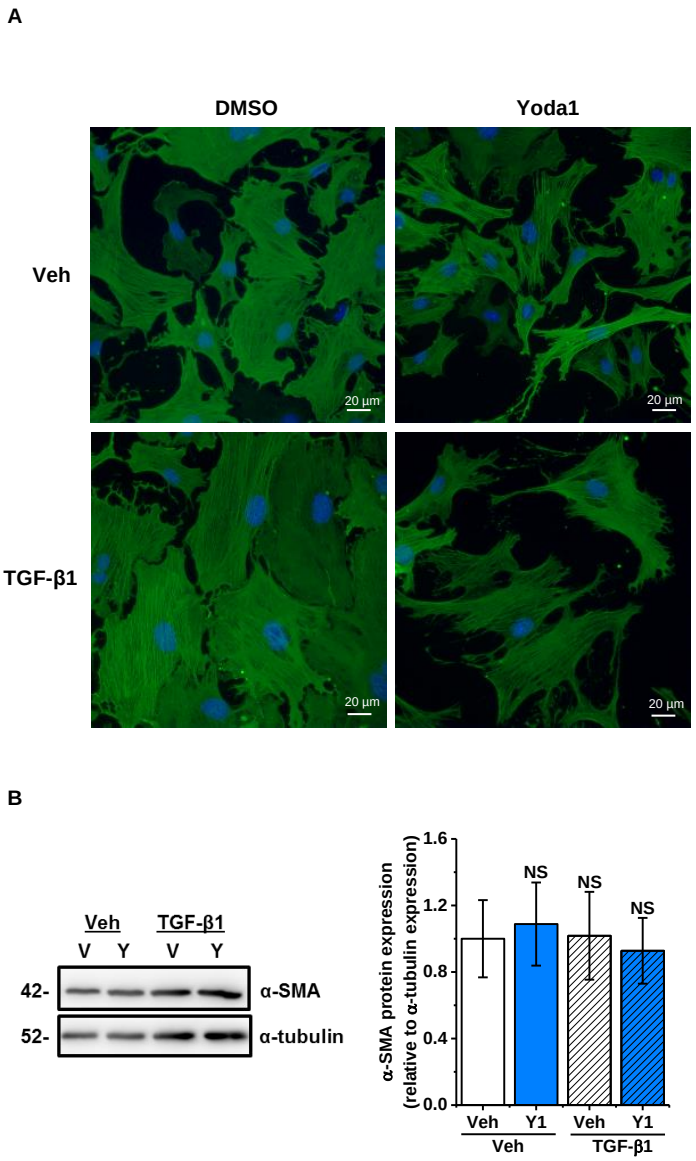

Figure 4.5 Effect of Yoda1 on TGF-β1-induced changes in cell morphology and α-SMA expression. (A) Representative images of cultured murine cardiac fibroblasts treated for 24 h with vehicle, 10 µM Yoda1, 10 ng/ml TGF-β1 or 10 ng/ml TGF-β1 plus Yoda1 and then immunostained for α-SMA (green); DAPI staining (blue) identifies nuclei. Scale bar = 20 µm. **(B)** Cells were treated for 24 h with vehicle, 10 µM Yoda1, 10 ng/ml TGF-β1 or 10 ng/ml TGF-β1 plus Yoda1 and probed for α-SMA protein; equal loading of samples was confirmed by probing for α-tubulin. Graph shows mean densitometric data, P=NS, not significant following an ANOVA with Tukey's post-hoc test (n=3).

4.4.2.2 The effect of Yoda1 on myofibroblast-mediated collagen gel contraction

The ability of fibroblasts to contract collagen gels is a marker of their differentiation to the myofibroblast phenotype, i.e. increased gel contraction correlates with increased myofibroblast activity. To functionally investigate the effect of Yoda1 on cardiac myofibroblast differentiation, collagen gel contraction assays were therefore employed. Collagen gels seeded with mouse cardiac fibroblasts were treated with TGF-β1 or vehicle, with and without Yoda1 for 24 h. As expected, there was a trend for TGF-β1 to reduce collagen gel weight and area, compared to untreated gels, which implies increased myofibroblast differentiation (Figure 4.6A-C). Yoda1 stimulated a significant 39% decrease in collagen gel weight and decreased the collagen gel area by a third, compared to unstimulated gels (Figure 4.6A-C), indicating even more pronounced myofibroblast differentiation than TGF-β1 treatment. These data suggest that Yoda1 is inducing myofibroblast differentiation, contrary to the previous gene expression data.

It was important to investigate if Yoda1-evoked myofibroblast differentiation was dependent on Piezo1. Yoda1-induced gel contraction was not affected by Piezo1-specific siRNA (Figure 4.6D-F). Further evidence that this effect was Piezo1-independent came from the use of compound 159, an alternative activator of Piezo1. This compound found in the analogue screen has similar properties and effects to Yoda1 and, when applied to murine cardiac fibroblasts, did not instigate a decrease in collagen gel weight or area as had been observed with Yoda1 (Figure 4.6D-F). These data imply that Yoda1 increases the ability of cardiac myofibroblasts to contract collagen gels in a Piezo1-independent manner.

A previous publication suggested that not all Yoda1 effects occur through Piezo1 and that Yoda1 could activate both the Akt and ERK signalling pathways in human endothelial cells independently of Piezo1 (Dela Paz and Frangos 2018). With this study in mind, it was investigated whether the ERK pathway was important for Yoda1-induced collagen gel contraction. Collagen gels seeded with mouse cardiac fibroblasts were pretreated for 1 h with an inhibitor of the ERK pathway, PD98059, and then treated with Yoda1 or vehicle for 24 h. Increased gel contraction following Yoda1 application was abolished in cells pretreated with

the ERK pathway inhibitor (Figure 4.7A-C). These data suggest that the ERK pathway is important for the Yoda1-evoked increase in collagen gel contraction.

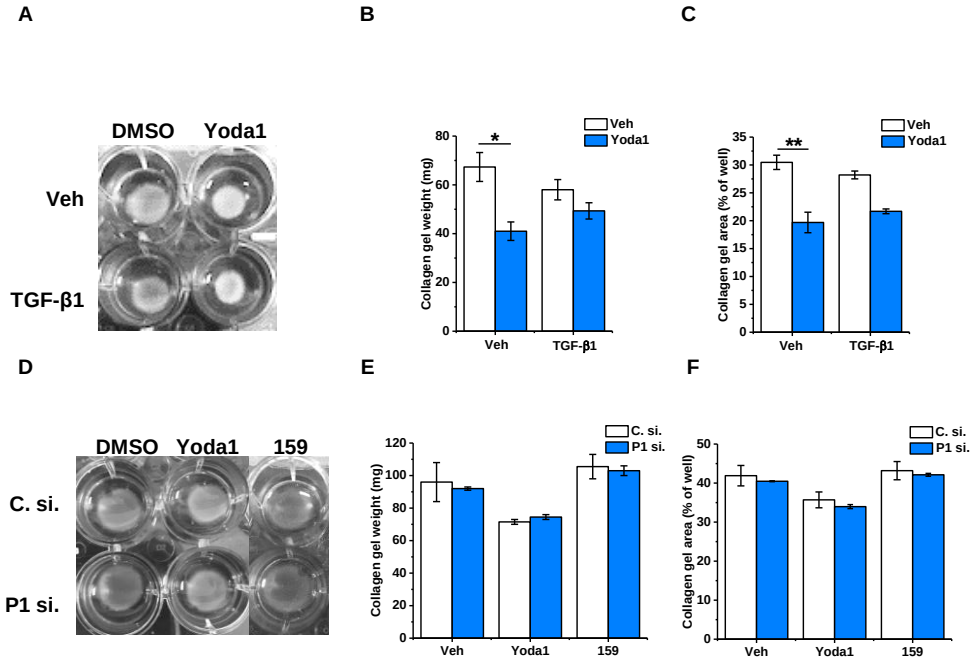

Figure 4.6 Effect of Piezo1 knockdown on Yoda1-evoked collagen gel contraction. (A) Representative images of contracted gels containing murine cardiac fibroblasts after 24 h treatment with vehicle, 10 µM Yoda1 or 10 ng/ml TGFβ +/- Yoda1. Mean data are illustrated in bar charts showing **(B)** collagen gel weight and **(C)** collagen gel area (as a % of the well) after 24 h treatment, *P<0.05, **P<0.01 following an ANOVA with Tukey's post-hoc test (n=3). **(D)** Representative images of contracted gels containing murine cardiac fibroblasts after 24 h treatment with vehicle, 10 µM Yoda1 or 10 µM compound 159 (a Piezo1 activator) following transfection with control (C) or Piezo1-specific (P1) siRNA. Mean data are shown in bar charts illustrating the **(E)** collagen gel weight and **(F)** collagen gel area (as a % of the well) after 24 h treatment, P=NS, not significant following an ANOVA with Tukey's post-hoc test (n=2).

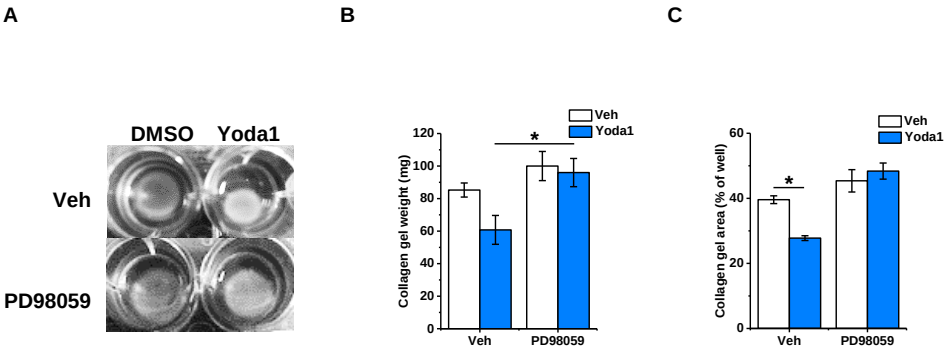

Figure 4.7 Role of the ERK pathway in Yoda1-evoked collagen gel contraction. (A) Representative images of contracted gels containing murine cardiac fibroblasts after 24 h treatment with vehicle or 10 µM Yoda1 following pretreatment for 1 h with vehicle or 30 µM PD98059 (ERK pathway inhibitor). Bar charts show mean data illustrating **(B)** collagen gel weight and **(C)** collagen gel area (as a % of the well), *P<0.05 following an ANOVA with Tukey's post-hoc test (n=4).

4.4.3 The effect of Yoda1 on Tenascin C

TNC, a matricellular protein discussed in Chapter 1, is the founding member of a family of four tenascins and was discovered to be highly expressed in embryonic ECM (Chiquet-Ehrismann *et al.* 1988). TNC is virtually undetected in healthy adult tissue but becomes transiently re-expressed upon myocardial injury and down-regulated following tissue repair (Willems, Arends and Daemen 1996). Increasing circulating TNC levels correlate with poor prognosis and mortality in patients following MI (Sato *et al.* 2006) and it is thought that the protein may promote tissue healing but enhance fibrosis and inflammation (Midwood *et al.* 2011). It had been established in the earlier screen that *Tnc* mRNA expression was increased in murine cardiac fibroblasts treated with Yoda1 for 24 h, compared to vehicle-treated cells (Figure 4.2I). Considering this, the investigation into the altered expression of TNC following Piezo1 activation was continued.

4.4.3.1 Yoda1 induces TNC mRNA expression in cardiac fibroblasts

In further experiments, *Tnc* mRNA expression was shown to increase in a time-dependent manner in response to Yoda1 (Figure 4.8A). After 6 h, *Tnc* mRNA expression was significantly increased by 15-fold, compared to the expression at 0 h or the expression when cells were treated with vehicle only (Figure 4.8A). Data were similar in human cardiac fibroblasts but over a slower time course, with *TNC* mRNA expression being significantly increased after 24 h Yoda1 treatment. The increase was not as substantial as that in mouse cells, with mRNA increasing by 5-fold compared to vehicle-treated cells (Figure 4.8B).

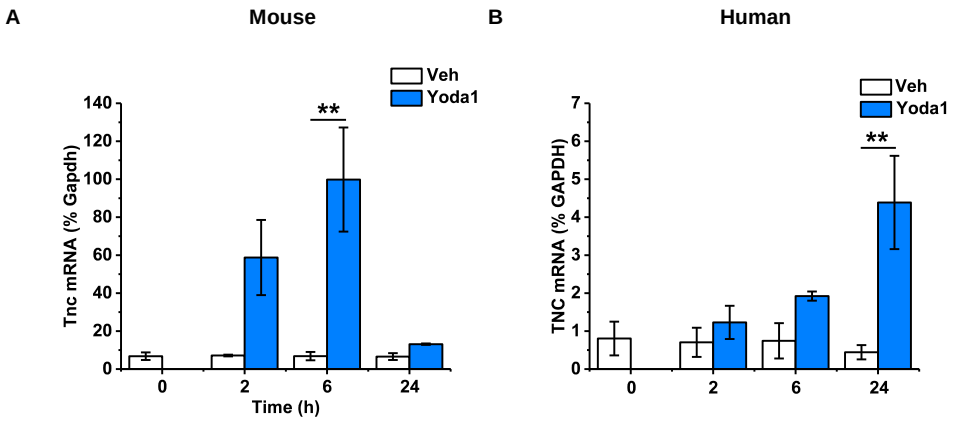

Figure 4.8 Effect of Yoda1 on Tnc / *TNC* mRNA expression in murine and human cardiac fibroblasts. (A) Murine and **(B)** human cardiac fibroblasts were exposed to vehicle or 10 μM Yoda1 for 2-24 h before measuring *Tnc* / *TNC* mRNA levels by RT-PCR, **P<0.01 following an ANOVA with Tukey's post-hoc test (n=3). Data are expressed relative to the housekeeper, *Gapdh* / *GAPDH*.

4.4.3.2 Yoda1 induces TNC protein expression in cardiac fibroblasts

Western blotting was performed to explore if there was also a change in TNC protein following Yoda1 treatment. TNC protein expression increased 2.5-fold following 24 h Yoda1 treatment in murine cardiac fibroblasts and this was maintained over 72 h of treatment (Figure 4.9A). A time course at earlier time points revealed a doubling in TNC protein expression following 6 h Yoda1 treatment, in comparison with vehicle-treated cells (Figure 4.9B). Therefore a 6 h time point was used for all future experiments investigating TNC mRNA and protein expression in mouse cells.

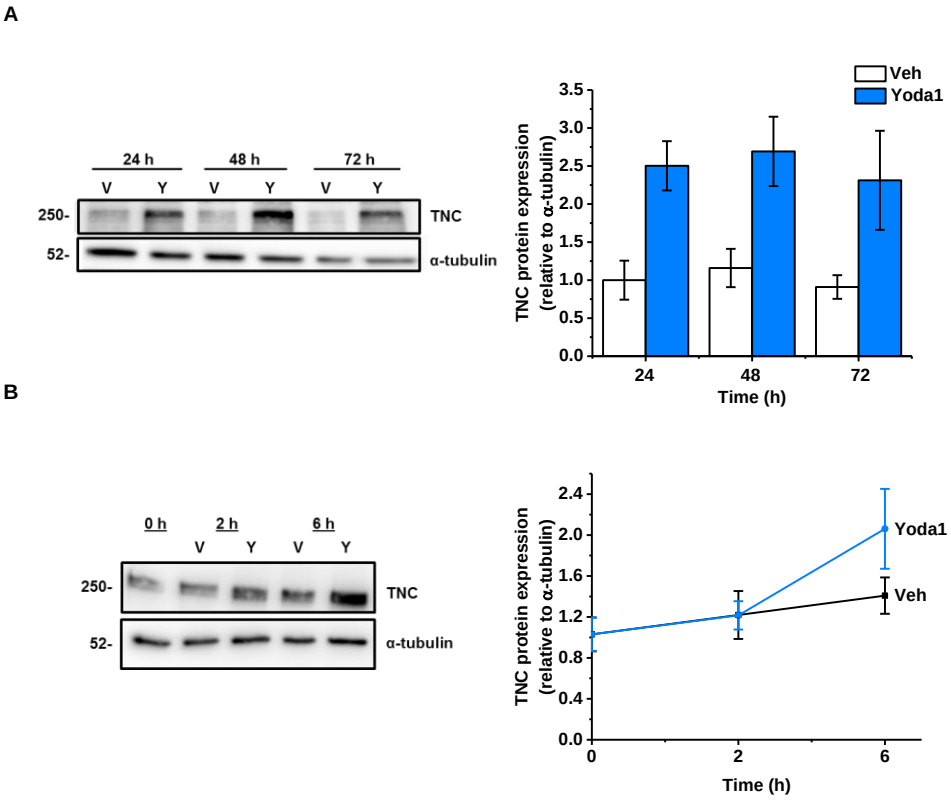

Figure 4.9 Effect of Yoda1 on TNC protein expression in murine cardiac fibroblasts. (A) Murine cardiac fibroblasts exposed to vehicle or 10 μM Yoda1 for 24-72 h before measuring TNC protein expression, mean data showing TNC expression relative to α-tubulin is shown on the right (n=3). **(B)** Murine cardiac fibroblasts exposed to vehicle or 10 μM Yoda1 for 2 or 6 h before measuring TNC protein expression, quantification relative to α-tubulin is shown on the right (n=3).

4.4.3.3 Yoda1-induced TNC expression is dependent on Piezo1

To investigate whether Yoda1-evoked *Tnc* mRNA expression was dependent on Piezo1, cardiac fibroblasts from Piezo1$^{+/-}$ heterozygous KO (Het) mice and gain-of-function Piezo1-mutated (M-R) mice were utilised. As expected, there was a 10-fold increase in *Tnc* mRNA expression after 6 h Yoda1 treatment in cardiac fibroblasts isolated from WT mice (Figure 4.10A). However, when Yoda1 was applied to cardiac fibroblasts isolated from Piezo1$^{+/-}$ (Het) mice, the respective increase in *Tnc* mRNA was reduced by ~50% (Figure 4.10A). The increase in *Tnc* mRNA expression was not observed when cardiac fibroblasts were treated with the inactive analogue of Yoda1, compound 2e, which was identified during the screening process in Chapter 3, implying that the response was Yoda1-specific. Furthermore, Yoda1-evoked TNC protein expression, was reduced by ~50% in cardiac fibroblasts from Piezo1$^{+/-}$ heterozygous knockout mice (Figure 4.10B).

A gain-of-function mutation in human Piezo1 (M2225R) which causes delayed inactivation kinetics of the channel (Albuisson *et al.* 2013) has been shown to lead to increased Yoda1-evoked Ca^{2+} influx in murine cardiac fibroblasts which have the equivalent mutation (M2220R) (Figure 3.27). The Yoda1-induced increase in *Tnc* mRNA expression in WT cardiac fibroblasts was increased a further 4-fold in M-R cells (Figure 4.10C). Similar changes were observed at the protein level (Figure 4.10D). These data imply that Yoda1-induced TNC expression is dependent on Piezo1 as two genetically modified mouse models with opposing Piezo1 activity showed a corresponding alteration of Yoda1-evoked TNC expression.

To further explore whether the increase in TNC protein expression was due to activation of Piezo1, siRNA targeting *Piezo1* was employed. As expected, there was a 3-fold increase in TNC protein expression after Yoda1 treatment in murine cardiac fibroblasts transfected with control siRNA, and importantly this response was attenuated to basal levels when cells were transfected with Piezo1 siRNA (Figure 4.11).

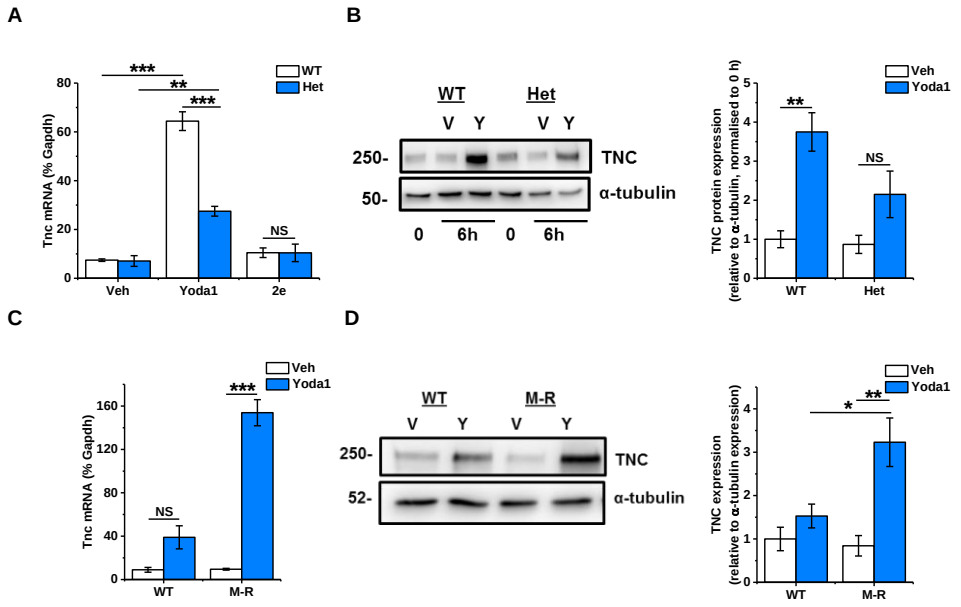

Figure 4.10 Effect of altering Piezo1 expression or activity on Yoda1-induced TNC expression. (A) Cardiac fibroblasts from wild-type (WT; n=4) and Piezo1$^{+/-}$ heterozygous knockout (Het; n=3) mice were treated with vehicle, 10 μM Yoda1 or compound 2e for 6 h before measuring *Tnc* mRNA expression relative to *Gapdh*, **P<0.01, ***P<0.001, P=NS, not significant following an ANOVA with Tukey's post-hoc test. **(B)** Cardiac fibroblasts from WT (n=4) and Het (n=3) mice were treated with vehicle or 10 μM Yoda1 for 6 h before measuring TNC protein expression. On the right, this is quantified relative to α-tubulin and normalised to the expression at 0 h, **P<0.01, p=NS, not significant following an ANOVA with Tukey's post-hoc test. **(C)** Cardiac fibroblasts from WT and gain-of-function Piezo1-mutated mice (M-R) mice were treated with vehicle or 10 μM Yoda1 for 6 h before measuring Tnc mRNA expression, relative to *Gapdh*, ***P<0.001, P=NS, not significant following an ANOVA with Tukey's post-hoc test (n=3). **(D)** Cardiac fibroblasts from WT and gain-of-function Piezo1-mutated mice (M-R) mice were treated with vehicle or 10 μM Yoda1 for 6 h before measuring TNC protein expression. On the right, quantified data are shown, relative to α-tubulin, *P<0.05, **P<0.01 following an ANOVA with Tukey's post-hoc test (n=3).

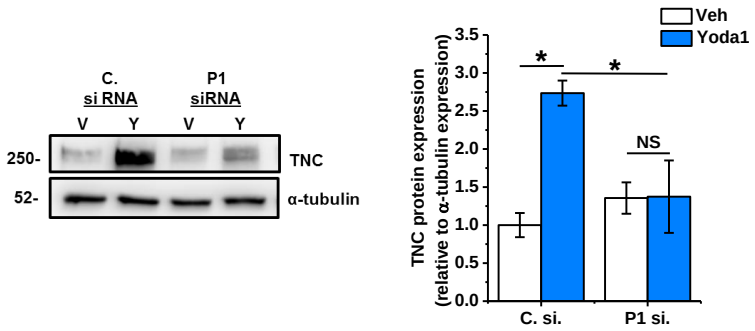

Figure 4.11 Effect of Piezo1 knockdown on Yoda1-induced TNC expression. Representative blot of murine cardiac fibroblasts transfected with either control (C) or Piezo1-specific (P1) siRNA before treatment with vehicle or 10 μM Yoda1 for 6 h. Samples were immunoblotted for TNC and re-probed with α-tubulin antibody to confirm equal protein loading. Graph on the right shows the mean densitometric data, *P<0.05, P=NS, not significant following an ANOVA with Tukey's post-hoc test (n=3).

4.4.3.4 Mechanical stress has no effect on TNC expression in cardiac fibroblasts

Yoda1 is a useful pharmacological tool with which to activate the Piezo1 channel and learn about its role in cardiac fibroblasts. However, it is crucial to investigate whether Yoda1 mimics mechanical activation of the channel which occurs *in vivo*. Therefore, in this section, different strategies were employed to stimulate mechanical stress in cardiac fibroblasts.

TNC is abundantly expressed in all musculoskeletal regions transmitting high mechanical forces from one tissue component to another (Järvinen *et al.* 2003) and demonstrates high expression at the branching point of arteries (Mackie *et al.* 1992). Thus, TNC is considered a mechanosensitive gene.

Firstly, the effects of shear stress were investigated. Murine cardiac fibroblasts subjected to 10 $dyn.cm^{-2}$ shear stress using an orbital shaker for 24 h had unaltered *Tnc* mRNA expression, compared to cells kept in parallel under static conditions (Figure 4.12A).

Secondly, murine cardiac fibroblasts were grown on tailored culture substrates (10 kPa, 30 kPa and tissue culture plastic which is approximately $1x10^6$ kPa) to determine whether the stiffness on which the cells grow affects *Tnc* mRNA expression. Increasing the stiffness of the substrate led to a trend of increased *Tnc* mRNA expression but this was not statistically significant (Figure 4.12B). This occurred independently of Piezo1 as it was not affected by Piezo1 gene silencing (Figure 4.12B).

Thirdly, cyclic stretching (1 Hz, 10% stretch) of human cardiac fibroblasts for 6 h increased *TNC* mRNA expression by approximately 25 % compared to cells kept under static conditions, although this was not statistically significant (Figure 4.12C). However, once more this was not dependent on Piezo1, as shown by silencing the *PIEZO1* gene (Figure 4.12C). Despite the previously discussed evidence that TNC is a mechanosensitive gene, none of the mechanical stimuli investigated in the present study modulated TNC expression. It may be that alternative stimuli which are able to mechanically activate Piezo1 could induce TNC expression in cardiac fibroblasts.

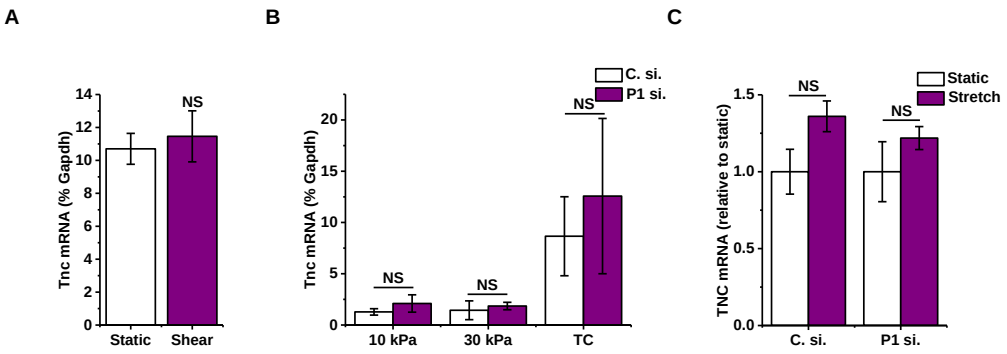

Figure 4.12 Effect of Piezo1 knockdown on *Tnc* / *TNC* mRNA expression induced by mechanical stimuli. (A) RT-PCR analysis of *Tnc* mRNA levels in murine cardiac fibroblasts exposed to 10 dyn.cm^{-2} shear stress for 24 h using an orbital shaker, compared to cells kept in parallel under static conditions, P=NS, not significant following a t-test (n=3). **(B)** RT-PCR analysis of *Tnc* mRNA expression when murine cardiac fibroblasts were plated on substrates of differing levels of stiffness for 24 h. TC=tissue culture plate (10^6 kPa). Cardiac fibroblasts were previously transfected with either control (C) or Piezo1-specific (P1) siRNA, P=NS, not significant following an ANOVA with Tukey's post-hoc test (n=3). **(C)** RT-PCR analysis of *TNC* mRNA expression after exposure of human cardiac fibroblasts to 6 h cyclic stretch (1 Hz, 10% stretch), compared to fibroblasts maintained in parallel under static conditions. Cardiac fibroblasts were previously transfected with either control (C) or Piezo1-specific (P1) siRNA. Data are normalised to static control, P=NS, not significant following an ANOVA with Tukey's post-hoc test (n=7). All expression levels are expressed relative to the relevant housekeeper, *Gapdh* / *GAPDH*.

4.4.4 The effect of Yoda1 on interleukin-6

IL-6 is a pleiotropic cytokine which has been shown to be mechanosensitive. Fibroblasts from several sources have been shown to secrete IL-6 in response to mechanical stretch (House *et al.* 2012; Skutek *et al.* 2001), including coronary artery fibroblasts which showed higher expression of IL-6 after 24 h of stretch (Li *et al.* 2013). IL-6 has pro-inflammatory, anti-inflammatory and fibrotic roles in the heart depending on the context and duration of its effect (Fontes, Rose and Čiháková 2015). *In vitro* studies have shown that IL-6 is secreted from cardiac fibroblasts in response to several well-known hypertrophic stimuli, including β-adrenergic receptor stimulation and Ang II (Porter and Turner 2009). IL-6 can directly induce cardiomyocyte hypertrophy *in vitro* (Zhao *et al.* 2016a; Ancey *et al.* 2003) and Ang II- or phenylephrine-induced cardiomyocyte hypertrophy is impaired in myocytes isolated from IL-6 KO mice (Zhao *et al.* 2016a), implying that IL-6 secretion is necessary for induction of myocyte hypertrophy by these stimuli. Given the causative link between mechanical stimulation and cardiac hypertrophy (Tarone and Lembo 2003), investigation into changes in IL-6 expression following Piezo1 activation was pursued further.

4.4.4.1 Yoda1 induces IL-6 mRNA expression and secretion

It was shown previously that 24 h Yoda1 treatment increased *Il6* mRNA expression in murine cardiac fibroblasts in a concentration dependent manner (Figure 4.2J). It was subsequently established that the increase in *Il6* mRNA expression occurred in a time-dependent manner with a significant increase being observed after 24 h (Figure 4.13A). The data were similar in human cardiac fibroblasts but, in these cells, a significant increase in *IL6* mRNA occurred earlier, with a doubling in expression after 2 h Yoda1 treatment (Figure 4.13B). The Yoda1-evoked increase in *Il6* mRNA expression in murine cardiac fibroblasts correlated with an increase in IL-6 secretion quantified using ELISA (Figure 4.14). In Yoda1-treated cells, the secretion of IL-6 was over 4-fold greater than that observed in vehicle-treated cells (Figure 4.14).

The inactive Yoda1 analogue, compound 2e (described in Section 3.4.4.2), did not induce Ca^{2+} influx (Figure 4.15A) or *Il6* mRNA expression (Figure 4.15B) in murine cardiac fibroblasts.

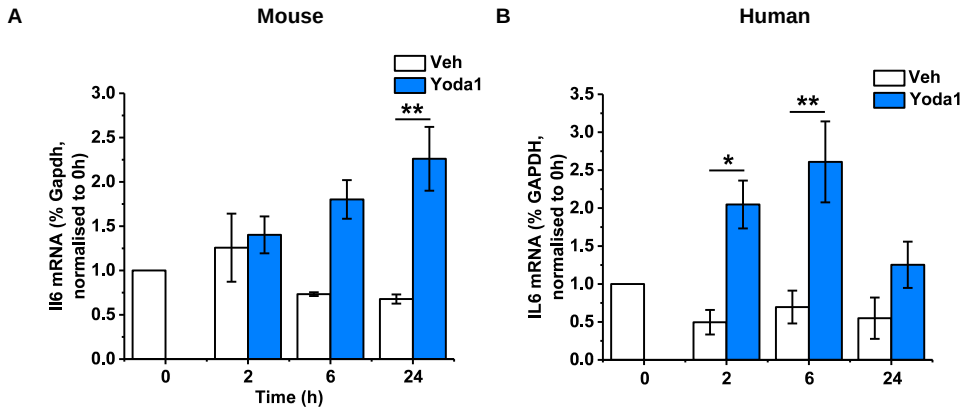

Figure 4.13 *Il6* / *IL6* mRNA expression following Yoda1 treatment in murine and human cardiac fibroblasts. (A) Murine and **(B)** human cardiac fibroblasts were exposed to vehicle or 10 μM Yoda1 for 2-24 h before measuring *Il6* / *IL6* mRNA levels by RT-PCR. Data are expressed as % of housekeeper, *Gapdh* / *GAPDH*, *P<0.05, **P<0.01 versus vehicle-treated cells following an ANOVA with Tukey's post-hoc test (n=3). Data are normalised to 0 h.

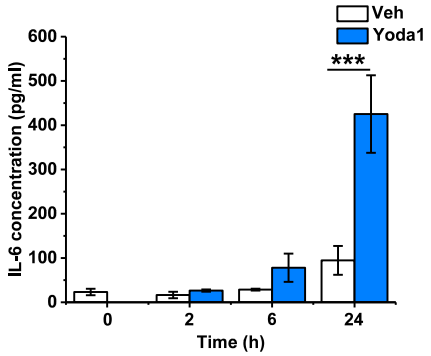

Figure 4.14 Effect of Yoda1 on IL-6 secretion from murine cardiac fibroblasts. Murine cardiac fibroblasts were exposed to vehicle or 10 μM Yoda1 for 2-24 h before analysing conditioned medium for IL-6 levels by ELISA, ***P<0.001 versus vehicle-treated cells following an ANOVA with Tukey's post-hoc test (n=3).

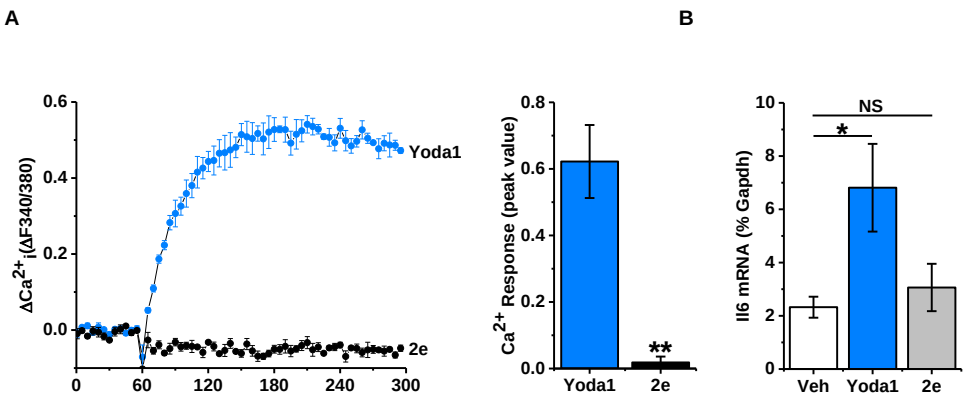

Figure 4.15 Effect of compound 2e, an inactive analogue of Yoda1, on Ca^{2+} entry and *Il6* mRNA expression in murine cardiac fibroblasts. (A) Representative Ca^{2+} traces illustrating Ca^{2+} entry evoked by 10 μM Yoda1 or compound 2e in murine cardiac fibroblasts. The mean data are shown to the right, **P<0.01 following a t-test (n/N=3/9). **(B)** Murine cardiac fibroblasts were treated with either vehicle, 10 μM Yoda1 or 10 μM compound 2e for 6 h before measuring *Il6* mRNA expression by RT-PCR. Data are expressed relative to the housekeeper, *Gapdh*, *P<0.05, p=NS, not significant versus vehicle-treated cells following an ANOVA with Tukey's post-hoc test (n=4).

4.4.4.2 Yoda1-evoked IL-6 expression and secretion are dependent on Piezo1

To investigate if Yoda1-evoked IL-6 induction was dependent on Piezo1, cardiac fibroblasts were isolated from Piezo1$^{+/-}$ heterozygous KO mice and gain-of-function Piezo1 (M-R) mice. The Yoda1-induced *Il6* mRNA expression was reduced by approximately 50 % in cardiac fibroblasts isolated from Piezo1$^{+/-}$ mice, compared to in cells from WT mice (Figure 4.16A). The Yoda1-induced increase in IL-6 protein secretion was also reduced by approximately 50 %, in cardiac fibroblasts isolated from hearts of Piezo1$^{+/-}$ Het mice compared to those from WT hearts (Figure 4.16B). This is in keeping with the reduction in Piezo1 expression and Ca^{2+} influx in response to Yoda1 in these cells (Figure 3.26). Similarly to the mRNA expression data, IL-6 secretion was unchanged following treatment of cardiac fibroblasts with compound 2e, an inactive analogue of Yoda1 (Figure 4.16B). Conversely, the Yoda1-induced increase in *Il6* mRNA expression after 6 h treatment was increased by 3-fold in cardiac fibroblasts isolated from gain-of-function M-R mice, compared with those from WT mice (Figure 4.16C).

To investigate further whether the induction in IL-6 was due to Piezo1, siRNA targeting Piezo1 in both murine and human cardiac fibroblasts was utilised. There was a doubling in *Il6* mRNA expression in control siRNA-transfected murine cardiac fibroblasts after Yoda1 treatment; this was reduced to basal levels in cells transfected with Piezo1-specific siRNA (Figure 4.17A). These data were replicated when conditioned media was analysed, as evidenced by the attenuation of IL-6 secretion from murine cardiac fibroblasts transfected with Piezo1-specific siRNA, compared to those transfected with control siRNA (Figure 4.17B).

A similar relationship was observed in human cardiac fibroblasts. Piezo1-specific siRNA successfully reduced *PIEZO1* mRNA expression by >75% (Figure 4.18A) and, subsequently, the Yoda1-evoked increase in *IL6* mRNA expression was attenuated back to basal levels (Figure 4.18B). The inactive Yoda1 analogue, 2e, had no effect on *IL6* mRNA expression, indicating a specific Yoda1 effect (Figure 4.18B). These data establish that Yoda1 induces IL-6 expression and secretion in cardiac fibroblasts via a Piezo1-dependent mechanism.

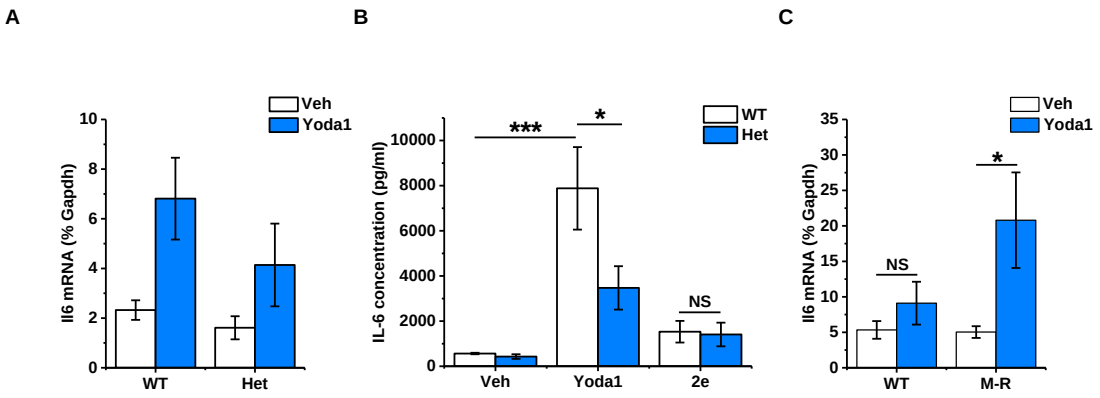

Figure 4.16 Effect of altering Piezo1 expression or activity on Yoda1-evoked *Il6* mRNA expression and IL-6 secretion. (A) Cardiac fibroblasts isolated from wild-type (WT; n=4) and Piezo1$^{+/-}$ heterozygous knockout (Het; n=3) mice were treated with vehicle or 10 μM Yoda1 for 6 h before measuring *Il6* mRNA expression, relative to *Gapdh*. **(B)** Cardiac fibroblasts from WT (n=4) and Het (n=3) mice were treated with vehicle, 10 μM Yoda1 or compound 2e for 24 h before measuring IL-6 levels in conditioned medium using ELISA, *P<0.05, ***P<0.001, P=NS, not significant following an ANOVA with Tukey's post-hoc test. **(C)** Cardiac fibroblasts isolated from WT (n=6) and gain-of-function Piezo1-mutated (M-R; n=7) mice were treated with vehicle or 10 μM Yoda1 for 6 h before measuring *Il6* mRNA expression, relative to *Gapdh*, *P<0.05, P=NS, not significant following an ANOVA with Tukey's post-hoc test.

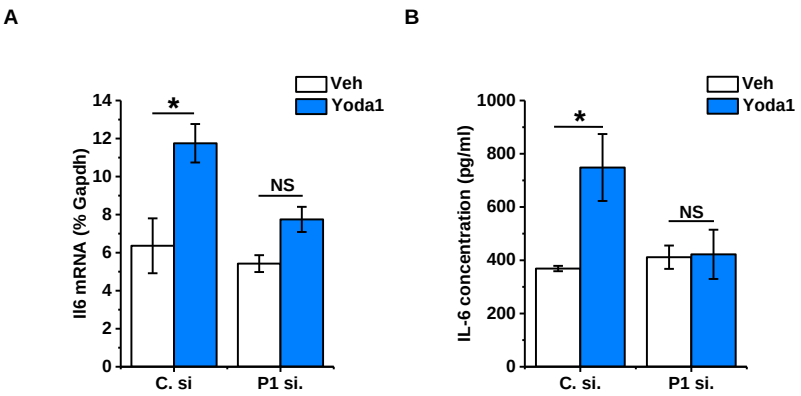

Figure 4.17 Effect of Piezo1 knockdown on Yoda1-induced IL-6 expression and secretion in murine cardiac fibroblasts. Cells were transfected with control (C) or Piezo1-specific (P1) siRNA and treated with either vehicle or 10 μM Yoda1 for 24 h before **(A)** measuring *Il6* mRNA expression, relative to *Gapdh* or **(B)** collecting conditioned media and measuring IL-6 levels by ELISA, *P<0.05, P=NS, not significant versus-vehicle-treated cells following an ANOVA with Tukey's post-hoc test (n=3).

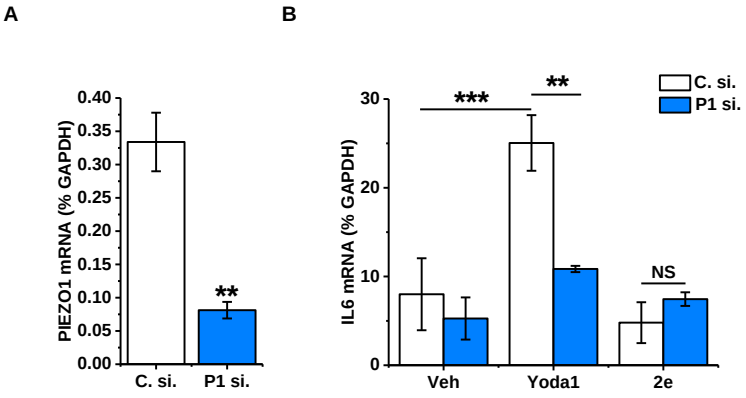

Figure 4.18 The effect of Piezo1 on Yoda1-evoked *IL6* mRNA expression in human cardiac fibroblasts. Human cardiac fibroblasts transfected with control (C) or Piezo1-specific (P1) siRNA were exposed to vehicle, 10 µM Yoda1 or compound 2e for 6 h before measuring **(A)** *PIEZO1* mRNA or **(B)** *IL6* mRNA by RT-PCR. Data are expressed as % of housekeeper, *GAPDH*, **P<0.01, ***P<0.001, P=NS, not significant following (A) a t-test and (B) an ANOVA with Tukey's post-hoc test (n=3).

4.4.4.3 The effect of mechanical stimuli on IL6 mRNA expression and secretion in cardiac fibroblasts

Fibroblasts from several sources have been shown to secrete IL-6 in response to mechanical stretch (House *et al.* 2012; Skutek *et al.* 2001). Therefore, it was explored whether mechanical activation of cardiac fibroblasts was coupled to IL-6 expression and whether this occurred via a Piezo1-dependent mechanism.

Exposing murine cardiac fibroblasts to 10 dyn.cm^{-2} shear stress for 24 h had no effect on *Il6* mRNA expression (Figure 4.19A). Tailored culture plates coated with fibronectin used to observe whether changes in substrate stiffness affect *Il6* mRNA expression revealed that plating murine cardiac fibroblasts on substrates of increasing stiffness for 24h led to a trend of increasing *Il6* mRNA expression; but gene silencing of Piezo1 suggested this was not a Piezo1-dependent effect (Figure 4.19B). Finally, cyclic stretching (1 Hz, 10% stretch) of human cardiac fibroblasts for 6 h did not induce an increase in *IL6* mRNA expression, in comparison with cells kept under static conditions (Figure 4.19C). Stretching of cells was performed on collagen-coated plates which had a stiffness of 930 kPa.

It was hypothesised that the stretch stimulus was not applied to cells for long enough; therefore, 24 h of 1 Hz, 10% stretch was tested. At this point, human cardiac fibroblasts were also transfected with Piezo2-specific siRNA in order to investigate if Piezo2 had a role in stretch-evoked IL-6 induction as both channels have previously been observed to function in tandem (Zeng *et al.* 2018). *PIEZO2* mRNA expression in human cardiac fibroblasts was reduced by 62% when cells were transfected with Piezo2-specific siRNA, in comparison with control siRNA-transfected cells; this was maintained when siRNA targeting *PIEZO1* and *PIEZO2* were used concurrently (48 h after transfection, data not shown, n=1).

When both *PIEZO1* and *PIEZO2* were silenced in human cardiac fibroblasts, there was no change in *IL6* mRNA expression following 24 h stretch on collagen-I-coated membranes, compared to cells kept under in parallel under static conditions (Figure 4.20A). However, a role for Piezo1 under basal conditions was indicated as there was a marked reduction in *IL6* mRNA expression in both static and stretched human cardiac fibroblasts transfected with Piezo1-specific siRNA or both Piezo1- and Piezo2-specific siRNAs, compared to control siRNA-transfected cells (Figure 4.20A). This did not occur in cells transfected only with Piezo2-specific siRNA (Figure 4.20A). It was investigated whether this correlated

with the amount of IL-6 secreted from human cardiac fibroblasts. There was a slight trend for an increase in IL-6 secretion when mechanical load was applied to cells but this was not statistically significant (Figure 4.20B). The data correlated with mRNA data; following 24 h cyclic stretching (1 Hz, 10% stretch), IL-6 secretion was reduced by >50 % in both static and stretched cells transfected with Piezo1-specific siRNA and with both Piezo1- and Piezo2-specific siRNAs, in comparison with cells transfected with control siRNA (Figure 4.20B). These data imply that, although Piezo1 activation using mechanical stimuli does not induce IL-6 production, Piezo1 may have a role in the basal production of IL-6 expression in cardiac fibroblasts. This effect was not seen when cardiac fibroblasts were plated on much softer substrates (10, 30 kPa) or tissue culture plastic (Figure 4.19B). The plates of 10/30 kPa stiffness were coated with fibronectin whereas the FlexCell plates utilised in the stretch experiment in Figure 4.20 were coated with collagen. Therefore, the effect which Piezo1 has on basal IL-6 levels appears to be dependent on the mechanical and/or chemical environment in which the cells are grown.

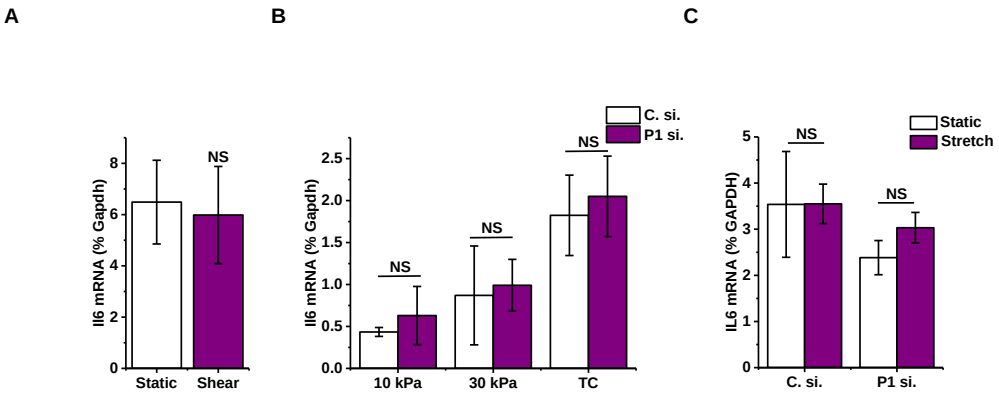

Figure 4.19 Effect of Piezo1 knockdown on *Il6* / *IL6* mRNA expression following application of mechanical stimuli. (A) RT-PCR analysis of *Il6* mRNA levels after murine cardiac fibroblasts were exposed to 24 h of 10 dyn.cm^{-2} shear stress, compared to cells kept under static conditions, P=NS, not significant following a t-test (n=3). **(B)** RT-PCR analysis of *Il6* mRNA expression after murine cardiac fibroblasts were plated on substrates of differing stiffness for 24 h. TC=tissue culture plate (10^{6} kPa). Cardiac fibroblasts were previously transfected with either control or Piezo1-specific siRNA, P=NS, not significant following an ANOVA with Tukey's post-hoc test (n=3). **(C)** RT-PCR analysis of *IL6* mRNA expression after exposure of human cardiac fibroblasts to 6 h cyclical stretch (1 Hz, 10% stretch), compared to fibroblasts maintained in parallel under static conditions. Cardiac fibroblasts were previously transfected with either control (C) or Piezo1-specific (P1) siRNA, P=NS, not significant following an ANOVA with Tukey's post-hoc test (n=10). All expression levels are expressed relative to the relevant housekeeper, *Gapdh* / *GAPDH*.

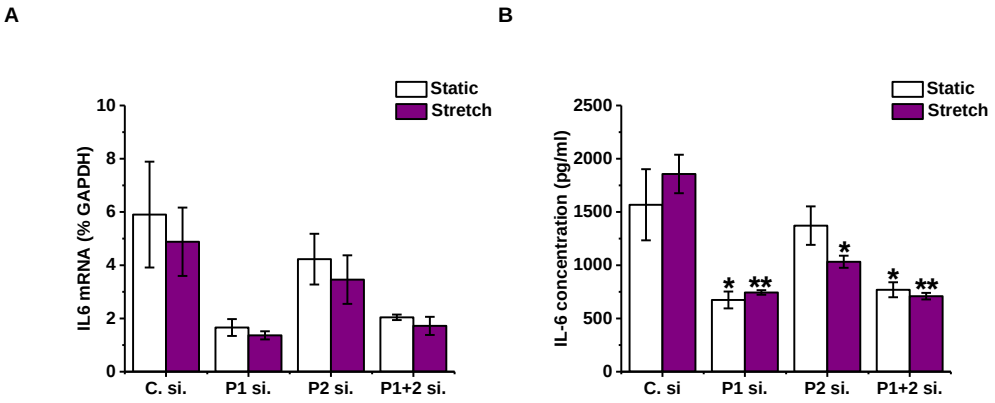

Figure 4.20 The effect of Piezo1 and Piezo2 knockdown on basal IL-6 levels in human cardiac fibroblasts. Human cardiac fibroblasts were transfected with either control (C) siRNA, Piezo1-specific (P1) siRNA, Piezo2-specific (P2) siRNA or Piezo1 plus Piezo1-specific (P1+2) siRNAs, before exposure to cyclical stretch (1 Hz, 10% stretch, 24 h). **(A)** *IL6* mRNA expression relative to *GAPDH* and **(B)** IL-6 levels in conditioned medium using ELISA, in comparison with fibroblasts maintained in parallel under static conditions, *P<0.05, **P<0.01 in comparison with control-siRNA transfected cells from the same group, following an ANOVA with Tukey's post-hoc test (n=3).

4.5 Discussion

The primary aim of this chapter was to investigate whether activation of the Piezo1 channel, using chemical activation such as Yoda1, or mechanical stimulation, leads to changes in the expression of genes associated with fibroblast function and cardiac remodelling.

Yoda1 was revealed to have no impact on the viability of murine cardiac fibroblasts after 24 h treatment, despite Yoda1 instigating cell death in endothelial cells after this prolonged period (Adam Hyman PhD thesis, 2018). Exposure to Yoda1 for 24 h modulated the expression of several genes in murine cardiac fibroblasts in a concentration-dependent manner, including increasing *Il6* and *Tnc* expression and decreasing *Acta2* (i.e. α-SMA), *Tgfb1* and *Postn* (i.e. periostin). Yoda1 had no effect on genes involved in ECM turnover (collagens, MMPs) or on *Piezo1* mRNA expression itself.

The decrease in *Acta2*, *Tgfb1* and *Postn* mRNA expression with Yoda1 was of interest as these molecules are key markers of myofibroblast differentiation. Further evidence for an effect of Yoda1 on fibroblast differentiation came from florescence microscopy illustrating that Yoda1 treatment induced a morphological change in cells towards a more spindle-like shape, similar to that observed in human cardiac fibroblasts after treatment with IL-1 (van Nieuwenhoven *et al.* 2013). A previous publication by Chubinskiy-Nadezhdin *et al.* (2019) on Piezo1 in a mouse fibroblast cell line also identified an altered cellular morphology caused by Yoda1 treatment. They observed increased cell perimeter and decreased roundness of cells following Yoda1 treatment, compared to vehicle-treated cells. This supports qRT-PCR data illustrating decreased mRNA expression of myofibroblast markers and the immunocytochemistry performed in the present study. Chubinskiy-Nadezhdin *et al.* (2019) also observed a concentration-dependent inhibition of cellular migration by Yoda1. Myofibroblasts are more migratory cells than fibroblasts and migrate to the wound area following cardiac injury (Baum and Duffy 2011). Therefore, knowledge that Yoda1 inhibits migration of fibroblasts correlates with the idea that Yoda1 induces the dedifferentiation of cardiac fibroblasts. These data combined suggest that Piezo1 activation is opposing myofibroblast differentiation. This observation is intriguing as mechanical stimulation is known to be an important driver of myofibroblast differentiation which, along with TGF-β, induces changes in gene expression,

including upregulation of α-SMA (Hinz and Gabbiani 2010). However, it is worth noting that although mRNA expression of *Acta2* and *Tgfb1* were decreased after 24 h Yoda1 treatment, there was no change in the overall expression over the entire 24 h. Further work using Piezo1-specific siRNA revealed that the Yoda1-evoked reduction in the expression of myofibroblast markers was not dependent on Piezo1. It was examined whether Yoda1 was able to oppose TGF-β-induced myofibroblast differentiation. Data obtained from immunocytochemistry and western blotting indicated that murine cells were already well differentiated in culture and the myofibroblast phenotype could not be induced any further. This prevented us investigating whether Yoda1 could oppose TGF-β-induced myofibroblast differentiation.

In the aforementioned study by van Nieuwenhoven *et al.* (2013), morphological changes induced by IL-1 were confirmed to be due to a reduced level of myofibroblast differentiation, as evidenced by an impaired capacity to contract collagen gels. In the present study, when murine cardiac fibroblasts were seeded into collagen gels, Yoda1 had the opposite effect and induced collagen gel contraction. This was suggested to be independent of Piezo1 as silencing Piezo1 using siRNA had no effect on Yoda1-evoked collagen gel contraction. Moreover, no effect was observed when gels were treated with compound 159, an agonist of Piezo1. It is possible that the outcome observed here is due to an off-target effect of Yoda1 or that the level of knockdown of Piezo1 is not sufficient to abolish the response. Further work would be essential in order to define if Piezo1 has a role in regulating myofibroblast differentiation; cardiac fibroblasts with a complete KO of Piezo1 would be helpful to confirm which theory is correct. From the contrasting evidence found during this study; Yoda1 does not appear to be inducing the "classical" myofibroblast phenotype. It may be that Yoda1 is inducing a phenotype with slightly different characteristics as recent studies have identified a range of phenotypes which serve different functions during post-MI cardiac remodelling (Ma *et al.* 2017; Fu *et al.* 2018).

It has been suggested that Yoda1 has Piezo1-independent effects in endothelial cells. Dela Paz and Frangos (2018) revealed that Yoda1-induced activation of both the Akt and ERK signalling pathways in human endothelial cells was not entirely dependent on Piezo1 activation. They came to this conclusion as, although both gadolinium and ruthenium red blocked Yoda1-induced Akt

phosphorylation and ruthenium red blocked Yoda1-induced ERK1/2 phosphorylation, the Piezo1 inhibitor GsMTx4 had no effect. They proposed that Yoda1 may be non-specific in its activation of Piezo1. However, the group did not attempt to knockdown Piezo1 using molecular methods; this would have been beneficial in order to come to a more definite conclusion. In the present study, ERK activation was investigated by pretreating collagen gels with an ERK pathway inhibitor; it was revealed that the ERK pathway may be involved in Yoda1-induced myofibroblast differentiation, independently of Piezo1 activation.

Following cardiac injury, TNC is thought to promote tissue healing but enhance fibrosis and inflammation (Midwood *et al.* 2011); increased circulating TNC levels have been shown to correlate with poor prognosis and mortality following MI (Sato *et al.* 2006). TNC has been associated with mechanical stress due to its high expression in locations which withstand high pressure such as myotendinous and myofascial junctions and the branching points of arteries (Mackie *et al.* 1992; Järvinen *et al.* 2003) and mechanical stimulation prompts TNC expression *in vitro* (Chiquet, Sarasa-Renedo and Tunç-Civelek 2004). In the present study, Yoda1 treatment led to increased TNC mRNA and protein expression in cardiac fibroblasts; this was dependent on Piezo1 based on studies utilising murine models with genetically modified Piezo and Piezo1-specific siRNA.

Lewis *et al.* (2017) state that, in the heart and arterial endothelial cells, mechanical forces from blood pressure oscillate sharply at frequencies of ~1-3 Hz (60–180 heart beats per minute), and that Piezo1 is able to respond to repetitive stimulation in this frequency range. This is in contrast to Piezo2, which the group suggest is not particularly efficient at continuously transducing high-frequency stimuli (Lewis *et al.* 2017). Cyclic stretching at 1 Hz has previously been employed to look at the effect of mechanical stress in the myocardium (Wong *et al.* 2018). To investigate if increased TNC expression in cardiac fibroblasts could be observed using mechanical, rather than chemical, activation of Piezo1, methods of applying mechanical stress were explored. Shear stress had no effect on *Tnc* mRNA expression in murine cardiac fibroblasts but this type of stress may be more relevant for endothelial cells, as cardiac fibroblasts are not in direct contact with blood flow. Therefore, an alternative method of inducing mechanical activation may be more appropriate. While increasing substrate

stiffness and cyclic stretch both caused trends for increased mRNA expression of *Tnc* / *TNC*, this was not statistically significant. Although there is evidence in the literature that TNC is a mechanosensitive gene in cardiac fibroblasts (Herum *et al.* 2017a), its expression was not induced using the particular mechanical stimuli applied in this study.

Cardiac fibroblasts secrete IL-6, a pleiotropic pro-inflammatory cytokine that promotes cardiac fibroblast proliferation and fibrosis (Banerjee *et al.* 2009), as well as cardiac hypertrophy through its actions on cardiomyocytes (Meléndez *et al.* 2010). It was revealed that Yoda1 increased *Il6* / *IL6* gene expression in both murine and human cardiac fibroblasts and increased secretion of IL-6 in murine cardiac fibroblasts. It was established that these effects were mediated via Piezo1 using various approaches. Interesting, this result may tie in with the previously discussed observation that Yoda1 evokes TNC expression, as inflammatory cytokines have been shown to induce TNC, which subsequently activates toll-like receptor 4 (TLR4) signalling, leading to increased cytokine secretion and additional TNC synthesis, creating a positive feedback loop (Midwood *et al.* 2009; Maqbool *et al.* 2016).

Mechanical stretching of cardiac fibroblasts induces the expression of several pro-fibrotic cytokines (Deb and Ubil 2014). IL-6 is also a mechanically-regulated gene, and increased IL-6 secretion occurs upon skeletal muscle contraction where it is thought to play a beneficial role (Pedersen and Fischer 2007). Fibroblasts from several sources have been shown to secrete IL-6 in response to mechanical stretch (House *et al.* 2012; Li *et al.* 2013; Skutek *et al.* 2001). However, the literature is varied; Tanaka *et al.* (2018) found that hydrostatic pressure inhibited *IL6* mRNA expression in human cardiac fibroblasts. A recent paper has shed light on Piezo1 activation and inflammation. Solis *et al.* (2019) very recently demonstrated that Piezo1 could sense cyclical hydrostatic pressure and initiate an inflammatory response in myeloid cells by triggering the expression of numerous pro-inflammatory mediators, including interleukins. Mice deficient in Piezo1 in innate immune cells had ablated pulmonary inflammation and increased susceptibility to bacterial infection; conversely, Piezo1 signalling exacerbated a model of pulmonary fibrosis. This study implicates force as a major signal dictating inflammation. In the present study, it was observed that IL-6 was

not induced by shear stress, altering substrate stiffness or cyclic stretching for 6 h.

Piezo1 and Piezo2 have previously been found to work in tandem, with both being required for arterial baroreceptor activity and function (Zeng *et al.* 2018). Genetic ablation of both Piezo1 and Piezo2 in the nodose and petrosal sensory ganglia of mice abolished drug-induced baroreflex and transgenic animals were found to have labile hypertension and increased blood pressure variability (Zeng *et al.* 2018). Cyclic stretching of cells was performed once more, this time for the longer period of 24 h and it was investigated whether both members of the Piezo1 family were involved in mechanically-induced IL-6. Although stretching of cells did not induce IL-6, knockdown of Piezo1 caused a reduction in basal levels of both IL-6 mRNA expression and secretion in both static and stretched cells. This indicates that Piezo1 may have a role in the production of IL-6 under basal conditions. However, Piezo1-specific siRNA did not reduce basal IL-6 levels in experiments where Yoda1 was applied to cells grown on normal tissue culture plates. A possible explanation for this is that stretched cardiac fibroblasts were seeded on collagen-coated silicon membranes (930 kPa), whereas cells treated with Yoda1 were plated on uncoated tissue culture plastic (10^6 kPa). This effect of Piezo1 knockdown on basal IL-6 levels did not occur in the experiment investigating substrates of 10 and 30 kPa stiffness but these varied greatly from the 930 kPa substrate utilised in the FlexCell experiments. These different effects on basal IL-6 secretion may be due to the surrounding environment, whether this be the stiffness or the coating of the substrate (FlexCell plates are collagen I-coated, whereas the plates used for the other experiment are coated with fibronectin). Cells continuously react to mechanical stresses inflicted on them by their environment and sense the stiffness of the substrate on which they adhere. Matrix rigidity is known to affect cell spreading areas, the stability of adhesion complexes and stress fibres, motility and cell proliferation (Lembong *et al.* 2015). It has previously been reported that substrate compliance modulates Ca^{2+} signalling in fibroblasts. When cells from a mouse fibroblast cell line are plated on a soft polyacrylamide gel, more cells exhibit calcium oscillations than in cultures on a rigid substrate in response to ATP stimulation and the stiffer substrate instigates a faster Ca^{2+} decay following excitation (Lembong *et al.* 2015). Moreover, growing rat subcutaneous myofibroblasts on silicone substrates and in collagen gels of

increasing stiffness or enhancing intracellular stress by altering cell adhesion and spreading increases the occurrence of Ca^{2+} oscillations (Godbout *et al.* 2013); this has been shown to correlate with contractile events in these cells (Castella *et al.* 2010). Therefore, it is evident that calcium events in fibroblasts are regulated by the mechanical environment. It has been established that the mechanical environment also has effects on Piezo1-mediated Ca^{2+} events; Ca^{2+} flickers which could be attributed to Piezo1 were found to be localised to regions of high-traction forces in human foreskin fibroblasts (Ellefsen *et al.* 2019).

To summarise, data discussed show that activation of Piezo1 in cardiac fibroblasts using Yoda1 leads to an increase in the expression of genes involved in cardiac remodelling. TNC and IL-6 are upregulated following myocardial injury; these genes were revealed to be amplified following Yoda1 treatment in cardiac fibroblasts in a Piezo1-dependent manner. These changes in gene expression could not be replicated when the channel was activated mechanically using shear stress or stretch. However, Piezo1 was indicated to play a role in the production of IL-6 under basal conditions in cardiac fibroblasts; this was dependent on the mechanical and/or chemical properties of the surrounding matrix.

Chapter 5 Role of p38α MAPK and Src signalling in Piezo1-induced IL-6 production

5.1 Introduction

In the previous chapter it was demonstrated that chemical activation of Piezo1 led to changes in the expression of genes which are important in fibroblast function and cardiac remodelling. The most well-defined evidence was for the pro-inflammatory cytokine, IL-6. Information on IL-6 is valuable in this setting as this cytokine is known to promote cardiac fibroblast proliferation and fibrosis (Banerjee *et al.* 2009) and the importance of cardiac fibroblast-derived IL-6 in modulating cardiac hypertrophy has been proposed (Bageghni *et al.* 2018). Therefore, the mechanism by which Piezo1 activation was coupled to IL-6 expression and secretion was interrogated.

5.2 Aim

The key aim of this chapter was to examine the downstream signalling events mediating Piezo1-induced IL-6 expression in cardiac fibroblasts.

5.3 Methods

PamChip multiplex serine/threonine and tyrosine kinase activity profiling were utilised to establish kinases activated by Yoda1 treatment in murine cardiac fibroblasts (Section 2.12). These arrays provided us with key data which was followed up by western blotting to confirm that kinases highlighted in the arrays were activated by Yoda1 treatment (Section 2.6). Piezo1-targeting siRNA was utilised to confirm the specificity of the data (Section 2.4) and pharmacological inhibitors were used to ascertain the hierarchy of the signalling pathway (Section 2.1). Finally, it was explored which members of a key kinase family activated by Yoda1 activation of Piezo1 were expressed in cardiac fibroblasts utilising RT-PCR (Section 2.5).

5.4 Results

5.4.1 Piezo1 activation induces MAP kinase signalling

PamChip multiplex serine/threonine kinase activity profiling was used to assess differences in kinase activity following treatment of murine cardiac fibroblasts with vehicle or 10 μM Yoda1 for 10 min. Combinatorial analysis of phosphorylation of 140 peptide substrates revealed predicted serine/threonine kinases that were activated downstream of Piezo1. The complete data set of kinases identified based on peptide substrate phosphorylation and ranked by median final score are shown in Table 5.1. Within the top hits, two major kinase families were identified; MAP kinases (extracellular signal-regulated kinases ERK1/2/5, c-Jun N-terminal kinases JNK1/2/3, p38 mitogen-activated protein kinases p38α/β/δ/γ) and cyclin-dependent kinases (CDKs1-7,9,11) (Figure 5.1). Kinase families activated can be seen more clearly in the dendrogram in Figure 5.2.

The primary role of CDK-family kinases is to phosphorylate cell cycle proteins and thereby regulate cell cycle progression; although it has also been reported that specific CDKs can regulate inflammatory gene expression through interaction with the NF-kB pathway (Schmitz and Kracht 2016). However, given that kinases within the NF-kB pathway (IKKα, IKKβ) were not revealed to be activated in response to Yoda1 (Table 5.1), the role of CDKs was not pursued further and the investigation was focussed on the MAP kinase families.

Ranking	Kinase Name	Median Final score	Mean Specificity Score	Mean Significance Score
1	p38[beta]	4.36	2.32	1.75
2	CDK5	4.28	2.47	1.63
3	p38[gamma]	4.10	1.97	1.28
4	CDK2	4.08	2.65	1.39
5	ERK2	4.04	2.70	1.39
6	ERK1	3.95	2.70	1.30
7	JNK2	3.88	2.70	1.19
8	p38[delta]	3.84	2.63	1.30
9	JNK3	3.76	2.70	1.04
10	JNK1	3.74	2.70	1.03
11	CDC2/CDK1	3.70	2.34	1.24
12	CDK11	3.40	1.78	1.65
13	CDK9	3.08	1.83	1.27
14	CDK6	2.99	1.55	1.50
15	CDK4	2.96	1.50	1.44
16	ERK5	2.86	1.74	1.04
17	CDK3	2.69	1.77	1.18
18	p38[alpha]	2.66	1.64	0.93
19	ICK	2.64	1.37	1.26
20	CDK7	2.40	1.44	0.93
21	CDKL2	2.22	1.22	1.00
22	CDKL5	2.11	1.16	0.94
23	GSK3[alpha]	1.91	0.93	0.75
24	TBK1	1.81	1.07	0.94
25	GSK3[beta]	1.64	0.87	0.65
26	ROCK1	1.52	0.80	0.71
27	AurA/Aur2	1.38	0.72	0.62
28	PKN1/PRK1	1.37	0.66	0.63
29	IKK[epsilon]	1.35	0.79	0.59
30	MSK1	1.29	0.73	0.55
31	RSK2	1.28	0.74	0.53
32	PCTAIRE2	1.17	0.63	0.54
33	RSK3	1.12	0.64	0.46
34	ARAF	1.01	0.61	0.41
35	BRAF	1.00	0.59	0.40
36	ROCK2	0.97	0.35	0.43
37	ADCK3	0.89	0.40	0.42
38	PKC[delta]	0.80	0.27	0.34
39	RSKL2	0.78	0.43	0.35
40	PAK1	0.78	0.43	0.35
41	Pim1	0.77	0.51	0.41
42	CDK10	0.76	0.40	0.39
43	AurB/Aur1	0.75	0.42	0.36
44	RSK1/p90RSK	0.72	0.39	0.33
45	Pim3	0.71	0.42	0.40
46	RAF1	0.70	0.36	0.33
47	PFTAIRE2	0.69	0.42	0.38
48	PKG1	0.69	0.30	0.36
49	Pim2	0.64	0.36	0.39
50	PKC[iota]	0.63	0.23	0.34
51	DAPK3	0.63	0.30	0.33
52	PKC[zeta]	0.62	0.29	0.37
53	CDKL1	0.62	0.30	0.37
54	MSK2	0.60	0.30	0.30
55	PKD1	0.60	0.32	0.28
56	DCAMKL1	0.59	0.29	0.29
57	PKC[beta]	0.57	0.24	0.33

Ranking	Kinase Name	Median Final score	Mean Specificity Score	Mean Significance Score
58	SGK1	0.56	0.28	0.27
59	CK2[alpha]1	0.56	0.33	0.23
60	HGK/ZC1	0.53	0.23	0.24
61	CHK1	0.51	0.23	0.30
62	Akt2/PKB[beta]	0.51	0.21	0.33
63	PRKY	0.46	0.29	0.31
64	PKG2	0.45	0.15	0.31
65	p70S6K	0.45	0.19	0.32
66	mTOR/FRAP	0.45	0.16	0.21
67	NuaK1	0.44	0.20	0.23
68	IKK[beta]	0.42	0.22	0.24
69	Akt1/PKB[alpha]	0.41	0.14	0.29
70	PKC[alpha]	0.39	0.10	0.30
71	PKC[epsilon]	0.35	0.11	0.28
72	MAPKAPK2	0.32	0.05	0.26
73	PKC[eta]	0.32	0.12	0.28
74	PKC[theta]	0.31	0.05	0.26
75	MAPKAPK3	0.30	0.03	0.26
76	PKC[gamma]	0.29	0.08	0.23
77	ANP[alpha]	0.25	0.04	0.22
78	PRKX	0.24	0.02	0.21
79	CK1[epsilon]	0.24	0.10	0.14
80	ATR	0.23	0.08	0.15
81	CK1[alpha]	0.22	0.12	0.20
82	PKA[alpha]	0.20	0.00	0.22
83	CHK2	0.20	0.02	0.18
84	p70S6K[beta]	0.20	0.02	0.19
85	PFTAIRE1	0.20	0.08	0.12
86	DAPK2	0.19	0.05	0.13
87	IKK[alpha]	0.18	0.09	0.13
88	AMPK[alpha]1	0.14	0.01	0.13
89	CaMK4	0.13	0.01	0.12
90	SGK2	0.10	0.00	0.10
91	CaMK2[alpha]	0.02	0.01	0.01

Table 5.1 Effect of Yoda1 on serine/threonine protein kinase activity. Mouse cardiac fibroblasts were stimulated with vehicle or 10 μM Yoda1 for 10 min before analysing serine/threonine protein kinase activity with PamChip multiplex kinase activity profiling (n=6). The complete data set of kinases identified are shown based on peptide substrate phosphorylation and ranked by median final score (combination of specificity and statistical significance).

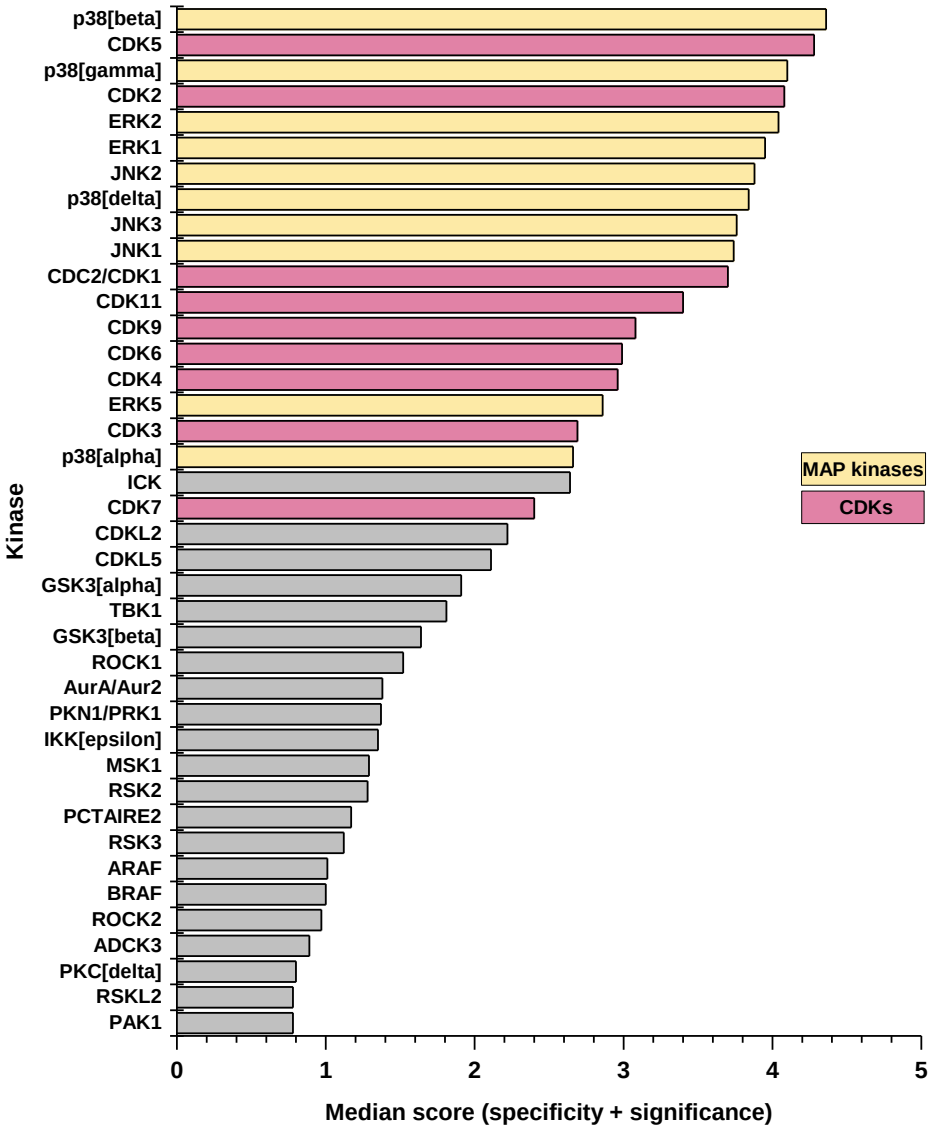

Figure 5.1 Top 40 serine/threonine protein kinases activated by Yoda1. Mouse cardiac fibroblasts were stimulated with vehicle or 10 μM Yoda1 for 10 min before analysing serine/threonine protein kinase activity with PamChip multiplex kinase activity profiling (n=6). Kinases identified based on peptide substrate phosphorylation and ranked by specificity and statistical significance; the top 40 hits from the analysis in Table 5.1 are shown. The top kinase families predicted to be activated by Yoda1 were the MAP kinases (ERK1/2/5, JNK1/2/3, p38α/β/γ/δ; yellow) and the cyclin-dependent kinases (CDKs1-7,9,11; pink).

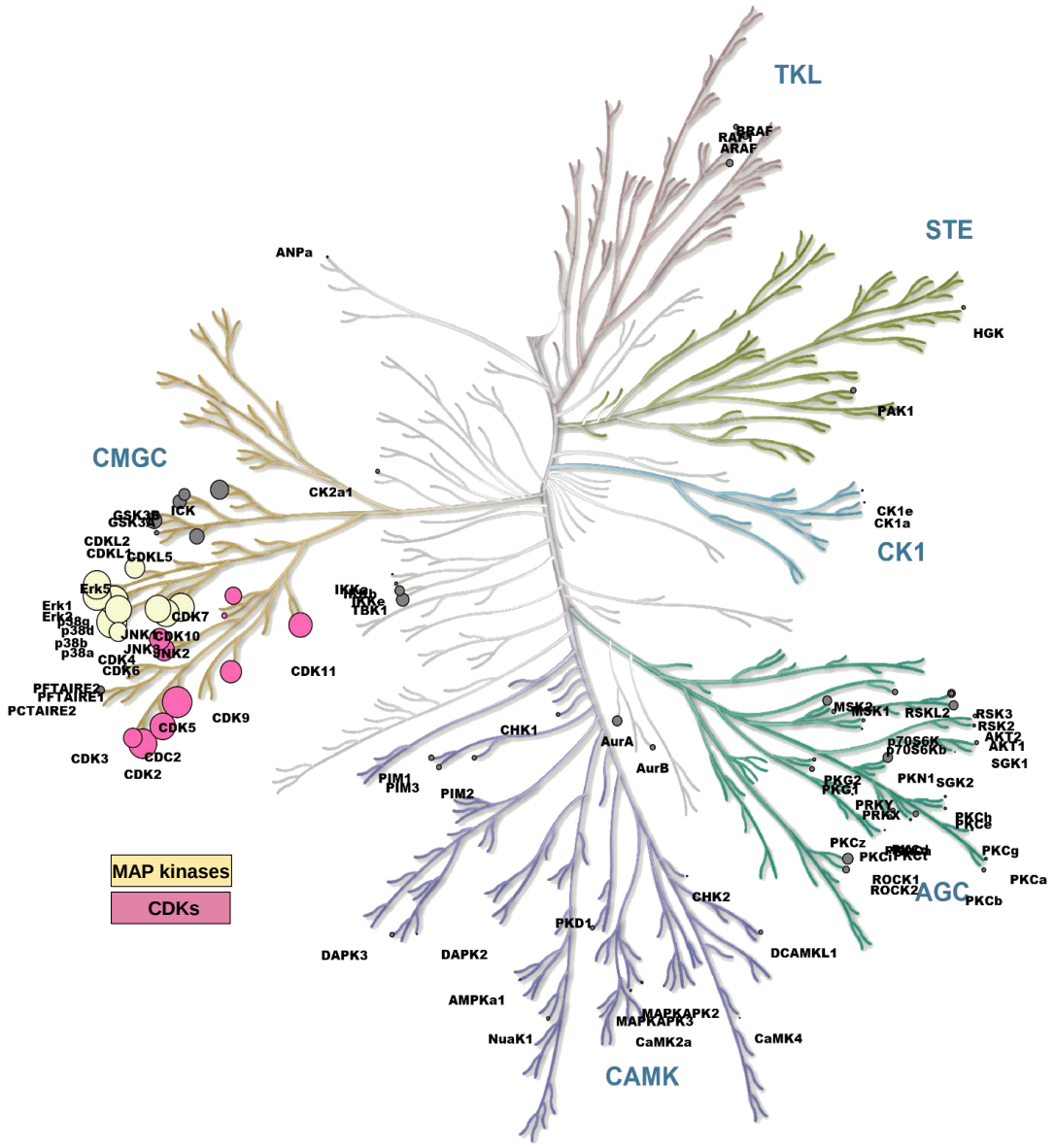

Figure 5.2 Dendrogram illustrating the effect of Yoda1 on serine/threonine protein kinase activity. KinMap-generated summary of serine/threonine protein kinase activity using PamChip multiplex kinase activity profiling shown in Table 5.1 and Figure 5.1. The top kinase families predicted to be activated by Yoda1 are illustrated by colour; MAP kinases (ERK1/2/5, JNK1/2/3, p38α/β/γ/δ; yellow) and cyclin-dependent kinases (CDKs1-7,9,11; pink). Circle size indicates median score (combination of specificity and significance).

5.4.2 Yoda1-evoked p38 MAPK and ERK phosphorylation

5.4.2.1 Yoda1 induces p38 MAPK and ERK phosphorylation in murine cardiac fibroblasts

The PamChip activity profiling revealed predictions of kinase activity based on phosphorylation sites derived from literature or computational predictions that are correlated with one or more upstream kinases; this explains why families of kinases are often highlighted in this array (see dendrogram in Figure 5.2). Of the four p38 subtypes, p38β had the highest ranking in the serine/threonine kinase activity profiling array following Yoda1 treatment (Table 5.1, Figure 5.1). This was followed by p38γ (ranking: 3rd), p38δ (ranking: 8th) and p38α (ranking: 18th) (Table 5.1, Figure 5.1). However, it is known that p38β is not expressed in cardiac fibroblasts and p38α is more highly expressed than p38δ or γ (Turner 2011; Sinfield *et al.* 2013). p38α has been reported to be involved in the production of IL-6 in cardiac fibroblasts (Du *et al.* 2005; Sinfield *et al.* 2013; Bageghni *et al.* 2018). Therefore, it was investigated whether the p38α MAPK pathway was stimulated following Piezo1 activation with Yoda1 in murine cardiac fibroblasts. Western blotting revealed that Yoda1 significantly increased p38 (i.e. p38α) phosphorylation by 3-fold after 10 min treatment, before returning to basal levels by 20-30 min (Figure 5.3A). Accordingly, 10 min Yoda1 treatment was utilised for future experiments.

Alongside the p38 family, members of the ERK family were also in the top 20 predicted serine/threonine kinases activated downstream of Piezo1 (ERK1 and ERK2 ranking: 6th and 5th respectively – Table 5.1, Figure 5.1). It was confirmed that ERK1 and 2 were also phosphorylated following Yoda1 treatment in murine cardiac fibroblasts by western blotting. There was a significant difference in ERK1/2 phosphorylation between vehicle-treated and Yoda1-treated cells after 10 and 20 min treatment (Figure 5.3B). The shortest time point in which Yoda1 was able to significantly phosphorylate ERK1/2 (10 min) was chosen for all further experiments.

Further studies revealed that both Yoda1-induced p38α and ERK1/2 phosphorylation occurred in a concentration-dependent manner, with maximal p38α phosphorylation occurring in response to 10 μM Yoda1 (Figure 5.4A,B). Therefore, this was the concentration used for subsequent experiments.

Correlating with earlier data on Ca^{2+} measurements and *Il6* mRNA expression (Figure 4.15A,B), neither p38α nor ERK1/2 were activated in response to the inactive Yoda1 analogue, 2e (Figure 5.4A,B). Compound 159, which was shown to induce Ca^{2+} entry in a similar manner to Yoda1 in murine cardiac fibroblasts (Figure 3.25B) also caused phosphorylation of p38α MAPK and ERK1/2, by a similar magnitude as 5 μM Yoda1, when applied to murine cardiac fibroblasts for 10 min (Figure 5.4A,B).

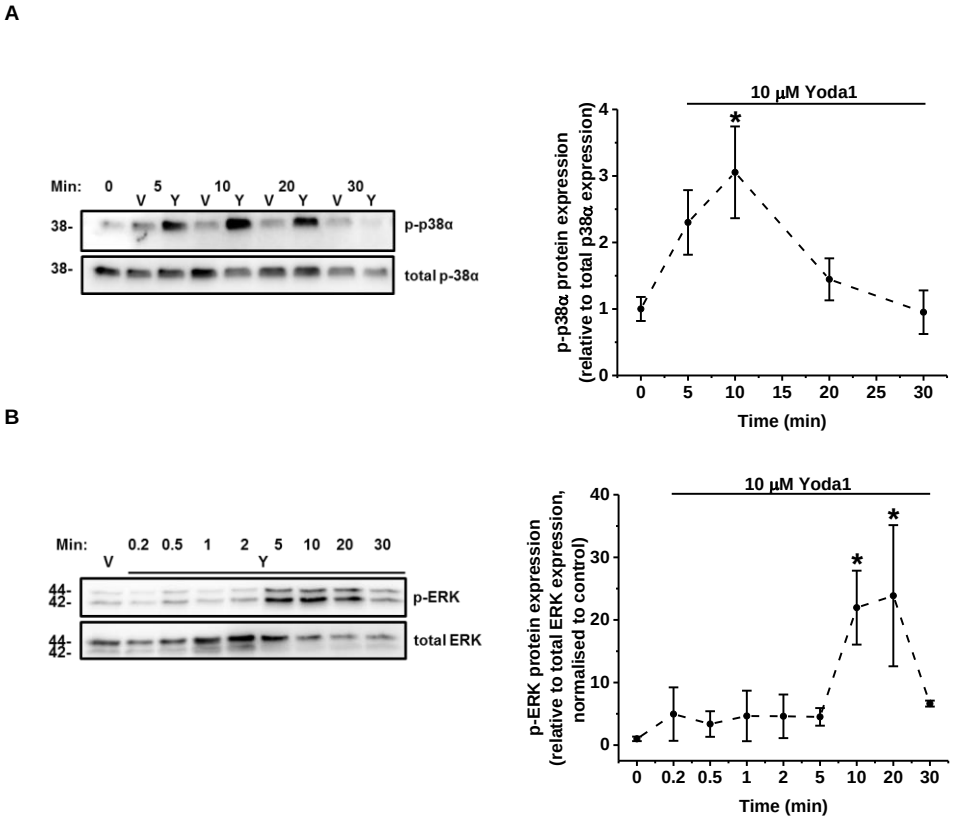

Figure 5.3 Time course of p38α and ERK1/2 activation following Yoda1 treatment. Murine cardiac fibroblasts were treated with vehicle (V) or 10 μM Yoda1 (Y) for 5-30 min. Samples were immunoblotted for **(A)** p-p38α expression and re-probed with total p38α antibody to confirm equal protein loading (n=6) or **(B)** p-ERK1/2 and reprobed with total ERK1/2 antibody to confirm equal protein loading (n=3). The bands at 44 kDa and 42 kDa represent ERK1 and ERK2, respectively. Graphs show mean densitometric data, *P<0.05 versus vehicle-treated cells following an ANOVA with Tukey's post-hoc test.

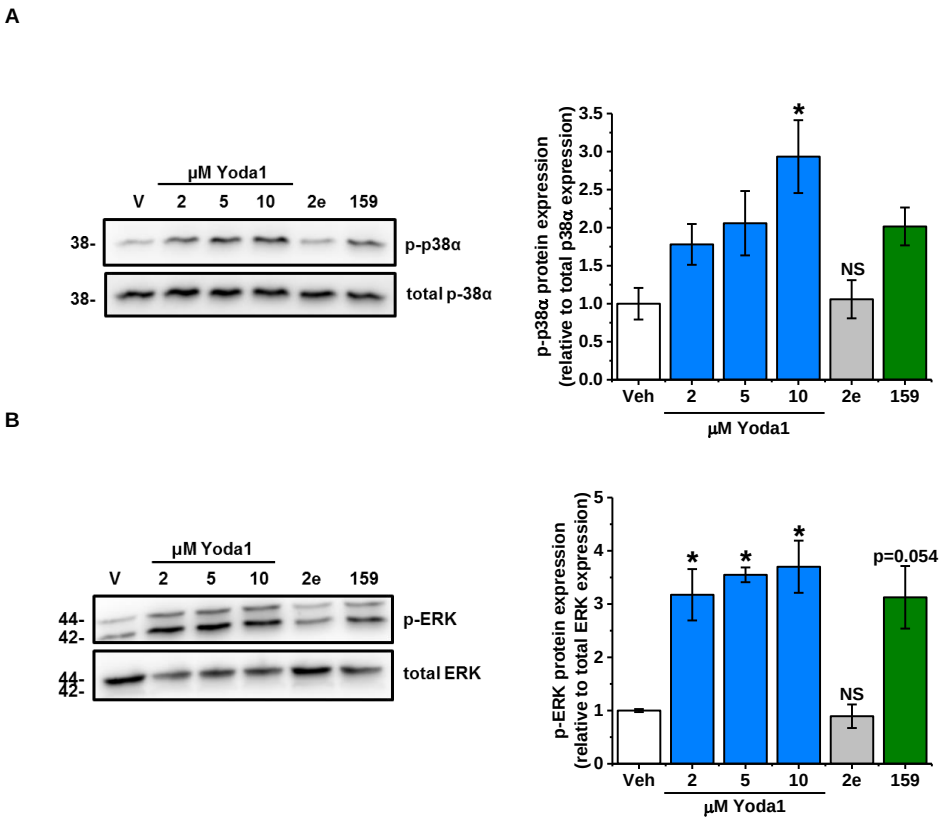

Figure 5.4 Effect of Yoda1 and its analogues on p38α MAPK and ERK1/2 phosphorylation. Murine cardiac fibroblasts were treated for 10 min with vehicle, varying concentrations of Yoda1 (2-10 μM), 10 μM compound 2e or 10 μM compound 159. Samples were immunoblotted for **(A)** p-p38α and reprobed with antibody for total p38α, to confirm equal protein loading (n=3) or **(B)** p-ERK1/2 and reprobed with antibody for total ERK1/2, to confirm equal protein loading (n=2). The bands at 44 kDa and 42 kDa represent ERK1 and ERK2, respectively. Graphs show mean densitometric data, *P<0.05, P=NS, not significant versus vehicle-treated cells following an ANOVA with Tukey's post-hoc test (n=3).

5.4.2.2 Yoda1-induced phosphorylation of p38α and ERK1/2 are dependent on Piezo1

It was important to ascertain if Yoda1-evoked phosphorylation of p38α and ERK1/2 were due to Piezo1 activation. Cardiac fibroblasts isolated from Piezo1$^{+/-}$ heterozygote KO mice (Het) displayed a marked reduction in the Yoda1-evoked p38α phosphorylation in comparison with cells from WT mice (Figure 5.5A). Conversely, cardiac fibroblasts isolated from gain-of-function M-R mice revealed increased Yoda1-induced p38α phosphorylation, compared to cardiac fibroblasts from WT mice (Figure 5.5B). Although not statistically significant, the basal level of p38α phosphorylation shows a trend for being increased in cardiac fibroblasts from M-R mice, compared to those from WT mice; this may be due to constitutive activity of Piezo1. This was observed occasionally but was not reproducible. These data indicate that Yoda1-evoked p38α activation is dependent on the activation/expression level of Piezo1 in murine cardiac fibroblasts.

To further confirm that Yoda1-evoked p38α activation was due to Piezo1, Piezo1 gene silencing was employed. Murine and human cardiac fibroblasts transfected with control siRNA exhibited a four-fold increase in p38α phosphorylation following Yoda1 treatment, compared to vehicle-treated cells (Figure 5.6A,B). Piezo1-specific siRNA reduced Yoda1-induced activation of p38α to basal levels in both murine (Figure 5.6A) and human (Figure 5.6B) cardiac fibroblasts. Similarly, Yoda1-induced ERK1/2 activation was inhibited by Piezo1 gene silencing (Figure 5.6C). Together, these data confirm the essential role of Piezo1 in Yoda1-induced p38α and ERK1/2 activation.

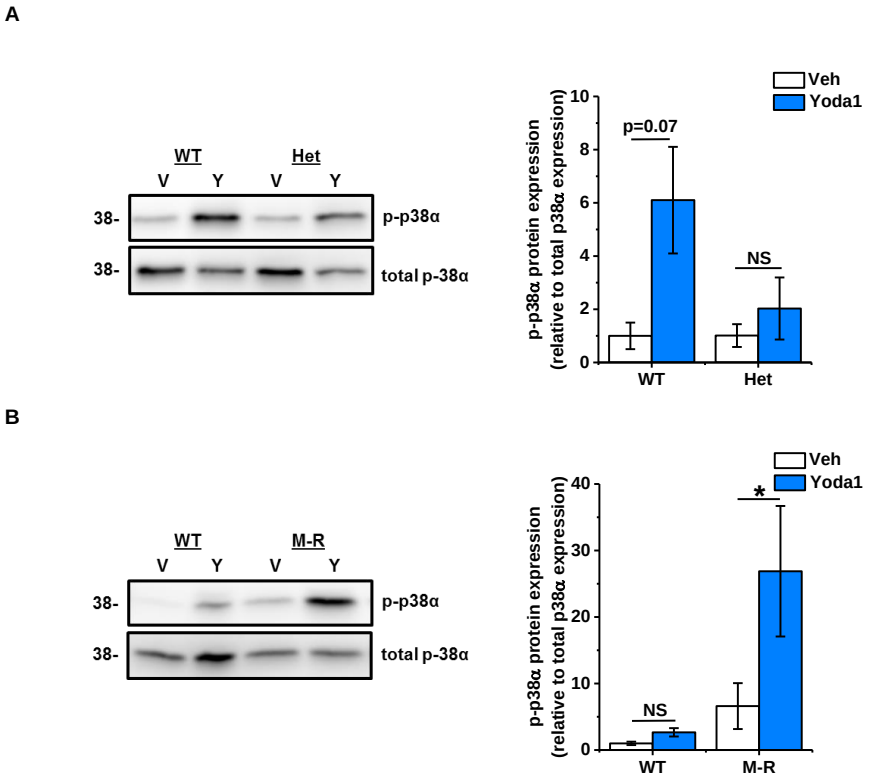

Figure 5.5 Effect of altering Piezo1 expression or activity on Yoda1-evoked phosphorylation of p38α. Cardiac fibroblasts isolated from **(A)** wild type (WT, n=3) and Piezo1$^{+/-}$ heterozygote knockout (Het, n=3) mice or **(B)** WT (n=6) and gain-of-function Piezo1-mutated (M-R, n=7) mice and treated with vehicle or 10 μM Yoda1 for 10 min. Samples were immunoblotted for p-p38α and reprobed with total p38α antibody to confirm equal protein loading. Graph shows mean densitometric data, *P<0.05, P=NS, not significant following an ANOVA with Tukey's post-hoc test.

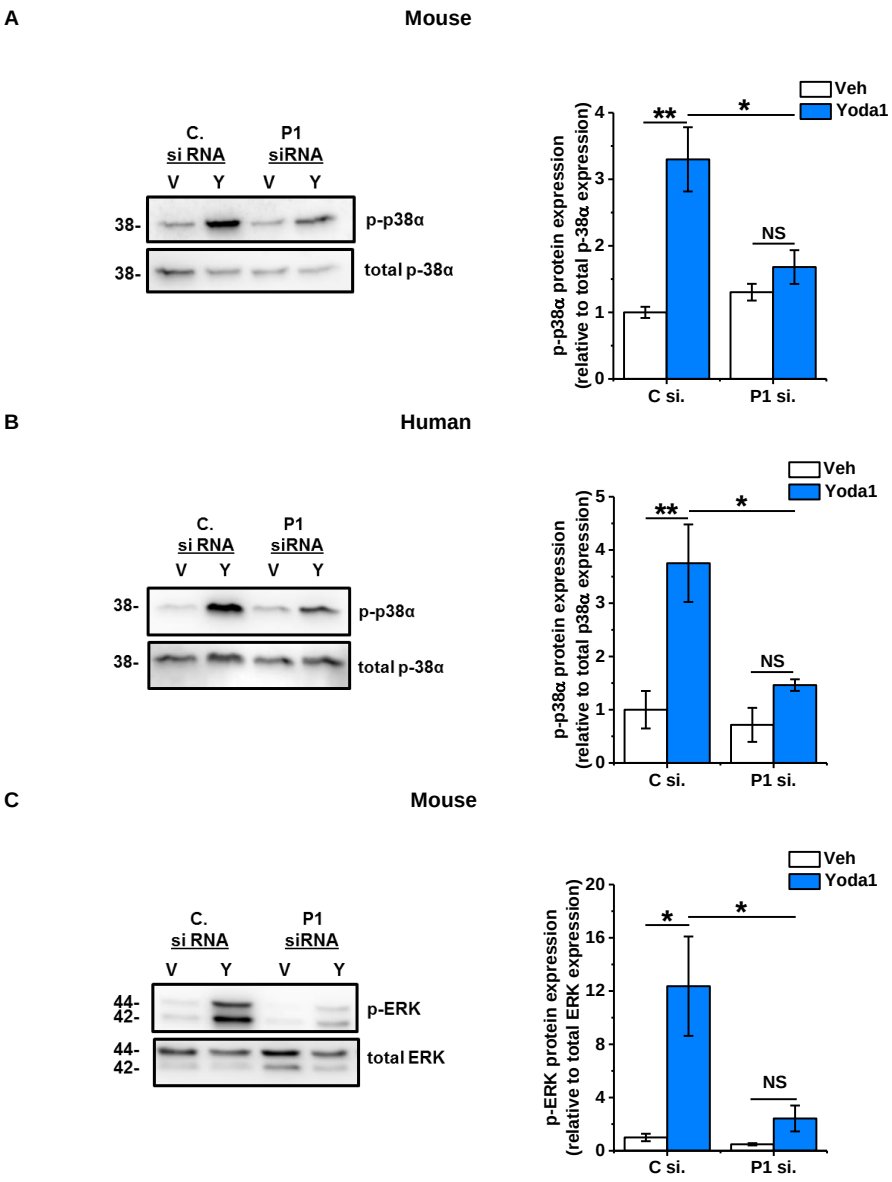

Figure 5.6 Effect of Piezo1 knockdown on Yoda1-evoked phosphorylation of p38α and ERK1/2 in murine and human cardiac fibroblasts. (A) Murine or **(B)** human cardiac fibroblasts were transfected with either control (C) or Piezo1-specific (P1) siRNA before treatment with vehicle or 10 μM Yoda1 for 10 min. Samples were immunoblotted for phospho-p38α antibody and reprobed with total p38α antibody to confirm equal protein loading. **(C)** Murine cardiac fibroblasts were transfected with either control (C) or Piezo1-specific (P1) siRNA prior to treatment with vehicle or 10 μM Yoda1 for 10 min. Samples were immunoblotted for p-ERK1/2 and reprobed with total ERK1/2 antibody to confirm equal protein loading. The bands at 44 kDa and 42 kDa represent ERK1 and ERK2, respectively. Graphs show mean densitometric data, *P<0.05, **P<0.01, P=NS, not significant following an ANOVA with Tukey's post-hoc test (n=3).

5.4.2.3 Yoda1-induced activation of p38α MAPK is reduced by a p38 inhibitor

p38α and β have high sequence homology and share sensitivity to pharmacological inhibition by pyridinyl imidazole molecules such as SB203580 whereas p38γ and δ have only 60% homology to p38α and are resistant to SB203580 inhibition (Eyers *et al.* 1999). Pretreatment of murine cardiac fibroblasts with SB203580 significantly reduced the Yoda1-induced phosphorylation of p38α by 65% in murine cardiac fibroblasts (Figure 5.7).

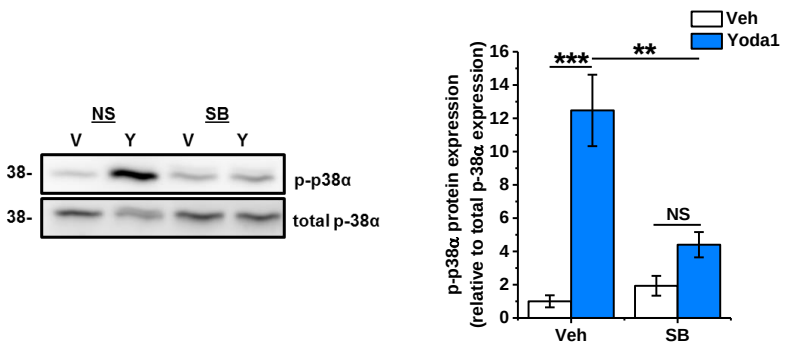

Figure 5.7 Effect of a p38 MAPK inhibitor on Yoda1-evoked p38α MAPK phosphorylation. Murine cardiac fibroblasts were exposed to 10 μM SB203580 for 1 h before treatment with vehicle or 10 μM Yoda1 for 10 min. Samples were immunoblotted for p-p38α and reprobed with total p38α, to confirm equal protein loading. Graph shows mean densitometric data, **P<0.01, ***P<0.001, P=NS, not significant following an ANOVA with Tukey's post-hoc test (n=3).

5.4.2.4 Yoda1-evoked p38α and ERK1/2 phosphorylation are dependent on Ca^{2+}

In order to confirm that the phosphorylation of p38α and ERK1/2 were due to Ca^{2+} entry into the cell upon Piezo1 activation by Yoda1, murine cardiac fibroblasts were treated with either vehicle or Yoda1 for 10 min in either standard DMEM media or in media containing 1.75 mM EGTA to chelate extracellular free Ca^{2+}. The Yoda1-induced phosphorylation of p38α that was observed in Ca^{2+}-containing medium was abolished in the absence of Ca^{2+} (Figure 5.8A). Similar data were obtained for ERK1/2 activation (Figure 5.8B). These data indicate that it is Ca^{2+} entry through the Piezo1 channel which is important for activation of these signalling cascades.

Together, these data illustrate that Piezo1 activation using Yoda1 and the subsequent Ca^{2+} influx leads to the phosphorylation of both p38α and ERK1/2.

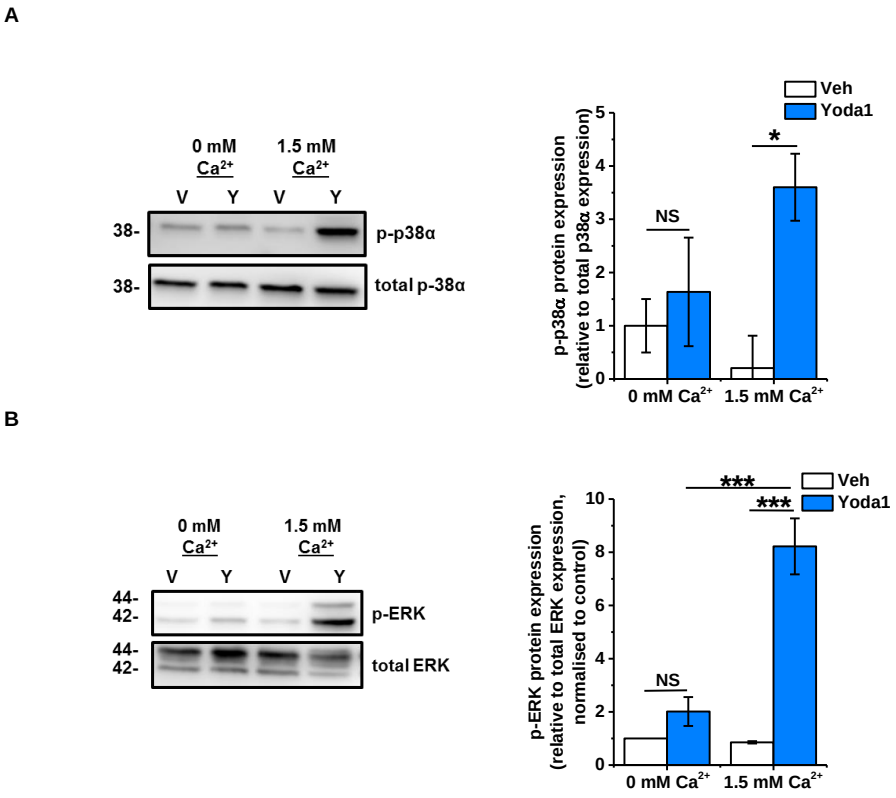

Figure 5.8 Effect of extracellular Ca^{2+} on Yoda1-induced p38α and ERK1/2 phosphorylation. Murine cardiac fibroblasts were treated for 10 min with vehicle or 10 μM Yoda1 in either standard DMEM or in DMEM containing 1.75 mM EGTA to chelate extracellular free Ca^{2+}. Samples were immunoblotted for **(A)** p-p38α and reprobed with total p38α antibody to confirm equal protein loading or **(B)** p-ERK1/2 and reprobed with total ERK1/2 antibody to confirm equal protein loading. The bands at 44 kDa and 42 kDa represent ERK1 and ERK2, respectively. Graphs show mean densitometric data, *P<0.05, ***P<0.001, P=NS, not significant following an ANOVA with Tukey's post-hoc test (n=3).

5.4.3 Yoda1-evoked IL-6 expression and secretion is abolished by a p38 inhibitor

Informed by the PamChip multiplex serine/threonine kinase activity profiling where three MAP kinase families were activated, subsequent experiments were undertaken to identify which family was required for the Piezo1-mediated induction of IL-6. Selective pharmacological inhibitors of the ERK (PD98059), JNK (SP600125) and p38 MAPK (SB203580) pathways were used. In addition, specific pharmacological inhibitors of pathways activated by Ca^{2+} entry were also tested: PI-3 kinase (LY294002), Ca^{2+}/calmodulin-dependent protein kinase II (KN-93) and NFAT (11R-VIVIT). There was a non-significant trend for KN-93 increasing basal *Il6* mRNA expression therefore this result was not studied further (Figure 5.9E). Of the pharmacological inhibitors, only SB203580 significantly reduced the Yoda1-induced increase in *Il6* mRNA expression back to basal levels (Figure 5.9), suggesting an important role for the p38 MAPK pathway in Yoda1-induced *Il6* gene expression, but not the other kinase pathways. In agreement, SB203580 also inhibited Yoda1-induced IL-6 protein secretion by 77% (Figure 5.10).

Together, these data imply that Ca^{2+}-induced p38 MAPK activation is essential for inducing the expression and secretion of IL-6 in response to Piezo1 activation.

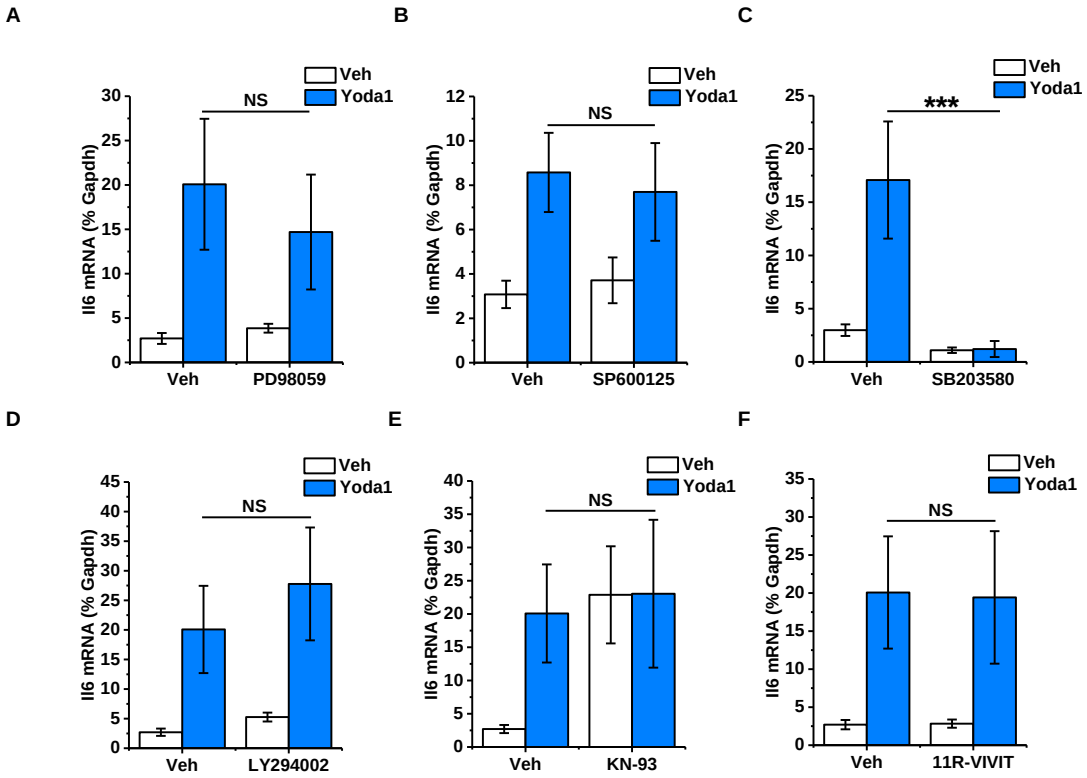

Figure 5.9 Effect of kinase inhibitors on Yoda1-evoked *Il6* mRNA expression in murine cardiac fibroblasts. RT-PCR analysis of *Il6* mRNA expression after exposure of murine cardiac fibroblasts to **(A)** 30 μM PD98059 (ERK pathway inhibitor), **(B)** 10 μM SP600125 (JNK inhibitor), **(C)** 10 μM SB203580 (p38 MAPK inhibitor), **(D)** 10 μM LY294002 (Phosphoinositide 3-kinase (PI3K)/Akt pathway inhibitor), **(E)** 10 μM KN-93 (CaM kinase II inhibitor) or **(F)** 10 μM 11R-VIVIT (NFAT Inhibitor) for 1 h followed by treatment with vehicle or 10 μM Yoda1 for a further 24 h. Expression is measured as % of housekeeping control, *Gapdh*, ***P<0.001, P=NS, not significant for effect of inhibitor following an ANOVA with Tukey's post-hoc test (n=7 for SB203580, n=5 for other inhibitors).

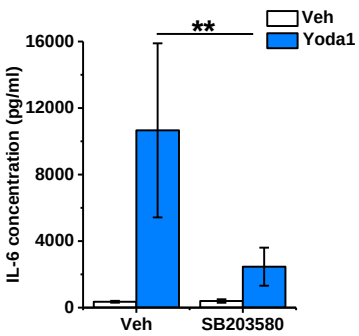

Figure 5.10 Effect of p38 inhibitor on Yoda1-induced IL-6 secretion from murine cardiac fibroblasts. Murine cardiac fibroblasts were pretreated with vehicle or 10 µM SB203580 for 1 h and then applied with either vehicle or 10 µM Yoda1 for 24 h before collecting conditioned media and measuring IL-6 levels by ELISA, **P<0.01 for effect of inhibitor following an ANOVA with Tukey's post-hoc test (n=6).

5.4.4 The role of Src-family kinases in Piezo1-induced p38α phosphorylation and IL-6 expression

5.4.4.1 Src-family and Src-related kinases are activated by Yoda1 treatment in murine cardiac fibroblasts

Having identified p38 MAPK as being important for Piezo1-mediated *Il6* mRNA expression, we sought to identify upstream tyrosine kinases that could couple Piezo1 activation and Ca^{2+} entry to p38 MAPK activation. Again PamChip multiplex kinase activity profiling was used, but this time, differences in activity of the tyrosine kinome were focussed on following treatment of murine cardiac fibroblasts with 10 µM Yoda1 for 10 min. Combinatorial analysis of phosphorylation of 196 peptide substrates (mapping to ~100 tyrosine kinases) generated predicted tyrosine kinases that were activated by Yoda1 (Table 5.2). Within the top hits were 8 SFKs (Lyn, Blk, Src, Hck, Fgr, Yes, Lck and Fyn) and 2 Src-related kinases (Frk and Srm) (Figure 5.11). Families of kinases are illustrated in a dendrogram in Figure 5.12.

Ranking	Kinase Name	Median Final score	Mean Specificity Score	Mean Significance Score
1	FRK	3.25	2.41	0.84
2	ALK	2.86	2.04	0.83
3	Lyn	2.83	1.65	0.84
4	BLK	2.71	1.91	0.86
5	Abl	2.38	1.65	0.80
6	Src	2.22	1.88	0.83
7	RYK	2.08	1.16	0.88
8	HCK	2.05	1.22	0.84
9	Fgr	2.02	1.12	0.84
10	Arg	2.02	1.32	0.82
11	Srm	2.01	1.16	0.80
12	IGF1R	2.00	1.51	0.84
13	InSR	1.98	1.23	0.84
14	Yes	1.92	1.18	0.84
15	Lck	1.91	1.31	0.79
16	LTK	1.75	0.95	0.82
17	Fyn	1.70	0.85	0.80
18	KDR	1.62	0.77	0.87
19	EphA1	1.53	0.80	0.80
20	EphA4	1.52	0.98	0.86
21	Tyro3/Sky	1.51	0.64	0.80
22	Axl	1.38	0.87	0.81
23	HER3	1.36	0.56	0.78
24	Met	1.34	0.51	0.82
25	CTK	1.32	0.56	0.80
26	FGFR3	1.29	0.47	0.76
27	Ron	1.28	0.47	0.76
28	TRKC	1.26	0.35	0.77
29	FLT3	1.24	0.40	0.81
30	FGFR2	1.24	0.48	0.78
31	FAK1	1.23	0.41	0.80
32	Ret	1.22	0.52	0.76
33	Fer	1.18	0.41	0.75
34	FmS/CSFR	1.15	0.44	0.78
35	PDGFR[beta]	1.15	0.40	0.73
36	CSK	1.15	0.35	0.77
37	EphA3	1.14	0.40	0.74
38	TRKA	1.12	0.31	0.77
39	EphA5	1.11	0.38	0.75
40	EphB3	1.11	0.39	0.72
41	Fes	1.10	0.41	0.74
42	EphA2	1.10	0.41	0.74
43	FLT4	1.06	0.31	0.79
44	FGFR1	1.05	0.22	0.79
45	Mer	1.04	0.30	0.77
46	CCK4/PTK7	1.04	0.25	0.80
47	Syk	1.03	0.31	0.77
48	FGFR4	1.03	0.34	0.79
49	Brk	1.02	0.23	0.79
50	HER4	0.98	0.23	0.78
51	TXK	0.97	0.24	0.76
52	TEC	0.95	0.20	0.75
53	BTK	0.95	0.24	0.74
54	TRKB	0.94	0.26	0.76
55	EphB2	0.91	0.25	0.66
56	EphA8	0.90	0.19	0.69
57	Etk/BMX	0.88	0.12	0.75

Ranking	Kinase Name	Median Final score	Mean Specificity Score	Mean Significance Score
58	EphB4	0.87	0.22	0.65
59	ITK	0.85	0.13	0.75
60	HER2	0.85	0.13	0.74
61	ZAP70	0.84	0.07	0.76
62	Lmr1	0.84	0.18	0.66
63	FAK2	0.83	0.13	0.74
64	IRR	0.83	0.19	0.65
65	EGFR	0.81	0.03	0.76
66	JAK2	0.80	0.05	0.74
67	PDGFR[alpha]	0.80	0.27	0.71
68	EphA7	0.80	0.16	0.64
69	Kit	0.76	0.06	0.71
70	FLT1	0.68	0.01	0.67
71	JAK1~b	0.68	0.10	0.60
72	DDR1	0.64	0.10	0.55
73	EphB1	0.60	0.04	0.54
74	Tyk2	0.51	0.02	0.50
75	JAK3	0.35	0.00	0.34

Table 5.2 Effect of Yoda1 on tyrosine protein kinase activity. PamChip multiplex kinase activity profiling of Yoda1-induced tyrosine kinase activity. Mouse cardiac fibroblasts (n=6) were treated with 10 µM Yoda1 for 10 min before extracting cell lysates and assessing activity of the tyrosine kinome (~100 TKs). The complete data set of kinases identified are shown based on peptide substrate phosphorylation and ranked by median final score (combination of specificity and statistical significance).

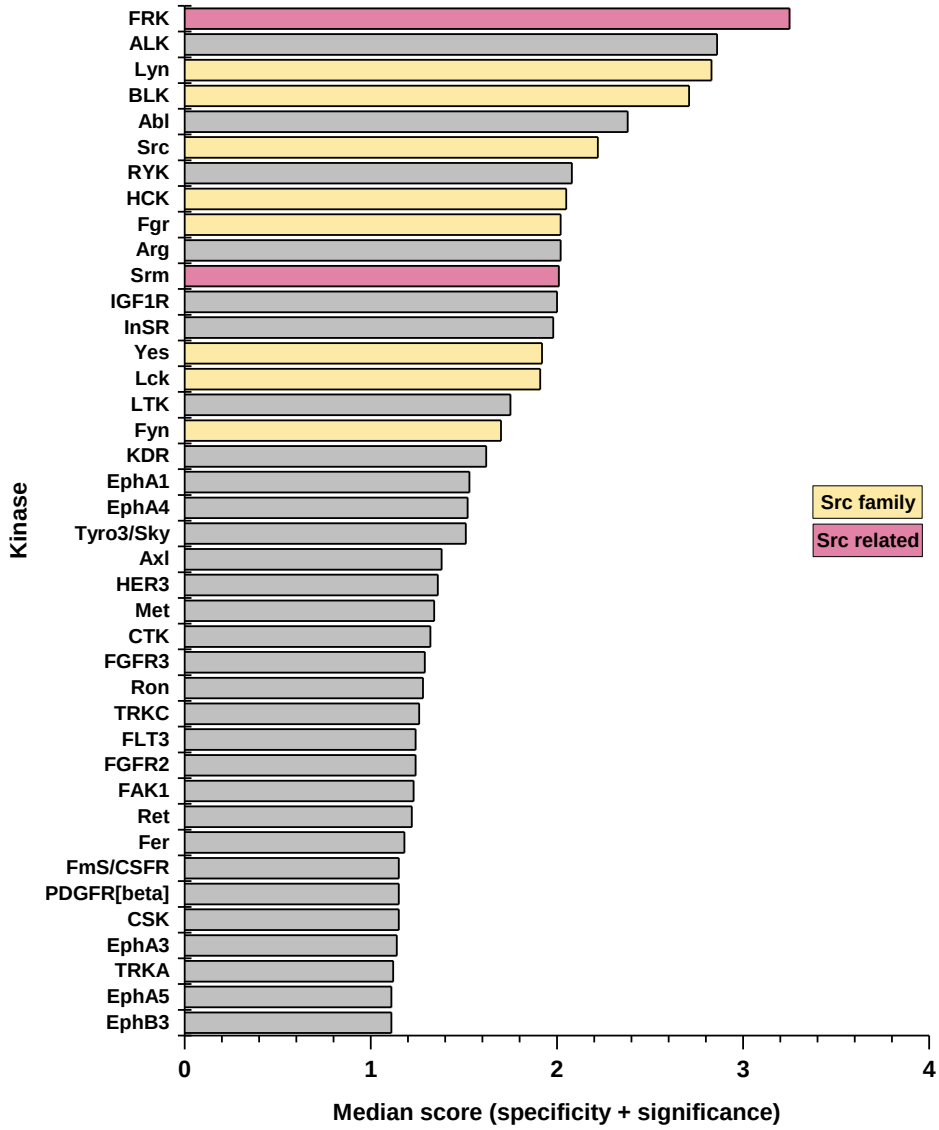

Figure 5.11 Top 40 tyrosine kinases activated by Yoda1. Mouse cardiac fibroblasts were stimulated with vehicle or 10 μM Yoda1 for 10 min before analysing tyrosine protein kinase activity with PamChip multiplex kinase activity profiling (n=6). Kinases were identified based on peptide substrate phosphorylation and ranked by specificity and statistical significance; the top 40 hits from Table 5.2 are shown. The top kinase families predicted to be activated by Yoda1 were the Src-family kinases (Lyn, Blk, Src, Hck, Fgr, Yes, Lck, Fyn; yellow) and the Src-related kinases (Frk, Srm, Brk; pink).

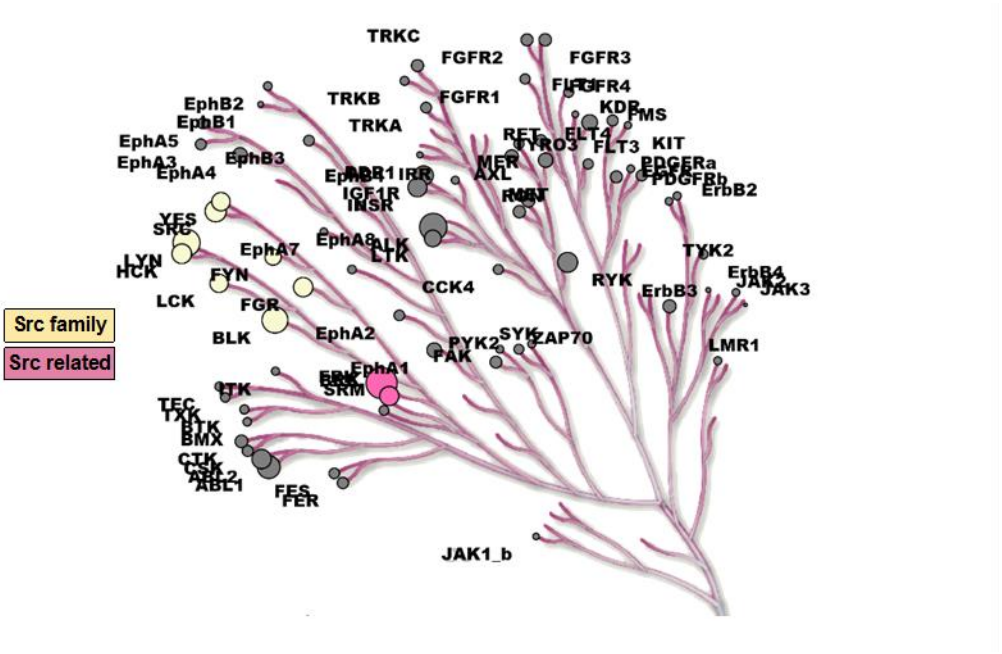

Figure 5.12 Dendrogram illustrating the effect of Yoda1 on tyrosine protein kinases. KinMap-generated summary of tyrosine protein kinase activity using PamChip multiplex kinase activity profiling shown in Table 5.2 and Figure 5.11. Circle size indicates median score (combination of specificity and significance). The top kinase families are illustrated by colour; Src-family kinases (yellow) and the Src-related kinases (pink).

5.4.4.2 A SFK inhibitor abolished Yoda1-evoked p38 MAPK and ERK1/2 phosphorylation

SFKs are the largest family of non-receptor protein tyrosine kinases; three members of the family (Src, Fyn, and Yes) are ubiquitously expressed, whereas the other members exhibit a more restricted expression pattern (Davis *et al.* 2001). To establish whether SFKs play a role in Yoda1-evoked p38 MAPK and/or ERK1/2 phosphorylation, an inhibitor of SFKs was used to pretreat murine cardiac fibroblasts. PP1 is an inhibitor of four of the SFKs; inhibiting Lck and Fyn at very low nanomolar concentrations and Src and Hck with slightly less potency (Hanke *et al.* 1996). PP1 pretreatment for 30 min prior to Yoda1 treatment revealed a substantial inhibitory effect on Yoda1-induced p38α MAPK phosphorylation in murine cardiac fibroblasts (Figure 5.13A). Pretreatment of murine cardiac fibroblasts with PP1 also eliminated ERK1/2 phosphorylation upon Yoda1 application (Figure 5.13B). These data indicate that SFKs are involved in Yoda1-evoked p38 MAPK and ERK1/2 activation.

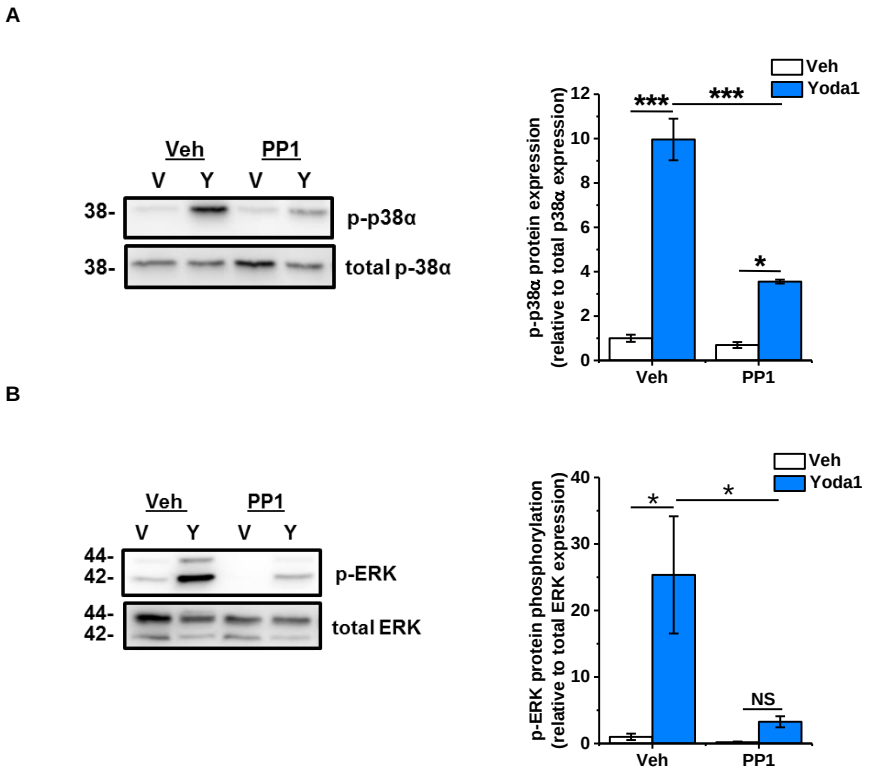

Figure 5.13 Effect of Src-family kinase inhibitor PP1 on Yoda1-induced p38α MAPK and ERK1/2 activation. Murine cardiac fibroblasts were pretreated with 5 μM PP1 or vehicle for 30 min, before treatment with vehicle or 10 μM Yoda1 for 10 min. Samples were immunoblotted for **(A)** p-p38α and reprobed with total p38α antibody or **(B)** p-ERK1/2 and reprobed with total ERK1/2 antibody to confirm equal protein loading. Graphs show mean densitometric data, *P<0.05, ***P<0.001, P=NS, not significant following an ANOVA with Tukey's post-hoc test (n=3).

5.4.4.3 A SFK inhibitor reduced Yoda1-evoked *Il6* expression

As PP1 was observed to reduce Yoda1-evoked phosphorylation of p38α MAPK, the next step was to investigate whether PP1 affected Yoda1-evoked *Il6* mRNA expression, which was previously shown to be dependent upon p38 MAPK (Figure 5.9). PP1 pretreatment abolished the Yoda-induced increase in *Il6* mRNA expression in murine cardiac fibroblasts (Figure 5.14). These data reveal SFKs as the link between activation of the Piezo1 channel and p38 MAPK activation, which subsequently leads to the induction of IL-6.

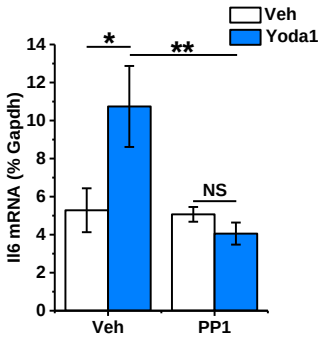

Figure 5.14 Effect of Src-family kinase inhibitor PP1 on Yoda1-induced *Il6* mRNA expression. RT-PCR analysis of *Il6* mRNA expression after exposure of murine cardiac fibroblasts to vehicle or 5 μM PP1 for 30 min, followed by treatment with vehicle or 10 μM Yoda1 for a further 24 h. Expression measured as % of housekeeping control, *Gapdh*, *P<0.05, **P<0.01, P=NS, not significant following an ANOVA with Tukey's post-hoc test (n=5).

5.4.4.4 A SFK inhibitor had no effect on Ca^{2+} entry through Piezo1

The effect of PP1 on Yoda1-evoked Ca^{2+} entry was investigated to ascertain whether the SFK inhibitor was interfering with Ca^{2+} entry through the activated Piezo1 channel, or whether the compound was having an effect further downstream. Fluorescence calcium imaging revealed that pretreatment of murine cardiac fibroblasts with PP1 had no effect on the Ca^{2+} entry seen upon application of 2 µM Yoda1, compared with cells pretreated with vehicle (Figure 5.15). These data indicate that SFKs are involved downstream of the Ca^{2+} influx induced following activation of Piezo1 with Yoda1, rather than interacting with the Piezo1 channel in some way.

Together, the results suggest that Yoda1-evoked Ca^{2+} entry through the Piezo1 channel instigates p38α MAPK phosphorylation and *Il6* mRNA expression through a SFK-dependent pathway.

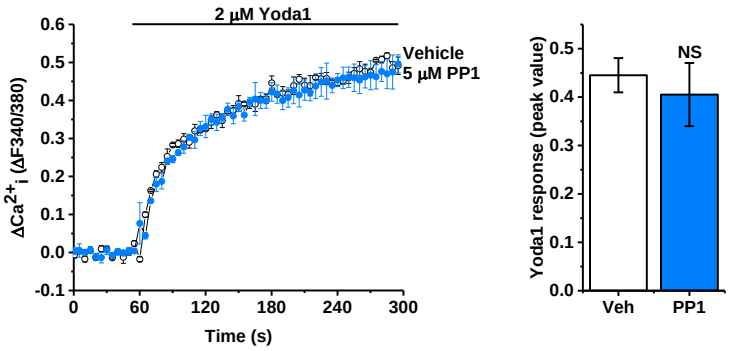

Figure 5.15 Effect of Src-family kinase inhibitor PP1 on Yoda1-induced Ca^{2+} entry. Representative intracellular Ca^{2+} traces and mean data after murine cardiac fibroblasts were exposed to 5 µM PP1 or vehicle for 30 min before activation of Piezo1 using 2 µM Yoda1, P=NS, not significant compared to vehicle-treated cells following a t-test (n/N=3/9).

5.4.4.5 Human cardiac fibroblasts express various SFKs

Expression of individual SFKs varies between different cell types; RT-PCR analysis was performed to determine which SFKs are expressed by cardiac fibroblasts. Human cardiac fibroblasts expressed mRNA encoding Fyn, Src, Lyn and Yes only (Figure 5.16A). Fyn and Yes kinase were most highly expressed and Src kinase was expressed at lower levels (approximately 25% of that of Fyn and Yes). These results were obtained using SYBR™ Green and in house designed primers, rather than Taqman primer/probe sets. Hence, products were run on a gel to confirm correct product size (Figure 5.16B). Primers were confirmed to be effective by including a commercial human brain sample as a control, which should express many members of the SFK family (Figure 5.16C). These results implicate Fyn, Src or Yes kinase, alone or in combination, as the SFKs responsible for Yoda1-evoked p38-dependent IL-6 expression in cardiac fibroblasts.

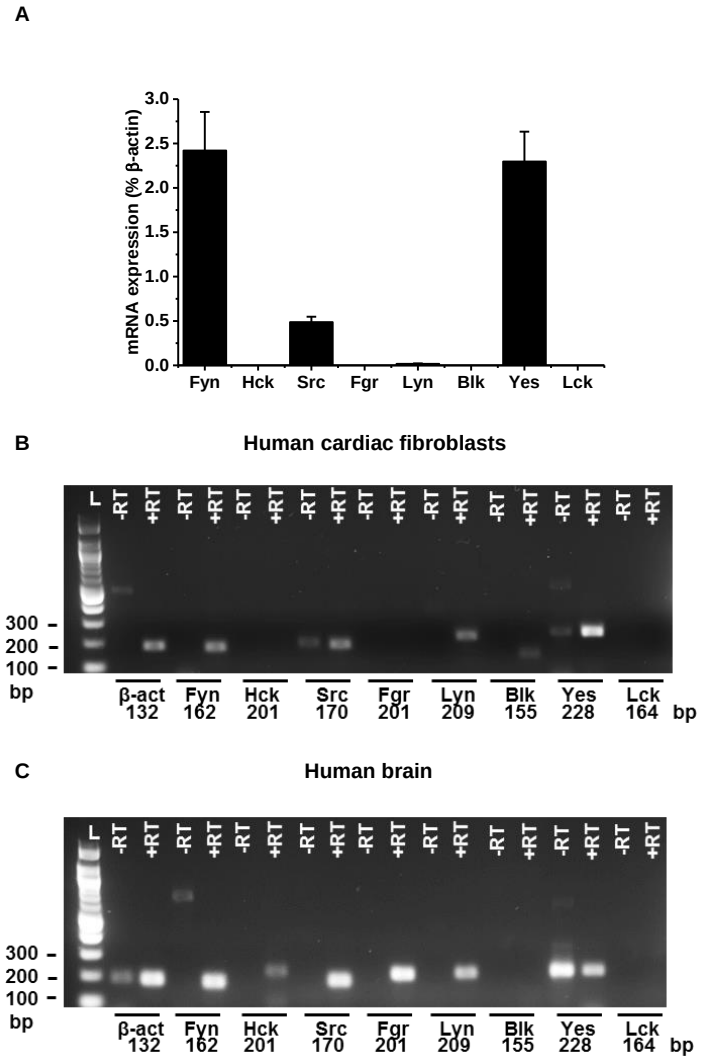

Figure 5.16 Expression of individual Src-family kinases in human cardiac fibroblasts. (A) RT-PCR analysis illustrating the differential expression of individual SFKs in human cardiac fibroblasts (n=4). Data are expressed relative to *β–ACTIN* housekeeping gene. **(B,C)** End-point PCR products obtained with primers for *Fyn*, *Hck*, *Src*, *Fgr*, *Lyn*, *Blk*, *Yes* and *Lck* in **(B)** human cardiac fibroblasts and **(C)** human brain mRNA after reverse transcriptase reaction (+RT) or without (-RT) to generate cDNA. Expected product sizes are shown beneath and L=100 bp ladder.

5.5 Discussion

Chemical activation of Piezo1, using Yoda1, initiates changes in the expression of genes associated with fibroblast function and cardiac remodelling. Of particular interest was the Yoda1-mediated increase in IL-6 expression and secretion in cardiac fibroblasts as this was revealed to be Piezo1-dependent. Piezo1 was also suggested to participate in maintaining basal levels of IL-6. IL-6 gene transcription in cardiac fibroblasts has been demonstrated to be induced via several different intracellular signalling pathways, including ERK, p38 MAPK and NF-κB (Vanden Berghe *et al.* 2000). In neonatal mouse cardiac fibroblasts, IL-6 expression was upregulated via activation of p38 MAPK following stimulation of the β2-adrenergic receptor (Yin *et al.* 2006). Yet, Ang II-evoked IL-6 production in neonatal rat cardiac fibroblasts required p38 MAPK and ERK activation (Sano *et al.* 2001), while Gα13 G-protein-induced IL-6 expression required NF-κB activation (Nagamatsu *et al.* 2006). Turner *et al.* (2007) found that TNF-α-evoked IL-6 expression in human cardiac fibroblasts occurred via p38 MAPK, PI3K/Akt and NF-κB pathways. These studies illustrate that the production of IL-6 expression in cardiac fibroblasts can arise following the activation of multiple pathways, depending on the initiating stimulus. The aim of this chapter was to establish the signalling pathway that coupled Piezo1 activation to IL-6 induction.

Multiplex serine/threonine kinase activity profiling revealed that, following Yoda1 treatment of murine cardiac fibroblasts, two major kinase families were activated: MAP kinases (extracellular signal-regulated kinases ERK1/2/5, c-Jun N-terminal kinases JNK1/2/3, p38 mitogen-activated protein kinases p38α/β/δ/γ) and cyclin-dependent kinases (CDKs1-7,9,11). Follow up experiments using western blotting revealed that both p38α MAPK and ERK1/2 were phosphorylated in murine cardiac fibroblasts applied with Yoda1 and these effects were both dependent on Piezo1 and extracellular Ca^{2+}. Further investigation using qRT-PCR demonstrated that it was p38 MAPK which was important for Yoda1-induced IL-6 expression and secretion in murine cardiac fibroblasts.

The p38 family of stress-activated MAPKs are known to play an important role in cardiac signalling and are activated in both acute and chronic cardiac pathologies (Zhang *et al.* 2003). The α subtype of the p38 family is the most abundantly expressed subtype and (along with p38β) can be inhibited by the pyridinyl imidazole class of compounds, including SB203580 (Turner 2011). Factors that

induce p38 signalling in cardiac fibroblasts are mostly stresses, including inflammatory cytokines (e.g. IL-1, TNF-α), profibrotic cytokines (e.g. TGF-β), DAMPs, G-protein coupled receptor agonists (e.g. Ang II, β-adrenoceptors), ischemia and mechanical stretch (Turner 2016; Sinfield *et al.* 2013; Dostal, Glaser and Baudino 2015; Turner 2014). In contrast, the ERK1/2 pathway is activated only to a smaller degree by stress stimuli; instead growth factors, serum, and phorbol esters strongly activate the pathway (Rose, Force and Wang 2010). Crosstalk has previously been demonstrated between ERK1/2 and p38 MAPK; Papakrivopoulou *et al.* (2004) found that both pathways were activated by cyclic mechanical load in cardiac fibroblasts and could regulate mechanical load-induced collagen I gene expression, albeit in opposite directions. Inhibition of ERK1/2 activity abolished expression whereas inhibition of p38 MAPK potentiated this process (Papakrivopoulou *et al.* 2004). These observations demonstrate a key role of these pathways in the regulation of pro-fibrotic gene expression induced by mechanical load.

SB203580, a compound confirmed to have suitable potency and selectivity for use as a p38 MAPK inhibitor in cell-based assays (Bain *et al.* 2007), was used to pretreat murine cardiac fibroblasts and was shown to abolish Yoda1-evoked *Il6* mRNA expression. It was also determined that SB203580 itself could substantially inhibit Yoda1-evoked p38α phosphorylation. This implies that p38α MAPK undergoes autophosphorylation upon Yoda1 treatment, which is prevented by reducing p38α MAPK activity via SB203580. Various upstream kinases are involved in the phosphorylation cascades leading to p38 activation, including MST1, MEKK1-4, MLK3, TAK1 and ASK1 at the MAPKKK level and MKK3/4/6 at the MAPKK level (Turner and Blythe 2019). Alternatively, p38 can also be activated by at least two non-canonical mechanisms, independently of upstream kinases. One of these is through TAB1 (TGF-β-activated protein 1 (TAK1)-binding protein 1), which binds to p38α MAPK and leads to its autophosphorylation (Tanno *et al.* 2003; Lu *et al.* 2006); this has been revealed to contribute to injury during myocardial ischemia (Tanno *et al.* 2003). Therefore, logically, as Yoda1 is inducing the autophosphorylation of p38, it is possible that TAB is important in this pathway, rather than classical MAPKKs.

The p38 pathway can regulate gene and protein expression via various approaches. These include: modulating chromatin structure by affecting DNA

methylation (Li *et al.* 2018), directly modifying gene transcription by phosphorylating transcription factors (Whitmarsh 2010) and regulating mRNA stability. The latter is mediated by the phosphorylation of RNA binding proteins, including HuR (human antigen R) which stabilises mRNA, and TTP (tristetraprolin) which partakes in mRNA destabilisation (Dean *et al.* 2004); the phosphorylation of both proteins leads to increased mRNA levels. RNA binding proteins bind to regulatory sites called adenosine/uridine-rich elements (AREs) in the 3′ untranslated regions (UTRs) of mRNAs (Bevilacqua *et al.* 2003). The majority of evidence implies that the p38 substrate, MAPK-activated protein kinase 2 (MK2), is involved in the phosphorylation of RNA binding proteins (Soni *et al.* 2019). Various proinflammatory cytokines secreted by cardiac fibroblasts, including IL-6, are modulated by p38-evoked MK2-mediated modulation of RNA-binding proteins (Turner and Blythe 2019). The p38 pathway can mediate myocardial IL-6 expression through multiple mechanisms; Ang II evokes *Il6* transcription via p38-mediated phosphorylation of the CREB transcription factor in rat cardiac fibroblasts (Sano *et al.* 2001) and IL-6 mRNA stability has been revealed to be promoted by p38α via the 3'-UTR (Zhao, Liu and Kirkwood 2008).

Transgenic mouse studies have demonstrated support for p38α playing a role in regulating fibroblast-derived IL-6 in various cardiac pathologies. Fibroblast-specific KO of *Mapk14*, the gene encoding p38α, revealed a critical role for this kinase in driving cardiac myofibroblast differentiation and fibrosis (Molkentin *et al.* 2017) and in stimulating IL-6-induced cardiac hypertrophy following chronic β-adrenergic stimulation (Bageghni *et al.* 2018). p38 signalling has also previously been demonstrated to be regulated by mechanical stress-evoked Piezo1 activation in mesenchymal stem cells (Sugimoto *et al.* 2017). These data combined therefore suggest it is possible that Piezo1-mediated activation of p38α in cardiac fibroblasts and the subsequent secretion of IL-6 may be important in cardiac remodelling.

Multiplex activity profiling of the tyrosine kinome revealed that Src-family and Src-related kinases may be the link between Piezo1-mediated Ca^{2+} influx and p38 activation. The activation of SFKs is achieved by either phosphorylation of Tyr416, dephosphorylation of Tyr527, or their association with different proteins, including ion channels (Bjorge, Jakymiw and Fujita 2000; Holmes *et al.* 1996). There is rich crosstalk between SFKs and the Ca^{2+} transient in activated cells.

The exchange is reciprocal; SFKs can play a part in pathways leading to the generation of the Ca^{2+} signal, as well as the Ca^{2+} signal being able to modulate the activity and function of SFKs (Anguita and Villalobo 2017). There is evidence that Src binds to regions of the α1c L-type Ca^{2+} channel to modulate channel activity (Dubuis *et al.* 2006). Moreover, it is known that SFKs interact with the Ca^{2+}-permeable TRP channels; Src interacts with TRPC channels via the SH2 domain and Fyn interacts with TRPC1/3/6/7 channels, regulating their functionality (Anguita and Villalobo 2017). This confirms the ability of SFKs to directly interact with ion channels. Reports of associations between Src kinase and Piezo1 have come to light in recent years. Wang *et al.* (2016) found that shear stress induced phosphorylation of Src kinase in endothelial cells and Zhong *et al.* (2019) demonstrated that Src kinase was cleaved in response to mechanical stretch in endothelial alveolar-capillary barriers; both processes occurred in a Piezo1-dependent manner. SFKs are also known upstream activators of the p38 MAPK pathway; Kim *et al.* (2008) reported that the GTPase, Rac1, was the link between Src kinase and p38 MAPK activation in a cancer cell line. Moreover, hypoxia-induced p38 MAPK activation and subsequent IL-6 production in mouse Kupffer cells and mechanically-activated calcium currents leading to activation of the ERK1/2 and p38 MAPK pathways in an osteoblast cell line were both found to involve upstream SFKs (Katz, Boland and Santillán 2006; Thobe *et al.* 2006). Therefore, it is postulated that SFKs may represent the link between Piezo1 activation and p38 MAPK activation in cardiac fibroblasts.

Utilisation of an inhibitor of SFKs (PP1) revealed a substantial inhibitory effect on Yoda1-induced p38α MAPK and ERK1/2 phosphorylation and reduced Yoda1-evoked *Il6* mRNA expression, implying that SFKs are indeed involved in Yoda1-evoked, p38 MAPK-mediated *Il6* expression. PP1 had no effect on Ca^{2+} influx, implying that SFKs are involved downstream of Ca^{2+} entry induced by Piezo1 activation using Yoda1, rather than interacting with the Piezo1 channel. RT-PCR data illustrating the expression levels of each member of the family suggested that either Src and/or Fyn kinase are involved in this pathway as PP1 inhibits only four of the kinases in the family (Fyn, Src, Lck and Hck) (Hanke *et al.* 1996) and, of these, only Src and Fyn kinase were found to be expressed in human cardiac fibroblasts. SFKs have a segment of residues called the unique domain which has a lack of sequence similarity among the different members; this is partly

conserved in Src, Fyn, and Yes (Amata, Maffei and Pons 2014). These 3 SFKs are often co-expressed and a deficiency in one can be compensated by the action of the others (Amata, Maffei and Pons 2014). This, along with the fact that Src and Fyn are similarly regulated (Ingley 2008), makes the study into individual SFKs more difficult.

Together, data in this chapter revealed that p38α MAPK and ERK1/2 are phosphorylated in cardiac fibroblasts upon Piezo1 activation by Yoda1. Phosphorylation was dependent on Piezo1 expression/activity and extracellular Ca^{2+}. Investigation into whether activation of these signalling pathways led to Yoda1-evoked IL-6 expression and secretion using a variety of pharmacological kinase inhibitors ascertained that only p38α MAPK was involved. Yoda1 treatment activated SFKs in cardiac fibroblasts; this was also dependent on Piezo1 and Ca^{2+} and occurred upstream of p38α MAPK activation. In summary, Ca^{2+} entry through Piezo1 leads to the phosphorylation of SFKs which cause the activation of p38α MAPK, with the end result being an induction in IL-6. This is summarised in Figure 5.17.

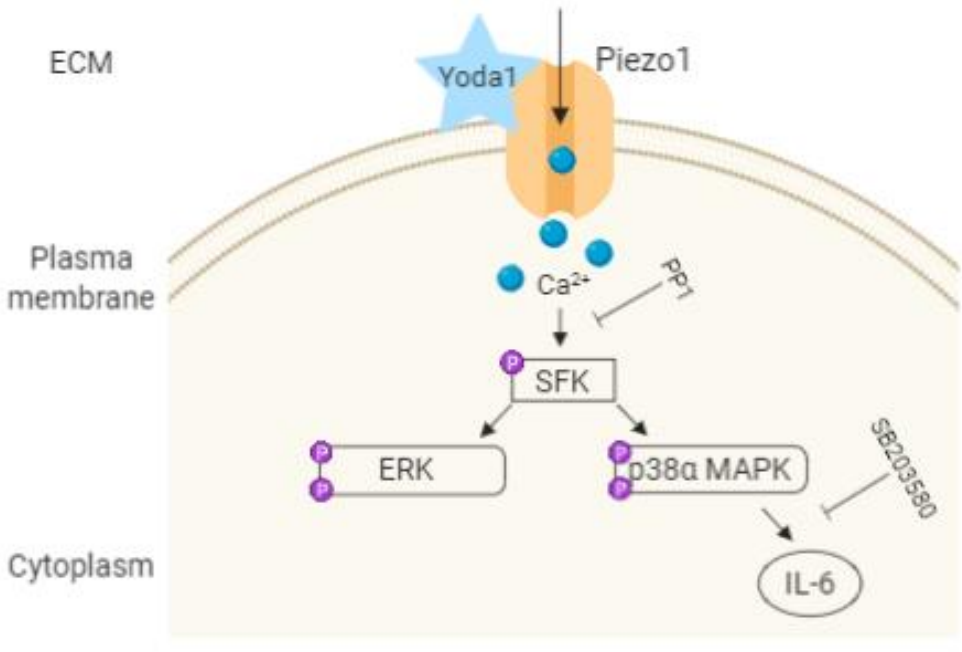

Figure 5.17 Schematic of the proposed mechanism linking Yoda1-mediated Piezo1 activation to IL-6 secretion. Yoda1 activates Piezo1 channels to cause Ca^{2+} influx, this activates Src-family kinases (SFK) which phosphorylate both extracellular signal-regulated kinases 1 and 2 (ERK) and p38 mitogen-activated protein kinase (MAPK). P38 MAPK activation stimulates interleukin-6 (IL-6) secretion. Inhibitory compounds used (PP1, SB203580) are also shown.

Chapter 6 The role of Piezo1 in cardiac fibroblasts *in vivo*

6.1 Introduction

In the previous three chapters, evidence was presented establishing that Piezo1 is expressed in cardiac fibroblasts and that its activation leads to changes in the expression of genes which are important for fibroblast function and cardiac remodelling. All experiments leading up to this point have been *in vitro* using cultured cardiac fibroblasts. To investigate the physiological role of Piezo1 in cardiac fibroblasts, it was necessary to develop a fibroblast-specific Piezo1 KO model. A global KO approach has been used previously to investigate endothelial-specific deletion of mouse Piezo1; it was discovered that this profoundly disturbed the developing vasculature and was embryonically lethal within days of the heart beating (Li *et al.* 2014).

6.2 Aims

The aim of this chapter was to generate and validate an inducible KO mouse model of Piezo1 specifically in cardiac fibroblasts in order to examine the role of Piezo1 in cardiac remodelling. The intention was to investigate whether cardiac function or molecular markers of remodelling were affected following cardiac injury in mice with fibroblast-specific deletion of Piezo1, in comparison with control mice.

6.3 Methods

Genetic manipulation to generate Piezo1 KO mice was performed using the *Cre-loxP* system (Section 2.13.4.1). Ca^{2+} measurements (Section 2.3) and RT-PCR (Section 2.5) were utilised to confirm KO of Piezo1. 10-12 week old mice underwent a surgical procedure, either a permanent left anterior descending (LAD) coronary artery ligation model of experimental MI (Section 2.13.5.1) or a pressure overload model caused by constriction of the transverse aorta (TAC) (Section 2.13.5.2). The following week, mice were injected with tamoxifen to induce *Cre* activity (Section 2.13.4.2) and cardiac function and gene expression were evaluated 4 weeks after surgery (Section 2.13.5.3).

6.4 Results

6.4.1 Fibroblast-specific Piezo1 knockout murine model

6.4.1.1 Generation of the fibroblast-specific Piezo1 knockout murine model

To study the role of cardiac fibroblast Piezo1 *in vivo*, C57BL/6 *Piezo1*$^{flx/flx}$ mice were crossed with C57BL/6 mice expressing Cre recombinase (*Col1a2-Cre-ER(T)*) to generate a tamoxifen-inducible fibroblast-specific Piezo1 KO murine model line (*Col1a2-Cre-Piezo1*$^{flx/flx}$). Fibroblast specificity of Cre expression (and hence Piezo1 deletion) was driven by a 6 kb transcriptional enhancer sub-cloned from the far-upstream region of the mouse collagen I alpha 2 gene (*Col1a2*), linked to an endogenous minimal promoter (Zheng *et al.* 2002). This method has previously been used successfully by our group to delete p38α and IL-1R1 in fibroblasts (Bageghni *et al.* 2018; Bageghni *et al.* 2019). *Cre*$^{-}$ *Piezo1*$^{flx/flx}$ mice were used as control animals and *Cre*$^{+}$ *Piezo1*$^{flx/flx}$ mice as experimental animals. Three week-old *Col1a2-Cre-Piezo1*$^{flx/flx}$ mice were injected intraperitoneally with tamoxifen, which induces the activity of Cre and, therefore, floxed gene deletion exclusively in fibroblasts. The strategy for breeding animals is illustrated in Section 2.14.4 (Figure 2.6) and information on how the deletion of Piezo1 is achieved using the *Cre-loxP* technique is detailed in Figure 2.7. Figure 6.1 displays examples of agarose gels used to identify the genotype of mice. Figure 6.1A illustrates PCR products attained using primers for *LoxP* confirming that all 6 *Col1a2-Cre-Piezo1*$^{flx/flx}$ mice have *LoxP* sites flanking exons 19-23 of Piezo1, as expected. Figure 6.1B reveals products from PCR using primers for *Cre*. Of the 6 *Col1a2-Cre-Piezo1*$^{flx/flx}$ mice, mice numbered 1, 3 and 4 were *Cre*$^{-}$ and 2, 5 and 6 were *Cre*$^{+}$. Following tamoxifen administration, deletion bands were detected in both ear notches and cultured cardiac fibroblasts from *Cre*$^{+}$ mice only, indicating that exons 19-23 of Piezo1 had been deleted (Figure 6.1C).

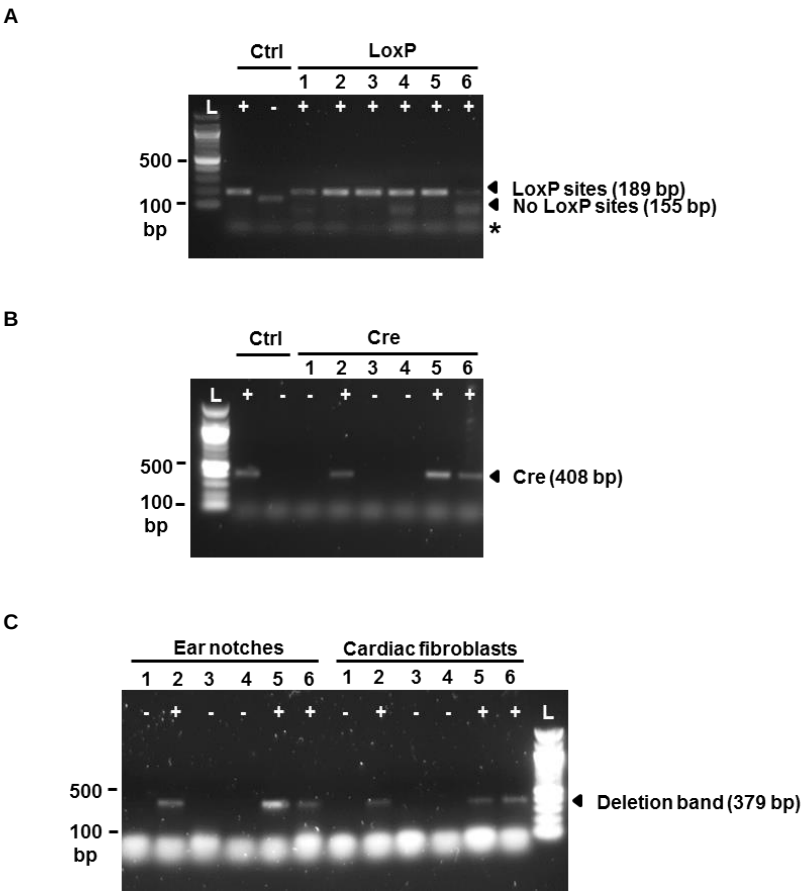

Figure 6.1 Validation of the fibroblast-specific Piezo1 knockout murine model. (A) PCR genotyping for presence of *LoxP* sites (189 bp) in DNA extracted from ear notches from mice 1-6. Band size was 155 bp if no *LoxP* sites were present. *Asterisk indicates non-specific bands. **(B)** PCR genotyping for presence of the *Cre* allele (408 bp) in DNA extracted from ear notches from mice 1-6. **(C)** PCR genotyping for presence of a band indicating a deletion of *Piezo1* (379 bp) in DNA extracted from ear notches and cultured cardiac fibroblasts from mice 1-6. This was performed using primers which were only capable of amplifying a product if exons 19-23 of Piezo1 had been deleted. Gels indicate positive and negative controls and L=100 bp ladder. Staining below 100 bp indicates primer dimers.

6.4.1.2 Validation of the fibroblast-specific Piezo1 knockout murine model

Despite *Piezo1* deletion bands being detected in *Cre*$^{+}$ samples, RT-PCR analysis and Ca^{2+} measurements revealed only a modest 20 % reduction in *Piezo1* mRNA expression and a lessening of 10 % in the Yoda1-evoked Ca^{2+} influx in cultured cardiac fibroblasts from tamoxifen-treated *Cre*$^{+}$ (Piezo1 KO) mice, compared to those from *Cre*$^{-}$ (Ctrl) mice (Figure 6.2A,B). ATP was used to confirm cell viability; the response was comparable in cardiac fibroblasts isolated from both control and Piezo1 KO animals (Figure 6.2C).

These data suggest that the (small) level of Piezo1 deletion observed at PCR and gene expression level was unlikely to be sufficient to observe functional effects *in vivo*. Therefore, a second strategy was adopted using a more potent version of *Cre*.

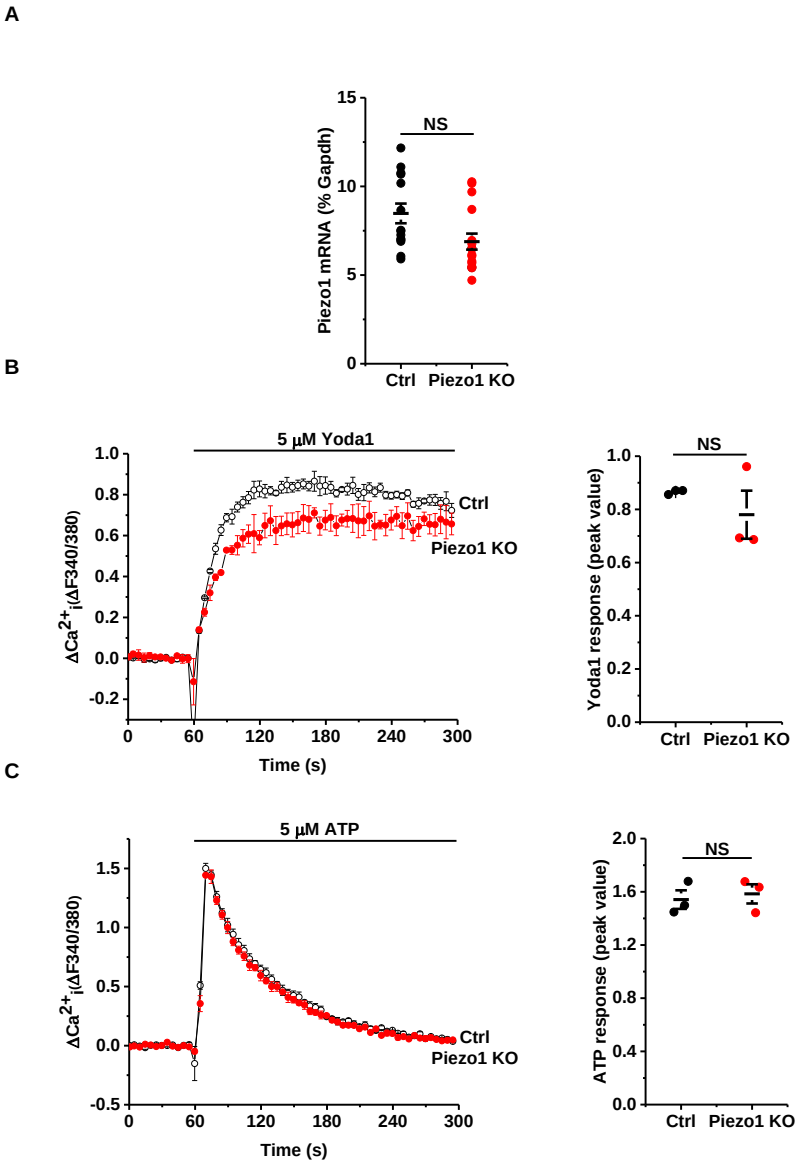

Figure 6.2 *Piezo1* mRNA expression and intracellular Ca^{2+} measurements following fibroblast-specific Piezo1 knockout. (A) RT-PCR analysis of *Piezo1* mRNA expression in cultured murine cardiac fibroblasts isolated from control and Piezo1 KO mice, P=NS, not significant following a t-test. Group sizes: control n=10, Piezo1 KO n=9. **(B, C)** Representative Ca^{2+} traces following **(B)** 5 µM Yoda or **(C)** 5 µM ATP application at 60 seconds in cardiac fibroblasts isolated from control and Piezo1 KO mice. The mean data are shown alongside, P=NS, not significant following t-tests (n/N=3/9).

6.4.2 Myofibroblast-specific Piezo1 knockout murine model

The second strategy involved generating an alternative KO murine model where C57BL/6 *Piezo1*$^{flx/flx}$ mice were crossed with C57BL/6 mice expressing Cre recombinase under control of the periostin (*Postn*) promoter (The Jackson Laboratory) to obtain a tamoxifen-inducible myofibroblast-specific Piezo1 KO murine model (*Postn-Cre-Piezo1*$^{flx/flx}$). This is a *Mer-Cre-Mer* (MCM) model; the tamoxifen inducible Cre recombinase is flanked by two modified estrogen receptor ligand binding domains and is more potent than the *ER*(*T*) Cre used in the *Col1a2*-promotor mice. This model has been used previously to investigate myofibroblast function following MI (Kanisicak *et al.* 2016).

Periostin expression in normal myocardium is high during the neonatal period, but subsequently falls to low levels (Frangogiannis 2012). Its expression reappears following cardiac injury as, irrespective of their lineage, periostin is a common marker for myofibroblasts in the adult mouse heart (Kanisicak *et al.* 2016). Therefore, cardiac injury is required prior to the administration of tamoxifen in order to induce periostin expression and the deletion. Cardiac hypertrophy, due to pressure overload induced by TAC, has been associated with cardiac periostin upregulation (Stansfield *et al.* 2009). Oka *et al.* (2007) revealed increased periostin expression 7 days after TAC surgery, which was absent in sham-operated animals. It has also been demonstrated that there is marked periostin expression 4 days after acute infarction in mice; this persisted for several weeks after the acute event (Stanton *et al.* 2000; Oka *et al.* 2007). On this basis, MI and TAC were the two methods utilised for generating cardiac injury.

6.4.2.1 Generation of the myofibroblast-specific Piezo1 knockout murine model

As with the previous model, *Cre*$^{-}$ *Piezo1*$^{flx/flx}$ mice were used as control animals and *Cre*$^{+}$ *Piezo1*$^{flx/flx}$ mice as experimental animals. An example DNA agarose gel used for identifying the genotype of each mouse is shown in Figure 6.3. In DNA isolated from ear notches of 8 mice, all animals were positive for *LoxP* sites, as expected, and of these, mice numbered 2, 5, 6 and 8 were *Cre*$^{+}$ and 1, 3, 4 and 7 were *Cre*$^{-}$. Mice underwent surgery at 10-12 weeks of age and were then injected intraperitoneally with tamoxifen for 5 consecutive days the following

week. This time point was chosen because, as previously discussed, periostin expression is upregulated 7 days after both TAC and MI induction in mice (Oka *et al.* 2007). 4 weeks after surgery, physiological measurements of cardiac function were obtained by Millar catheter analysis. Stroke volume (SV), ejection fraction (EF), end systolic/diastolic volume (ESV/EDV), end systolic/diastolic pressure (ESP/EDP) and myocardial contractility (dP/dt_{max}) were calculated. Cardiac hypertrophy was investigated by calculating heart weight/tibia length (HW/TL) and heart weight/body weight (HW/BW) ratios. Cardiac gene expression was also investigated using RT-PCR. The timeline for experimentation is shown in Figure 6.4.

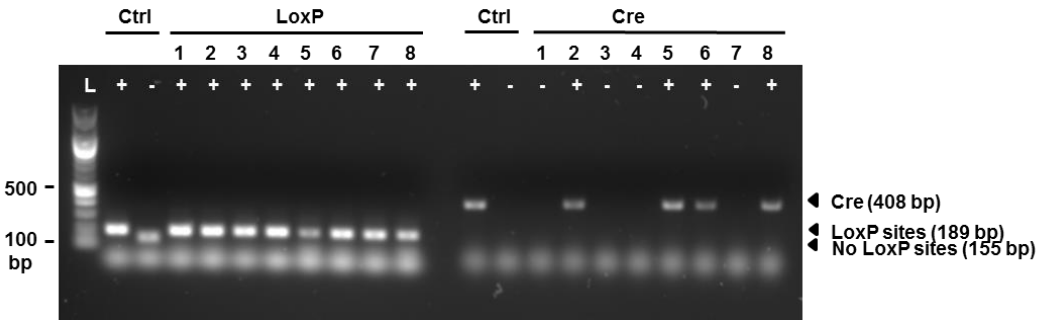

Figure 6.3 Validation of the myofibroblast-specific knockout of Piezo1 murine model. PCR genotyping in *Postn-Cre-Piezo1*$^{flx/flx}$ mice for presence of *LoxP* sites (189 bp; band size was 155 bp if no *LoxP* sites were present) and the *Cre* allele (408 bp) in DNA extracted from ear notches from 8 mice. Gels indicate positive and negative controls and L=100 bp ladder. Staining below 100 bp indicates primer dimers.

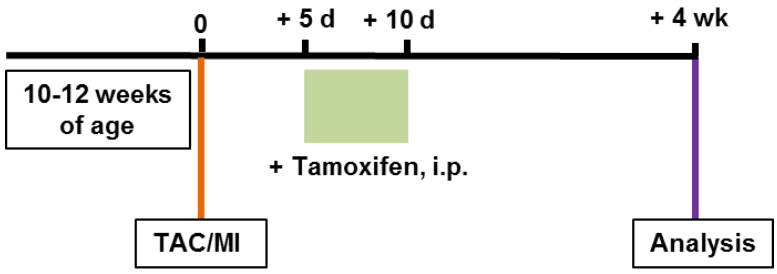

Figure 6.4 Timeline for the TAC- and MI-induced models of cardiac injury. Experimental timeline indicating the timing of tamoxifen injection and experimental myocardial infarction (MI) / thoracic aortic constriction (TAC) in 10-12 week old *Postn-Cre-Piezo1*$^{flx/flx}$ mice, as well as timings for collection of RNA and measurement of cardiac function by pressure-volume (P-V) conductance catheter.

6.4.2.2 MI-induced cardiac injury

Ligation of the coronary artery to induce MI was chosen as one of two methods for inducing cardiac injury in mice. MI is characterised by ischaemic necrosis, left ventricular dilatation and at a later stage, collagen deposition, which results in the formation of a scar. *Cre*$^{-}$ animals were referred to as “Ctrl MI” and *Cre*$^{+}$ animals as “KO MI” throughout; these animals were compared to animals undergoing a sham procedure (surgery without ligation of the coronary artery).

6.4.2.2.1 Validation of MI-induced Piezo1 deletion

RNA taken from the apex of the heart was analysed for *Postn* and *Piezo1* mRNA expression in mice 4 weeks following surgery. There appeared to be no difference in *Postn* mRNA expression between sham-operated mice and mice which underwent MI (Figure 6.5A). There was also no correlation between *Piezo1* expression and whether mice were Ctrl or had KO of Piezo1 (Figure 6.5B).

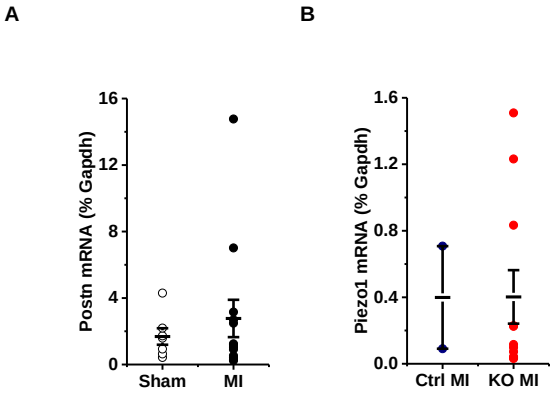

Figure 6.5 *Postn* and *Piezo1* expression levels following MI-induced cardiac injury in mice with myofibroblast-specific deletion of *Piezo1*. RT-PCR analysis for **(A)** *Postn* and **(B)** *Piezo1* mRNA expression 4 weeks after mice underwent surgery. Individual data and mean ± SEM are shown. Expression is measured as % of housekeeping control, *Gapdh*. Group sizes for *Postn* expression: sham, n=7; MI, n=13. Group sizes for Piezo1 expression: control MI, n=2; KO MI, n=11. Sham data were taken from Bageghni *et al.* (2019); all animals were male.

6.4.2.2.2 Effect of Piezo1 deletion on cardiac function

A summary of physiological measurements of cardiac function 4 weeks after surgery for all three groups of mice (sham, Ctrl MI and KO MI) is shown in Table 6.1. Measurements of stroke volume and ejection fraction showed a decrease from 17 µl in sham animals to 12 µl in Ctrl animals and 62 % in sham animals to 41 % in Ctrl animals, respectively (Figure 1.6A,B). However, other cardiac parameters expected to be affected following MI induction, e.g. an increase in end systolic and diastolic volumes (Bageghni *et al.* 2019), were unchanged in Ctrl MI mice, in comparison with sham-operated mice (Figure 6.6C,D). Due to the lack of an induction of *Postn* mRNA expression and therefore, a lack of Piezo1 KO (Figure 6.5) in Cre^{+} mice, it was difficult to ascertain the impact of myofibroblast-specific Piezo1 deletion. Very low sample numbers in the control group also make any evaluation of results difficult.

Parameter	Sham (n=12)	Ctrl MI (n=2)	KO MI (n=11)
Ejection fraction (%)	62.15 ± 3.61	41.13 ± 6.06	39.26 ± 4.37
End systolic volume (µl)	12.19 ± 1.78	16.82 ± 1.58	15.29 ± 2.65
End diastolic volume (µl)	26.94 ± 1.92	26.98 ± 7.06	24.25 ± 2.83
Cardiac output (µl/min)	9800 ± 684	6836 ± 1566	5020 ± 585
Stroke volume (µl)	16.72 ± 0.88	12.17 ± 3.7	8.85 ± 1.12
Heart rate (bpm)	584.5 ± 21.9	575.6 ± 46.3	572.9 ± 14.1
End systolic pressure (mmHg)	103.15 ± 4.23	102.26 ± 8.74	100.19 ± 2.65
End diastolic pressure (mmHg)	10.66 ± 1.78	8.72 ± 2.84	7.59 ± 1.96
$dPdt_{max}$ (mmHg/sec)	11510 ± 802	9328 ± 2731	10620 ± 692
$dPdt_{min}$ (mmHg/sec)	-10285 ± 621	-9307 ± 3543	-8471 ± 728
Arterial blood pressure (mmHg)	71.6 ± 3.1	77.0 ± 2.0	74.2 ± 4.9

Table 6.1 Effect of myofibroblast-specific Piezo1 deletion on cardiac function 4 weeks after myocardial infarction. Cardiac parameters were assessed by Millar pressure-volume conductance catheter. Sham = from a previous study (Bageghni *et al.* 2019) (n=12); Ctrl MI = *Cre^- Postn-Cre-Piezo1$^{flx/flx}$* mice after MI (n=2); KO MI = *Cre^+ Postn-Cre-Piezo1$^{flx/flx}$* mice after MI (n=11). Data are mean values ± SEM. All animals were male.

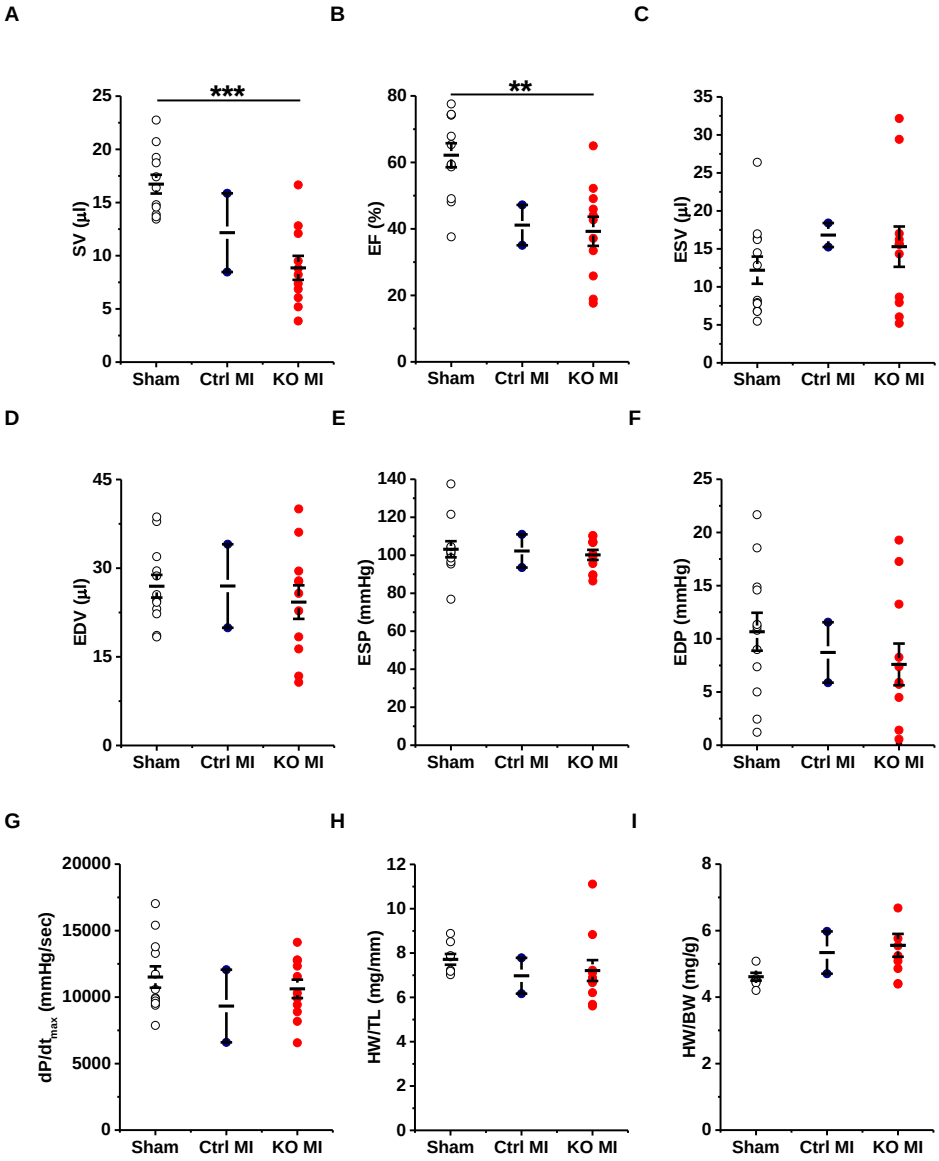

Figure 6.6 Effect of myofibroblast-specific Piezo1 KO on cardiac function and size following MI-induced cardiac injury. PV conductance catheter data from sham, control and myofibroblast-specific Piezo1 KO mice 4 weeks after surgery. Individual data and mean ± SEM are shown. Group sizes: sham (n=12), control MI (n=2), KO MI (n=11) for **(A)** SV, stroke volume; **(B)** EF, ejection fraction; **(C)** ESV, end systolic volume; **(D)** EDV, end diastolic volume; **(E)** ESP, end systolic pressure; **(F)** EDP, end diastolic pressure; **(G)** dP/dt_{max}, maximal rate of rise of left ventricular pressure and a measure of myocardial contractility. Group sizes: sham (n=8), control MI (n=2), KO MI (n=11) for **(H)** HW/TL, heart weight/tibia length and **(I)** HW/BW, height weight/body weight. Sham data were taken from Bageghni *et al.* (2019); all animals were male, **P<0.01, ***P<0.001 following an ANOVA with Tukey's post-hoc test.

6.4.2.2.3 Effect of Piezo1 deletion on cardiac gene expression

Messenger RNA expression of various ECM regulatory genes (*Mmp3*, *Tnc*, *Col1a1*, *Col3a1*), hypertrophy markers (*Mhy7*, *Nppa*), an inflammatory gene (*Il6*) and a myofibroblast marker (*Acta2*) were analysed in MI hearts and compared to sham hearts. Despite data indicating that mice which underwent surgery to induce MI had reduced stroke volume and ejection fraction (Figure 6.6B), there were no obvious differences in the mRNA expression levels of these genes between sham and Ctrl MI mice 4 weeks after surgery (Figure 6.7). Although expression levels of all the genes appeared to be increased in KO MI mice, compared to both sham and Ctrl MI animals (Figure 6.7), this could not be fully elaborated on due to a lack of an induction of *Postn* mRNA expression and a lack of Piezo1 KO in *Cre*$^{+}$ animals (Figure 1.5).

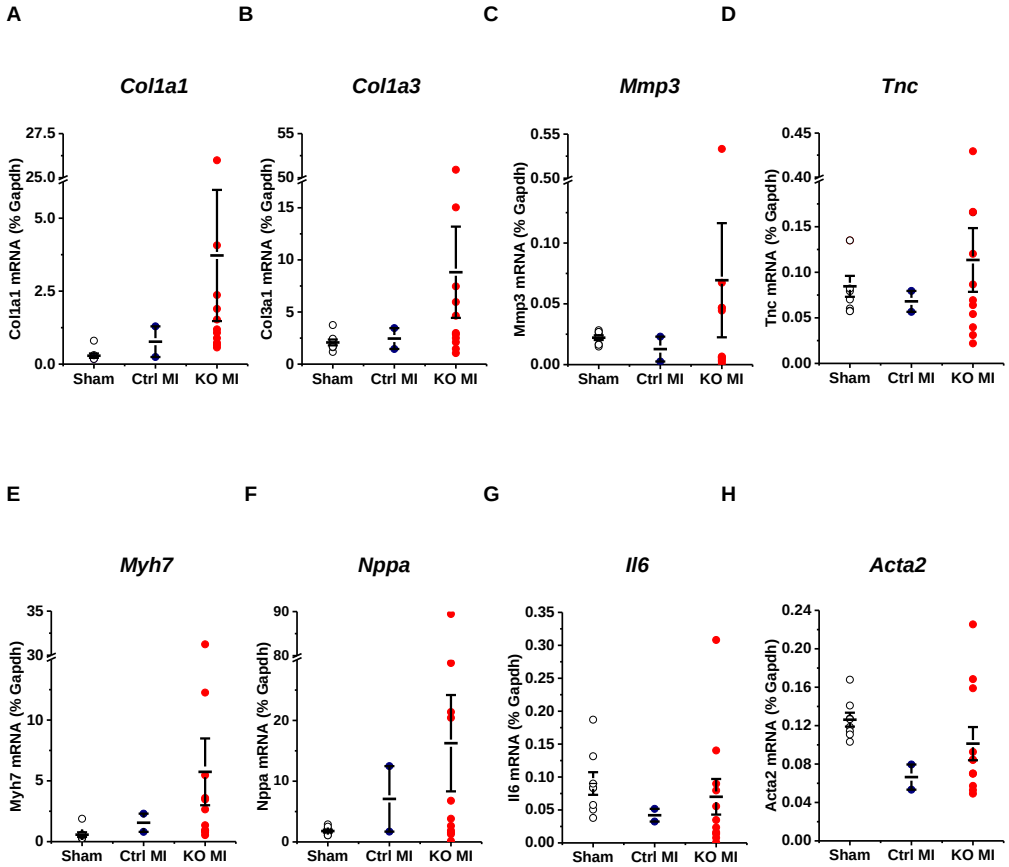

Figure 6.7 Effect of myofibroblast-specific Piezo1 KO on markers of hypertrophy and cardiac dysfunction following MI-induced cardiac injury. Real-time RT-PCR analysis of cardiac mRNA levels in hearts from sham, control and Piezo1 KO mice 4 weeks after MI for **(A)** *Col1a1*, **(B)** *Col1a3*, **(C)** *Mmp3*, **(D)** *Tnc*, **(E)** *Myh7*, **(F)** *Nppa*, **(G)** *Il6* and **(H)** *Acta2*. Individual data and mean ± SEM are shown. Expression is measured as % of housekeeping control, *Gapdh*. Group sizes: sham (n=8), control (n=2), KO (n=11). Sham data were taken from Bageghni *et al.* (2019); all animals were male.

6.4.2.3 TAC-induced cardiac injury

When the load on the heart is excessive, a number of compensatory mechanisms maintain circulatory function. TAC causes pressure overload which leads to cardiac remodelling within 7 days (Herum *et al.* 2015) and was chosen as the second technique for inducing cardiac injury. This procedure often leads to cardiac hypertrophy, a physiological, compensatory response to pressure or volume overload which results in increased cardiac myocyte size. When the increased work exceeds the reserve of the compensatory mechanisms, the heart is incapable to meet the demands imposed and overt congestive heart failure ensues (Spann 1969). The murine TAC model was first validated by Rockman *et al.* (1991) and is now a useful tool to mimic cardiac hypertrophy and heart failure development. *Cre*$^{-}$ animals are referred to as “Ctrl TAC” and *Cre*$^{+}$ animals as “KO TAC” throughout; these animals were compared to animals undergoing a sham procedure (surgery without banding of the aorta).

6.4.2.3.1 Validation of TAC-induced Piezo1 deletion

RNA was isolated from the apex of the heart from sham and TAC-operated animals and analysed for *Postn* and *Piezo1* mRNA expression. There was a clear, but somewhat variable, increase in *Postn* mRNA expression in hearts following TAC surgery, compared to sham-operated hearts, as has been reported previously, but this was not statistically significant with the small number of animals used (Figure 6.8A). There was also decreased *Piezo1* expression in all KO TAC mice, compared to those in the Ctrl TAC group but, again, this was not statistically significant (Figure 6.8B).

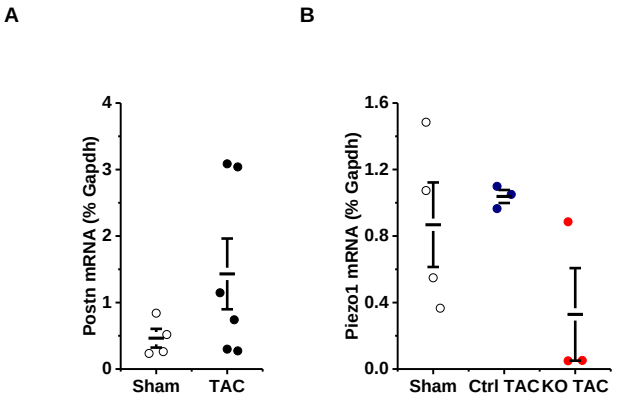

Figure 6.8 *Postn* and *Piezo1* expression levels following TAC-induced cardiac injury in mice with myofibroblast-specific deletion of *Piezo1*. RT-PCR analysis for **(A)** *Postn* and **(B)** *Piezo1* mRNA expression 4 weeks after control and Piezo1 KO mice underwent TAC surgery, compared to sham animals. Individual data and mean ± SEM are shown. Expression is measured as % of housekeeping control, *Gapdh*. Group sizes for *Postn* expression: sham n=4, TAC n=6. Group sizes for *Piezo1* expression: sham n=4, Ctrl TAC n=3, KO TAC n=3; all animals were female.

6.4.2.3.2 Effect of Piezo1 deletion on cardiac function

The data discussed here are viewed as pilot data due to the small number of animals utilised. A summary of each parameter of cardiac function measured in all three groups of animals is summarised in Table 6.2. Physiological measurements of cardiac function 4 weeks after surgery revealed ejection fraction was reduced by almost half in TAC-operated mice, compared to sham animals (Figure 6.9B). As expected, Ctrl mice displayed decreased stroke volume (Figure 6.9A) and raised end systolic and diastolic pressures (Figure 6.9C,D) 4 weeks after TAC surgery, in comparison with sham-operated animals. There was no difference in the ratios of HW/TL or HW/BW between sham-operated and mice which underwent TAC (Figure 6.9E,F). This indicates that cardiac dysfunction, but not overt hypertrophy, was achieved following TAC surgery. The most obvious difference between control (Ctrl TAC) and experimental (KO TAC) animals was in end diastolic pressure. This parameter was markedly increased in Ctrl TAC mice, in comparison with sham-operated mice; this increase was not evident in KO TAC mice (Figure 6.9D). This result may indicate that a deletion in Piezo1 is beneficial as mice lacking Piezo1 exhibit lower end diastolic pressure following TAC-induced cardiac injury.

Parameter	Sham (n=3)	Ctrl TAC (n=3)	KO TAC (n=3)
Ejection fraction (%)	61.95 ± 7.68	34.11 ± 1.97	37.91 ± 5.21
End systolic volume (µl)	10.49 ± 3.76	16.98 ± 2.97	17.51 ± 1.18
End diastolic volume (µl)	25.43 ± 3.85	24.82 ± 3.92	27.97 ± 3.48
Cardiac output (µl/min)	8672 ± 1289	4770 ± 850	6062 ± 1351
Stroke volume (µl)	15.74 ± 2.22	8.19 ± 1.12	10.59 ± 2.40
Heart rate (bpm)	550.0 ± 7.1	575.7 ± 24.2	578.1 ± 29.7
End systolic pressure (mmHg)	96.91 ± 2.70	125.06 ± 10.80	130.43 ± 7.33
End diastolic pressure (mmHg)	8.68 ± 2.84	17.04 ± 3.07	5.979 ± 1.23
$dPdt_{max}$ (mmHg/sec)	10753 ± 265	10479 ± 1802	13756 ± 1141
$dPdt_{min}$ (mmHg/sec)	-8090 ± 737	-10215 ± 2490	-12706 ± 972
Arterial blood pressure (mmHg)	84.3 ± 8.2	78.0 ± 5.1	77.6 ± 2.7

Table 6.2 Effect of cardiac fibroblast-specific Piezo1 deletion on cardiac function 4 weeks after thoracic aortic constriction. Cardiac parameters were assessed by Millar pressure-volume conductance catheter. Sham = *Cre*$^{+}$ *Postn-Cre-Piezo1*$^{flx/flx}$ mice (n=3); Ctrl TAC = *Cre*$^{-}$ *Postn-Cre-Piezo1*$^{flx/flx}$ mice after TAC (n=3); KO TAC = *Cre*$^{+}$ *Postn-Cre-Piezo1*$^{flx/flx}$ mice after TAC (n=3). Data are mean values ± SEM; all animals were female.

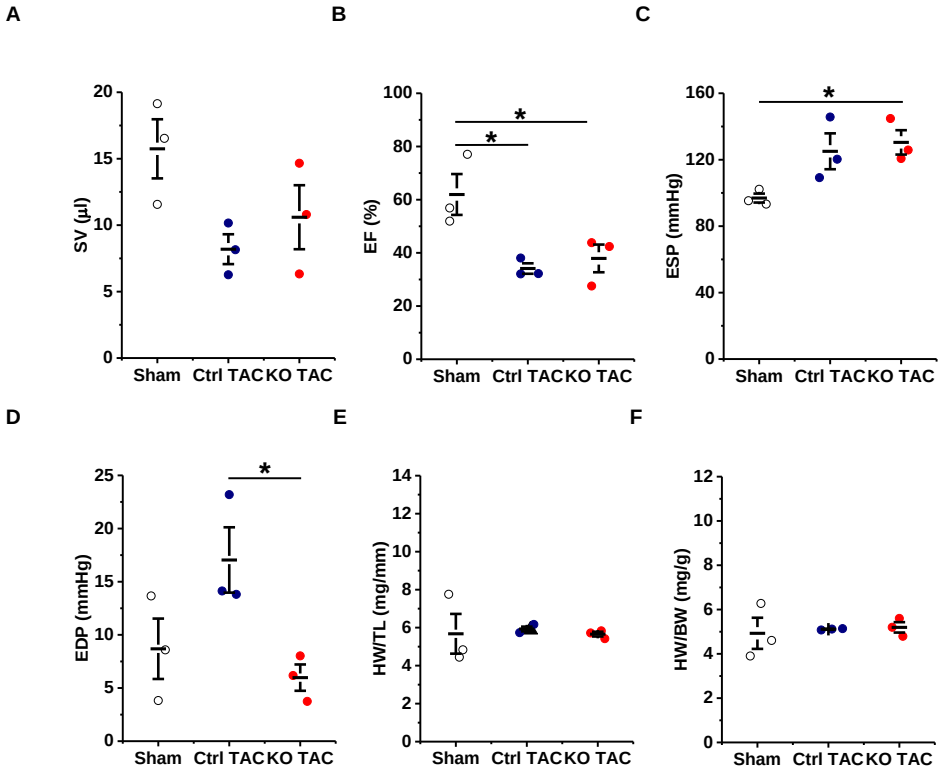

Figure 6.9 Effect of myofibroblast-specific Piezo1 KO on cardiac function and size following TAC-induced cardiac injury. PV conductance catheter data from sham, control and myofibroblast-specific Piezo1 KO mice 4 weeks after TAC. Individual data and mean ± SEM are shown. **(A)** SV, stroke volume; **(B)** EF, ejection fraction; **(C)** ESP, end systolic pressure; **(D)** EDP, end diastolic pressure; **(E)** HW/TL, heart weight/tibia length and **(F)** HW/BW, height weight/body weight. Group sizes: sham (n=3), Ctrl TAC (n=3), KO TAC (n=3). All animals were female, *P<0.05 following an ANOVA with Tukey's post-hoc test.

6.4.2.3.3 Effect of Piezo1 deletion on cardiac gene expression

Assessment of gene expression by RT-PCR revealed that, although not statistically significant, *Acta2* and *Il6* mRNA expression were increased in Ctrl TAC mice compared to sham-operated animals; these increases were absent in KO TAC mice (Figure 6.10A,B). Increased expression levels of markers of cardiomyocyte hypertrophy (β-MHC; *Myh7*, ANF; *Nppa*) were observed in Ctrl TAC mice compared to sham-operated animals (Figure 6.10C,D), indicating TAC caused molecular changes at a cellular level suggesting cardiomyocyte hypertrophy. These increases were again lost in KO TAC mice (Figure 6.10C,D). These data imply reduced numbers of myofibroblasts and diminished levels of inflammation and cardiac hypertrophy following TAC in myofibroblast-specific Piezo1 KO mice, compared to Ctrl mice. These data, similarly to the data on cardiac parameters, may signify that myofibroblast Piezo1 plays a detrimental role in cardiac remodelling and, therefore, may be a therapeutic target.

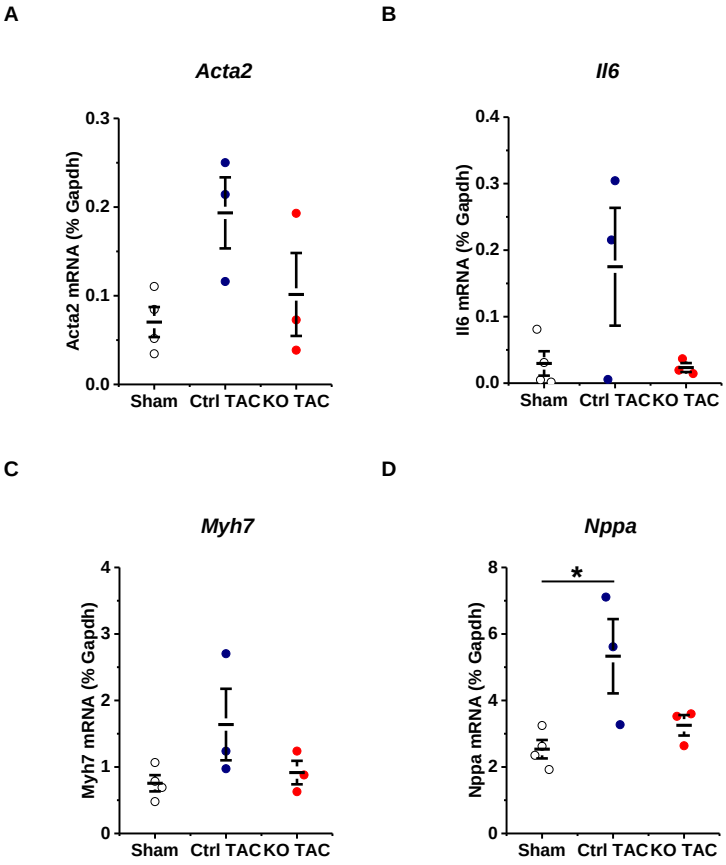

Figure 6.10 Effect of myofibroblast-specific Piezo1 KO on markers of hypertrophy and cardiac dysfunction following TAC-induced cardiac injury. Real-time RT-PCR analysis of cardiac mRNA levels in hearts from sham, control and Piezo1 KO mice 4 weeks after TAC surgery for **(A)** *Acta2*, **(B)** *Il6*, **(C)** *Myh*7 and **(D)** *Nppa*. Individual data and mean ± SEM are shown. Expression is measured as % of housekeeping control, *Gapdh*. Group sizes: sham (n=4), Ctrl TAC (n=3), KO TAC (n=3); all animals were female, *P<0.05 following an ANOVA with Tukey's post-hoc test.

6.5 Discussion

The final aim of this project was to investigate the role of Piezo1 *in vivo* in modulating cardiac remodelling using a mouse model. Two cell-specific KO mouse models were utilised to investigate the role of Piezo1 in cardiac function.

Fibroblast-specific Piezo1 KO

The model used in this study, a tamoxifen-inducible fibroblast-specific KO murine model based on use of a *Cre-lox* system involving *Col1a2* promoter-driven *Cre*(*ERT*), has been frequently used to delete certain genes in fibroblasts prior to investigation into the role of a protein in a specific tissue (Swonger *et al.* 2016). Following tamoxifen injections administered at 3 weeks of age, RT-PCR analysis and Ca^{2+} measurements revealed a 20 % reduction in *Piezo1* mRNA expression and a lessening of 10 % in the Yoda1-evoked Ca^{2+} influx in cultured cardiac fibroblasts from tamoxifen-treated Cre^{+} (Piezo1 KO) mice, compared to those from Cre^{-} (Ctrl) mice. Group sizes were relatively large but these data did not reach statistical significance. The most commonly utilised method for administering tamoxifen is intraperitoneal injection, as performed here, because the amount of administered compound can be more easily controlled (Whitfield, Littlewood and Soucek 2015). However, to assess if the KO was incomplete due to a lack of technical expertise whilst injecting tamoxifen, tamoxifen citrate-containing mouse chow at a treatment dosage of 400 mg/kg (Harlan laboratories) was used as an alternative. Andersson *et al.* (2010) have previously had success using this protocol. Treatment was planned to be given to 5 week-old mice for 2 weeks. Mice were given access to tamoxifen-containing chow and weighed daily; however, mice lost over 10 % body weight within the first few days so had to be culled according to HO project licence guidelines.

Tamoxifen-inducible fibroblast-specific KO models have been previously been developed in our group for a number of genes, including p38α and the IL-1 receptor, IL-1R1 (Bageghni *et al.* 2018; Bageghni *et al.* 2019). It has previously been shown that, using this genetic approach, a 50 % reduction in both *Mapk14* mRNA expression and p38α protein expression could be achieved in cultured cardiac fibroblasts from p38 KO mice, compared to control mice (Bageghni *et al.* 2018). However, Bageghni *et al.* (2019) found that this method was ineffective at diminishing IL1R1 expression in cardiac fibroblasts, despite their previous success with p38α (Bageghni *et al.* 2018). To overcome this, a modified strategy

was adopted to generate a hemizygous mouse line with global deletion of one *Il1r1* allele, with the remaining allele being floxed (Bageghni *et al.* 2019). This is a suitable tactic for targeting genes whose heterozygous ($^{+/-}$) KO does not cause a phenotype (Feil, Valtcheva and Feil 2009). However, as previously discussed, this was not feasible in the case of Piezo1 as the global Piezo1 heterozygous KO mouse has a cardiovascular phenotype (Li *et al.* 2014). Therefore, in comparison with previous data of a similar nature, it was judged that the level of Piezo1 KO achieved in the *Col1a2* promoter-driven *Cre*(*ERT*) mouse was not sufficient to observe functional effects *in vivo*. Thus, a second strategy was adopted using a more potent version of *Cre*.

Myofibroblast-specific Piezo1 KO

There are other benefits to the subsequent model other than a more potent version of *Cre* as, whilst the *Col1a2* promoter-driven model is useful for studying the role of specific fibroblast proteins, it has drawbacks. It targets all fibroblasts (not only those in the heart) and the KO is usually induced at 2-3 weeks of age, long before cardiac remodelling is induced. For therapeutic relevance, the KO should be performed after the injury, but the *Col1a2* promoter is less active in adult mice (Ponticos *et al.* 2004). To avoid these issues, a transgenic mouse line exploiting the periostin (*Postn*) promoter was utilised to direct expression of Cre recombinase exclusively in cardiac myofibroblasts (Kanisicak *et al.* 2016; Meng *et al.* 2018). Periostin is not expressed in the heart under normal physiological conditions but is highly expressed by resident fibroblasts when they adopt a myofibroblast phenotype (Dixon, Landry and Rattan 2019). Therefore, this method provides a highly selective, targeted system enabling the investigation of the specific role of Piezo1 in modulating fibroblast phenotype and cardiac remodelling after injury. *Cre* activation exclusively in cardiac myofibroblasts in the injured heart has been generated following both MI and TAC induction in these mice previously so these were the techniques chosen to evoke myocardial injury (Kanisicak *et al.* 2016; Khalil *et al.* 2017).

Myocardial infarction

Following surgery to induce MI, there was no difference observed between *Postn* and *Piezo1* mRNA expression in Ctrl MI and KO MI mice. It is well established that low reliability and reproducibility are problems in MI models. The coronary anatomy varies in mice, posing challenges for surgical ligation and the result is

inconsistent MI sizes post ligation (Chen *et al.* 2017). Therefore, caution was taken when analysing the data. An ejection fraction of 62 % in sham animals was reduced to 41 % in Ctrl MI animals. It must be kept in mind that a small number of replicates in the control group make the results difficult to interpret but these data were in keeping with previous studies which utilised LAD coronary artery ligation to induce MI and suggested a heart failure phenotype (Bageghni *et al.* 2018). However, the other cardiac parameters measured were unaffected by surgery to induce MI. This was in agreement with RT-PCR analysis which showed that there were no significant increases in any of the remodelling genes investigated following MI induction, in comparison with sham animals. Increases in all of the genes studied have previously been shown to be increased following LAD coronary artery ligation (Bageghni *et al.* 2019). Therefore, as this model could not be validated by an increase in *Postn* mRNA expression in MI animals and a subsequent decrease in *Piezo1* mRNA expression in KO MI animals, the role of myofibroblast Piezo1 could not be evaluated using this model. It is worth noting for any future work that a permanent LAD ligation model of MI was utilised in the present study; investigations with an ischemia-reperfusion model of MI more closely resembles the clinical scenario in which the majority of patients undergo revascularisation (van Zuylen *et al.* 2015). However, the permanent ligation model is useful for understanding direct mechanisms without the confounding element of reperfusion.

Thoracic aortic constriction

The average expression of *Postn* mRNA was tripled in TAC-operated mice, compared to mice which underwent a sham procedure, indicating that cardiac injury had been induced in these animals. *Piezo1* mRNA expression in control and experimental mice following TAC was not statistically significantly different, presumably due to variation and the low number of replicates. However, all values for *Piezo1* mRNA expression in the KO animals were reduced compared to Ctrl animals, hinting that the induction of cardiac injury by performing TAC, followed by tamoxifen administration generated a deletion of Piezo1. Mice which underwent TAC displayed reduced cardiac function, as shown by an ejection fraction which was reduced by almost half and a doubling in end diastolic pressure. There was no difference observed in the ratios between HW/TL or HW/BW between sham-operated and TAC-operated mice, indicating that the

cardiac dysfunction had not yet manifested into overt hypertrophy. However, increased expression levels of markers of cardiomyocyte hypertrophy (β-MHC; *Myh7*, ANF; *Nppa*) were observed in Ctrl TAC mice compared to sham-operated animals. Piezo1 deletion in mice resulted in a loss of the TAC-induced increase in end diastolic pressure and increased expression of markers of hypertrophy observed in Ctrl TAC mice. This may signify that a deletion in myofibroblast Piezo1 is beneficial in cardiac remodelling following pressure overload and, therefore, the ion channel may be a therapeutic target.

The most promising data for inducing cardiac injury and observing a KO of Piezo1 was performing TAC on mice. This is a more apt method to use to study the mechanosensitive ion channel, Piezo1, due to TAC inducing pressure overload, rather than MI. This study has provided preliminary data on the role of Piezo1 in cardiac function. Data suggest that a lack of Piezo1 may be beneficial in pressure overload-induced cardiac remodelling. However, a limitation is the numbers of animals used; larger data sets are essential in order to deduce more accurate conclusions. Future work would include studying specific features of remodelling using histological staining to strengthen the conclusions drawn here. It is also important to consider that transgene integration of *Cre* can cause unanticipated side effects. *Cre* toxicity can occur when expression is high or when *Cre* recognises genomic sequences resembling *loxP* sites; *Cre* has also been shown to cause damage to DNA in the absence of a floxed sequence (Loonstra *et al.* 2001). Cardiomyocyte-specific *Cre* mice have displayed molecular signs of cardiac toxicity by 3 months of age and exhibit decreased cardiac function by 6 months of age compared to WT littermates (Pugach *et al.* 2015). This highlights the importance of using *Cre* mice as controls in conditional KO studies.

In summary, the lack of Piezo1 KO in experimental animals, compared to control animals following the induction of MI and the very low number of replicates in the control group made it difficult to ascertain the impact of myofibroblast-specific Piezo1 deletion using this model. However, following TAC-induced pressure overload, a KO of Piezo1 appeared to be achieved. The induction of TAC caused cardiac dysfunction and, in terms of the effect of Piezo1 KO, there was a significant difference in end diastolic pressure between control and Piezo1 KO mice; the increase in end diastolic pressure observed in control mice following TAC was reduced in Piezo1 KO mice to levels observed in sham-operated

animals. There were trends for and significant increases in *Acta2*, *Il6*, *Myh7* and *Nppa* mRNA expression in Ctrl TAC mice compared to sham-operated animals; these changes were also absent in KO TAC mice. These data indicate that cardiac fibroblast Piezo1 has a detrimental effect in cardiac hypertrophy and that its deletion may be beneficial under these conditions. However, care must be taken when interpreting the data due to the small number of replicates. Further work would be essential in order to draw more accurate conclusions.

Chapter 7 Final discussion, future directions and conclusion

7.1 Summary of results

Using a combination of mouse and human cardiac fibroblasts cultured *in vitro*, it has been demonstrated that:

Chapter 3

- Cardiac fibroblasts express Piezo1 mRNA and protein
- Yoda1, the chemical activator of Piezo1, rapidly and potently activates Ca^{2+} entry
- Dooku1, a Yoda1 analogue, can inhibit Yoda1-evoked Ca^{2+} in both Piezo1-overpressing cells and cardiac fibroblasts
- Acute pharmacological inhibition, genetically modified mouse models and siRNA knockdown of *Piezo1* mRNA expression verifies that Yoda1-mediated Ca^{2+} entry occurs via activation of endogenous Piezo1
- Mechanical force applied using cell-attached patch clamp electrophysiology activates Piezo1 channels

Chapter 4

- Yoda1-mediated activation of Piezo1 alters the expression of genes associated with cardiac remodelling
- Yoda1 increases *Il6* and *Tnc* mRNA expression in a Piezo1-dependent manner; an inactive analogue of Yoda1, 2e, has no effect
- Activation of Piezo1 stimulates IL-6 secretion
- Piezo1 is important for basal levels of *IL6* mRNA expression; this is dependent on substrate stiffness or composition

Chapter 5

- Yoda1 triggers MAPK signalling
- Piezo1 activation induces the concentration-dependent phosphorylation of p38 MAPK and ERK1/2 after 10 min of treatment; 2e has no effect
- Compound 159, an analogue with better ADME properties then Yoda1, evokes similar levels of p38α MAPK and ERK1/2 phosphorylation

- Yoda1-mediated p38α MAPK and ERK1/2 phosphorylation is dependent upon extracellular Ca^{2+}
- P38 MAPK, rather than ERK1/2, is responsible for Yoda1-evoked IL-6 expression and secretion
- SFKs are also activated by Yoda1 and this precedes p38 MAPK phosphorylation; of the SFKs, Fyn, Src and Yes kinases are expressed

Chapter 6

Genetic manipulation using *Cre-loxP* technology to generate Piezo1 KO mice and experimental models of cardiac injury revealed:

- A myofibroblast-specific Piezo1 KO mouse model could be successfully generated
- TAC is effective at inducing pressure overload and cardiac dysfunction in mice
- TAC, followed by tamoxifen administration, induces a deletion of myofibroblast Piezo1
- A deletion of myofibroblast Piezo1 may be beneficial in pressure overload-induced cardiac dysfunction

7.2 Final discussion

Prior to this study, there was a lack of knowledge on Piezo1 in cardiac fibroblasts, despite confirmation that *Piezo1* mRNA is expressed in the murine heart (Coste *et al.* 2010) and that cardiac fibroblasts express other mechanically-activated ion channels (Yue, Xie and Nattel 2011). In the present study, it was established for the first time that *Piezo1* mRNA is expressed in cardiac fibroblasts. *Piezo1* mRNA expression was higher than the expression of its family member, *Piezo2*, and higher in cardiac fibroblasts than in cardiomyocytes. Piezo1 protein could also be detected in cardiac fibroblasts; this protein formed a Ca^{2+}-permeable channel which could be activated by a chemical agonist of Piezo1, Yoda1, and mechanical stimuli. Piezo1 could be activated by pressure induced by cell-attached patch clamp electrophysiology but not by hypotonic stress in cardiac fibroblasts, indicating that activation of the channel is dependent on the type of mechanical stimuli.

Following cardiac injury, cardiac fibroblasts secrete ECM proteins and cytokines, which contribute to healing and cardiac remodelling (Humeres and Frangogiannis 2019). Piezo1 activation using Yoda1 induced the expression of two key cardiac remodelling genes, TNC and IL-6, which are both upregulated following cardiac injury (Imanaka-Yoshida *et al.* 2001; Nian *et al.* 2004). Both proteins are initially cardioprotective after insult but subsequently promote adverse cardiac remodelling and become detrimental (Midwood *et al.* 2011; Fontes, Rose and Čiháková 2015). This implies that reduced Piezo1 activity may be beneficial post-cardiac injury. This links to a study by Bae, Sachs and Gottlieb (2015) which demonstrated that low pH, as observed in pathological conditions such as ischemia, can stabilise the inactivated state of Piezo1; this may be an attempt by the body to attenuate unfavourable Piezo1 activity when necessary.

The mechanism for Piezo1-mediated IL-6 secretion was uncovered in this study. It was verified that Ca^{2+} influx through the activated Piezo1 channel led to activation of SFKs, which preceded the activation of p38 MAPK and culminated in the secretion of IL-6. Extensive data have demonstrated a critical role of inflammation in the fibrotic response. Persistently elevated IL-6 levels lead to chronic inflammation; this is associated with hypertrophy, fibrosis and ultimately heart failure (Fontes, Rose and Čiháková 2015). Notably, Piezo1 has recently been identified to initiate an inflammatory response in myeloid cells by sensing cyclical hydrostatic pressure (Solis *et al.* 2019).

The gene expression data correlates with the preliminary data gathered on the role of Piezo1 *in vivo* following cardiac injury using a novel myofibroblast-specific Piezo1 KO murine model. These data hinted that a lack of myofibroblast Piezo1 may be beneficial in pressure overload-induced cardiac remodelling, as mice with a deletion of myofibroblast Piezo1 had improved end diastolic pressure and reduced inflammation and cardiac hypertrophy following TAC-induced cardiac dysfunction, compared to control mice. Other studies have suggested that inhibiting Piezo1 may be beneficial in disease states. Mechanical strain leads to Piezo1-mediated Ca^{2+} influx in chondrocytes and inhibition of the channel protects articular chondrocytes from mechanically induced cell death, which may be relevant in arthritis following traumatic joint injury (Lee *et al.* 2014). In addition, blockade of Piezo1 channels and deletion of pancreatic acinar cell Piezo1 has been demonstrated to protect mice from pressure-induced pancreatitis, this is

due to the inhibition of the excessive cytoplasmic calcium signals (Romac *et al.* 2018).

The present study has revealed that Ca^{2+} signals through Piezo1 are important for inducing IL-6 expression and secretion through a novel signalling pathway in cardiac fibroblasts. Early studies indicate that this inflammatory signal may be important in pressure overload-induced cardiac remodelling. It is conceivable that, within the context of cardiac pathophysiology, dampening Piezo1 activity could offer a novel target in the search for therapeutic interventions for cardiac hypertrophy and fibrosis, and therefore, heart failure.

7.3 Clinical relevance

The British Heart Foundation state that, in the UK today, over 7 million people are living with cardiovascular disease and this is the cause of a quarter of all deaths (www.bhf.org.uk). Half a million people in the UK have been officially diagnosed with the devastating disorder that is heart failure; a rise in cardiovascular risk factors, improved survival from ischaemic heart disease and population ageing have contributed to a sustained increase in prevalence (Taylor *et al.* 2019). Current treatment options for heart failure patients include angiotensin-converting enzyme (ACE) inhibitors, angiotensin receptor blockers (ARBs), beta blockers, mineralocorticoid receptor antagonists and diuretics. Cardiac fibrosis is a hallmark of the majority of cardiac pathologies, therefore anti-fibrotic strategies are acknowledged as hopeful approaches in the treatment of cardiac dysfunction. While not approved for the treatment of cardiac fibrosis specifically, several of these therapeutic agents, including ACE inhibitors and ARBs, have been revealed to exert pleiotropic effects on fibroblasts that underlie some of their potential benefits in cardiac fibrosis (Porter and Turner 2009; Yue *et al.* 2013). This implies that improved therapeutics for cardiac fibrosis are imperative in the treatment of heart failure.

As the preliminary *in vivo* data in this study hints that a lack of myofibroblast Piezo1 may be beneficial following pressure overload-induced cardiac injury, it would be useful to assess whether a Piezo1 blocker had a comparable effect. Unfortunately current inhibitors of Piezo1 are non-specific inhibitors of many mechanosensitive ion channels (Coste *et al.* 2010) but screening of small

molecules, as described in Chapter 3, is currently ongoing, with the aim of discovering a more specific antagonist of Piezo1. It would be essential to ensure a potential therapeutic drug had good ADME properties (e.g. solubility, half-life and clearance rate) and would need to be utilised successfully *in vivo* first.

However, due to Piezo1 being expressed in a diverse number of tissues, having many different roles and being activated my numerous types of mechanical stimuli (Coste *et al.* 2010), an attempt to target the ion channel therapeutically may present difficulties. It would require drugs to act in a tissue-specific manner. It has been established that global or endothelial-specific deletion of mouse Piezo1 profoundly disturbs the developing vasculature and is embryonic lethal within days of the heart beating (Li *et al.* 2014). Targeting Piezo1 later in life may have a less disastrous effect as adult mice are able to survive following conditional disruption of Piezo1 in the endothelium but were established to display disadvantageous effects in the cardiovascular system, in terms of their physical performance (Rode *et al.* 2017). It would need to be carefully considered when was the optimum time to target Piezo1. As previously discussed, both loss- and gain-of-function mutations in Piezo1 have been attributed to diseases in humans (Martin-Almedina, Mansour and Ostergaard 2018) which implies that tight regulation of Piezo1 is vital. It may be necessary to modulate the gating rather than completely inhibit the channel; this may become more realistic with the current increase in knowledge surrounding residues important for Piezo1 gating (Zheng, Gracheva and Bagriantsev 2019). In order to entirely comprehend conformational changes associated with Piezo1 activation, it will be critical to capture Piezo1 and Piezo2 structures in activated and inactivated states.

7.4 Future work

7.4.1 Is substrate stiffness and/or composition important for Yoda1-mediated IL-6 levels?

Piezo1-specific siRNA was established to reduce basal levels of IL-6 mRNA expression and secretion. This appeared to be dependent on the mechanical and/or chemical environment which the cells are grown on as Piezo1-specific siRNA had an effect on basal levels of IL-6 only when cardiac fibroblasts were

plated on collagen-coated silicon membranes (930 kPa); there was no effect when cells were plated on tissue culture plastic (10^6 kPa) or on very soft fibronectin-coated membranes (10/30 kPa). As previously discussed, substrate compliance has been demonstrated to modulate Ca^{2+} signalling in fibroblasts (Godbout *et al.* 2013; Lembong *et al.* 2015). To confirm these findings, it could be investigated whether pressure-induced ionic currents or Yoda1-induced Ca^{2+} oscillations were reduced when cardiac fibroblasts were cultured on soft hydrogels, compared to on stiffer substrates by patch clamp recording and single cell imaging, respectively, or whether altering the coating of the membranes had an impact. This could be executed using control and Piezo1-specific siRNA to confirm that it is the nature of the substrate which is important for the magnitude of Ca^{2+} entry through Piezo1.

7.4.2 What is the mechanism responsible for the effect of Yoda1 on myofibroblast phenotype?

It appears that the effects of Yoda1 on cardiac fibroblast differentiation are non-specific. However, it is possible that the outcome observed here is due to incomplete knockdown of Piezo1 not being sufficient to abolish the response. Future work could involve using cardiac fibroblasts with a complete KO of Piezo1 to verify this, e.g. in cells isolated from the myofibroblast-specific Piezo1 KO mouse. In this study, it was hinted at that the ERK pathway may be involved in the Yoda1-mediated increase in collagen gel contraction. The ERK pathway has previously been demonstrated to be involved in TGF-β1-stimulated fibroblast to myofibroblast differentiation (Midgley *et al.* 2013).

7.4.3 What is the mechanism leading to Yoda1-evoked TNC expression?

This study demonstrated that Yoda1-evoked Piezo1 activation upregulated TNC expression in both mouse and human cardiac fibroblasts. It is believed that the mechanism responsible for this is not similar to that for Yoda1-induced IL-6 secretion as a p38 inhibitor had no effect on Yoda1-induced TNC expression (data not shown). However, it was not explored whether Yoda1-mediated TNC

expression was affected by the other pharmacological inhibitors used in this thesis. Correlating with data obtained in this study, antagonists of the ERK and p38 MAPK pathways had no effect on cyclic strain-induced tenascin-C induction in chick embryo fibroblasts (Chiquet, Sarasa-Renedo and Tunç-Civelek 2004). However, a specific inhibitor of Rho-dependent kinase strongly attenuated this response, indicating that the regulation of TNC in fibroblasts by cyclic strain requires Rho/ROCK signalling (Chiquet, Sarasa-Renedo and Tunç-Civelek 2004). Future work could be to use alternative inhibitors, including Y-27632, a highly potent and selective ROCK inhibitor, to ascertain the molecular mechanisms occurring which lead to this change in TNC expression.

7.4.4 Which specific Src-family kinases are activated by Piezo1 activation and are important for p38 signalling and altered gene expression?

PamChip multiplex tyrosine kinase activity profiling in mouse cardiac fibroblasts revealed that Piezo1 activation induced the activation of multiple SFKs. Follow-up expression studies revealed that human cardiac fibroblasts express Src, Fyn and Yes kinases, but none of the other family members. Further work would involve investigating specifically which of the kinases are activated by Yoda1. To do this, cardiac fibroblasts would be treated with Yoda1 and then activated SFKs would be immunoprecipitated using a phospho-Src family antibody, followed by western blot with expression antibodies for Src, Fyn and Yes. The role of Piezo1 could be confirmed using cells transfected with Piezo1-specific or control siRNA and similar experiments could be undertaken using cyclical stretch (Flexcell, 10% strain, 1 Hz) to compare SFK activation in response to chemical and mechanical stimulation of Piezo1, in addition to in response to being plated on altered ECM substrates. It is currently unknown which specific family members are responsible for Yoda1-induced p38 activation and IL-6 expression. To determine this, siRNA gene silencing could be used to knockdown the individual kinases. IL-6 mRNA expression (qRT-PCR) and protein secretion (ELISA) would be analysed in Src/Fyn/Yes-silenced cells to see which member was responsible.

7.4.5 Do Src-family kinases bind to Piezo1?

One limitation of studying Piezo1 at the protein level is the lack of an antibody able to specifically and strongly detect endogenous Piezo1. BEEC4 was developed for the lab by Cambridge Bioscience but is restricted to detecting overexpressed Piezo1 by western blotting; no endogenous Piezo1 band could be detected in murine cardiac fibroblasts (data not shown). The generation of Piezo1-HA mice, using CRISPR technology, has been used in this thesis to confirm that endogenous Piezo1 is expressed in murine cardiac fibroblasts using an anti-HA antibody and western blotting. The development of these mice facilitates further experiments. Piezo1-HA immunoprecipitation experiments could be performed to allow investigation into endogenous Piezo1 interactions, such as whether SFK directly interact with the Piezo1 channel following activation using Yoda1. The influence of chemical or mechanical Piezo1 activation (Yoda1 or cell-stretching respectively) and the influence of the ECM substrate on Piezo1/SFK interactions could also be investigated.

7.4.6 What is the functional role of Piezo1 in cardiac fibroblasts?

Cardiac fibroblasts undergo increased proliferation and migration post cardiac injury (Porter and Turner 2009) and Piezo1 has been demonstrated to have a role in these functions in other cell types (McHugh *et al.* 2012; Gudipaty *et al.* 2017). In addition to assessing myofibroblast differentiation using the collagen gel contraction assay, proliferation could be assessed using the IncuCyte-FLR live cell imaging system and migration using the scratch wound or Boyden chamber assays (Riches *et al.* 2009). Utilising control and Piezo1-specific siRNA would aid in elucidating if Piezo1 has a role in important cardiac fibroblast functions. Yoda1 could also be used to treat cells to see if activating the Piezo1 channel had any effect on these cell functions. The suggestions for future work are illustrated in Figure 7.1.

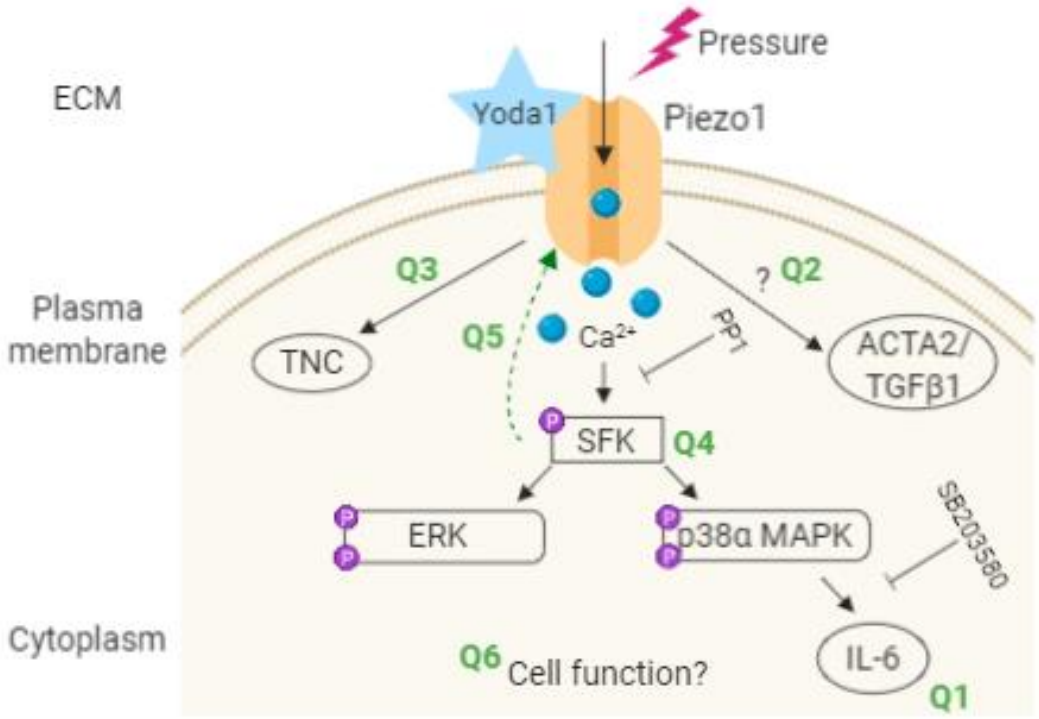

Figure 7.1 Schematic of the proposed mechanism linking Yoda1-mediated Piezo1 activation to IL-6 secretion in cardiac fibroblasts, with proposed questions for future *in vitro* study. Q1 - Is substrate stiffness and/or composition important for Yoda1-mediated IL-6 levels? **Q2** - What is the mechanism responsible for the effect of Yoda1 on myofibroblast phenotype? **Q3** - What is the mechanism leading to Yoda1-evoked TNC expression? **Q4** - Which specific Src-family kinases are activated by Piezo1 activation and are important for p38 signalling and altered gene expression? **Q5** - Do Src-family kinases bind to Piezo1? **Q6** - What is the functional role of Piezo1 in cardiac fibroblasts?

7.4.7 Further investigation into the role of Piezo1 *in vivo*

Preliminary data were gathered on the role of Piezo1 following myocardial injury using a novel myofibroblast-specific Piezo1 KO murine model; it was implied that a lack of myofibroblast Piezo1 may be beneficial following pressure overload-induced cardiac injury. Further work to add replicates to these data sets would allow more accurate conclusions to be drawn. It would also be necessary to confirm that the deletion of Piezo1 was confined to the myofibroblast population, with no effect on other cell types; this could be done using the MACS magnetic antibody cell separation approach, as utilised earlier in this thesis. In addition to

investigating gene expression of markers of hypertrophy, it would be useful to examine histological sections for fibrosis, cardiomyocyte hypertrophy and the accumulation of inflammatory cells and myofibroblasts. Doppler echocardiography could also be utilised to assess myocardial function (e.g. ejection fraction, fractional shortening, ventricle wall thickness) every fortnight following cardiac injury to evaluate the progression to heart failure. It would be appealing to induce hypertrophy and cardiac fibrosis using an alternative method, to investigate whether there are similarities with the TAC data. Systemic infusion of the β-adrenergic agonist, isoproterenol, is known to promote overt hypertrophy (Murray, Prabhu and Chandrasekar 2000; Jaffré *et al.* 2009). Mini-osmotic pumps could be implanted in mice subcutaneously and either saline or isoproterenol infused for 2 weeks, before the assessment of cardiac function (Bageghni *et al.* 2018).

7.5 Conclusion

Modulation of Piezo1 channel activity is implicated in a growing number of human diseases, including cardiovascular disease. The overall aim of this study was to gain an understanding of the role of Piezo1 in cardiac fibroblasts. Investigation revealed expression of Piezo1 in mouse and human cardiac fibroblasts and it was demonstrated that the channel could be activated using chemical and mechanical stimuli. Activation of Piezo1 using its agonist, Yoda1, led to changes in the expression of key cardiac remodelling genes, including TNC and IL-6. IL-6 is a cytokine with considerable importance in cardiac hypertrophy and fibrosis. Exploration into the mechanism by which Yoda1 induces IL-6 secretion revealed a downstream pathway linking Ca^{2+} entry through the Piezo1 channel and activation of both SFK and p38 MAPK to IL-6 secretion. It was also demonstrated that Piezo1 was a regulator of basal levels of IL-6; this was dependent on the surrounding mechanical and chemical environment. *In vivo* investigation into the role of Piezo1 revealed that the protein may have a role in pressure overload-induced cardiac dysfunction but more exploration is warranted to confirm the role of Piezo1 in cardiac remodelling. These novel findings may improve understanding of how cardiac fibroblasts sense mechanical stimuli in order to affect cell signalling and function and modulate cardiac structure and function.

List of References

ABRAHAM, D. M., T. E. LEE, L. J. WATSON, L. MAO, G. CHANDOK, H.-G. WANG, S. FRANGAKIS, G. S. PITT, S. H. SHAH, M. J. WOLF and H. A. ROCKMAN. 2018. The Two-Pore Domain Potassium Channel TREK-1 Mediates Cardiac Fibrosis and Diastolic Dysfunction. *The Journal of Clinical Investigation,* **128**(11), pp.4843-4855.

ADAPALA, R. K., R. J. THOPPIL, D. J. LUTHER, S. PARUCHURI, J. G. MESZAROS, W. M. CHILIAN and C. K. THODETI. 2013. TRPV4 Channels Mediate Cardiac Fibroblast Differentiation by Integrating Mechanical and Soluble Signals. *Journal of Molecular and Cellular Cardiology,* **54**, pp.45-52.

AIKAWA, R., T. NAGAI, S. KUDOH, Y. ZOU, M. TANAKA, M. TAMURA, H. AKAZAWA, H. TAKANO, R. NAGAI and I. KOMURO. 2002. Integrins Play a Critical Role in Mechanical Stress-Induced p38 MAPK Activation. *Hypertension,* **39**(2), pp.233-238.

ALBERTS, J. A., LEWIS J., RAFF M., ROBERTS K., WALTER P. 2002. Ion Channels and the Electrical Properties of Membranes*. Molecular Biology of the Cell*. 4th ed. Garland Science.

ALBUISSON, J., S. E. MURTHY, M. BANDELL, B. COSTE, H. LOUIS-DIT-PICARD, J. MATHUR, M. FÉNÉANT-THIBAULT, G. TERTIAN, J.-P. DE JAUREGUIBERRY, P.-Y. SYFUSS, S. CAHALAN, L. GARÇON, F. TOUTAIN, P. SIMON ROHRLICH, J. DELAUNAY, V. PICARD, X. JEUNEMAITRE and A. PATAPOUTIAN. 2013. Dehydrated Hereditary Stomatocytosis Linked to Gain-of-Function Mutations in Mechanically Activated PIEZO1 Ion Channels. *Nature Communications,* **4**, pp.1884-1884.

AMATA, I., M. MAFFEI and M. PONS. 2014. Phosphorylation of Unique Domains of Src Family Kinases. *Frontiers in Genetics,* **5**, pp.181-181.

ANCEY, C., E. MENET, P. CORBI, S. FREDJ, M. GARCIA, C. RÜCKER-MARTIN, J. BESCOND, F. MOREL, J. WIJDENES, J.-C. LECRON and D. POTREAU. 2003. Human Cardiomyocyte Hypertrophy Induced In Vitro by Gp130 Stimulation. *Cardiovascular Research,* **59**(1), pp.78-85.

ANDERSSON, K. B., L. H. WINER, H. K. MØRK, J. D. MOLKENTIN and F. JAISSER. 2010. Tamoxifen Administration Routes and Dosage for Inducible Cre-Mediated Gene Disruption in Mouse Hearts. *Transgenic Research,* **19**(4), pp.715-725.

ANDOLFO, I., S. L. ALPER, L. DE FRANCESCHI, C. AURIEMMA, R. RUSSO, L. DE FALCO, F. VALLEFUOCO, M. R. ESPOSITO, D. H. VANDORPE, B. E. SHMUKLER, R. NARAYAN, D. MONTANARO, M. D'ARMIENTO, A. VETRO, I. LIMONGELLI, O. ZUFFARDI, B. E. GLADER, S. L. SCHRIER, C. BRUGNARA, G. W. STEWART, J. DELAUNAY and A. IOLASCON. 2013. Multiple Clinical Forms of Dehydrated Hereditary Stomatocytosis Arise from Mutations in PIEZO1. *Blood,* **121**(19), p3925.

ANGUITA, E. and A. VILLALOBO. 2017. Src-family Tyrosine Kinases and the Ca2+ Signal. *Biochimica et Biophysica Acta (BBA) - Molecular Cell Research,* **1864**(6), pp.915-932.

BAE, C., R. GNANASAMBANDAM, C. NICOLAI, F. SACHS and P. A. GOTTLIEB. 2013. Xerocytosis is Caused by Mutations That Alter the Kinetics of the Mechanosensitive Channel PIEZO1. *Proceedings of the National Academy of Sciences,* **110**(12), pp.E1162-E1168.

BAE, C., F. SACHS and P. A. GOTTLIEB. 2011. The Mechanosensitive Ion Channel Piezo1 is Inhibited by the Peptide GsMTx4. *Biochemistry,* **50**(29), pp.6295-6300.

BAE, C., F. SACHS and P. A. GOTTLIEB. 2015. Protonation of the Human PIEZO1 Ion Channel Stabilizes Inactivation. *The Journal of Biological Chemistry,* **290**(8), pp.5167-5173.

BAGEGHNI, S. A., K. E. HEMMINGS, N. Y. YULDASHEVA, A. MAQBOOL, F. O. GAMBOA-ESTEVES, N. E. HUMPHREYS, M. S. JACKSON, C. P. DENTON, S. FRANCIS, K. E. PORTER, J. F. X. AINSCOUGH, E. PINTEAUX, M. J. DRINKHILL and N. A. TURNER. 2019. Fibroblast-Specific Deletion of IL-1 Receptor-1 Reduces Adverse Cardiac Remodeling Following Myocardial Infarction. *JCI Insight,* **4**(17).

BAGEGHNI, S. A., K. E. HEMMINGS, N. ZAVA, C. P. DENTON, K. E. PORTER, J. F. X. AINSCOUGH, M. J. DRINKHILL and N. A. TURNER. 2018. Cardiac Fibroblast-specific p38α MAP Kinase Promotes Cardiac Hypertrophy via a Putative Paracrine Interleukin-6 Signaling Mechanism. *The FASEB Journal,* **32**(9), pp.4941-4954.

BAIN, J., L. PLATER, M. ELLIOTT, N. SHPIRO, C. J. HASTIE, H. MCLAUCHLAN, I. KLEVERNIC, J. S. C. ARTHUR, D. R. ALESSI and P. COHEN. 2007. The Selectivity of Protein Kinase Inhibitors: a Further Update. *The Biochemical Journal,* **408**(3), pp.297-315.

BANERJEE, I., J. W. FUSELER, A. R. INTWALA and T. A. BAUDINO. 2009. IL-6 Loss Causes Ventricular Dysfunction, Fibrosis, Reduced Capillary Density, and Dramatically Alters the Cell Populations of the Developing and Adult Heart. *American Journal of Physiology-Heart and Circulatory Physiology,* **296**(5), pp.H1694-H1704.

BANERJEE, I., J. W. FUSELER, R. L. PRICE, T. K. BORG and T. A. BAUDINO. 2007. Determination of Cell Types and Numbers During Cardiac Development in the Neonatal and Adult Rat and Mouse. *American Journal of Physiology-Heart and Circulatory Physiology,* **293**(3), pp.H1883-H1891.

BARTON, P. J. R., E. J. BIRKS, L. E. FELKIN, M. E. CULLEN, M. U. KOBAN and M. H. YACOUB. 2003. Increased Expression of Extracellular Matrix Regulators TIMP1 and MMP1 in Deteriorating Heart Failure. *The Journal of Heart and Lung Transplantation,* **22**(7), pp.738-744.

BAUER, C. C., J. P. BOYLE, K. E. PORTER and C. PEERS. 2010. Modulation of Ca2+ Signalling in Human Vascular Endothelial Cells by Hydrogen Sulfide. *Atherosclerosis,* **209**(2), pp.374-380.

BAUM, J. and H. S. DUFFY. 2011. Fibroblasts and Myofibroblasts: What are we Talking About? *Journal of Cardiovascular Pharmacology,* **57**(4), pp.376-379.

BELLIN, R. M., J. D. KUBICEK, M. J. FRIGAULT, A. J. KAMIEN, R. L. STEWARD, H. M. BARNES, M. B. DIGIACOMO, L. J. DUNCAN, C. K. EDGERLY, E. M. MORSE, C. Y. PARK, J. J. FREDBERG, C.-M. CHENG and P. R. LEDUC. 2009. Defining the Role of Syndecan-4 in Mechanotransduction Using Surface-Modification Approaches. *Proceedings of the National Academy of Sciences,* **106**(52), pp.22102-22107.

BENAMER, N., C. VASQUEZ, V. M. MAHONEY, M. J. STEINHARDT, W. A. COETZEE and G. E. MORLEY. 2013. Fibroblast KATP Currents Modulate Myocyte Electrophysiology in Infarcted Hearts. *American Journal of Physiology-Heart and Circulatory Physiology,* **304**(9), pp.H1231-H1239.

BERRIDGE, M. J., P. LIPP and M. D. BOOTMAN. 2000. The Versatility and Universality of Calcium Signalling. *Nature Reviews Molecular Cell Biology,* **1**(1), pp.11-21.

BERRY, M. F., A. J. ENGLER, Y. J. WOO, T. J. PIROLLI, L. T. BISH, V. JAYASANKAR, K. J. MORINE, T. J. GARDNER, D. E. DISCHER and H. L. SWEENEY. 2006. Mesenchymal Stem Cell Injection after Myocardial Infarction Improves Myocardial Compliance. *American Journal of Physiology-Heart and Circulatory Physiology,* **290**(6), pp.H2196-H2203.

BERS, D. M., D. A. EISNER and H. H. VALDIVIA. 2003. Sarcoplasmic Reticulum Ca2+ and Heart Failure. *Circulation Research,* **93**(6), pp.487-490.

BERS, D. M. and T. GUO. 2005. Calcium Signaling in Cardiac Ventricular Myocytes. *Annals of the New York Academy of Sciences,* **1047**(1), pp.86-98.

BEVILACQUA, A., M. C. CERIANI, S. CAPACCIOLI and A. NICOLIN. 2003. Post-transcriptional Regulation of Gene Expression by Degradation of Messenger RNAs. *Journal of Cellular Physiology,* **195**(3), pp.356-372.

BEYDER, A., J. L. RAE, C. BERNARD, P. R. STREGE, F. SACHS and G. FARRUGIA. 2010. Mechanosensitivity of Nav1.5, a Voltage-Sensitive Sodium Channel. *The Journal of Physiology,* **588**(Pt 24), pp.4969-4985.

BIERNACKA, A. and N. G. FRANGOGIANNIS. 2011. Aging and Cardiac Fibrosis. *Aging and Disease,* **2**(2), pp.158-173.

BJORGE, J. D., A. JAKYMIW and D. J. FUJITA. 2000. Selected Glimpses into the Activation and Function of Src Kinase. *Oncogene,* **19**(49), pp.5620-5635.

BLANKENBERG, S., H. J. RUPPRECHT, O. POIRIER, C. BICKEL, M. SMIEJA, G. HAFNER, J. MEYER, F. CAMBIEN and L. TIRET. 2003. Plasma Concentrations and Genetic Variation of Matrix Metalloproteinase 9 and Prognosis of Patients With Cardiovascular Disease. *Circulation,* **107**(12), pp.1579-1585.

BOGOYEVITCH, M. A., P. E. GLENNON, M. B. ANDERSSON, A. CLERK, A. LAZOU, C. J. MARSHALL, P. J. PARKER and P. H. SUGDEN. 1994. Endothelin-1 and Fibroblast Growth Factors Stimulate the Mitogen-Activated Protein Kinase Signaling Cascade in Cardiac Myocytes. The Potential Role of the Cascade in the Integration of Two Signaling Pathways Leading to Myocyte Hypertrophy. *Journal of Biological Chemistry,* **269**(2), pp.1110-9.

BOMBELI, T., A. KARSAN, J. F. TAIT and J. M. HARLAN. 1997. Apoptotic Vascular Endothelial Cells Become Procoagulant. *Blood,* **89**(7), pp.2429-2442.

BORDER, W. A. and N. A. NOBLE. 1994. Transforming Growth Factor β in Tissue Fibrosis. *New England Journal of Medicine,* **331**(19), pp.1286-1292.

BOURON, A., K. KISELYOV and J. OBERWINKLER. 2015. Permeation, Regulation and Control of Expression of TRP Channels by Trace Metal Ions. *Pflugers Archiv : European Journal of Physiology,* **467**(6), pp.1143-1164.

BOYMAN, L., G. S. B. WILLIAMS, D. KHANANSHVILI, I. SEKLER and W. J. LEDERER. 2013. NCLX: the Mitochondrial Sodium Calcium Exchanger. *Journal of Molecular and Cellular Cardiology,* **59**, pp.205-213.

BUJAK, M. and N. G. FRANGOGIANNIS. 2007. The Role of TGF-β Signaling in Myocardial Infarction and Cardiac Remodeling. *Cardiovascular Research,* **74**(2), pp.184-195.

BURSAC, N. 2014. Cardiac Fibroblasts in Pressure Overload Hypertrophy: the Enemy Within? *The Journal of Clinical Investigation,* **124**(7), pp.2850-2853.

CAHALAN, S. M., V. LUKACS, S. S. RANADE, S. CHIEN, M. BANDELL and A. PATAPOUTIAN. 2015. Piezo1 Links Mechanical Forces to Red Blood Cell Volume. *ELife,* **4**, pe07370.

CAI, C.-L., J. C. MARTIN, Y. SUN, L. CUI, L. WANG, K. OUYANG, L. YANG, L. BU, X. LIANG, X. ZHANG, W. B. STALLCUP, C. P. DENTON, A. MCCULLOCH, J. CHEN and S. M. EVANS. 2008. A Myocardial Lineage Derives from Tbx18 Epicardial Cells. *Nature,* **454**(7200), pp.104-108.

CAMELLITI, P., T. K. BORG and P. KOHL. 2005. Structural and Functional Characterisation of Cardiac Fibroblasts. *Cardiovascular Research,* **65**(1), pp.40-51.

CARTLEDGE, J. E., C. KANE, P. DIAS, M. TESFOM, L. CLARKE, B. MCKEE, S. AL AYOUBI, A. CHESTER, M. H. YACOUB, P. CAMELLITI and C. M. TERRACCIANO. 2015. Functional Crosstalk Between Cardiac Fibroblasts and Adult Cardiomyocytes by Soluble Mediators. *Cardiovascular Research,* **105**(3), pp.260-270.

CARTWRIGHT, E. J., D. OCEANDY, C. AUSTIN and L. NEYSES. 2011. Ca2+ Signalling in Cardiovascular Disease: the Role of the Plasma Membrane Calcium Pumps. *Science China Life Sciences,* **54**(8), pp.691-698.

CARVER, W., M. L. NAGPAL, M. NACHTIGAL, T. K. BORG and L. TERRACIO. 1991. Collagen Expression in Mechanically Stimulated Cardiac Fibroblasts. *Circulation Research,* **69**(1), pp.116-122.

CASTELLA, L. F., L. BUSCEMI, C. GODBOUT, J.-J. MEISTER and B. HINZ. 2010. A New Lock-Step Mechanism of Matrix Remodelling Based on Subcellular Contractile Events. *Journal of Cell Science,* **123**(10), pp.1751-1760.

CATTERALL, W. A. 2011. Voltage-Gated Calcium Channels. *Cold Spring Harbor Perspectives in Biology,* **3**(8), pp.a003947-a003947.

CHA, H.-N., J. H. CHOI, Y.-W. KIM, J.-Y. KIM, M.-W. AHN and S.-Y. PARK. 2010. Metformin Inhibits Isoproterenol-Induced Cardiac Hypertrophy in Mice. *The Korean Journal of Physiology & Pharmacology : official journal of the Korean Physiological Society and the Korean Society of Pharmacology,* **14**(6), pp.377-384.

CHAPMAN, D., K. T. WEBER and M. EGHBALI. 1990. Regulation of Fibrillar Collagen Types I and III and Basement Membrane Type IV Collagen Gene Expression in Pressure Overloaded Rat Myocardium. *Circulation Research,* **67**(4), pp.787-794.

CHATELIER, A., A. MERCIER, B. TREMBLIER, O. THÉRIAULT, M. MOUBARAK, N. BENAMER, P. CORBI, P. BOIS, M. CHAHINE and J. F. FAIVRE. 2012. A Distinct de Novo Expression of Nav1.5 Sodium Channels in Human Atrial Fibroblasts Differentiated into Myofibroblasts. *The Journal of Physiology,* **590**(17), pp.4307-4319.

CHEN, J.-B., W.-J. LIU, H. CHE, J. LIU, H.-Y. SUN and G.-R. LI. 2012. Adenosine-5'-Triphosphate Up-Regulates Proliferation of Human Cardiac Fibroblasts. *British Journal of Pharmacology,* **166**(3), pp.1140-1150.

CHEN, J.-B., R. TAO, H.-Y. SUN, H.-F. TSE, C.-P. LAU and G.-R. LI. 2010. Multiple Ca2+ Signaling Pathways Regulate Intracellular Ca2+ Activity in Human Cardiac Fibroblasts. *Journal of Cellular Physiology,* **223**(1), pp.68-75.

CHEN, J., D. K. CEHOLSKI, L. LIANG, K. FISH and R. J. HAJJAR. 2017. Variability in Coronary Artery Anatomy Affects Consistency of Cardiac Damage After Myocardial Infarction in Mice. *American Journal of Physiology-Heart and Circulatory Physiology,* **313**(2), pp.H275-H282.

CHEN, K., J. L. MEHTA, D. LI, L. JOSEPH and J. JOSEPH. 2004. Transforming Growth Factor β; Receptor Endoglin Is Expressed in Cardiac Fibroblasts and Modulates Profibrogenic Actions of Angiotensin II. *Circulation Research,* **95**(12), pp.1167-1173.

CHEN, W. and N. G. FRANGOGIANNIS. 2013. Fibroblasts in Post-infarction Inflammation and Cardiac Repair. *Biochimica et Biophysica Acta (BBA) - Molecular Cell Research,* **1833**(4), pp.945-953.

CHIQUET-EHRISMANN, R., P. KALLA, C. A. PEARSON, K. BECK and M. CHIQUET. 1988. Tenascin Interferes with Fibronectin Action. *Cell,* **53**(3), pp.383-390.

CHIQUET, M., L. GELMAN, R. LUTZ and S. MAIER. 2009. From Mechanotransduction to Extracellular Matrix Gene Expression in Fibroblasts. *Biochimica et Biophysica Acta (BBA) - Molecular Cell Research,* **1793**(5), pp.911-920.

CHIQUET, M., A. SARASA-RENEDO and V. TUNÇ-CIVELEK. 2004. Induction of Tenascin-C by Cyclic Tensile Strain versus Growth Factors: Distinct Contributions by Rho/ROCK and MAPK Signaling Pathways. *Biochimica et Biophysica Acta (BBA) - Molecular Cell Research,* **1693**(3), pp.193-204.

CHRISTENSEN, A. P. and D. P. COREY. 2007. TRP Channels in Mechanosensation: Direct or Indirect Activation? *Nature Reviews Neuroscience,* **8**, p510.

CHUBINSKIY-NADEZHDIN, V. I., V. Y. VASILEVA, I. O. VASSILIEVA, A. V. SUDARIKOVA, E. A. MORACHEVSKAYA and Y. A. NEGULYAEV. 2019. Agonist-induced Piezo1 Activation Suppresses Migration of Transformed Fibroblasts. *Biochemical and Biophysical Research Communications,* **514**(1), pp.173-179.

CLAPHAM, D. E. 1995. Calcium Signaling. *Cell,* **80**(2), pp.259-268.

CLAPHAM, D. E. 2007. Calcium Signaling. *Cell,* **131**(6), pp.1047-1058.

CLEMENTE, C. F. M. Z., T. F. TORNATORE, T. H. THEIZEN, A. C. DECKMANN, T. C. PEREIRA, I. LOPES-CENDES, J. R. M. SOUZA and K. G. FRANCHINI. 2007. Targeting Focal Adhesion Kinase With Small Interfering RNA Prevents and Reverses Load-Induced Cardiac Hypertrophy in Mice. *Circulation Research,* **101**(12), pp.1339-1348.

COLES, B., C. A. FIELDING, S. ROSE-JOHN, J. SCHELLER, S. A. JONES and V. B. O'DONNELL. 2007. Classic Interleukin-6 Receptor Signaling and Interleukin-6 Trans-signaling Differentially Control Angiotensin II-Dependent Hypertension, Cardiac Signal Transducer and Activator of Transcription-3 Activation, and Vascular Hypertrophy In Vivo. *The American Journal of Pathology,* **171**(1), pp.315-325.

COSTE, B., J. MATHUR, M. SCHMIDT, T. J. EARLEY, S. RANADE, M. J. PETRUS, A. E. DUBIN and A. PATAPOUTIAN. 2010. Piezo1 and Piezo2 are Essential Components of Distinct Mechanically Activated Cation Channels. *Science (New York, N.Y.),* **330**(6000), pp.55-60.

COSTE, B., B. XIAO, J. S. SANTOS, R. SYEDA, J. GRANDL, K. S. SPENCER, S. E. KIM, M. SCHMIDT, J. MATHUR, A. E. DUBIN, M. MONTAL and A. PATAPOUTIAN. 2012. Piezo Proteins are Pore-Forming Subunits of Mechanically Activated Channels. *Nature,* **483**(7388), pp.176-181.

COUCHMAN, J. R. 2010. Transmembrane Signaling Proteoglycans. *Annual Review of Cell and Developmental Biology,* **26**(1), pp.89-114.

COX, C. D., C. BAE, L. ZIEGLER, S. HARTLEY, V. NIKOLOVA-KRSTEVSKI, P. R. ROHDE, C.-A. NG, F. SACHS, P. A. GOTTLIEB and B. MARTINAC. 2016. Removal of the Mechanoprotective Influence of the Cytoskeleton Reveals PIEZO1 is Gated by Bilayer Tension. *Nature Communications,* **7**, p10366.

CRITCHLEY, D. R. 2009. Biochemical and Structural Properties of the Integrin-Associated Cytoskeletal Protein Talin. *Annual Review of Biophysics,* **38**(1), pp.235-254.

CUTHBERTSON, K. 2019. Design and Synthesis of Small Molecules for the Modulation of Piezo1 Function. PhD thesis, University of Leeds.

DALLA COSTA, A. P., C. F. M. Z. CLEMENTE, H. F. CARVALHO, J. B. CARVALHEIRA, W. NADRUZ, JR and K. G. FRANCHINI. 2009. FAK Mediates the Activation of Cardiac Fibroblasts Induced by Mechanical Stress Through Regulation of the mTOR Complex. *Cardiovascular Research,* **86**(3), pp.421-431.

DARBY, I. A., B. LAVERDET, F. BONTÉ and A. DESMOULIÈRE. 2014. Fibroblasts and Myofibroblasts in Wound Healing. *Clinical, Cosmetic and Investigational Dermatology,* **7**, pp.301-311.

DARDIK, A., L. CHEN, J. FRATTINI, H. ASADA, F. AZIZ, F. A. KUDO and B. E. SUMPIO. 2005. Differential Effects of Orbital and Laminar Shear Stress on Endothelial Cells. *Journal of Vascular Surgery,* **41**(5), pp.869-880.

DAVIS, J., A. R. BURR, G. F. DAVIS, L. BIRNBAUMER and J. D. MOLKENTIN. 2012. A TRPC6-Dependent Pathway for Myofibroblast Transdifferentiation and Wound Healing In Vivo. *Developmental Cell,* **23**(4), pp.705-715.

DAVIS, M. J., X. WU, T. R. NURKIEWICZ, J. KAWASAKI, P. GUI, M. A. HILL and E. WILSON. 2001. Regulation of Ion Channels by Protein Tyrosine Phosphorylation. *American Journal of Physiology-Heart and Circulatory Physiology,* **281**(5), pp.H1835-H1862.

DE NADAL, E. and F. POSAS. 2010. Multilayered Control of Gene Expression by Stress-Activated Protein Kinases. *The EMBO Journal,* **29**(1), pp.4-13.

DEALMEIDA, A. C., R. J. VAN OORT and X. H. T. WEHRENS. 2010. Transverse Aortic Constriction in Mice. *Journal of Visualized Experiments : JoVE,* (38), p1729.

DEAN, J. L. E., G. SULLY, A. R. CLARK and J. SAKLATVALA. 2004. The Involvement of AU-Rich Element-Binding Proteins in p38 Mitogen-Activated Protein Kinase Pathway-Mediated mRNA Stabilisation. *Cellular Signalling,* **16**(10), pp.1113-1121.

DEB, A. and E. UBIL. 2014. Cardiac Fibroblast in Development and Wound Healing. *Journal of Molecular and Cellular Cardiology,* **70**, pp.47-55.

DEL MÁRMOL, J. I., K. K. TOUHARA, G. CROFT and R. MACKINNON. 2018. Piezo1 Forms a Slowly-Inactivating Mechanosensory Channel in Mouse Embryonic Stem Cells. *ELife,* **7**, pe33149.

DELA PAZ, N. G. and J. A. FRANGOS. 2018. Yoda1-Induced Phosphorylation of Akt and ERK1/2 Does Not Require Piezo1 Activation. *Biochemical and Biophysical Research Communications,* **497**(1), pp.220-225.

DENTON, C. P., G. E. LINDAHL, K. KHAN, X. SHIWEN, V. H. ONG, N. J. GASPAR, K. LAZARIDIS, D. R. EDWARDS, A. LEASK, M. EASTWOOD, P. LEONI, E. A. RENZONI, G. BOU GHARIOS, D. J. ABRAHAM and C.

M. BLACK. 2005. Activation of Key Profibrotic Mechanisms in Transgenic Fibroblasts Expressing Kinase-deficient Type II Transforming Growth Factor-β Receptor (TβRIIΔk). *Journal of Biological Chemistry,* **280**(16), pp.16053-16065.

DENTON, C. P., B. ZHENG, X. SHIWEN, Z. ZHANG, G. BOU-GHARIOS, H. EBERSPAECHER, C. M. BLACK and B. DE CROMBRUGGHE. 2001. Activation of a Fibroblast-Specific Enhancer of the Proα2(I) Collagen Gene in Tight-Skin Mice. *Arthritis & Rheumatism,* **44**(3), pp.712-722.

DERYNCK, R. and Y. E. ZHANG. 2003. Smad-Dependent and Smad-Independent Pathways in TGF-β Family Signalling. *Nature,* **425**(6958), pp.577-584.

DETTMAN, R. W., W. DENETCLAW, C. P. ORDAHL and J. BRISTOW. 1998. Common Epicardial Origin of Coronary Vascular Smooth Muscle, Perivascular Fibroblasts, and Intermyocardial Fibroblasts in the Avian Heart. *Developmental Biology,* **193**(2), pp.169-181.

DI VIRGILIO, F., T. H. STEINBERG and S. C. SILVERSTEIN. 1989. Chapter 21 Organic-Anion Transport Inhibitors to Facilitate Measurement of Cytosolic Free Ca2+ with Fura-2. *In:* A. M. TARTAKOFF, ed. *Methods in Cell Biology.* Academic Press, pp.453-462.

DIXON, I. M. C., N. M. LANDRY and S. G. RATTAN. 2019. Periostin Reexpression in Heart Disease Contributes to Cardiac Interstitial Remodeling by Supporting the Cardiac Myofibroblast Phenotype. *In:* A. KUDO, ed. *Periostin.* Singapore: Springer Singapore, pp.35-41.

DOBACZEWSKI, M., W. CHEN and N. G. FRANGOGIANNIS. 2011. Transforming Growth Factor (TGF)-β Signaling in Cardiac Remodeling. *Journal of Molecular and Cellular Cardiology,* **51**(4), pp.600-606.

DOBACZEWSKI, M., C. GONZALEZ-QUESADA and N. G. FRANGOGIANNIS. 2010. The Extracellular Matrix as a Modulator of the Inflammatory and Reparative Response Following Myocardial Infarction. *Journal of Molecular and Cellular Cardiology,* **48**(3), pp.504-511.

DOSTAL, D., S. GLASER and T. A. BAUDINO. 2015. Cardiac Fibroblast Physiology and Pathology. *Comprehensive Physiology.* pp.887-909.

DRIESEN, R. B., C. K. NAGARAJU, J. ABI-CHAR, T. COENEN, P. J. LIJNEN, R. H. FAGARD, K. R. SIPIDO and V. V. PETROV. 2014. Reversible and Irreversible Differentiation of Cardiac Fibroblasts. *Cardiovascular Research,* **101**(3), pp.411-422.

DU, J.-H., N. XU, Y. SONG, M. XU, Z.-Z. LU, C. HAN and Y.-Y. ZHANG. 2005. AICAR Stimulates IL-6 Production via p38 MAPK in Cardiac Fibroblasts in Adult Mice: A possible role for AMPK. *Biochemical and Biophysical Research Communications,* **337**(4), pp.1139-1144.

DUBIN, A. E., M. SCHMIDT, J. MATHUR, M. J. PETRUS, B. XIAO, B. COSTE and A. PATAPOUTIAN. 2012. Inflammatory Signals Enhance Piezo2-Mediated Mechanosensitive Currents. *Cell Reports,* **2**(3), pp.511-517.

DUBUIS, E., N. ROCKLIFFE, M. HUSSAIN, M. BOYETT, D. WRAY and D. GAWLER. 2006. Evidence for Multiple Src Binding Sites on the α1c L-Type Ca2+ Channel and Their Roles in Activity Regulation. *Cardiovascular Research,* **69**(2), pp.391-401.

DUPONT, S., L. MORSUT, M. ARAGONA, E. ENZO, S. GIULITTI, M. CORDENONSI, F. ZANCONATO, J. LE DIGABEL, M. FORCATO, S. BICCIATO, N. ELVASSORE and S. PICCOLO. 2011. Role of YAP/TAZ in Mechanotransduction. *Nature,* **474**, p179.

DUYGU, B. and P. A. DA COSTA MARTINS. 2015. miR-21: a Star Player in Cardiac Hypertrophy. *Cardiovascular Research,* **105**(3), pp.235-237.

EDELMAN, J. L., M. KAJIMURA, E. WOLDEMUSSIE and G. SACHS. 1994. Differential Effects of Carbachol on Calcium Entry and Release in CHO Cells Expressing the m3 Muscarinic Receptor. *Cell Calcium,* **16**(3), pp.181-193.

EDER, P. and J. D. MOLKENTIN. 2011. TRPC Channels As Effectors of Cardiac Hypertrophy. *Circulation Research,* **108**(2), pp.265-272.

EGHBALI, M., R. TOMEK, C. WOODS and B. BHAMBI. 1991. Cardiac Fibroblasts are Predisposed to Convert into Myocyte Phenotype: Specific Effect of Transforming Growth Factor Beta. *Proceedings of the National Academy of Sciences of the United States of America,* **88**(3), pp.795-799.

EHRLICH, H. P., G. M. ALLISON and M. LEGGETT. 2006. The Myofibroblast, Cadherin, α Smooth Muscle Actin and the Collagen Effect. *Cell Biochemistry and Function,* **24**(1), pp.63-70.

EISENHOFFER, G. T., P. D. LOFTUS, M. YOSHIGI, H. OTSUNA, C.-B. CHIEN, P. A. MORCOS and J. ROSENBLATT. 2012. Crowding Induces Live Cell Extrusion to Maintain Homeostatic Cell Numbers in Epithelia. *Nature,* **484**(7395), pp.546-549.

ELLEFSEN, K. L., J. R. HOLT, A. C. CHANG, J. L. NOURSE, J. ARULMOLI, A. H. MEKHDJIAN, H. ABUWARDA, F. TOMBOLA, L. A. FLANAGAN, A. R. DUNN, I. PARKER and M. M. PATHAK. 2019. Myosin-II Mediated Traction Forces Evoke Localized Piezo1-Dependent Ca2+ Flickers. *Communications Biology,* **2**(1), p298.

ELOSEGUI-ARTOLA, A., I. ANDREU, A. E. M. BEEDLE, A. LEZAMIZ, M. UROZ, A. J. KOSMALSKA, R. ORIA, J. Z. KECHAGIA, P. RICO-LASTRES, A.-L. LE ROUX, C. M. SHANAHAN, X. TREPAT, D. NAVAJAS, S. GARCIA-MANYES and P. ROCA-CUSACHS. 2017. Force Triggers YAP Nuclear Entry by Regulating Transport across Nuclear Pores. *Cell,* **171**(6), pp.1397-1410.e14.

ERTEL, E. A., K. P. CAMPBELL, M. M. HARPOLD, F. HOFMANN, Y. MORI, E. PEREZ-REYES, A. SCHWARTZ, T. P. SNUTCH, T. TANABE, L. BIRNBAUMER, R. W. TSIEN and W. A. CATTERALL. 2000. Nomenclature of Voltage-Gated Calcium Channels. *Neuron,* **25**(3), pp.533-535.

EVANS, E. L., K. CUTHBERTSON, N. ENDESH, B. RODE, N. M. BLYTHE, A. J. HYMAN, S. J. HALL, H. J. GAUNT, M. J. LUDLOW, R. FOSTER and D. J. BEECH. 2018. Yoda1 Analogue (Dooku1) Which Antagonizes Yoda1-Evoked Activation of Piezo1 and Aortic Relaxation. *British Journal of Pharmacology,* **175**(10), pp.1744-1759.

EYERS, P. A., P. VAN DEN IJSSEL, R. A. QUINLAN, M. GOEDERT and P. COHEN. 1999. Use of a Drug-Resistant Mutant of Stress-Activated Protein Kinase 2a/p38 to Validate the In Vivo Specificity of SB 203580. *FEBS Letters,* **451**(2), pp.191-196.

FAN, D., A. TAKAWALE, J. LEE and Z. KASSIRI. 2012. Cardiac Fibroblasts, Fibrosis and Extracellular Matrix Remodeling in Heart Disease. *Fibrogenesis & Tissue Repair,* **5**(1), pp.15-15.

FAUCHERRE, A., H. MOHA OU MAATI, N. NASR, A. PINARD, A. THERON, G. ODELIN, J. P. DESVIGNES, D. SALGADO, G. COLLOD BEROUD, J. F. AVIERINOS, G. LEBON, S. ZAFFRAN and C. JOPLING. 2019. Piezo1 is Required for Outflow Tract and Aortic Valve Development. *BioRxiv*, p528588.

FEDERMANN, M. and O. M. HESS. 1994. Differentiation between Systolic and Diastolic Dysfunction. *European Heart Journal,* **15**(suppl_D), pp.2-6.

FEETHAM, C. H., N. NUNN, R. LEWIS, C. DART and R. BARRETT-JOLLEY. 2015. TRPV4 and K(Ca) Ion Channels Functionally Couple as Osmosensors in the Paraventricular Nucleus. *British Journal of Pharmacology,* **172**(7), pp.1753-1768.

FEIL, S., N. VALTCHEVA and R. FEIL. 2009. Inducible Cre Mice. *In:* W. WURST and R. KÜHN, eds. *Gene Knockout Protocols: Second Edition.* Totowa, NJ: Humana Press, pp.343-363.

FONTES, J. A., N. R. ROSE and D. ČIHÁKOVÁ. 2015. The Varying Faces of IL-6: From Cardiac Protection to Cardiac Failure. *Cytokine,* **74**(1), pp.62-68.

FOTIOU, E., S. MARTIN-ALMEDINA, M. A. SIMPSON, S. LIN, K. GORDON, G. BRICE, G. ATTON, I. JEFFERY, D. C. REES, C. MIGNOT, J. VOGT, T. HOMFRAY, M. P. SNYDER, S. G. ROCKSON, S. JEFFERY, P. S. MORTIMER, S. MANSOUR and P. OSTERGAARD. 2015. Novel Mutations in PIEZO1 Cause an Autosomal Recessive Generalized Lymphatic Dysplasia with Non-Immune Hydrops Fetalis. *Nature Communications,* **6**, pp.8085-8085.

FOUNTOULAKI, K., N. DAGRES and E. K. ILIODROMITIS. 2015. Cellular Communications in the Heart. *Cardiac Failure Review,* **1**(2), pp.64-68.

FRANGOGIANNIS, N. G. 2012. Matricellular Proteins in Cardiac Adaptation and Disease. *Physiological Reviews,* **92**(2), pp.635-688.

FU, X., H. KHALIL, O. KANISICAK, J. G. BOYER, R. J. VAGNOZZI, B. D. MALIKEN, M. A. SARGENT, V. PRASAD, I. VALIENTE-ALANDI, B. C. BLAXALL and J. D. MOLKENTIN. 2018. Specialized Fibroblast Differentiated States Underlie Scar Formation in the Infarcted Mouse Heart. *The Journal of Clinical Investigation,* **128**(5), pp.2127-2143.

FUJIU, K. and R. NAGAI. 2014. Fibroblast-Mediated Pathways in Cardiac Hypertrophy. *Journal of Molecular and Cellular Cardiology,* **70**, pp.64-73.

GABBIANI, G. 2003. The Myofibroblast in Wound Healing and Fibrocontractive Diseases. *The Journal of Pathology,* **200**(4), pp.500-503.

GABBIANI, G., G. B. RYAN and G. MAJNO. 1971. Presence of Modified Fibroblasts in Granulation Tissue and their Possible Role in Wound Contraction. *Experientia,* **27**(5), pp.549-550.

GE, J., W. LI, Q. ZHAO, N. LI, M. CHEN, P. ZHI, R. LI, N. GAO, B. XIAO and M. YANG. 2015. Architecture of the Mammalian Mechanosensitive Piezo1 Channel. *Nature,* **527**, p64.

GIBSON, D. G., L. YOUNG, R.-Y. CHUANG, J. C. VENTER, C. A. HUTCHISON III and H. O. SMITH. 2009. Enzymatic Assembly of DNA Molecules up to Several Hundred Kilobases. *Nature Methods,* **6**, p343.

GIUSTI, B., E. STICCHI, R. DE CARIO, A. MAGI, S. NISTRI and G. PEPE. 2017. Genetic Bases of Bicuspid Aortic Valve: The Contribution of Traditional and High-Throughput Sequencing Approaches on Research and Diagnosis. *Frontiers in Physiology,* **8**, pp.612-612.

GNANASAMBANDAM, R., C. BAE, P. A. GOTTLIEB and F. SACHS. 2015. Ionic Selectivity and Permeation Properties of Human PIEZO1 Channels. *PLOS ONE,* **10**(5), pp.e0125503-e0125503.

GODBOUT, C., L. FOLLONIER CASTELLA, E. A. SMITH, N. TALELE, M. L. CHOW, A. GARONNA and B. HINZ. 2013. The Mechanical Environment Modulates Intracellular Calcium Oscillation Activities of Myofibroblasts. *PLOS ONE,* **8**(5), pe64560.

GONZÁLEZ, A., S. RAVASSA, B. LÓPEZ, M. U. MORENO, J. BEAUMONT, G. S. JOSÉ, R. QUEREJETA, A. BAYÉS-GENÍS and J. DÍEZ. 2018. Myocardial Remodeling in Hypertension. *Hypertension,* **72**(3), pp.549-558.

GOONETILLEKE, L. and J. QUAYLE. 2012. TREK-1 K+ Channels in the Cardiovascular System: Their Significance and Potential as a Therapeutic Target. *Cardiovascular Therapeutics,* **30**(1), pp.e23-e29.

GRAY, M. O., C. S. LONG, J. E. KALINYAK, H.-T. LI and J. S. KARLINER. 1998. Angiotensin II Stimulates Cardiac Myocyte Hypertrophy via Paracrine Release of TGF-β1 and Endothelin-1 from Fibroblasts. *Cardiovascular Research,* **40**(2), pp.352-363.

GRYNKIEWICZ, G., M. POENIE and R. Y. TSIEN. 1985. A New Generation of Ca2+ Indicators with Greatly Improved Fluorescence Properties. *Journal of Biological Chemistry,* **260**(6), pp.3440-3450.

GUDIPATY, S. A., J. LINDBLOM, P. D. LOFTUS, M. J. REDD, K. EDES, C. F. DAVEY, V. KRISHNEGOWDA and J. ROSENBLATT. 2017. Mechanical Stretch Triggers Rapid Epithelial Cell Division through Piezo1. *Nature,* **543**(7643), pp.118-121.

GUILLUY, C., V. SWAMINATHAN, R. GARCIA-MATA, E. T. O'BRIEN, R. SUPERFINE and K. BURRIDGE. 2011. The Rho GEFs LARG and GEF-H1 Regulate the Mechanical Response to Force on Integrins. *Nature Cell Biology,* **13**(6), pp.722-727.

GURNEY, A. and B. MANOURY. 2008. Two-Pore Potassium Channels in the Cardiovascular System. *European Biophysics Journal,* **38**(3), p305.

HAMILL, O. P. and B. MARTINAC. 2001. Molecular Basis of Mechanotransduction in Living Cells. *Physiological Reviews,* **81**(2), pp.685-740.

HANKE, J. H., J. P. GARDNER, R. L. DOW, P. S. CHANGELIAN, W. H. BRISSETTE, E. J. WERINGER, B. A. POLLOK and P. A. CONNELLY. 1996. Discovery of a Novel, Potent, and Src Family-selective Tyrosine Kinase Inhibitor: STUDY OF Lck- AND FynT-DEPENDENT T CELL ACTIVATION. *Journal of Biological Chemistry,* **271**(2), pp.695-701.

HARADA, M., X. LUO, X. Y. QI, A. TADEVOSYAN, A. MAGUY, B. ORDOG, J. LEDOUX, T. KATO, P. NAUD, N. VOIGT, Y. SHI, K. KAMIYA, T. MUROHARA, I. KODAMA, J.-C. TARDIF, U. SCHOTTEN, D. R. VAN WAGONER, D. DOBREV and S. NATTEL. 2012. Transient Receptor Potential Canonical-3 Channel-Dependent Fibroblast Regulation in Atrial Fibrillation. *Circulation,* **126**(17), pp.2051-2064.

HEEREBEEK, L. V., N. HAMDANI, M. L. HANDOKO, I. FALCAO-PIRES, R. J. MUSTERS, K. KUPREISHVILI, A. J. J. IJSSELMUIDEN, C. G. SCHALKWIJK, J. G. F. BRONZWAER, M. DIAMANT, A. BORBÉLY, J. V. D. VELDEN, G. J. M. STIENEN, G. J. LAARMAN, H. W. M. NIESSEN and W. J. PAULUS. 2008. Diastolic Stiffness of the Failing Diabetic Heart. *Circulation,* **117**(1), pp.43-51.

HEINEKE, J. and J. D. MOLKENTIN. 2006. Regulation of Cardiac Hypertrophy by Intracellular Signalling Pathways. *Nature Reviews Molecular Cell Biology,* **7**(8), pp.589-600.

HELDIN, C.-H. and A. MOUSTAKAS. 2016. Signaling Receptors for TGF-β Family Members. *Cold Spring Harbor Perspectives in Biology,* **8**(8), pa022053.

HERUM, K., I. LUNDE, B. SKRBIC, W. LOUCH, A. HASIC, S. BOYE, A. UNGER, S.-H. BRORSON, I. SJAASTAD, T. TØNNESSEN, W. LINKE, M. GOMEZ

and G. CHRISTENSEN. 2015. Syndecan-4 is a Key Determinant of Collagen Cross-Linking and Passive Myocardial Stiffness in the Pressure-Overloaded Heart. *Cardiovascular Research*.

HERUM, K. M., J. CHOPPE, A. KUMAR, A. J. ENGLER and A. D. MCCULLOCH. 2017a. Mechanical Regulation of Cardiac Fibroblast Profibrotic Phenotypes. *Molecular Biology of the Cell,* **28**(14), pp.1871-1882.

HERUM, K. M., I. G. LUNDE, A. D. MCCULLOCH and G. CHRISTENSEN. 2017b. The Soft- and Hard-Heartedness of Cardiac Fibroblasts: Mechanotransduction Signaling Pathways in Fibrosis of the Heart. *Journal of Clinical Medicine,* **6**(5), p53.

HERUM, K. M., I. G. LUNDE, B. SKRBIC, G. FLORHOLMEN, D. BEHMEN, I. SJAASTAD, C. R. CARLSON, M. F. GOMEZ and G. CHRISTENSEN. 2013. Syndecan-4 Signaling via NFAT Regulates Extracellular Matrix Production and Cardiac Myofibroblast Differentiation in Response to Mechanical Stress. *Journal of Molecular and Cellular Cardiology,* **54**, pp.73-81.

HILGE, M. 2012. Ca2+ Regulation of Ion Transport in the Na+/Ca2+ Exchanger. *Journal of Biological Chemistry,* **287**(38), pp.31641-31649.

HINZ, B. 2015. The Extracellular Matrix and Transforming Growth Factor-β1: Tale of a Strained Relationship. *Matrix Biology,* **47**, pp.54-65.

HINZ, B. and G. GABBIANI. 2010. Fibrosis: Recent Advances in Myofibroblast Biology and New Therapeutic Perspectives. *F1000 Biology Reports,* **2**, pp.78-78.

HINZ, B., D. MASTRANGELO, C. E. ISELIN, C. CHAPONNIER and G. GABBIANI. 2001. Mechanical Tension Controls Granulation Tissue Contractile Activity and Myofibroblast Differentiation. *The American Journal of Pathology,* **159**(3), pp.1009-1020.

HINZ, B., S. H. PHAN, V. J. THANNICKAL, A. GALLI, M.-L. BOCHATON-PIALLAT and G. GABBIANI. 2007. The Myofibroblast: One Function, Multiple Origins. *The American Journal of Pathology,* **170**(6), pp.1807-1816.

HIROTA, H., K. YOSHIDA, T. KISHIMOTO and T. TAGA. 1995. Continuous Activation of Gp130, a Signal-Transducing Receptor Component for Interleukin 6-Related Cytokines, Causes Myocardial Hypertrophy in Mice. *Proceedings of the National Academy of Sciences of the United States of America,* **92**(11), pp.4862-4866.

HOLMES, T. C., D. A. FADOOL, R. REN and I. B. LEVITAN. 1996. Association of Src Tyrosine Kinase with a Human Potassium Channel Mediated by SH3 Domain. *Science,* **274**(5295), pp.2089-2091.

HOUSE, M., P. TANG, J. DANIEL, D. KAPLAN and S. SOCRATE. 2012. 510: Mechanical Stretch Increases Production of Inflammatory Cytokines from Cervical Fibroblasts in 2D and 3D culture. *American Journal of Obstetrics & Gynecology,* **206**(1), pS231.

HSIEH, A. H., C. M.-H. TSAI, Q.-J. MA, T. LIN, A. J. BANES, F. J. VILLARREAL, W. H. AKESON and K.-L. PAUL SUNG. 2000. Time-Dependent Increases in Type-III Collagen Gene Expression in Medial Collateral Ligament Fibroblasts under Cyclic Strains. *Journal of Orthopaedic Research,* **18**(2), pp.220-227.

HUDON-DAVID, F., F. BOUZEGHRANE, P. COUTURE and G. THIBAULT. 2007. Thy-1 Expression by Cardiac Fibroblasts: Lack of Association with Myofibroblast Contractile Markers. *Journal of Molecular and Cellular Cardiology,* **42**(5), pp.991-1000.

HUMERES, C. and N. G. FRANGOGIANNIS. 2019. Fibroblasts in the Infarcted, Remodeling, and Failing Heart. *JACC: Basic to Translational Science,* **4**(3), pp.449-467.

HUTCHINSON, K. R., C. K. LORD, T. A. WEST and J. A. STEWART, JR. 2013. Cardiac Fibroblast-Dependent Extracellular Matrix Accumulation is Associated with Diastolic Stiffness in Type 2 Diabetes. *PLOS ONE,* **8**(8), pp.e72080-e72080.

HYMAN, A. J. 2018. Modulation of Piezo1 by Lipids and Synthetic Small-Molecules. PhD thesis, University of Leeds.

IMANAKA-YOSHIDA, K., M. HIROE, T. NISHIKAWA, S. ISHIYAMA, T. SHIMOJO, Y. OHTA, T. SAKAKURA and T. YOSHIDA. 2001. Tenascin-C Modulates Adhesion of Cardiomyocytes to Extracellular Matrix during Tissue Remodeling after Myocardial Infarction. *Laboratory Investigation,* **81**, p1015.

INGLEY, E. 2008. Src Family Kinases: Regulation of their Activities, Levels and Identification of New Pathways. *Biochimica et Biophysica Acta (BBA) - Proteins and Proteomics,* **1784**(1), pp.56-65.

IYER, R. P., M. JUNG and M. L. LINDSEY. 2016. MMP-9 Signaling in the Left Ventricle Following Myocardial Infarction. *American Journal of Physiology-Heart and Circulatory Physiology,* **311**(1), pp.H190-H198.

IZUMO, S., B. NADAL-GINARD and V. MAHDAVI. 1988. Protooncogene Induction and Reprogramming of Cardiac Gene Expression Produced by Pressure Overload. *Proceedings of the National Academy of Sciences,* **85**(2), p339.

JAFARNEJAD, M., W. E. CROMER, R. R. KAUNAS, S. L. ZHANG, D. C. ZAWIEJA and J. E. M. JR. 2015. Measurement of Shear Stress-Mediated Intracellular Calcium Dynamics in Human Dermal Lymphatic Endothelial Cells. *American Journal of Physiology-Heart and Circulatory Physiology,* **308**(7), pp.H697-H706.

JAFFRÉ, F., P. BONNIN, J. CALLEBERT, H. DEBBABI, V. SETOLA, S. DOLY, L. MONASSIER, B. METTAUER, B. C. BLAXALL, J.-M. LAUNAY and L. MAROTEAUX. 2009. Serotonin and Angiotensin Receptors in Cardiac Fibroblasts Coregulate Adrenergic-Dependent Cardiac Hypertrophy. *Circulation Research,* **104**(1), pp.113-123.

JANICKI, J. S. and G. L. BROWER. 2002. The Role of Myocardial Fibrillar Collagen in Ventricular Remodeling and Function. *Journal of Cardiac Failure,* **8**(6, Part B), pp.S319-S325.

JÄRVINEN, T. A. H., L. JÓZSA, P. KANNUS, T. L. N. JÄRVINEN, T. HURME, M. KVIST, M. PELTO-HUIKKO, H. KALIMO and M. JÄRVINEN. 2003. Mechanical Loading Regulates the Expression of Tenascin-C in the Myotendinous Junction and Tendon but does not Induce De Novo Synthesis in the Skeletal Muscle. *Journal of Cell Science,* **116**(5), pp.857-866.

JIN, B., J. ZHU, H.-M. SHI, Z.-C. WEN and B.-W. WU. 2018. YAP Activation Promotes the Transdifferentiation of Cardiac Fibroblasts to Myofibroblasts in Matrix Remodeling of Dilated Cardiomyopathy. *Brazilian Journal of Medical and Biological Research = Revista Brasileira de Pesquisas Medicas e Biologicas,* **52**(1), pp.e7914-e7914.

JIN, Y., J. LI, Y. WANG, R. YE, X. FENG, Z. JING and Z. ZHAO. 2015. Functional Role of Mechanosensitive Ion Channel Piezo1 in Human Periodontal Ligament Cells. *The Angle Orthodontist,* **85**(1), pp.87-94.

JOURDAN-LESAUX, C., J. ZHANG and M. L. LINDSEY. 2010. Extracellular Matrix Roles During Cardiac Repair. *Life Sciences,* **87**(13), pp.391-400.

KAHAN, T. and L. BERGFELDT. 2005. Left Ventricular Hypertrophy in Hypertension: its Arrhythmogenic Potential. *Heart (British Cardiac Society),* **91**(2), pp.250-256.

KAINULAINEN, T., A. PENDER, M. D'ADDARIO, Y. FENG, P. LEKIC and C. A. MCCULLOCH. 2002. Cell Death and Mechanoprotection by Filamin A in Connective Tissues after Challenge by Applied Tensile Forces. *Journal of Biological Chemistry,* **277**(24), pp.21998-22009.

KAMO, T., H. AKAZAWA and I. KOMURO. 2015. Cardiac Nonmyocytes in the Hub of Cardiac Hypertrophy. *Circulation Research,* **117**(1), pp.89-98.

KANISICAK, O., H. KHALIL, M. J. IVEY, J. KARCH, B. D. MALIKEN, R. N. CORRELL, M. J. BRODY, S.-C. J. LIN, B. J. ARONOW, M. D. TALLQUIST and J. D. MOLKENTIN. 2016. Genetic Lineage Tracing Defines Myofibroblast Origin and Function in the Injured Heart. *Nature Communications,* **7**, p12260.

KATSUMI, A., A. W. ORR, E. TZIMA and M. A. SCHWARTZ. 2004. Integrins in Mechanotransduction. *Journal of Biological Chemistry,* **279**(13), pp.12001-12004.

KATZ, S., R. BOLAND and G. SANTILLÁN. 2006. Modulation of ERK 1/2 and p38 MAPK Signaling Pathways by ATP in Osteoblasts: Involvement of Mechanical Stress-Activated Calcium Influx, PKC and Src Activation. *The International Journal of Biochemistry & Cell Biology,* **38**(12), pp.2082-2091.

KENDALL, R. T. and C. A. FEGHALI-BOSTWICK. 2014. Fibroblasts in Fibrosis: Novel Roles and Mediators. *Frontiers in Pharmacology,* **5**, pp.123-123.

KHALIL, H., O. KANISICAK, V. PRASAD, R. N. CORRELL, X. FU, T. SCHIPS, R. J. VAGNOZZI, R. LIU, T. HUYNH, S.-J. LEE, J. KARCH and J. D. MOLKENTIN. 2017. Fibroblast-Specific TGF-β-Smad2/3 Signaling Underlies Cardiac Fibrosis. *The Journal of Clinical Investigation,* **127**(10), pp.3770-3783.

KIM, D. 1993. Novel Cation-Selective Mechanosensitive Ion Channel in the Atrial Cell Membrane. *Circulation Research,* **72**(1), pp.225-231.

KIM, M.-J., J.-Y. BYUN, C.-H. YUN, I.-C. PARK, K.-H. LEE and S.-J. LEE. 2008. c-Src-p38 Mitogen-Activated Protein Kinase Signaling Is Required for Akt Activation in Response to Ionizing Radiation. *Molecular Cancer Research,* **6**(12), pp.1872-1880.

KIMURA, T., K. SHIRAISHI, A. FURUSHO, S. ITO, S. HIRAKATA, N. NISHIDA, K. YOSHIMURA, K. IMANAKA-YOSHIDA, T. YOSHIDA, Y. IKEDA, T. MIYAMOTO, T. UENO, K. HAMANO, M. HIROE, K. AONUMA, M. MATSUZAKI, T. IMAIZUMI and H. AOKI. 2014. Tenascin C Protects Aorta from Acute Dissection in Mice. *Scientific Reports,* **4**, pp.4051-4051.

KIRICHOK, Y., G. KRAPIVINSKY and D. E. CLAPHAM. 2004. The Mitochondrial Calcium Uniporter is a Highly Selective Ion Channel. *Nature,* **427**(6972), pp.360-364.

KIS, K., X. LIU and J. S. HAGOOD. 2011. Myofibroblast Differentiation and Survival in Fibrotic Disease. *Expert Reviews in Molecular Medicine,* **13**, pe27.

KISELEVA, I., A. KAMKIN, P. KOHL and M. J. LAB. 1996. Calcium and Mechanically Induced Potentials in Fibroblasts of Rat Atrium. *Cardiovascular Research,* **32**(1), pp.98-111.

KONDRATSKYI, A., K. KONDRATSKA, R. SKRYMA and N. PREVARSKAYA. 2015. Ion Channels in the Regulation of Apoptosis. *Biochimica et Biophysica Acta (BBA) - Biomembranes,* **1848**(10, Part B), pp.2532-2546.

KONG, P., P. CHRISTIA, A. SAXENA, Y. SU and N. G. FRANGOGIANNIS. 2013. Lack of Specificity of Fibroblast-Specific Protein 1 in Cardiac Remodeling and Fibrosis. *American journal of physiology. Heart and Circulatory Physiology,* **305**(9), pp.H1363-H1372.

KRISHNA, M. and H. NARANG. 2008. The Complexity of Mitogen-Activated Protein Kinases (MAPKs) Made Simple. *Cellular and Molecular Life Sciences,* **65**(22), pp.3525-3544.

KRISTIANSEN, S. B., O. HENNING, R. K. KHARBANDA, J. E. NIELSEN-KUDSK, M. R. SCHMIDT, A. N. REDINGTON, T. T. NIELSEN and H. E. BØTKER. 2005. Remote Preconditioning Reduces Ischemic Injury in the Explanted Heart by a KATP Channel-Dependent Mechanism. *American Journal of Physiology-Heart and Circulatory Physiology,* **288**(3), pp.H1252-H1256.

KULKARNI, A. B., C. G. HUH, D. BECKER, A. GEISER, M. LYGHT, K. C. FLANDERS, A. B. ROBERTS, M. B. SPORN, J. M. WARD and S. KARLSSON. 1993. Transforming Growth Factor Beta 1 Null Mutation in Mice Causes Excessive Inflammatory Response and Early Death. *Proceedings of the National Academy of Sciences of the United States of America,* **90**(2), pp.770-774.

KUNISADA, K., E. TONE, Y. FUJIO, H. MATSUI, K. YAMAUCHI-TAKIHARA and T. KISHIMOTO. 1998. Activation of gp130 Transduces Hypertrophic Signals via STAT3 in Cardiac Myocytes. *Circulation,* **98**(4), pp.346-352.

KYRIAKIS, J. M. and J. AVRUCH. 2001. Mammalian Mitogen-Activated Protein Kinase Signal Transduction Pathways Activated by Stress and Inflammation. *Physiological Reviews,* **81**(2), pp.807-869.

LACROIX, J. J., W. M. BOTELLO-SMITH and Y. LUO. 2018. Probing the Gating Mechanism of the Mechanosensitive Channel Piezo1 with the Small Molecule Yoda1. *Nature Communications,* **9**(1), p2029.

LAHOZ, C. and J. M. MOSTAZA. 2007. Atherosclerosis As a Systemic Disease. *Revista Española de Cardiología (English Edition),* **60**(2), pp.184-195.

LEASK, A. and D. J. ABRAHAM. 2004. TGF-β Signaling and the Fibrotic Response. *The FASEB Journal,* **18**(7), pp.816-827.

LEE, W., H. A. LEDDY, Y. CHEN, S. H. LEE, N. A. ZELENSKI, A. L. MCNULTY, J. WU, K. N. BEICKER, J. COLES, S. ZAUSCHER, J. GRANDL, F. SACHS, F. GUILAK and W. B. LIEDTKE. 2014. Synergy between Piezo1 and Piezo2 Channels Confers High-Strain Mechanosensitivity to Articular Cartilage. *Proceedings of the National Academy of Sciences of the United States of America,* **111**(47), pp.E5114-E5122.

LEMBONG, J., B. SABASS, B. SUN, M. E. ROGERS and H. A. STONE. 2015. Mechanics Regulates ATP-Stimulated Collective Calcium Response in Fibroblast Cells. *Journal of the Royal Society, Interface,* **12**(108), pp.20150140-20150140.

LEWIS, A. H., A. F. CUI, M. F. MCDONALD and J. GRANDL. 2017. Transduction of Repetitive Mechanical Stimuli by Piezo1 and Piezo2 Ion Channels. *Cell Reports,* **19**(12), pp.2572-2585.

LEWIS, A. H. and J. GRANDL. 2015. Mechanical Sensitivity of Piezo1 Ion Channels Can be Tuned by Cellular Membrane Tension. E*Life,* **4**, pe12088.

LI, G.-R., H.-Y. SUN, J.-B. CHEN, Y. ZHOU, H.-F. TSE and C.-P. LAU. 2009. Characterization of Multiple Ion Channels in Cultured Human Cardiac Fibroblasts. *PLOS ONE,* **4**(10), pp.e7307-e7307.

LI, J., B. HOU, S. TUMOVA, K. MURAKI, A. BRUNS, M. J. LUDLOW, A. SEDO, A. J. HYMAN, L. MCKEOWN, R. S. YOUNG, N. Y. YULDASHEVA, Y. MAJEED, L. A. WILSON, B. RODE, M. A. BAILEY, H. R. KIM, Z. FU, D. A. L. CARTER, J. BILTON, H. IMRIE, P. AJUH, T. N. DEAR, R. M. CUBBON, M. T. KEARNEY, K. R. PRASAD, P. C. EVANS, J. F. X. AINSCOUGH and D. J. BEECH. 2014. Piezo1 Integration of Vascular Architecture with Physiological Force. *Nature,* **515**, p279.

LI, J., Y. ZHANG, L. CUI, J. WANG, X. PANG, Y. LAI, Y. YAO, X. LIU and Y. LI. 2013. Mechanical Stretch Changes Coronary Artery Fibroblasts Function by Upregulating HSF1 Protein Expression. *International Journal of Biological Macromolecules,* **59**, pp.105-110.

LI, Q., Y. XU, X. LI, Y. GUO and G. LIU. 2012. Inhibition of Rho-Kinase Ameliorates Myocardial Remodeling and Fibrosis in Pressure Overload and Myocardial Infarction: Role of TGF-β1–TAK1. *Toxicology Letters,* **211**(2), pp.91-97.

LI, X., E. SHANG, Q. DONG, Y. LI, J. ZHANG, S. XU, Z. ZHAO, W. SHAO, C. LV, Y. ZHENG, H. WANG, X. LEI, B. ZHU and Z. ZHANG. 2018. Small Molecules Capable of Activating DNA Methylation-Repressed Genes Targeted by the p38 Mitogen-Activated Protein Kinase Pathway. *The Journal of Biological Chemistry,* **293**(19), pp.7423-7436.

LIANG, J., B. HUANG, G. YUAN, Y. CHEN, F. LIANG, H. ZENG, S. ZHENG, L. CAO, D. GENG and S. ZHOU. 2017. Stretch-Activated Channel Piezo1 is Up-Regulated in Failure Heart and Cardiomyocyte Stimulated by AngII. *American Journal of Translational Research,* **9**(6), pp.2945-2955.

LIJNEN, P. J., V. V. PETROV and R. H. FAGARD. 2001. Angiotensin II-Induced Stimulation of Collagen Secretion and Production in Cardiac Fibroblasts is Mediated via Angiotensin II Subtype 1 Receptors. *Journal of the Renin-Angiotensin-Aldosterone System,* **2**(2), pp.117-122.

LIU, C. and C. MONTELL. 2015. Forcing open TRP channels: Mechanical Gating as a Unifying Activation Mechanism. *Biochemical and Biophysical Research Communications,* **460**(1), pp.22-25.

LIU, S., D. A. CALDERWOOD and M. H. GINSBERG. 2000. Integrin Cytoplasmic Domain-Binding Proteins. *Journal of Cell Science,* **113**(20), pp.3563-3571.

LOONSTRA, A., M. VOOIJS, H. B. BEVERLOO, B. A. ALLAK, E. VAN DRUNEN, R. KANAAR, A. BERNS and J. JONKERS. 2001. Growth Inhibition and DNA Damage Induced by Cre Recombinase in Mammalian Cells. *Proceedings of the National Academy of Sciences of the United States of America,* **98**(16), pp.9209-9214.

LU, D., S. SOLEYMANI, R. MADAKSHIRE and P. A. INSEL. 2012. ATP Released from Cardiac Fibroblasts via Connexin Hemichannels Activates Profibrotic P2Y2 Receptors. *FASEB journal : official publication of the Federation of American Societies for Experimental Biology,* **26**(6), pp.2580-2591.

LU, G., Y. J. KANG, J. HAN, H. R. HERSCHMAN, E. STEFANI and Y. WANG. 2006. TAB-1 Modulates Intracellular Localization of p38 MAP Kinase and Downstream Signaling. *Journal of Biological Chemistry,* **281**(9), pp.6087-6095.

LUKACS, V., J. MATHUR, R. MAO, P. BAYRAK-TOYDEMIR, M. PROCTER, S. M. CAHALAN, H. J. KIM, M. BANDELL, N. LONGO, R. W. DAY, D. A. STEVENSON, A. PATAPOUTIAN and B. L. KROCK. 2015. Impaired

PIEZO1 Function in Patients with a Novel Autosomal Recessive Congenital Lymphatic Dysplasia. *Nature Communications,* **6**, p8329.

MA, S., S. CAHALAN, G. LAMONTE, N. D. GRUBAUGH, W. ZENG, S. E. MURTHY, E. PAYTAS, R. GAMINI, V. LUKACS, T. WHITWAM, M. LOUD, R. LOHIA, L. BERRY, S. M. KHAN, C. J. JANSE, M. BANDELL, C. SCHMEDT, K. WENGELNIK, A. I. SU, E. HONORE, E. A. WINZELER, K. G. ANDERSEN and A. PATAPOUTIAN. 2018. Common PIEZO1 Allele in African Populations Causes RBC Dehydration and Attenuates Plasmodium Infection. *Cell,* **173**(2), pp.443-455.e12.

MA, Y., L. E. DE CASTRO BRÁS, H. TOBA, R. P. IYER, M. E. HALL, M. D. WINNIFORD, R. A. LANGE, S. C. TYAGI and M. L. LINDSEY. 2014. Myofibroblasts and the Extracellular Matrix Network in Post-Myocardial Infarction Cardiac Remodeling. *Pflugers Archiv : European journal of Physiology,* **466**(6), pp.1113-1127.

MA, Y., R. P. IYER, M. JUNG, M. P. CZUBRYT and M. L. LINDSEY. 2017. Cardiac Fibroblast Activation Post-Myocardial Infarction: Current Knowledge Gaps. *Trends in Pharmacological Sciences,* **38**(5), pp.448-458.

MACKIE, E. J., T. SCOTT-BURDEN, A. W. HAHN, F. KERN, J. BERNHARDT, S. REGENASS, A. WELLER and F. R. BÜHLER. 1992. Expression of Tenascin by Vascular Smooth Muscle Cells. Alterations in Hypertensive Rats and Stimulation by Angiotensin II. *The American Journal of Pathology,* **141**(2), pp.377-388.

MAHAUT-SMITH, M. P., K. A. TAYLOR and R. J. EVANS. 2016. Calcium Signalling through Ligand-Gated Ion Channels such as P2X1 Receptors in the Platelet and other Non-Excitable Cells. *In:* J. A. ROSADO, ed. *Calcium Entry Pathways in Non-excitable Cells.* Cham: Springer International Publishing, pp.305-329.

MANSO, A. M., S.-M. KANG and R. S. ROSS. 2009. Integrins, Focal Adhesions, and Cardiac Fibroblasts. *Journal of Investigative Medicine : the official publication of the American Federation for Clinical Research,* **57**(8), pp.856-860.

MANSO, A. M., R. LI, S. J. MONKLEY, N. M. CRUZ, S. ONG, D. H. LAO, Y. E. KOSHMAN, Y. GU, K. L. PETERSON, J. CHEN, E. D. ABEL, A. M. SAMAREL, D. R. CRITCHLEY and R. S. ROSS. 2013. Talin1 has Unique Expression versus Talin 2 in the Heart and Modifies the Hypertrophic Response to Pressure Overload. *The Journal of Biological Chemistry,* **288**(6), pp.4252-4264.

MAQBOOL, A., E. J. SPARY, I. W. MANFIELD, M. RUHMANN, L. ZULIANI-ALVAREZ, F. O. GAMBOA-ESTEVES, K. E. PORTER, M. J. DRINKHILL, K. S. MIDWOOD and N. A. TURNER. 2016. Tenascin C Upregulates Interleukin-6 Expression in Human Cardiac Myofibroblasts via Toll-Like Receptor 4. *World Journal of Cardiology,* **8**(5), pp.340-350.

MARKS, A. R. 1997. Intracellular Calcium-Release Channels: Regulators of Cell Life and Death. *American Journal of Physiology-Heart and Circulatory Physiology,* **272**(2), pp.H597-H605.

MARTIN-ALMEDINA, S., S. MANSOUR and P. OSTERGAARD. 2018. Human Phenotypes Caused by PIEZO1 Mutations; One Gene, Two Overlapping Phenotypes? *The Journal of Physiology,* **596**(6), pp.985-992.

MARTINAC, B. 2004. Mechanosensitive Ion Channels: Molecules of Mechanotransduction. *Journal of Cell Science,* **117**(12), pp.2449-2460.

MARTINO, F., A. R. PERESTRELO, V. VINARSKÝ, S. PAGLIARI and G. FORTE. 2018. Cellular Mechanotransduction: From Tension to Function. *Frontiers in Physiology,* **9**(824).

MARTINS, J. R., D. PENTON, R. PEYRONNET, M. ARHATTE, C. MORO, N. PICARD, B. KURT, A. PATEL, E. HONORÉ and S. DEMOLOMBE. 2016. Piezo1-Dependent Regulation of Urinary Osmolarity. *Pflügers Archiv - European Journal of Physiology,* **468**(7), pp.1197-1206.

MATTHEWS, B. D., D. R. OVERBY, R. MANNIX and D. E. INGBER. 2006. Cellular Adaptation to Mechanical Stress: Role of Integrins, Rho, Cytoskeletal Tension and Mechanosensitive Ion Channels. *Journal of Cell Science,* **119**(3), p508.

MCHUGH, B. J., R. BUTTERY, Y. LAD, S. BANKS, C. HASLETT and T. SETHI. 2010. Integrin Activation by Fam38A Uses a Novel Mechanism of R-Ras Targeting to the Endoplasmic Reticulum. *Journal of Cell Science,* **123**(Pt 1), pp.51-61.

MCHUGH, B. J., A. MURDOCH, C. HASLETT and T. SETHI. 2012. Loss of the Integrin-Activating Transmembrane Protein Fam38A (Piezo1) Promotes a Switch to a Reduced Integrin-Dependent Mode of Cell Migration. *PLOS ONE,* **7**(7), pp.e40346-e40346.

MCMULLEN, J. R., T. SHIOI, W.-Y. HUANG, L. ZHANG, O. TARNAVSKI, E. BISPING, M. SCHINKE, S. KONG, M. C. SHERWOOD, J. BROWN, L. RIGGI, P. M. KANG and S. IZUMO. 2004. The Insulin-like Growth Factor 1 Receptor Induces Physiological Heart Growth via the Phosphoinositide 3-Kinase(p110α) Pathway. *Journal of Biological Chemistry,* **279**(6), pp.4782-4793.

MEIER, H., J. BULLINGER, G. MARX, A. DETEN, L. C. HORN, B. RAßLER, H. G. ZIMMER and W. BRIEST. 2009. Crucial Role of Interleukin-6 in the Development of Norepinephrine-induced Left Ventricular Remodeling in Mice. *Cellular Physiology and Biochemistry,* **23**(4-6), pp.327-334.

MELÉNDEZ, G. C., J. L. MCLARTY, S. P. LEVICK, Y. DU, J. S. JANICKI and G. L. BROWER. 2010. Interleukin 6 mediates Myocardial Fibrosis, Concentric Hypertrophy, and Diastolic Dysfunction in Rats. *Hypertension (Dallas, Tex. : 1979),* **56**(2), pp.225-231.

MENG, Q., B. BHANDARY, M. S. BHUIYAN, J. JAMES, H. OSINSKA, I. VALIENTE-ALANDI, K. SHAY-WINKLER, J. GULICK, J. D. MOLKENTIN, B. C. BLAXALL and J. ROBBINS. 2018. Myofibroblast-Specific TGFb Receptor II Signaling in the Fibrotic Response to Cardiac Myosin Binding Protein C-Induced Cardiomyopathy. *Circulation Research,* **123**(12), pp.1285-1297.

MIDGLEY, A. C., M. ROGERS, M. B. HALLETT, A. CLAYTON, T. BOWEN, A. O. PHILLIPS and R. STEADMAN. 2013. Transforming Growth Factor-β1 (TGF-β1)-Stimulated Fibroblast to Myofibroblast Differentiation is Mediated by Hyaluronan (HA)-Facilitated Epidermal Growth Factor Receptor (EGFR) and CD44 Co-Localization in Lipid Rafts. *The Journal of Biological Chemistry,* **288**(21), pp.14824-14838.

MIDWOOD, K., S. SACRE, A. M. PICCININI, J. INGLIS, A. TREBAUL, E. CHAN, S. DREXLER, N. SOFAT, M. KASHIWAGI, G. OREND, F. BRENNAN and B. FOXWELL. 2009. Tenascin-C is an Endogenous Activator of Toll-Like Receptor 4 that is Essential for Maintaining Inflammation in Arthritic Joint Disease. *Nature Medicine,* **15**, p774.

MIDWOOD, K. S., T. HUSSENET, B. LANGLOIS and G. OREND. 2011. Advances in Tenascin-C Biology. *Cellular and Molecular Life Sciences,* **68**(19), p3175.

MIYAMOTO, T., T. MOCHIZUKI, H. NAKAGOMI, S. KIRA, M. WATANABE, Y. TAKAYAMA, Y. SUZUKI, S. KOIZUMI, M. TAKEDA and M. TOMINAGA. 2014. Functional Role for Piezo1 in Stretch-Evoked Ca^{2+} Influx and ATP Release in Urothelial Cell Cultures. *The Journal of Biological Chemistry,* **289**(23), pp.16565-16575.

MOHAMED, T. M. A., R. ABOU-LEISA, N. STAFFORD, A. MAQSOOD, M. ZI, S. PREHAR, F. BAUDOIN-STANLEY, X. WANG, L. NEYSES, E. J. CARTWRIGHT and D. OCEANDY. 2016. The Plasma Membrane Calcium ATPase 4 Signalling in Cardiac Fibroblasts Mediates Cardiomyocyte Hypertrophy. *Nature Communications,* **7**, pp.11074-11074.

MOLKENTIN, J. D., D. BUGG, N. GHEARING, L. E. DORN, P. KIM, M. A. SARGENT, J. GUNAJE, K. OTSU and J. DAVIS. 2017. Fibroblast-Specific Genetic Manipulation of p38 Mitogen-Activated Protein Kinase In Vivo Reveals Its Central Regulatory Role in Fibrosis. *Circulation,* **136**(6), pp.549-561.

MOORE-MORRIS, T., N. GUIMARÃES-CAMBOA, I. BANERJEE, A. C. ZAMBON, T. KISSELEVA, A. VELAYOUDON, W. B. STALLCUP, Y. GU, N. D. DALTON, M. CEDENILLA, R. GOMEZ-AMARO, B. ZHOU, D. A. BRENNER, K. L. PETERSON, J. CHEN and S. M. EVANS. 2014. Resident Fibroblast Lineages Mediate Pressure Overload-Induced Cardiac Fibrosis. *The Journal of Clinical Investigation,* **124**(7), pp.2921-2934.

MOSTERD, A. and A. W. HOES. 2007. Clinical Epidemiology of Heart Failure. *Heart (British Cardiac Society),* **93**(9), pp.1137-1146.

MOUTON, A. J., Y. MA, O. J. RIVERA GONZALEZ, M. J. DASEKE, E. R. FLYNN, T. C. FREEMAN, M. R. GARRETT, K. Y. DELEON-PENNELL and M. L. LINDSEY. 2019. Fibroblast Polarization over the Myocardial Infarction Time Continuum Shifts Roles from Inflammation to Angiogenesis. *Basic Research in Cardiology,* **114**(2), p6.

MURAKI, K., Y. IWATA, Y. KATANOSAKA, T. ITO, S. OHYA, M. SHIGEKAWA and Y. IMAIZUMI. 2003. TRPV2 Is a Component of Osmotically Sensitive Cation Channels in Murine Aortic Myocytes. *Circulation Research,* **93**(9), pp.829-838.

MURRAY, D. R., S. D. PRABHU and B. CHANDRASEKAR. 2000. Chronic β-Adrenergic Stimulation Induces Myocardial Proinflammatory Cytokine Expression. *Circulation,* **101**(20), pp.2338-2341.

MURTHA, L. A., M. J. SCHULIGA, N. S. MABOTUWANA, S. A. HARDY, D. W. WATERS, J. K. BURGESS, D. A. KNIGHT and A. J. BOYLE. 2017. The Processes and Mechanisms of Cardiac and Pulmonary Fibrosis. *Frontiers in Physiology,* **8**, pp.777-777.

NAG, A. C. 1980. Study of Non-Muscle Cells of the Adult Mammalian Heart: a Fine Structural Analysis and Distribution. *Cytobios,* **28**(109), pp.41-61.

NAGAMATSU, Y., M. NISHIDA, N. ONOHARA, M. FUKUTOMI, Y. MARUYAMA, H. KOBAYASHI, Y. SATO and H. KUROSE. 2006. Heterotrimeric G Protein Galpha13-Induced Induction of Cytokine mRNAs Through Two Distinct Pathways in Cardiac Fibroblasts. *Journal of Pharmacological Sciences,* **101**(2), pp.144-150.

NAGASE, H., R. VISSE and G. MURPHY. 2006. Structure and Function of Matrix Metalloproteinases and TIMPs. *Cardiovascular Research,* **69**(3), pp.562-573.

NI, J., Z. DONG, W. HAN, D. KONDRIKOV and Y. SU. 2013. The Role of RhoA and Cytoskeleton in Myofibroblast Transformation in Hyperoxic Lung Fibrosis. *Free Radical Biology & Medicine,* **61**, pp.26-39.

NIAN, M., P. LEE, N. KHAPER and P. LIU. 2004. Inflammatory Cytokines and Postmyocardial Infarction Remodeling. *Circulation Research,* **94**(12), pp.1543-1553.

NISHIDA, M. and H. KUROSE. 2008. Roles of TRP Channels in the Development of Cardiac Hypertrophy. *Naunyn-Schmiedeberg's Archives of Pharmacology,* **378**(4), pp.395-406.

OKA, T., J. XU, R. A. KAISER, J. MELENDEZ, M. HAMBLETON, M. A. SARGENT, A. LORTS, E. W. BRUNSKILL, G. W. DORN, 2ND, S. J. CONWAY, B. J. ARONOW, J. ROBBINS and J. D. MOLKENTIN. 2007. Genetic Manipulation of Periostin Expression Reveals a Role in Cardiac Hypertrophy and Ventricular Remodeling. *Circulation Research,* **101**(3), pp.313-321.

PANDYA, K. and O. SMITHIES. 2011. α-MyHC and Cardiac Hypertrophy. *Circulation Research,* **109**(6), pp.609-610.

PAPAKRIVOPOULOU, J., G. E. LINDAHL, J. E. BISHOP and G. J. LAURENT. 2004. Differential Roles of Extracellular Signal-Regulated Kinase 1/2 and p38MAPK in Mechanical Load-Induced Procollagen α1(I) Gene Expression in Cardiac Fibroblasts. *Cardiovascular Research,* **61**(4), pp.736-744.

PATEL, A. J. and E. HONORÉ. 2001. Properties and Modulation of Mammalian 2P Domain K+ Channels. *Trends in Neurosciences,* **24**(6), pp.339-346.

PATHAK, M. M., J. L. NOURSE, T. TRAN, J. HWE, J. ARULMOLI, D. T. T. LE, E. BERNARDIS, L. A. FLANAGAN and F. TOMBOLA. 2014. Stretch-Activated Ion Channel Piezo1 Directs Lineage Choice in Human Neural Stem Cells. *Proceedings of the National Academy of Sciences of the United States of America,* **111**(45), pp.16148-16153.

PATIL, V. C., H. V. PATIL, K. B. SHAH, J. D. VASANI and P. SHETTY. 2011. Diastolic Dysfunction in Asymptomatic Type 2 Diabetes Mellitus with Normal Systolic Function. *Journal of Cardiovascular Disease Research,* **2**(4), pp.213-222.

PEDERSEN, B. K. and C. P. FISCHER. 2007. Beneficial Health Effects of Exercise – the Role of IL-6 as a Myokine. *Trends in Pharmacological Sciences,* **28**(4), pp.152-156.

PELLIEUX, C., A. FOLETTI, G. PEDUTO, J. F. AUBERT, J. NUSSBERGER, F. BEERMANN, H. R. BRUNNER and T. PEDRAZZINI. 2001. Dilated Cardiomyopathy and Impaired Cardiac Hypertrophic Response to Angiotensin II in Mice Lacking FGF-2. *The Journal of Clinical Investigation,* **108**(12), pp.1843-1851.

PEREZ, D. M., R. S. PAPAY and T. SHI. 2009. Alpha1-Adrenergic Receptor Stimulates Interleukin-6 Expression and Secretion Through both mRNA Stability and Transcriptional Regulation: Involvement of p38 Mitogen-Activated Protein Kinase and Nuclear Factor-kappaB. *Molecular Pharmacology,* **76**(1), pp.144-152.

PEYRONNET, R., J. M. NERBONNE and P. KOHL. 2016. Cardiac Mechano-Gated Ion Channels and Arrhythmias. *Circulation Research,* **118**(2), pp.311-329.

PHATHARAJAREE, W., A. PHROMMINTIKUL and N. CHATTIPAKORN. 2007. Matrix Metalloproteinases and Myocardial Infarction. *The Canadian Journal of Cardiology,* **23**(9), pp.727-733.

PIEK, A., R. A. DE BOER and H. H. W. SILLJÉ. 2016. The Fibrosis-Cell Death Axis in Heart Failure. *Heart Failure Reviews,* **21**(2), pp.199-211.

PINTO, A. R., A. ILINYKH, M. J. IVEY, J. T. KUWABARA, M. L. D'ANTONI, R. DEBUQUE, A. CHANDRAN, L. WANG, K. ARORA, N. A. ROSENTHAL and M. D. TALLQUIST. 2016. Revisiting Cardiac Cellular Composition. *Circulation Research,* **118**(3), pp.400-409.

PONTICOS, M., D. ABRAHAM, C. ALEXAKIS, Q.-L. LU, C. BLACK, T. PARTRIDGE and G. BOU-GHARIOS. 2004. Col1a2 Enhancer Regulates Collagen Activity during Development and in Adult Tissue Repair. *Matrix Biology,* **22**(8), pp.619-628.

PORRELLO, E. R. and E. N. OLSON. 2014. A Neonatal Blueprint for Cardiac Regeneration. *Stem Cell Research,* **13**(3 Pt B), pp.556-570.

PORTER, K. E. and N. A. TURNER. 2009. Cardiac Fibroblasts: At the Heart of Myocardial Remodeling. *Pharmacology & Therapeutics,* **123**(2), pp.255-278.

PRABHU, S. D. and N. G. FRANGOGIANNIS. 2016. The Biological Basis for Cardiac Repair After Myocardial Infarction: From Inflammation to Fibrosis. *Circulation Research,* **119**(1), pp.91-112.

PUGACH, E. K., P. A. RICHMOND, J. G. AZOFEIFA, R. D. DOWELL and L. A. LEINWAND. 2015. Prolonged Cre Expression Driven by the α-Myosin Heavy Chain Promoter can be Cardiotoxic. *Journal of Molecular and Cellular Cardiology,* **86**, pp.54-61.

RAKESH, K., B. YOO, I.-M. KIM, N. SALAZAR, K.-S. KIM and H. A. ROCKMAN. 2010. Beta-Arrestin-Biased Agonism of the Angiotensin Receptor Induced by Mechanical Stress. *Science Signaling,* **3**(125), pp.ra46-ra46.

RANADE, S. S., Z. QIU, S.-H. WOO, S. S. HUR, S. E. MURTHY, S. M. CAHALAN, J. XU, J. MATHUR, M. BANDELL, B. COSTE, Y.-S. J. LI, S. CHIEN and A. PATAPOUTIAN. 2014. Piezo1, a Mechanically Activated Ion Channel, is Required for Vascular Development in Mice. *Proceedings of the National Academy of Sciences of the United States of America,* **111**(28), pp.10347-10352.

REED, A., P. KOHL and R. PEYRONNET. 2014. Molecular Candidates for Cardiac Stretch-Activated Ion Channels. *Global Cardiology Science & Practice,* **2014**(2), pp.9-25.

RETAILLEAU, K., F. DUPRAT, M. ARHATTE, S. S. RANADE, R. PEYRONNET, J. R. MARTINS, M. JODAR, C. MORO, S. OFFERMANNS, Y. FENG, S. DEMOLOMBE, A. PATEL and E. HONORÉ. 2015. Piezo1 in Smooth Muscle Cells Is Involved in Hypertension-Dependent Arterial Remodeling. *Cell Reports,* **13**(6), pp.1161-1171.

RICHES, K., M. E. MORLEY, N. A. TURNER, D. J. O'REGAN, S. G. BALL, C. PEERS and K. E. PORTER. 2009. Chronic Hypoxia Inhibits MMP-2 Activation and Cellular Invasion in Human Cardiac Myofibroblasts. *Journal of Molecular and Cellular Cardiology,* **47**(3), pp.391-399.

RITTER, O. and L. NEYSES. 2003. The Molecular Basis of Myocardial Hypertrophy and Heart Failure. *Trends in Molecular Medicine,* **9**(7), pp.313-321.

ROBERTSON, I. B., M. HORIGUCHI, L. ZILBERBERG, B. DABOVIC, K. HADJIOLOVA and D. B. RIFKIN. 2015. Latent TGF-β-Binding Proteins.

Matrix Biology : Journal of the International Society for Matrix Biology, **47**, pp.44-53.

ROCKMAN, H. A., R. S. ROSS, A. N. HARRIS, K. U. KNOWLTON, M. E. STEINHELPER, L. J. FIELD, J. ROSS, JR. and K. R. CHIEN. 1991. Segregation of Atrial-Specific and Inducible Expression of an Atrial Natriuretic Factor Transgene in an In Vivo Murine Model of Cardiac Hypertrophy. *Proceedings of the National Academy of Sciences of the United States of America,* **88**(18), pp.8277-8281.

RODE, B., J. SHI, N. ENDESH, M. J. DRINKHILL, P. J. WEBSTER, S. J. LOTTEAU, M. A. BAILEY, N. Y. YULDASHEVA, M. J. LUDLOW, R. M. CUBBON, J. LI, T. S. FUTERS, L. MORLEY, H. J. GAUNT, K. MARSZALEK, H. VISWAMBHARAN, K. CUTHBERTSON, P. D. BAXTER, R. FOSTER, P. SUKUMAR, A. WEIGHTMAN, S. C. CALAGHAN, S. B. WHEATCROFT, M. T. KEARNEY and D. J. BEECH. 2017. Piezo1 Channels Sense Whole Body Physical Activity to Reset Cardiovascular Homeostasis and Enhance Performance. *Nature Communications,* **8**(1), p350.

ROMAC, J. M. J., R. A. SHAHID, S. M. SWAIN, S. R. VIGNA and R. A. LIDDLE. 2018. Piezo1 is a Mechanically Activated Ion Channel and Mediates Pressure Induced Pancreatitis. *Nature Communications,* **9**(1), pp.1715-1715.

ROMERO, L. O., A. E. MASSEY, A. D. MATA-DABOIN, F. J. SIERRA-VALDEZ, S. C. CHAUHAN, J. F. CORDERO-MORALES and V. VÁSQUEZ. 2019. Dietary Fatty Acids Fine-Tune Piezo1 Mechanical Response. *Nature Communications,* **10**(1), p1200.

ROSE, B. A., T. FORCE and Y. WANG. 2010. Mitogen-Activated Protein Kinase Signaling in the Heart: Angels versus Demons in a Heart-Breaking Tale. *Physiological Reviews,* **90**(4), pp.1507-1546.

ROSKOSKI, R. 2004. Src Protein–Tyrosine Kinase Structure and Regulation. *Biochemical and Biophysical Research Communications,* **324**(4), pp.1155-1164.

ROSKOSKI, R. 2005. Src Kinase Regulation by Phosphorylation and Dephosphorylation. *Biochemical and Biophysical Research Communications,* **331**(1), pp.1-14.

ROSS, G. R., T. BAJWA, JR., S. EDWARDS, L. EMELYANOVA, F. RIZVI, E. L. HOLMUHAMEDOV, P. WERNER, F. X. DOWNEY, A. J. TAJIK and A. JAHANGIR. 2017. Enhanced Store-Operated Ca(2+) Influx and ORAI1 Expression in Ventricular Fibroblasts from Human Failing Heart. *Biology Open,* **6**(3), pp.326-332.

ROSS, G. R. and A. JAHANGIR. 2016. Functional Alterations of Ion Channels from Cardiac Fibroblasts in Heart Diseases. *Journal of Patient-Centered Research and Reviews,* **3**, pp.207-216.

ROSSI, M. A. and S. V. CARILLO. 1991. Cardiac Hypertrophy Due to Pressure and Volume Overload: Distinctly Different Biological Phenomena? *International Journal of Cardiology,* **31**(2), pp.133-141.

ROTH, G. A., C. JOHNSON, A. ABAJOBIR, F. ABD-ALLAH, S. F. ABERA, G. ABYU, M. AHMED, B. AKSUT, T. ALAM, K. ALAM, F. ALLA, N. ALVIS-GUZMAN, S. AMROCK, H. ANSARI, J. ÄRNLÖV, H. ASAYESH, T. M. ATEY, L. AVILA-BURGOS, A. AWASTHI, A. BANERJEE, A. BARAC, T. BÄRNIGHAUSEN, L. BARREGARD, N. BEDI, E. BELAY KETEMA, D. BENNETT, G. BERHE, Z. BHUTTA, S. BITEW, J. CARAPETIS, J. J. CARRERO, D. C. MALTA, C. A. CASTAÑEDA-ORJUELA, J. CASTILLO-

RIVAS, F. CATALÁ-LÓPEZ, J.-Y. CHOI, H. CHRISTENSEN, M. CIRILLO, L. COOPER, M. CRIQUI, D. CUNDIFF, A. DAMASCENO, L. DANDONA, R. DANDONA, K. DAVLETOV, S. DHARMARATNE, P. DORAIRAJ, M. DUBEY, R. EHRENKRANZ, M. EL SAYED ZAKI, E. J. A. FARAON, A. ESTEGHAMATI, T. FARID, M. FARVID, V. FEIGIN, E. L. DING, G. FOWKES, T. GEBREHIWOT, R. GILLUM, A. GOLD, P. GONA, R. GUPTA, T. D. HABTEWOLD, N. HAFEZI-NEJAD, T. HAILU, G. B. HAILU, G. HANKEY, H. Y. HASSEN, K. H. ABATE, R. HAVMOELLER, S. I. HAY, M. HORINO, P. J. HOTEZ, K. JACOBSEN, S. JAMES, M. JAVANBAKHT, P. JEEMON, D. JOHN, J. JONAS, Y. KALKONDE, C. KARIMKHANI, A. KASAEIAN, Y. KHADER, A. KHAN, Y.-H. KHANG, S. KHERA, A. T. KHOJA, J. KHUBCHANDANI, D. KIM, D. KOLTE, S. KOSEN, K. J. KROHN, G. A. KUMAR, G. F. KWAN, D. K. LAL, A. LARSSON, S. LINN, A. LOPEZ, P. A. LOTUFO, H. M. A. EL RAZEK*, et al.* 2017. Global, Regional, and National Burden of Cardiovascular Diseases for 10 Causes, 1990 to 2015. *Journal of the American College of Cardiology,* **70**(1), pp.1-25.

RUSTAD, K., V. W WONG and G. GURTNER. 2013. The Role of Focal Adhesion Complexes in Fibroblast Mechanotransduction During Scar Formation. *Differentiation; Research in Biological Diversity,* **86**.

RUWHOF, C. and A. VAN DER LAARSE. 2000. Mechanical Stress-Induced Cardiac Hypertrophy: Mechanisms and Signal Transduction Pathways. *Cardiovascular Research,* **47**(1), pp.23-37.

RUWHOF, C., A. E. T. VAN WAMEL, J. M. EGAS and A. VAN DER LAARSE. 2000. Cyclic Stretch Induces the Release of Growth Promoting Factors from Cultured Neonatal Cardiomyocytes and Cardiac Fibroblasts. *Molecular and Cellular Biochemistry,* **208**(1), pp.89-98.

SAMUEL, C. S., E. N. UNEMORI, I. MOOKERJEE, R. A. D. BATHGATE, S. L. LAYFIELD, J. MAK, G. W. TREGEAR and X.-J. DU. 2004. Relaxin Modulates Cardiac Fibroblast Proliferation, Differentiation, and Collagen Production and Reverses Cardiac Fibrosis in Vivo. *Endocrinology,* **145**(9), pp.4125-4133.

SANO, M., K. FUKUDA, T. SATO, H. KAWAGUCHI, M. SUEMATSU, S. MATSUDA, S. KOYASU, H. MATSUI, K. YAMAUCHI-TAKIHARA, M. HARADA, Y. SAITO and S. OGAWA. 2001. ERK and p38 MAPK, but not NF-κB, Are Critically Involved in Reactive Oxygen Species-Mediated Induction of IL-6 by Angiotensin II in Cardiac Fibroblasts. *Circulation Research,* **89**(8), pp.661-669.

SANTIAGO, J.-J., A. L. DANGERFIELD, S. G. RATTAN, K. L. BATHE, R. H. CUNNINGTON, J. E. RAIZMAN, K. M. BEDOSKY, D. H. FREED, E. KARDAMI and I. M. C. DIXON. 2010. Cardiac Fibroblast to Myofibroblast Differentiation In Vivo and In Vitro: Expression of Focal Adhesion Components in Neonatal and Adult Rat Ventricular Myofibroblasts. *Developmental Dynamics,* **239**(6), pp.1573-1584.

SANTULLI, G., R. NAKASHIMA, Q. YUAN and A. R. MARKS. 2017. Intracellular Calcium Release Channels: an Update. *The Journal of Physiology,* **595**(10), pp.3041-3051.

SARRAZY, V., A. KOEHLER, M. L. CHOW, E. ZIMINA, C. X. LI, H. KATO, C. A. CALDARONE and B. HINZ. 2014. Integrins αvβ5 and αvβ3 Promote Latent TGF-β1 Activation by Human Cardiac Fibroblast Contraction. *Cardiovascular Research,* **102**(3), pp.407-417.

SATO, A., K. AONUMA, K. IMANAKA-YOSHIDA, T. YOSHIDA, M. ISOBE, D. KAWASE, N. KINOSHITA, Y. YAZAKI and M. HIROE. 2006. Serum Tenascin-C Might Be a Novel Predictor of Left Ventricular Remodeling and Prognosis After Acute Myocardial Infarction. *Journal of the American College of Cardiology,* **47**(11), pp.2319-2325.

SATOH, S., H. TANAKA, Y. UEDA, J.-I. OYAMA, M. SUGANO, H. SUMIMOTO, Y. MORI and N. MAKINO. 2007. Transient receptor potential (TRP) Protein 7 acts as a G Protein-Activated Ca2+ Channel Mediating Angiotensin II-Induced Myocardial Apoptosis. *Molecular and Cellular Biochemistry,* **294**(1), pp.205-215.

SCHIRONE, L., M. FORTE, S. PALMERIO, D. YEE, C. NOCELLA, F. ANGELINI, F. PAGANO, S. SCHIAVON, A. BORDIN, A. CARRIZZO, C. VECCHIONE, V. VALENTI, I. CHIMENTI, E. DE FALCO, S. SCIARRETTA and G. FRATI. 2017. A Review of the Molecular Mechanisms Underlying the Development and Progression of Cardiac Remodeling. *Oxidative Medicine and Cellular Longevity,* **2017**, pp.3920195-3920195.

SCHLAEPFER, D. D. and T. HUNTER. 1998. Integrin Signalling and Tyrosine Phosphorylation: Just the FAKs? *Trends in Cell Biology,* **8**(4), pp.151-157.

SCHMIDT, C., F. WIEDMANN, S. M. KALLENBERGER, A. RATTE, J. S. SCHULTE, B. SCHOLZ, F. U. MÜLLER, N. VOIGT, M.-P. ZAFEIRIOU, J. R. EHRLICH, U. TOCHTERMANN, G. VERES, A. RUHPARWAR, M. KARCK, H. A. KATUS and D. THOMAS. 2017. Stretch-Activated Two-Pore-Domain (K2P) Potassium Channels in the Heart: Focus on Atrial Fibrillation and Heart Failure. *Progress in Biophysics and Molecular Biology,* **130**, pp.233-243.

SCHMITZ, M. L. and M. KRACHT. 2016. Cyclin-Dependent Kinases as Coregulators of Inflammatory Gene Expression. *Trends in Pharmacological Sciences,* **37**(2), pp.101-113.

SCHROER, A. K. and W. D. MERRYMAN. 2015. Mechanobiology of Myofibroblast Adhesion in Fibrotic Cardiac Disease. *Journal of Cell Science,* **128**(10), pp.1865-1875.

SEDGWICK, B., K. RICHES-SUMAN, S. A. BAGEGHNI, D. J. O'REGAN, K. E. PORTER and N. A. TURNER. 2014. Investigating Inherent Functional Differences between Human Cardiac Fibroblasts Cultured from Non-Diabetic and Type 2 Diabetic Donors. *Cardiovascular Pathology*, **23**(4), pp. 204-210.

SEONG, J., A. TAJIK, J. SUN, J.-L. GUAN, M. J. HUMPHRIES, S. E. CRAIG, A. SHEKARAN, A. J. GARCÍA, S. LU, M. Z. LIN, N. WANG and Y. WANG. 2013. Distinct Biophysical Mechanisms of Focal Adhesion Kinase Mechanoactivation by Different Extracellular Matrix Proteins. *Proceedings of the National Academy of Sciences of the United States of America,* **110**(48), pp.19372-19377.

SHAH, M., D. M. FOREMAN and M. W. FERGUSON. 1995. Neutralisation of TGF-beta 1 and TGF-beta 2 or Exogenous Addition of TGF-beta 3 to Cutaneous Rat Wounds Reduces Scarring. *Journal of Cell Science,* **108**(3), p985.

SHI, Y. and J. MASSAGUÉ. 2003. Mechanisms of TGF-β Signaling from Cell Membrane to the Nucleus. *Cell,* **113**(6), pp.685-700.

SHIMAZAKI, M., K. NAKAMURA, I. KII, T. KASHIMA, N. AMIZUKA, M. LI, M. SAITO, K. FUKUDA, T. NISHIYAMA, S. KITAJIMA, Y. SAGA, M. FUKAYAMA, M. SATA and A. KUDO. 2008. Periostin is Essential for

Cardiac Healing after Acute Myocardial Infarction. *The Journal of Experimental Medicine,* **205**(2), pp.295-303.

SHIMIZU, I. and T. MINAMINO. 2016. Physiological and Pathological Cardiac Hypertrophy. *Journal of Molecular and Cellular Cardiology,* **97**, pp.245-262.

SINFIELD, J. K., A. DAS, D. J. O'REGAN, S. G. BALL, K. E. PORTER and N. A. TURNER. 2013. p38 MAPK alpha Mediates Cytokine-Induced IL-6 and MMP-3 Expression in Human Cardiac Fibroblasts. *Biochemical and Biophysical Research Communications,* **430**(1), pp.419-424.

SKUTEK, M., M. VAN GRIENSVEN, J. ZEICHEN, N. BRAUER and U. BOSCH. 2001. Cyclic Mechanical Stretching Enhances Secretion of Interleukin 6 in Human Tendon Fibroblasts. *Knee Surgery, Sports Traumatology, Arthroscopy,* **9**(5), pp.322-326.

SMART, N., M. H. MOJET, D. S. LATCHMAN, M. S. MARBER, M. R. DUCHEN and R. J. HEADS. 2006. IL-6 Induces PI 3-Kinase and Nitric Oxide-Dependent Protection and Preserves Mitochondrial Function in Cardiomyocytes. *Cardiovascular Research,* **69**(1), pp.164-177.

SNIDER, P., K. N. STANDLEY, J. WANG, M. AZHAR, T. DOETSCHMAN and S. J. CONWAY. 2009. Origin of Cardiac Fibroblasts and the Role of Periostin. *Circulation Research,* **105**(10), pp.934-947.

SOATTIN, L., M. FIORE, P. GAVAZZO, F. VITI, P. FACCI, R. RAITERI, F. DIFATO, M. PUSCH and M. VASSALLI. 2016. The Biophysics of Piezo1 and Piezo2 Mechanosensitive Channels. *Biophysical Chemistry,* **208**, pp.26-33.

SOLIS, A. G., P. BIELECKI, H. R. STEACH, L. SHARMA, C. C. D. HARMAN, S. YUN, M. R. DE ZOETE, J. N. WARNOCK, S. D. F. TO, A. G. YORK, M. MACK, M. A. SCHWARTZ, C. S. DELA CRUZ, N. W. PALM, R. JACKSON and R. A. FLAVELL. 2019. Mechanosensation of Cyclical Force by PIEZO1 is Essential for Innate Immunity. *Nature,* **573**(7772), pp.69-74.

SOLON, J., I. LEVENTAL, K. SENGUPTA, P. C. GEORGES and P. A. JANMEY. 2007. Fibroblast Adaptation and Stiffness Matching to Soft Elastic Substrates. *Biophysical Journal,* **93**(12), pp.4453-4461.

SONI, S., M. K. SAROCH, B. CHANDER, N. V. TIRPUDE and Y. S. PADWAD. 2019. MAPKAPK2 Plays a Crucial Role in the Progression of Head and Neck Squamous Cell Carcinoma by Regulating Transcript Stability. *Journal of Experimental & Clinical Cancer Research,* **38**(1), p175.

SOUDERS, C. A., S. L. K. BOWERS and T. A. BAUDINO. 2009. Cardiac Fibroblast. *Circulation Research,* **105**(12), pp.1164-1176.

SPANN, J. F. 1969. Heart Failure and Ventricular Hypertrophy: Altered Cardiac Contractility and Compensatory Mechanisms. *The American Journal of Cardiology,* **23**(4), pp.504-510.

STAFFORD, N., C. WILSON, D. OCEANDY, L. NEYSES and E. J. CARTWRIGHT. 2017. The Plasma Membrane Calcium ATPases and Their Role as Major New Players in Human Disease. *Physiological Reviews,* **97**(3), pp.1089-1125.

STANSFIELD, W. E., N. M. ANDERSEN, R.-H. TANG and C. H. SELZMAN. 2009. Periostin is a Novel Factor in Cardiac Remodeling after Experimental and Clinical Unloading of the Failing Heart. *The Annals of Thoracic Surgery,* **88**(6), pp.1916-1921.

STANTON, L. W., L. J. GARRARD, D. DAMM, B. L. GARRICK, A. LAM, A. M. KAPOUN, Q. ZHENG, A. A. PROTTER, G. F. SCHREINER and R. T.

WHITE. 2000. Altered Patterns of Gene Expression in Response to Myocardial Infarction. *Circulation Research,* **86**(9), pp.939-945.

STEWART, S., A. JENKINS, S. BUCHAN, A. MCGUIRE, S. CAPEWELL and J. J. J. V. MCMURRAY. 2002. The Current Cost of Heart Failure to the National Health Service in the UK. *European Journal of Heart Failure,* **4**(3), pp.361-371.

STREHLER, E. E. and D. A. ZACHARIAS. 2001. Role of Alternative Splicing in Generating Isoform Diversity Among Plasma Membrane Calcium Pumps. *Physiological Reviews,* **81**(1), pp.21-50.

SUCHYNA, T. M., J. H. JOHNSON, K. HAMER, J. F. LEYKAM, D. A. GAGE, H. F. CLEMO, C. M. BAUMGARTEN and F. SACHS. 2000. Identification of a Peptide Toxin from Grammostola spatulata Spider Venom That Blocks Cation-Selective Stretch-Activated Channels. *The Journal of General Physiology,* **115**(5), pp.583-598.

SUCHYNA, T. M., S. E. TAPE, R. E. KOEPPE, O. S. ANDERSEN, F. SACHS and P. A. GOTTLIEB. 2004. Bilayer-Dependent Inhibition of Mechanosensitive Channels by Neuroactive Peptide Enantiomers. *Nature,* **430**(6996), pp.235-240.

SUGDEN, P. H. and A. CLERK. 1998. "Stress-Responsive" Mitogen-Activated Protein Kinases (c-Jun N-Terminal Kinases and p38 Mitogen-Activated Protein Kinases) in the Myocardium. *Circulation Research,* **83**(4), pp.345-352.

SUGIMOTO, A., A. MIYAZAKI, K. KAWARABAYASHI, M. SHONO, Y. AKAZAWA, T. HASEGAWA, K. UEDA-YAMAGUCHI, T. KITAMURA, K. YOSHIZAKI, S. FUKUMOTO and T. IWAMOTO. 2017. Piezo Type Mechanosensitive Ion Channel Component 1 Functions as a Regulator of the Cell Fate Determination of Mesenchymal Stem Cells. *Scientific Reports,* **7**(1), pp.17696-17696.

SVEC, D., A. TICHOPAD, V. NOVOSADOVA, M. W. PFAFFL and M. KUBISTA. 2015. How Good is a PCR Efficiency Estimate: Recommendations for Precise and Robust qPCR Efficiency Assessments. *Biomolecular Detection and Quantification,* **3**, pp.9-16.

SWONGER, J. M., J. S. LIU, M. J. IVEY and M. D. TALLQUIST. 2016. Genetic Tools for Identifying and Manipulating Fibroblasts in the Mouse. *Differentiation; Research in Biological Diversity,* **92**(3), pp.66-83.

SYEDA, R., M. N. FLORENDO, C. D. COX, J. M. KEFAUVER, J. S. SANTOS, B. MARTINAC and A. PATAPOUTIAN. 2016. Piezo1 Channels Are Inherently Mechanosensitive. *Cell Reports,* **17**(7), pp.1739-1746.

SYEDA, R., J. XU, A. E. DUBIN, B. COSTE, J. MATHUR, T. HUYNH, J. MATZEN, J. LAO, D. C. TULLY, I. H. ENGELS, H. M. PETRASSI, A. M. SCHUMACHER, M. MONTAL, M. BANDELL and A. PATAPOUTIAN. 2015. Chemical Activation of the Mechanotransduction Channel Piezo1. *ELife,* **4**, pe07369.

TAKADA, Y., X. YE and S. SIMON. 2007. The Integrins. *Genome Biology,* **8**(5), pp.215-215.

TALMAN, V. and H. RUSKOAHO. 2016. Cardiac Fibrosis in Myocardial Infarction-From Repair and Remodeling to Regeneration. *Cell and Tissue Research,* **365**(3), pp.563-581.

TANAKA, R., M. UMEMURA, M. NARIKAWA, T. FUJITA, U. YOKOYAMA, T. ISHIGAMI, K. KIMURA, K. TAMURA and Y. ISHIKAWA. 2018. Hydrostatic Pressure Suppresses Fibrotic Changes via Akt/GSK-3 Signaling in Human Cardiac Fibroblasts. *Physiological Reports,* **6**(9), pp.e13687-e13687.

TANG, M., W. ZHANG, H. LIN, H. JIANG, H. DAI and Y. ZHANG. 2007. High Glucose Promotes the Production of Collagen Types I and III by Cardiac Fibroblasts through a Pathway Dependent on Extracellular-Signal-Regulated Kinase 1/2. *Molecular and Cellular Biochemistry,* **301**(1), pp.109-114.

TANNO, M., R. BASSI, D. A. GOROG, A. T. SAURIN, J. JIANG, R. J. HEADS, J. L. MARTIN, R. J. DAVIS, R. A. FLAVELL and M. S. MARBER. 2003. Diverse Mechanisms of Myocardial p38 Mitogen-Activated Protein Kinase Activation. *Circulation Research,* **93**(3), pp.254-261.

TARONE, G. and G. LEMBO. 2003. Molecular Interplay between Mechanical and Humoral Signalling in Cardiac Hypertrophy. *Trends in Molecular Medicine,* **9**(9), pp.376-382.

TAYLOR, C. J., J. M. ORDÓÑEZ-MENA, A. K. ROALFE, S. LAY-FLURRIE, N. R. JONES, T. MARSHALL and F. D. R. HOBBS. 2019. Trends in Survival After a Diagnosis of Heart Failure in the United Kingdom 2000-2017: population based cohort study. *BMJ,* **364**, pl223.

THOBE, B. M., M. FRINK, M. A. CHOUDHRY, M. G. SCHWACHA, K. I. BLAND and I. H. CHAUDRY. 2006. Src Family Kinases Regulate p38 MAPK-Mediated IL-6 Production in Kupffer Cells Following Hypoxia. *American Journal of Physiology-Cell Physiology,* **291**(3), pp.C476-C482.

TOMASEK, J. J., G. GABBIANI, B. HINZ, C. CHAPONNIER and R. A. BROWN. 2002. Myofibroblasts and Mechano-Regulation of Connective Tissue Remodelling. *Nature Reviews Molecular Cell Biology,* **3**(5), pp.349-363.

TRAVERS, J. G., F. A. KAMAL, J. ROBBINS, K. E. YUTZEY and B. C. BLAXALL. 2016. Cardiac Fibrosis: The Fibroblast Awakens. *Circulation Research,* **118**(6), pp.1021-1040.

TURNER, N. A. 2011. Therapeutic Regulation of Cardiac Fibroblast Function: Targeting Stress-Activated Protein Kinase Pathways. *Future Cardiology,* **7**(5), pp.673-691.

TURNER, N. A. 2014. Effects of Interleukin-1 on Cardiac Fibroblast Function: Relevance to Post-Myocardial Infarction Remodelling. *Vascular Pharmacology,* **60**(1), pp.1-7.

TURNER, N. A. 2016. Inflammatory and Fibrotic Responses of Cardiac Fibroblasts to Myocardial Damage Associated Molecular Patterns (DAMPs). *Journal of Molecular and Cellular Cardiology,* **94**, pp.189-200.

TURNER, N. A. and N. M. BLYTHE. 2019. Cardiac Fibroblast p38 MAPK: A Critical Regulator of Myocardial Remodeling. *Journal of Cardiovascular Development and Disease,* **6**(3), p27.

TURNER, N. A., R. S. MUGHAL, P. WARBURTON, D. J. O'REGAN, S. G. BALL and K. E. PORTER. 2007. Mechanism of TNFα-Induced IL-1α, IL-1β and IL-6 Expression in Human Cardiac Fibroblasts: Effects of Statins and Thiazolidinediones. *Cardiovascular Research,* **76**(1), pp.81-90.

TURNER, N. A. and K. E. PORTER. 2012. Regulation of Myocardial Matrix Metalloproteinase Expression and Activity by Cardiac Fibroblasts. *IUBMB Life,* **64**(2), pp.143-150.

TURNER, N. A. and K. E. PORTER. 2013. Function and Fate of Myofibroblasts After Myocardial Infarction. *Fibrogenesis & Tissue Repair,* **6**(1), pp.5-5.

TURNER, N. A., K. E. PORTER, W. H. T. SMITH, H. L. WHITE, S. G. BALL and A. J. BALMFORTH. 2003. Chronic β2-adrenergic Receptor Stimulation Increases Proliferation of Human Cardiac Fibroblasts via an Autocrine Mechanism. *Cardiovascular Research,* **57**(3), pp.784-792.

VAKILI, B. A., P. M. OKIN and R. B. DEVEREUX. 2001. Prognostic Implications of Left Ventricular Hypertrophy. *American Heart Journal,* **141**(3), pp.334-341.

VALIENTE-ALANDI, I., A. E. SCHAFER and B. C. BLAXALL. 2016. Extracellular Matrix-Mediated Cellular Communication in the Heart. *Journal of Molecular and Cellular Cardiology,* **91**, pp.228-237.

VAN DEN BORNE, S. W. M., J. DIEZ, W. M. BLANKESTEIJN, J. VERJANS, L. HOFSTRA and J. NARULA. 2009. Myocardial Remodeling after Infarction: the Role of Myofibroblasts. *Nature Reviews Cardiology,* **7**, p30.

VAN NIEUWENHOVEN, F. A., K. E. HEMMINGS, K. E. PORTER and N. A. TURNER. 2013. Combined Effects of Interleukin-1α and Transforming Growth Factor-β1 on Modulation of Human Cardiac Fibroblast Function. *Matrix Biology,* **32**(7), pp.399-406.

VAN PUTTEN, S., Y. SHAFIEYAN and B. HINZ. 2016. Mechanical Control of Cardiac Myofibroblasts. *Journal of Molecular and Cellular Cardiology,* **93**, pp.133-142.

VAN WAGONER, D. R. and M. LAMORGESE. 1994. Ischemia Potentiates the Mechanosensitive Modulation of Atrial ATP-Sensitive Potassium Channels a. *Annals of the New York Academy of Sciences,* **723**(1), pp.392-395.

VAN WAMEL, A. J. E. T., C. RUWHOF, L. E. J. M. VAN DER VALK-KOKSHOORN, P. I. SCHRIERN and A. VAN DER LAARSE. 2001. The Role of Angiotensin II, Endothelin-1 and Transforming Growth Factor-β as Autocrine/Paracrine Mediators of Stretch-Induced Cardiomyocyte hypertrophy. *Molecular and Cellular Biochemistry,* **218**(1), pp.113-124.

VAN ZUYLEN, V.-L., M. C. DEN HAAN, H. ROELOFS, W. E. FIBBE, M. J. SCHALIJ and D. E. ATSMA. 2015. Myocardial Infarction Models in NOD/Scid Mice for Cell Therapy Research: Permanent Ischemia vs Ischemia-Reperfusion. *SpringerPlus,* **4**, pp.336-336.

VANDEN BERGHE, W., L. VERMEULEN, G. DE WILDE, K. DE BOSSCHER, E. BOONE and G. HAEGEMAN. 2000. Signal Transduction by Tumor Necrosis Factor and Gene Regulation of the Inflammatory Cytokine Interleukin-6. *Biochemical Pharmacology,* **60**(8), pp.1185-1195.

VANDESOMPELE, J., K. DE PRETER, F. PATTYN, B. POPPE, N. VAN ROY, A. DE PAEPE and F. SPELEMAN. 2002. Accurate Normalization of Real-Time Quantitative RT-PCR Data by Geometric Averaging of Multiple Internal Control Genes. *Genome Biology,* **3**(7), pp.RESEARCH0034-RESEARCH0034.

VANHOUTTE, D., M. SCHELLINGS, Y. PINTO and S. HEYMANS. 2006. Relevance of Matrix Metalloproteinases and their Inhibitors after Myocardial Infarction: A temporal and spatial window. *Cardiovascular Research,* **69**(3), pp.604-613.

VERDECCHIA, P., G. SCHILLACI, M. GUERRIERI, C. GATTESCHI, G. BENEMIO, F. BOLDRINI and C. PORCELLATI. 1990. Circadian Blood Pressure Changes and Left Ventricular Hypertrophy in Essential Hypertension. *Circulation,* **81**(2), pp.528-536.

VILLARREAL, F. J., A. A. LEE, W. H. DILLMANN and F. J. GIORDANO. 1996. Adenovirus-Mediated Overexpression of Human Transforming Growth Factor-b1 in Rat Cardiac Fibroblasts, Myocytes and Smooth Muscle Cells. *Journal of Molecular and Cellular Cardiology,* **28**(4), pp.735-742.

VRIENS, J., H. WATANABE, A. JANSSENS, G. DROOGMANS, T. VOETS and B. NILIUS. 2004. Cell Swelling, Heat, and Chemical Agonists Use Distinct

Pathways for the Activation of the Cation Channel TRPV4. *Proceedings of the National Academy of Sciences of the United States of America,* **101**(1), pp.396-401.

WANG, J., H. CHEN, A. SETH and C. A. MCCULLOCH. 2003. Mechanical Force Regulation of Myofibroblast Differentiation in Cardiac Fibroblasts. *American Journal of Physiology-Heart and Circulatory Physiology,* **285**(5), pp.H1871-H1881.

WANG, S., R. CHENNUPATI, H. KAUR, A. IRING, N. WETTSCHURECK and S. OFFERMANNS. 2016. Endothelial Cation Channel PIEZO1 Controls Blood Pressure by Mediating Flow-Induced ATP Release. *The Journal of Clinical Investigation,* **126**(12), pp.4527-4536.

WANG, Y., S. CHI, H. GUO, G. LI, L. WANG, Q. ZHAO, Y. RAO, L. ZU, W. HE and B. XIAO. 2018. A Lever-Like Transduction Pathway for Long-Distance Chemical- and Mechano-Gating of the Mechanosensitive Piezo1 Channel. *Nature Communications,* **9**(1), pp.1300-1300.

WERNER, F., M. K. JAIN, M. W. FEINBERG, N. E. S. SIBINGA, A. PELLACANI, P. WIESEL, M. T. CHIN, J. N. TOPPER, M. A. PERRELLA and M.-E. LEE. 2000. Transforming Growth Factor-β1 Inhibition of Macrophage Activation Is Mediated via Smad3. *Journal of Biological Chemistry,* **275**(47), pp.36653-36658.

WHITFIELD, J., T. LITTLEWOOD and L. SOUCEK. 2015. Tamoxifen Administration to Mice. *Cold Spring Harbor Protocols,* **2015**(3), ppdb.prot077966.

WHITMARSH, A. J. 2010. A Central Role for p38 MAPK in the Early Transcriptional Response to Stress. *BMC Biology,* **8**(1), p47.

WILLEMS, I. E., M. G. HAVENITH, J. G. DE MEY and M. J. DAEMEN. 1994. The Alpha-Smooth Muscle Actin-Positive Cells in Healing Human Myocardial Scars. *The American Journal of Pathology,* **145**(4), pp.868-875.

WILLEMS, I. E. M. G., J.-W. ARENDS and M. J. A. P. DAEMEN. 1996. Tenascin and Fibronectin Expression in Healing Human Myocardial Scars. *The Journal of Pathology,* **179**(3), pp.321-325.

WILSON, C. and S. E. DRYER. 2014. A Mutation in TRPC6 Channels Abolishes their Activation by Hypoosmotic Stretch but Does Not Affect Activation by Diacylglycerol or G Protein Signaling Cascades. *American Journal of Physiology-Renal Physiology,* **306**(9), pp.F1018-F1025.

WIPFF, P.-J., D. B. RIFKIN, J.-J. MEISTER and B. HINZ. 2007. Myofibroblast Contraction Activates Latent TGF-beta1 from the Extracellular Matrix. *The Journal of Cell Biology,* **179**(6), pp.1311-1323.

WONG, T.-Y., W.-C. JUANG, C.-T. TSAI, C.-J. TSENG, W.-H. LEE, S.-N. CHANG and P.-W. CHENG. 2018. Mechanical Stretching Simulates Cardiac Physiology and Pathology through Mechanosensor Piezo1. *Journal of Clinical Medicine,* **7**(11), p410.

WOO, S.-H., V. LUKACS, J. C. DE NOOIJ, D. ZAYTSEVA, C. R. CRIDDLE, A. FRANCISCO, T. M. JESSELL, K. A. WILKINSON and A. PATAPOUTIAN. 2015. Piezo2 is the Principal Mechanotransduction Channel for Proprioception. *Nature Neuroscience,* **18**(12), pp.1756-1762.

WOO, S.-H., S. RANADE, A. D. WEYER, A. E. DUBIN, Y. BABA, Z. QIU, M. PETRUS, T. MIYAMOTO, K. REDDY, E. A. LUMPKIN, C. L. STUCKY and A. PATAPOUTIAN. 2014. Piezo2 is Required for Merkel-Cell Mechanotransduction. *Nature,* **509**(7502), pp.622-626.

XIA, Y., K. LEE, N. LI, D. CORBETT, L. MENDOZA and N. G. FRANGOGIANNIS. 2009. Characterization of the Inflammatory and Fibrotic Response in a

Mouse Model of Cardiac Pressure Overload. *Histochemistry and Cell Biology,* **131**(4), pp.471-481.

YANCY, C. W., M. JESSUP, B. BOZKURT, J. BUTLER, D. E. CASEY, M. H. DRAZNER, G. C. FONAROW, S. A. GERACI, T. HORWICH, J. L. JANUZZI, M. R. JOHNSON, E. K. KASPER, W. C. LEVY, F. A. MASOUDI, P. E. MCBRIDE, J. J. V. MCMURRAY, J. E. MITCHELL, P. N. PETERSON, B. RIEGEL, F. SAM, L. W. STEVENSON, W. H. W. TANG, E. J. TSAI and B. L. WILKOFF. 2013. 2013 ACCF/AHA Guideline for the Management of Heart Failure: Executive Summary. *Circulation,* **128**(16), pp.1810-1852.

YANG, X.-N., Y.-P. LU, J.-J. LIU, J.-K. HUANG, Y.-P. LIU, C.-X. XIAO, A. JAZAG, J.-L. REN and B. GULENG. 2014. Piezo1 Is as a Novel Trefoil Factor Family 1 Binding Protein that Promotes Gastric Cancer Cell Mobility In Vitro. *Digestive Diseases and Sciences,* **59**(7), pp.1428-1435.

YASUDA, N., S.-I. MIURA, H. AKAZAWA, T. TANAKA, Y. QIN, Y. KIYA, S. IMAIZUMI, M. FUJINO, K. ITO, Y. ZOU, S. FUKUHARA, S. KUNIMOTO, K. FUKUZAKI, T. SATO, J. GE, N. MOCHIZUKI, H. NAKAYA, K. SAKU and I. KOMURO. 2008. Conformational Switch of Angiotensin II Type 1 Receptor Underlying Mechanical Stress-Induced Activation. *EMBO reports,* **9**(2), pp.179-186.

YIN, F., Y.-Y. WANG, J.-H. DU, C. LI, Z.-Z. LU, C. HAN and Y.-Y. ZHANG. 2006. Noncanonical cAMP Pathway and p38 MAPK Mediate β2-Adrenergic Receptor-Induced IL-6 Production in Neonatal Mouse Cardiac Fibroblasts. *Journal of Molecular and Cellular Cardiology,* **40**(3), pp.384-393.

YOKOYAMA, T., K. SEKIGUCHI, T. TANAKA, K. TOMARU, M. ARAI, T. SUZUKI and R. NAGAI. 1999. Angiotensin II and Mechanical Stretch Induce Production of Tumor Necrosis Factor in Cardiac Fibroblasts. *American Journal of Physiology-Heart and Circulatory Physiology,* **276**(6), pp.H1968-H1976.

YUE, L., J. XIE and S. NATTEL. 2011. Molecular Determinants of Cardiac Fibroblast Electrical Function and Therapeutic Implications for Atrial Fibrillation. *Cardiovascular Research,* **89**(4), pp.744-753.

YUE, Z., Y. ZHANG, J. XIE, J. JIANG and L. YUE. 2013. Transient Receptor Potential (TRP) Channels and Cardiac Fibrosis. *Current Topics in Medicinal Chemistry,* **13**(3), pp.270-282.

ZARYCHANSKI, R., V. P. SCHULZ, B. L. HOUSTON, Y. MAKSIMOVA, D. S. HOUSTON, B. SMITH, J. RINEHART and P. G. GALLAGHER. 2012. Mutations in the Mechanotransduction Protein PIEZO1 are Associated with Hereditary Xerocytosis. *Blood,* **120**(9), pp.1908-1915.

ZEISBERG, E. M. and R. KALLURI. 2010. Origins of Cardiac Fibroblasts. *Circulation Research,* **107**(11), pp.1304-1312.

ZEISBERG, E. M., O. TARNAVSKI, M. ZEISBERG, A. L. DORFMAN, J. R. MCMULLEN, E. GUSTAFSSON, A. CHANDRAKER, X. YUAN, W. T. PU, A. B. ROBERTS, E. G. NEILSON, M. H. SAYEGH, S. IZUMO and R. KALLURI. 2007. Endothelial-to-Mesenchymal Transition Contributes to Cardiac Fibrosis. *Nature Medicine,* **13**, p952.

ZENG, W.-Z., K. L. MARSHALL, S. MIN, I. DAOU, M. W. CHAPLEAU, F. M. ABBOUD, S. D. LIBERLES and A. PATAPOUTIAN. 2018. PIEZOs Mediate Neuronal Sensing of Blood Pressure and the Baroreceptor Reflex. *Science (New York, N.Y.),* **362**(6413), pp.464-467.

ZHANG, B., J. JIANG, Z. YUE, S. LIU, Y. MA, N. YU, Y. GAO, S. SUN, S. CHEN and P. LIU. 2016. Store-Operated Ca2+ Entry (SOCE) Contributes to Angiotensin II-Induced Cardiac Fibrosis in Cardiac Fibroblasts. *Journal of Pharmacological Sciences,* **132**(3), pp.171-180.

ZHANG, W., V. ELIMBAN, M. S. NIJJAR, S. K. GUPTA and N. S. DHALLA. 2003. Role of Mitogen-Activated Protein Kinase in Cardiac Hypertrophy and Heart Failure. *Experimental and Clinical Cardiology,* **8**(4), pp.173-183.

ZHANG, X., T. ZHANG, J. WU, X. YU, D. ZHENG, F. YANG, T. LI, L. WANG, Y. ZHAO, S. DONG, X. ZHONG, S. FU, C. Q. XU, F. LU and W. H. ZHANG. 2014. Calcium Sensing Receptor Promotes Cardiac Fibroblast Proliferation and Extracellular Matrix Secretion. *Cellular Physiology and Biochemistry,* **33**(3), pp.557-568.

ZHAO, L., G. CHENG, R. JIN, M. R. AFZAL, A. SAMANTA, Y.-T. XUAN, M. GIRGIS, H. K. ELIAS, Y. ZHU, A. DAVANI, Y. YANG, X. CHEN, S. YE, O.-L. WANG, L. CHEN, J. HAUPTMAN, R. J. VINCENT and B. DAWN. 2016a. Deletion of Interleukin-6 Attenuates Pressure Overload-Induced Left Ventricular Hypertrophy and Dysfunction. *Circulation Research,* **118**(12), pp.1918-1929.

ZHAO, Q., K. WU, J. GENG, S. CHI, Y. WANG, P. ZHI, M. ZHANG and B. XIAO. 2016b. Ion Permeation and Mechanotransduction Mechanisms of Mechanosensitive Piezo Channels. *Neuron,* **89**(6), pp.1248-1263.

ZHAO, Q., H. ZHOU, S. CHI, Y. WANG, J. WANG, J. GENG, K. WU, W. LIU, T. ZHANG, M.-Q. DONG, J. WANG, X. LI and B. XIAO. 2018. Structure and Mechanogating Mechanism of the Piezo1 Channel. *Nature,* **554**, p487.

ZHAO, W., M. LIU and K. L. KIRKWOOD. 2008. p38alpha Stabilizes Interleukin-6 mRNA via Multiple AU-Rich Elements. *The Journal of Biological Chemistry,* **283**(4), pp.1778-1785.

ZHENG, B., Z. ZHANG, C. M. BLACK, B. DE CROMBRUGGHE and C. P. DENTON. 2002. Ligand-Dependent Genetic Recombination in Fibroblasts : a Potentially Powerful Technique for Investigating Gene Function in Fibrosis. *The American Journal of Pathology,* **160**(5), pp.1609-1617.

ZHENG, W., E. O. GRACHEVA and S. N. BAGRIANTSEV. 2019. A Hydrophobic Gate in the Inner Pore Helix is the Major Determinant of Inactivation in Mechanosensitive Piezo Channels. *ELife,* **8**, pe44003.

ZHONG, M., W. WU, H. KANG, Z. HONG, S. XIONG, X. GAO, J. REHMAN, Y. A. KOMAROVA and A. B. MALIK. 2019. Alveolar Stretch Activation of Endothelial Piezo1 Protects Adherens Junctions and Lung Vascular Barrier. *American Journal of Respiratory Cell and Molecular Biology,* **0**(ja), pnull.

ZHU, J. and W. CARVER. 2012. Effects of Interleukin-33 on Cardiac Fibroblast Gene Expression and Activity. *Cytokine,* **58**(3), pp.368-379.